ISSN 2408-2384 (ONLINE)

Environment and Natural Resources Journal

Volume 22 Number 5 September - October 2024

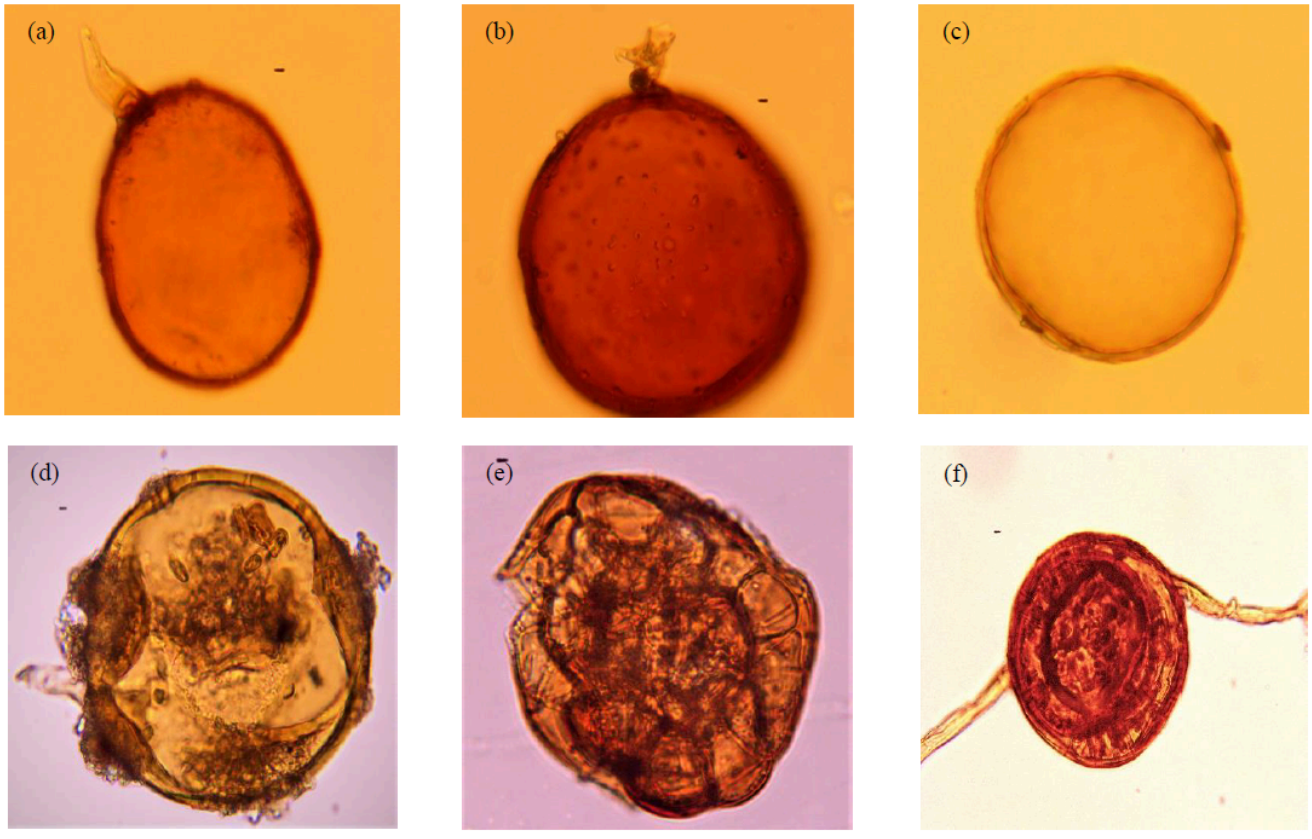

Tentative identification of spores; (a) *Glomus mossae*, (b) *G. macrocarpon*, (c) *Acaulospora* sp., (d) *Gigaspora* sp., (e) *Sclerocystis* sp., (f) *Glomus multicauli*

Source: Paul S, Parkash V, Kaundal R, Dhara B, Thapa M, Mitra AK. Seasonal diversity of Arbuscular Mycorrhizal Fungi (AMF) in the mangrove forests of Bakkhali, Sundarban, India. Page 420-430.

Environment and Natural Resources Journal (EnNRJ)
Volume 22, Number 5, September - October 2024 ISSN: 2408-2384 (Online)

AIMS AND SCOPE

The Environment and Natural Resources Journal is a peer-reviewed journal, which provides insight scientific knowledge into the diverse dimensions of integrated environmental and natural resource management. The journal aims to provide a platform for exchange and distribution of the knowledge and cutting-edge research in the fields of environmental science and natural resource management to academicians, scientists and researchers. The journal accepts a varied array of manuscripts on all aspects of environmental science and natural resource management. The journal scope covers the integration of multidisciplinary sciences for prevention, control, treatment, environmental clean-up and restoration. The study of the existing or emerging problems of environment and natural resources in the region of Southeast Asia and the creation of novel knowledge and/or recommendations of mitigation measures for sustainable development policies are emphasized.

The subject areas are diverse, but specific topics of interest include:

- Biodiversity
- Climate change
- Detection and monitoring of polluted sources e.g., industry, mining
- Disaster e.g., forest fire, flooding, earthquake, tsunami, or tidal wave
- Ecological/Environmental modelling
- Emerging contaminants/hazardous wastes investigation and remediation
- Environmental dynamics e.g., coastal erosion, sea level rise
- Environmental assessment tools, policy and management e.g., GIS, remote sensing, Environmental Management System (EMS)
- Environmental pollution and other novel solutions to pollution
- Remediation technology of contaminated environments
- Transboundary pollution
- Waste and wastewater treatments and disposal technology

Schedule
Environment and Natural Resources Journal (EnNRJ) is published 6 issues per year in January-February, March-April, May-June, July-August, September-October, and November-December.

Publication Fees
There is no cost of the article-processing and publication.

Ethics in publishing
EnNRJ follows closely a set of guidelines and recommendations published by Committee on Publication Ethics (COPE).

Environment and Natural Resources Journal (EnNRJ)
Volume 22, Number 5, September - October 2024 ISSN: 2408-2384 (Online)

Editorial Office Address
Research Management and Administration Section,
Faculty of Environment and Resource Studies, Mahidol University
999, Phutthamonthon Sai 4 Road, Salaya, Phutthamonthon, Nakhon Pathom, Thailand, 73170
Phone +662 441 5000 ext. 2108 Fax. +662 441 9509-10
Website: https://ph02.tci-thaijo.org/index.php/ennrj/index
E-mail: ennrjournal@gmail.com

Environment and Natural Resources Journal (EnNRJ)

Volume 22, Number 5, September - October 2024 ISSN: 2408-2384 (Online)

CONTENT

Environment and Natural Resources Journal

Volume 22
Issue 5
2024

Modeling the Bioclimatic Range of *Musa ingens* (Giant Highland Banana) under Conditions of Climate Change Scenarios

Septianto Aldiansyah[1*] and Risna[2]

[1]*Department of Geography, Faculty of Mathematics and Natural Sciences, University of Indonesia, Jalan Margonda Raya, Depok 16424, Jawa Barat, Indonesia*
[2]*Department of Microbiology, Faculty of Mathematics and Natural Sciences, IPB University, Jalan Merantil, Bogor 16680, Jawa Barat, Indonesia*

ARTICLE INFO

Received: 1 Jan 2024
Received in revised: 21 Jul 2024
Accepted: 26 Jul 2024
Published online: 14 Aug 2024
DOI: 10.32526/ennrj/22/20240002

Keywords:
Climate change/ Predicted area/ Distribution/ Climate factor/ Giant highland banana/ *Musa ingens*

*** Corresponding author:**
E-mail:
septianto.aldiansyah@ui.ac.id

ABSTRACT

Climate change significantly impacts living organisms, leading to alterations in their range, distribution, and abundance. This study estimates the potential distribution of representatives of the family *Musaceae*, noted for their large size and importance to tropical ecosystems. We focus on *Musa ingens* Simmonds 1960 and employ bioclimatic variables and in situ datasets to model its species distribution. We differentiate potential distribution areas for *M. ingens* and present a prognostic map of its distribution under four climate change scenarios. Precipitation during the warmest quarter emerges as the primary factor influencing the spatial distribution of *M. ingens*. Under the RCP (Representative Concentration Pathway) 6.0 scenario, the potential distribution shows an initial decrease, followed by a significant increase by 2070. Meanwhile, the RCP 8.5 scenario indicates an increase in 2050, with a subsequent six percent decrease in 2070. Under the RCP 4.5 scenario for 2050, the species distribution shifts regionally, particularly around the Osua Trikora Mountains and the highlands of the Giluwe Mountains to Mount Victoria. By 2070, the feasible area is expected to expand. Notably, the RCP 2.6 scenario for 2070 predicts a dramatic reduction in habitable area around Mount Bintang Lestari, on the border between Indonesia and Papua New Guinea, rendering the entire lowland region of Papua uninhabitable. Consequently, a sharp decline in the population of *M. ingens* in this area is predicted.

1. INTRODUCTION

Climate projections indicate that tropical regions are expected to experecience significantly warmer and more severe compared to other part of the world (Gasparrini et al., 2017; Serdeczny et al., 2017; Siyum, 2020). According to the IPCC's recent multi-model mean, Northeastern United States, Central America, West and South Africa, and Southeast Asia are projected to become drier by 2100, while other already wet tropical regions will become even wetter (Lee et al., 2021). Studies by Feng and Zhang (2015) and Greve and Seneviratne (2015) suggest that wet areas will experience increased precipitation, whereas dry areas will see reduced rainfall. However, Knutti and Sedláček (2013) and McSweeney and Jones (2013) have noted that tropical regions show the lowest consensus among climate models regarding future weather changes. This uncertainty is compounded by smaller-scale assessments (Platts et al., 2015; Rahn et al., 2018). Given the prejected increase in temperatures, reduced rainfall intensity represents a potential worst-case scenario for future crop growth.

Climatic factors have long been recognized as influential in ecological studies (Thiele, 1977). Determining optimal temperature and humidity across season is crucial for understanding species habitats predicting changes in their distribution area. *Musa ingens* Simmonds 1960 is an important component of tropical ecosystems, producing over 125 million tons annually and ranking among the world's most

Citation: Aldiansyah S, Risna. Modeling the bioclimatic range of *Musa ingens* (giant highland banana) under conditions of climate change scenarios. Environ. Nat. Resour. J. 2024;22(5):394-407. (https://doi.org/10.32526/ennrj/22/20240002)

important fruit crops (FAO, 2018). Every parts of the plant is utilized in daily life (Kennedy, 2009). *M. ingens* can reach heights of 15 m (Argent, 1976; WCSP, 2018), thriving in the highlands of Papua New Guinea's main island within primary montane rainforest and exhibiting intolerance to high temperatures (Simmonds, 1960; Argent, 1976). Such topographic conditions are influenced by biotic and abiotic stresses, including climate factors such as salinity (8.0), relative humidity (15%), heat stress (>15ºC), and cold temperature stress (<0ºC). As a native plant of tropical regions, *M. ingens* thrives best at temperature between 31ºC and 32ºC with adequate nutrient and water availability (Kallow et al., 2020; Joshi et al., 2023), facilitating early flowering and higher yields in favorable environments (Ravi and Vaganan, 2016). Recorded collections indicate its presence predominantly in the Central Range montane rainforests ecoregion, with occurence also noted in the Huon Peninsula montane rainforests and Southeastern Papuan rainforests ecoregions (Olson et al., 2001). Studies have additionaly documented its presence in the Arfak Mountains, Indonesia (Sadsoeitoeboen et al., 2021).

The population of *M. ingens* significantly surpasses the threshold for threatened status, owing to its widespread distribution ascross numerouslocations. While specific population trends remains unclear, it is believed to be abundant in the central highlands of Papua New Guinea (Plummer et al., 2020), thus classified as Least Concern by conservation standards. However, habitat fragmentation poses a significant threat to this species (Butler, 2006; WWF, 2019; Mongabay, 2019). Factors such as timber extraction, subsistence, and industrial agriculture expansion, mining activities (Butler, 2006; WWF, 2019; Mongabay, 2019), along with local cultural practices (Sterly, 1997; Kennedy, 2009; Lentfer, 2009) contribute to this fragmentation. Furthermore, while *M. ingens* holds holticultural value, its cultivation outside its native climate presents considerable challenges (Plummer et al., 2020).

Although the anthropogenic factors mentioned are a concern for the survival of this species (Plummer et al., 2020), it appears that climate change has significantly altered the distribution of species such as bananas in the wild and has the potential to affect interactions between plants, pests, and diseases and the humans, animal, and plants hosts (Bebber, 2019; Watts et al., 2023; Abdoussalami et al., 2023). Empirical studies show that competition for water resources between trees may worsen under increasingly hot and dry climate conditions, thereby impacting distribution and productivity (Lott et al., 2009; Abdulai et al., 2018; Blaser et al., 2018). Bebber's (2019) in-depth study found that the increase in risk to the survival of banana species over the last 60 years was influenced by temperature. Therefore, little is known about the influence of climate change on the distribution of bananas, especially *M. ingens*.

Climate change is seen to affect the cycle and habitat range of the *M. ingens* species. In this contex, investigating the potential distribution of species becomes interesting, although some rare species are no less important. The species studied in this research has Least Concern (LC) status according to the IUCN Red List. It is very interesting to predict changes in the potential distribution of this species range in the next 30-50 years due to the influence of global climate change. This research aims to predict trends in changes in the potential distribution of *M. ingens* under various global climate change scenarios for 2050 and 2070.

2. METHODOLOGY

Research material was obtained from the Global Biodiversity Information Facility (GBIF) open database, initially comprising data from 37 sites. However, only 19 sites were used after eliminating duplicate data, coordinate errors, and data without coordinates (GBIF, 2023). We then validate these data with our colleagues through the framework of the Scientific Collaboration Agreement. The data collection covered the time range from 1963 to 2023, with occurences distributed in Indonesia (5 occurrences) and Papua New Guinea (14 occurrences) (Figure 1).

Bioclimatic modeling (Aldiansyah and Wahid, 2023; Aldiansyah and Wahid, 2024) uses 2.5 km resolution WorldClim data from the global climate database (www.worldclim.org) with 19 bioclimatic variables. The model is built from the Community Climate System Model 4 (CCSM 4). This data was chosen considering the development of all CCSM components from the previous version, particularly in the annual water storage cycle in tropical regions which is much improved (Gent et al., 2011). To enchance the prediction quality of the CSSM dataset, we first reduce the long-term bias and then compare it with the adequate Climate Forecast System Reanalysis (CFSR) dataset. Bearing in mind that varying degrees

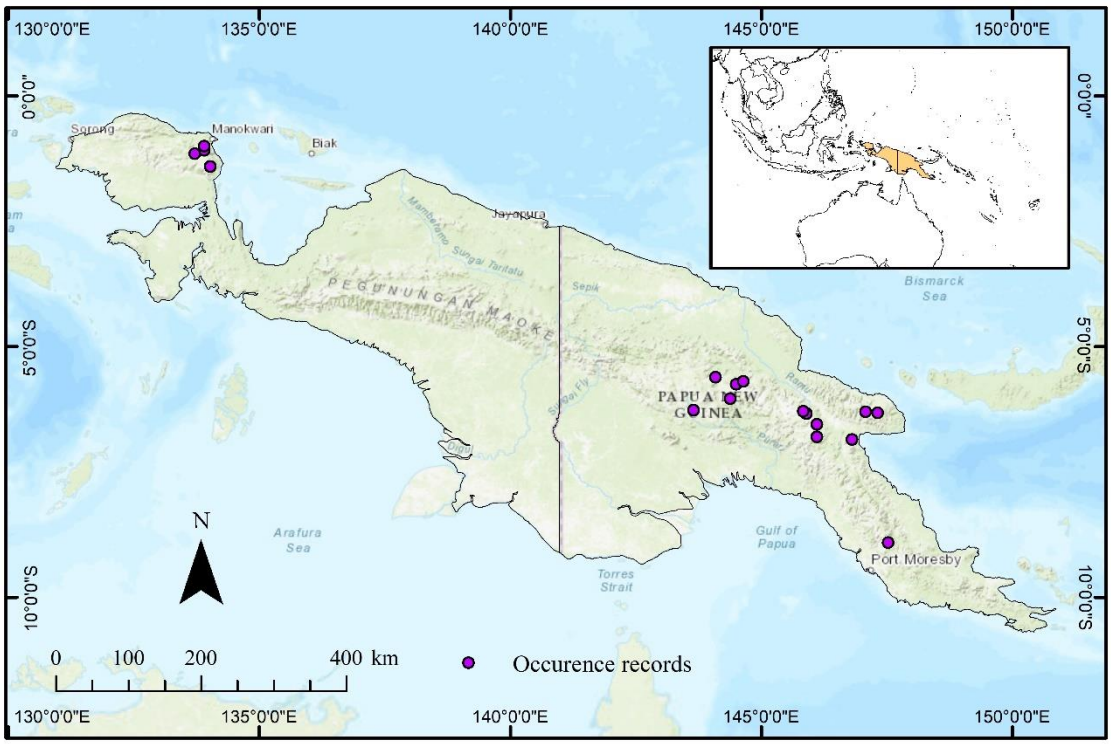

Figure 1. Study area

of bias can be found throughout the atmosphere at the study location for each of these variables, both spatially and temporally. This is due to the CCSM grid being too coarse, which produced significant biases for surface variables such as temperature, relative humidity, geopotential height, wind, and meridionality, especially in complex orographic conditions. We found consistency between CCSM and CFSR mixing ratio climatologies, particularly over complex terrain across the study area. Although it did not directly correct the mixing ratio data, the temperature and relative humidity corrections and subsequent mixing ratio calculations produce a climatology consistent with CFSR. This research calculates future climate predictions through representative concentration pathway (RCP) scenarios. The model provides four scenarios by dividing the radiation dose based on greenhouse gas concentrations: RCP2.6 (implies temperature increase on the planet to 0.9ºC on an average); RCP4.5 (increase to 1.9ºC); RCP6.0 (increase to 2.4ºC); RCP8.5 (increase to 4.1ºC). This model was chosen considering the resulting statistical similarity of the current climate compared to previous climate models (Lee et al., 2014; Ruosteenoja et al., 2016). We selected historical periods according to the latest recommendations of the World Meteorological Organization (WMO, 2017). Applying timeline scales in the past, we modeled for the 2050s and 2070s in each scenario and compared them with the present time model.

This research uses ArcGIS 10.4.1 for layer work and estimated potential reach using the SDM package in R (RStudio Team, 2020), identifying the most influential variables in each scenario. Several R packages were employed in bioclimatic modeling. Package “dismo” is used to load climate variables, while “mapview” is used to see the point of occurrences. Package “usdm” to test collinearity among the climatic variables by providing functions “vifstep” and “vifcor”. We use the Variance Inflation Factor (VIF) to overcome the collinearity problem between predictor variables. Therefore, we did not include highly correlated variables to obtain an accurate model (Aldiansyah and Wahid, 2023; Aldiansyah and Wahid, 2024). A total of 19 bioclimatic variables were selected using VIF values. VIF reflects how much the standard error increases due to the multicollinearity of the variables included in the model. The correlation threshold was set at 0.7 (Table 1). Library “sdm” is used to run the algorithm of species distribution models. This package combines different parallel implementations of niche ecology and machine learning models on a single platform and uses an object-oriented, reproducible, and extensible approach in R (Naimi and Araújo, 2016). To predict

species probabilities, the "sdmData" package was used to generate 200 pseudo-absence records which were used against 19 presence-only records to calibrate the model. The algorithm is run using bootstrap with two replications and applied to all scenarios. We used the Learning Vector Quantization (LVQ) algorithm to determine the most important factors from each selected predictor variable. LVQ is a supervised classifier that was introduced by Kohonen (1995). LVQ has been used in various studies for environmental sciences (Pourghasemi and Kerle, 2016), flood susceptibility mapping (Termeh et al., 2018; Aldiansyah and Wardani, 2023), landslide susceptibility mapping (Rahmati et al., 2016; Aldiansyah and Wardani, 2024), wildfire mapping (Aldiansyah and Madani, 2024) species distribution mapping (Aldiansyah and Risna, 2023; Aldiansyah et al., 2024). The LVQ was worked by searching for the shortest distance to the value and eliminating the noise, which could potentially interfere with the process of convergence in the forecasting system in large data (Kohonen, 1995).

Table 1. Bioclimatic variables and their computed variance inflation factor (VIF) obtained from the Worldclim database for modeling the bioclimatic range of *Musa ingens*

Bioclimatic variable	Variable description	Unit	VIF
Bio1	Annual mean temperature	ºC	304.41
Bio2	**Mean diurnal range [mean of monthly (maximum temp.-minimum temp.)]**	**ºC**	**1.82**
Bio3	Isothermality (Bio2/Bio7) (× 100)	ºC	17.33
Bio4	Temperature seasonality (standard deviation × 100)	ºC	51.69
Bio5	Maximum temperature of the warmest month	ºC	11.12
Bio6	Minimum temperature of the coldest month	ºC	28.13
Bio7	Temperature annual range (Bio5-Bio6)	ºC	66.07
Bio8	**Mean temperature of wettest quarter**	**ºC**	**1.45**
Bio9	**Mean temperature of driest quarter**	**ºC**	**2.43**
Bio10	Mean temperature of warmest quarter	ºC	521.09
Bio11	Mean temperature of coldest quarter	ºC	80.91
Bio12	Annual precipitation	mm	19.32
Bio13	**Precipitation of wettest month**	**mm**	**2.78**
Bio14	**Precipitation of driest month**	**mm**	**2.08**
Bio15	**Precipitation seasonality (coefficient of variation)**	**mm**	**1.94**
Bio16	Precipitation of wettest quarter	mm	117.25
Bio17	Precipitation of driest quarter	mm	242.24
Bio18	**Precipitation of warmest quarter**	**mm**	**1.84**
Bio19	**Precipitation of coldest quarter**	**mm**	**2.13**

Note: The variables in bold text are those that were selected based on VIF for predicting the bioclimatic range of *Musa ingens*.

Model verification in this study employs several metrics includin Receiver Operating Characteristics-Area Under Curve (ROC-AUC) (Shabani et al., 2016), Correlation (COR), True Skill Statistics (TSS) (Fourcade et al., 2018) Deviance (Agresti, 2018), Prevalence (Allouche et al., 2006), and Calibration (Fieberg et al., 2018). The ROC-AUC evaluates the model's ability to distinguish between presence and absence data, with values ranging from 0 to 1; an AUC>0.7 indicates good model performance. COR assesses the strength of the relationship between climate variables and species presence. TSS measures relationship between observations and predictions, with values ranging from-1 to +1; a TSS closer to +1 indicates stronger the relationship between the two variables. Deviance represents model error, with values closer to 0 indicating lower error rates. Prevalence measures the proportion of sites where the species is present. Calibration tests the accuracy of model estimates, with values closer to 1 indicating better model calibration. Model accuracy was verified using a random split of presence data: 70% for model training and 30% for testing. A binarization prediction threshold was set based on model performance, considering predictions above the 10^{th} percentile threshold as potential distribution for species. This approach identifies 90% of analyzed presence point within the "potential" range, while disregarding 10% classified as unpotential for climate niche modeling.

3. RESULTS AND DISCUSSION

AUC is used to estimate the model's performance in recognizing the presence or absence of a species in a location. The obtained maps reliably characterize the peculiarities of the distribution of the studied species. In this research model, the average AUC obtained was 0.96, indicating a high model significance with a 97% probability of correctly predicting the presence of the studied species at the recorded points (Table 2). Meanwhile, the average values of COR, TSS, Deviance, Prevalence, and Calibration are 0.91, 0.93, 0.13, 0.14, and 0.80 respectively.

Table 2. Evaluation model of *Musa ingens* according to each scenario

Scenario	AUC	COR	TSS	Deviance	Prevalence	Calibration
Present time	0.98	0.95	0.92	0.09	0.16	0.79
RCP2.6 2050	0.97	0.96	0.93	0.21	0.10	0.89
RCP2.6 2070	0.94	0.93	0.92	0.11	0.10	0.80
RCP4.5 2050	0.97	0.93	0.93	0.10	0.19	0.81
RCP4.5 2070	0.96	0.81	0.96	0.17	0.05	0.74
RCP6.0 2050	0.97	0.79	0.97	0.13	0.21	0.77
RCP6.0 2070	0.93	0.92	0.92	0.09	0.02	0.91
RCP8.5 2050	0.97	0.95	0.91	0.08	0.17	0.81
RCP8.5 2070	0.96	0.93	0.95	0.15	0.27	0.66

Modeling problems generally suggest supplementing the constructed model with points of absence. In this study, the number of absence points was randomly selected as 200 points. According to Phillips et al. (2017), model adequacy will be determined by the choice of traits. This method used all bioclimatic parameters from the WorldClim dataset for this purpose. In case of limited species presence, resampling techniques are generally applied to duplicate the presence data, for example, N=100. However, this is greatly influenced by regional coverage in different cases. Thus, there is considerable variation depending on the type of modeling approach, species, and regional coverage. Modelers therefore need to be aware that the results obtained will include some degree of uncertainty, particularly due to climate (Thuiller et al., 2004; Araújo et al., 2005; IPCC, 2013; Casajus et al., 2016; Quillfeldt et al., 2017). Casajus et al. (2016) proposed an objective approach to selecting climate scenarios for a species. However, there are no definite guidelines for choosing the best type of setting or climate variable, which also depends on the specific periods to be considered and the magnitude of environmental changes (Araújo et al., 2004). This implies that when climate change occurs, the dynamics of the home range can be influenced by intrinsic population dynamics (Lawton, 1993). However, if strong environmental changes occur, species distribution dynamics will be strongly influenced by these changes (Araújo et al., 2004). Many invasive plant species have characteristics that can increase their dominance in transitional climate scenarios (Dukes and Mooney, 1999), as seen in several relatives of the *Musa* species. Additionally, potential new areas may emerge in previously unsuitable or marginal areas, while previously suitable areas may become unsuitable or marginal habitats (Araújo et al., 2004; Hirzel et al., 2002; Hirzel et al., 2006).

This research found that only in the RCP6.0 2070s scenario was the bio13 variable used along with other variables. Meanwhile, other present-time and future scenarios ignore Bio13 variables. The contributing variables in the present time variables are precipitation of warmest quarter, precipitation of driest month, and precipitation of coldest quarter. This contribution analysis remains the same in RCP2.6 and RCP8.5 in 2070, and RCP6.0 in 2070.

Analysis of variables contributions to the 2050 projections across all scenarios highlights the highest significance of precipitation in the warmest quarter, particularly under RCP6.0. Precipitation in the driest month also show significant influence across all scenarios for 2050, whereas in RCP4.5, precipitation of coldest quarter becomes more significant compared to other scenarios. Moving to 2070, precipitation of warmest quarter emerges as most significant under RCP2.6, RCP6.0, and RCP8.5, alongside continued significant of precipitation in the driest month. Notably, precipitation in the driest month takes precendence in importance under RCP4.5. Overall, the

contribution of bioclimatic variables is likely to vary in shaping the future spatial distribution of *M. ingens*. Nonetheless, across all models, precipitation of warmest quarter and driest month consistently emerge as crucial variables, except in RCP4.5 where the driest month takes precedence (Figure 2).

This research models nine bioclimatic regions, including projection for 2050 and 2070 under four climate scenarios. Each model identifies four regions with varying probabilities of species presence: 0.8-1.0 -the most probable presence likelihood; 0.6-0.8 -high presence likelihood; 0.5-0.6 -moderate presence likelihood; 0.3-0.5 -low presence likelihood; and value below 0.3 -indicatingno presence likelihood. The threshold value 0.3 corresponds of the 10 percentiles.

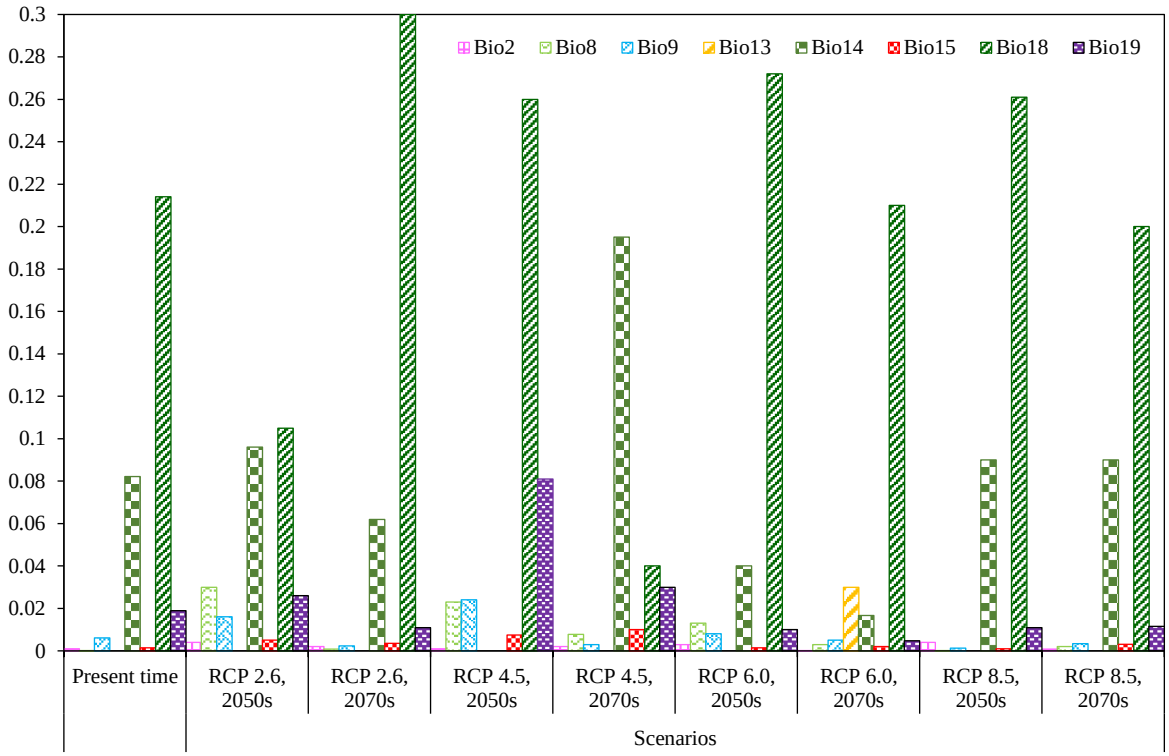

Figure 2. Variable importance

The current bioclimatic model of *M. ingens* identifies several key areas with high likelihood of species presence, including the Arfak mountains (2,955 m.a.s.l.), the Weyland mountains (3,891 m.a.s.l.), from Angemuk Peak (3,949 m.a.s.l.) to Osua Trikora Peak (4,750 m.a.s.l.) in Indonesia, as well as Mount Kabangama (4,104 m.a.s.l.), Mount Wilhelm (4,509 m.a.s.l.), Mount Michael (3,647 m.a.s.l.), Mount Piora (1,722 m.a.s.l.), Mount Victoria (4,038 m.a.s.l.), Mount Sibium (2,295 m.a.s.l.), Mount Suckling (3,676 m.a.s.l.), Mount Simpson (2,883 m.a.s.l.), including McAdam National Park (1.18 km^2) in Papua New Guinea. This area zones with a high probability of species presence (Figure 3). The Gauttier Mountains (2,230 m.a.s.l.), Cyclops Mountains (2,160 m.a.s.l.), and Wondiwoi Mountains (2,251 m.a.s.l.) are area with a moderate probability of species presence. The bioclimatic area with the highest probability of species presence covers 233,628 km^2, with moderate presence covering 97,653 km^2, and with low presence covering 447,407 km^2.

In the context of the RCP 2.6 scenario, there is a notable shift in the zone of high probability of species presence towards the western part of the region, centered around Weyland and Undundi-Wandandi (3,640 m.a.s.l.) (Figure 4). While the area with a very high probability remains with in the contemporary model, there is regional expansion into the high probability zone, notably across the temperate zone. Changes from McAdam National Park to the Simpson Mountains are expected to reduce the bioclimatic range of the region. Areas classified as high and medium probability of species presence have expanded to 341,840 km^2 and 107,874 km^2 respectively, while those with a low probability have decreased to 328,975 km^2.

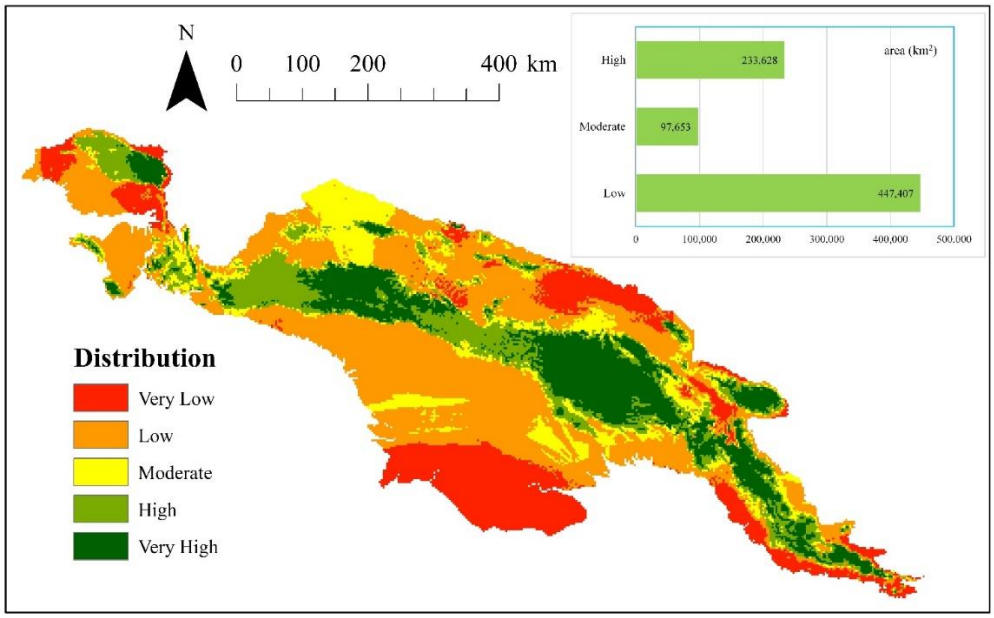

Figure 3. Present bioclimatic area in *Musa ingens*

According to the RCP 2.6 model scenario in 2070, the total area of the bioclimatic area significant changes, resulting in a notable shift in the ratio of area to potential distribution (Figure 4). Areas with high probability decreased by half to 161,091 km^2, while areas with low probability increased nearly double to 594,596 km^2 (Table 3). This change is driven by the RCP 2.6 climate scenario, which predicts rising temperatures due to increased greenhouse gas emissions until 2070. The bioclimatic conditions in 2070 are anticipated to differ significantly from current conditions, with a marked decline in potential area. This decrease is influenced by varying emissions scenarios, predicting a reduction in CO_2 levels from 380 to 100 ppm (IPCC, 2013). This reduction is associated with temperature increases ranging from 0.3ºC to 2.6ºC and 0.9ºC to 6.8ºC by 2100. Extreme low CO_2 levels (<100 ppm) can threaten plant growth, leading to slow growth and increased drought susceptibility even under optimal conditions near the equator. Consequently, only a few plant species may thrive even in the best conditions.

According to the scenario 4.5 projections for 2050, adecline in areas of moderate potential probability is observed compared to the contemporary model. This indicates changes in bioclimatic parameters and deteriorating environmental conditions in most areas, except around Puncak Jaya (4,884 m.a.s.l.). These changes may result from increased seasonal temperature contrasts. The most potential area for the studied species have decrease significantly compared to the current distribution, now covering only 55,482 km^2, with some regions becoming unsuitable (Figure 5). High potential probability is now primarily confined to the Osua Trikora Mountains and the highlands of the Giluwe Mountains (4,367 m.a.s.l.) to Mount Victoria. This scenario represents the most severe changes, with the sharpest decline in potential area.

In the 2070 scenario 4.5, the potential area expands compared to 2050 (high: 139,169 km^2) and the current distribution area (moderate: 307,264 km^2) (Figure 5). The area with low potential decreases to 332,254 km^2, extending its probability to the eastern and southern sides of the region. The most significant changes were observed in the amplitude of the driest monthly temperatures and the average precipitation during the warmest and coldest months. Compared to the current climate, future projections (PACCSAP, 2011) suggest a warmer and wetter, with the rainfall expected to change by ±25%, temperature increase by 1.4ºC to 3.1ºC, and sea level rising by 19 cm to 85 cm. These changes imply an increase in surface temperature of 1.0ºC to 4.2ºC, contributing to a sea level rise of 1.0ºC to 3.0ºC. Additionally, sea water is predicted to become more acidic, dropping by 0.3 to 0.4 pH units due to the increasing CO_2 absortion. Many plant and animal species may struggle to adapt to the impacts of RCP 4.5 (IPCC, 2014). In this scenario, carbon levels are estimated to reach 600 ppm by 2070. Small plants are predicted to decompose and released CO_2 while larger plants may survive longer by absorbing carbon from decaying vegetation. This dynamic explains the observed improvement in this scenario.

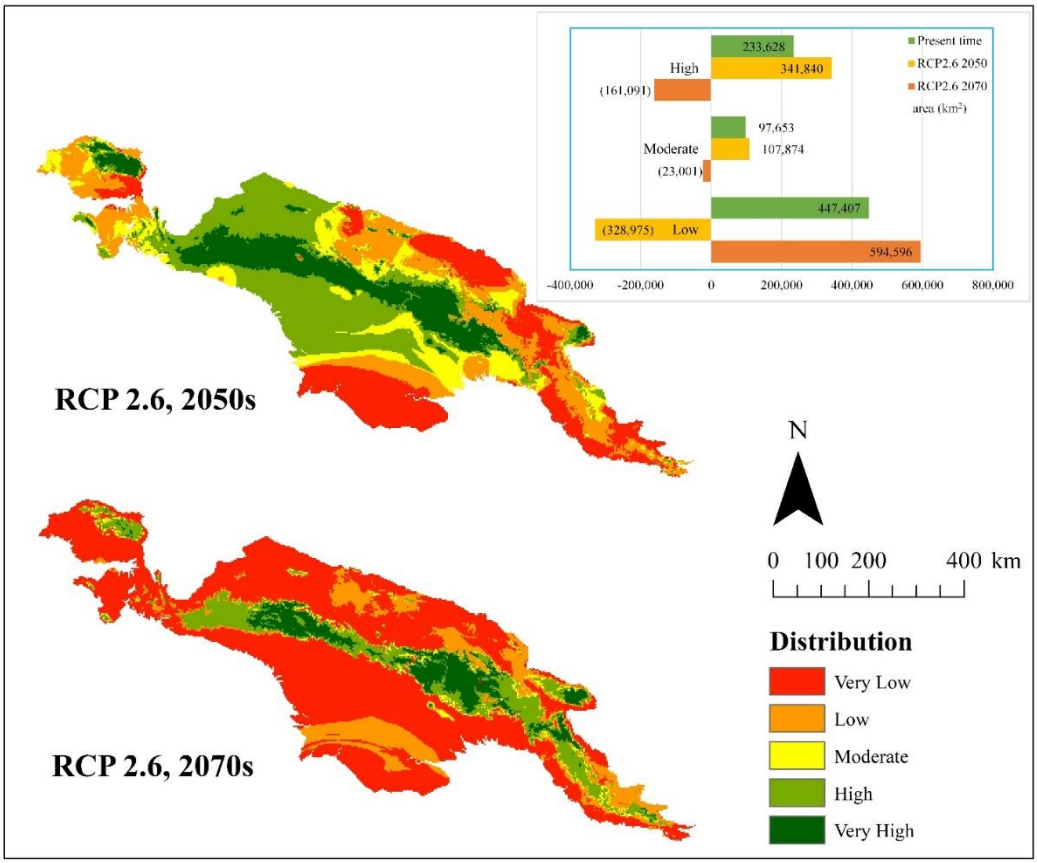

Figure 4. Bioclimatic range of *Musa ingens* to 2050 and 2070 according to RCP 2.6 scenario

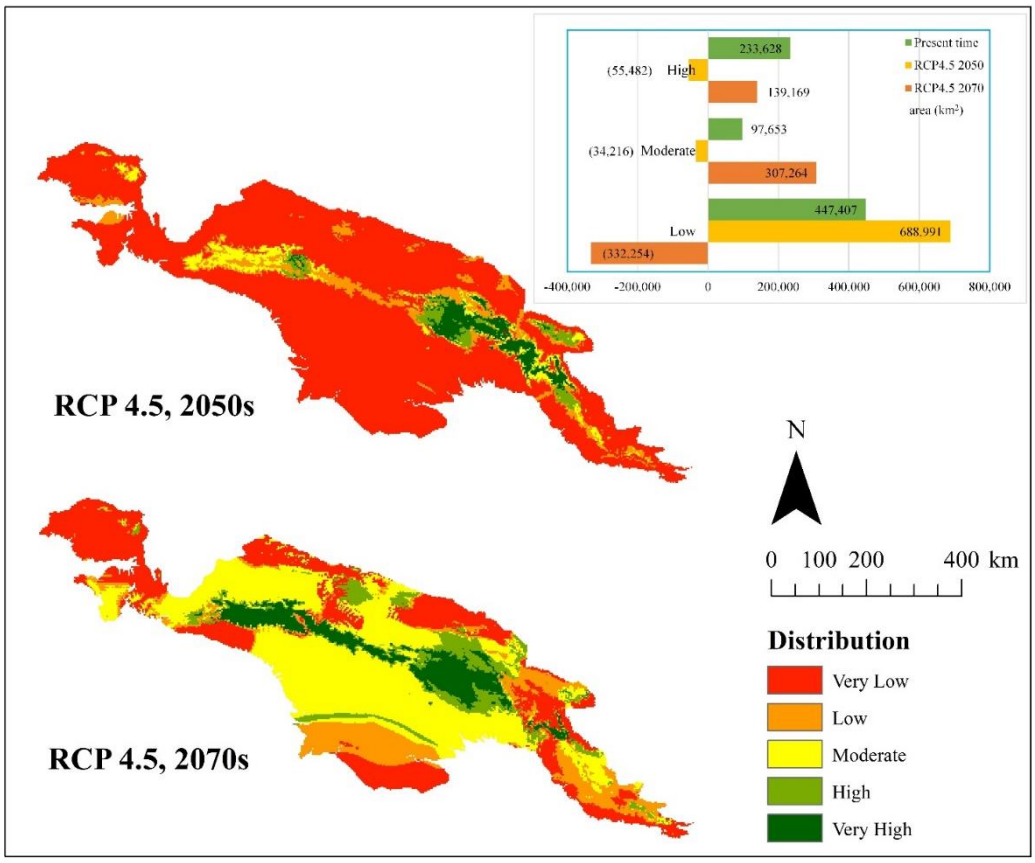

Figure 5. Bioclimatic range of *Musa ingens* to 2050 and 2070 according to RCP 4.5 scenario

According to the prognostic model of the RCP.6.0 scenario, areas with a marginal distribution index of 0.5-0.6 will decrease by 2050 (Figure 6). The area with the highest potential distribution index covers 124,294 km^2, which is 2.5 times lower than the previous model. In contrast, the area with marginal index has decreased significantly, covering only 28,312 km^2. The main contribution to this significant change is influenced by three factors, namely precipitation of warmest quarter, mean temperature of wettest quarter, and precipitation of driest month. The territorial reach is very limited, concentrated around Mount Bintang Lestari (3,745 m.a.s.l.) on the border of Indonesia and Papua New Guinea. Therefore, there is a trend similar to the RCP 4.5 scenario for 2050, where the high potential area decreases, but recovers by 2070 (Figure 6). A similar pattern is observed in areas with marginal potential; however, this is inversely proportional to the RCP 6.0 scenario for 2070, which shows a decrease in probability, covering 26,323 km^2. The difference in altitude, coupled with a gradual but significant increase in temperature from highlands to lowlands, indicates that *M. ingens* doest not grow well. This observation is supported by Argent (1976), who reported a very high intolerance to continuous temperature changes. However, with even sunlight as projected, the canopy of *M. ingens* will receive prolonged shade from largertrees in lowland areas. Unlike other banana subspecies that struggle in low light conditions (Simmonds, 1962), *M. ingens* is relatively shade tolerant.

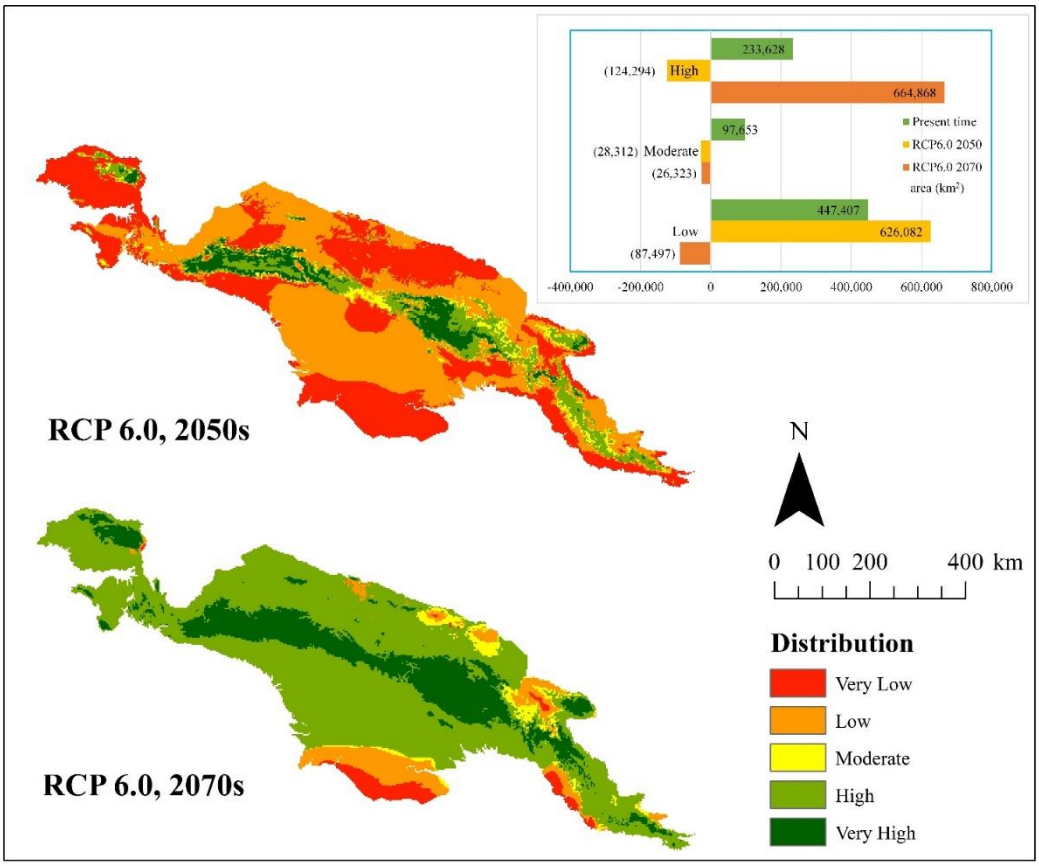

Figure 6. Bioclimatic range of *Musa ingens* to 2050 and 2070 according to RCP 6.0 scenario

The RCP 8.5 scenario shows the most favorablechanges, with minimal significant changes occurring in each region, and an expansion of the bioclimatic area. The highland areas along the island of Papua significantly influence the surrounding lower land areas (Figure 7).

The model in this study shows that the total range does not change significantly. Some factors also show a higher level of importance, and regional distribution is improving. In the “lower” scenario, the area with conditions that have the potential to worsen decrease significantly. However, this area is larger

than areas with high potential. This means that by 2070, the average annual temperature for inland, and higher mountain areas will increase by 28.10ºC to 30.20ºC, and 25.10ºC to 37.2ºC respectively. This implies that spatial and temporal variability in temperature will be small (>1.2ºC) compared to current variability, supporting an average annual temperature of around 30±2ºC throughout the region. The temperature increase is estimated at 0.32ºC by 2050 and 0.46ºC by 2070. This change is expected to continue due to increasing greenhouse gas emissions (Canadell and Raupach, 2008; Rahmstorf et al., 2007). Annual and seasonal rainfall is expected to increase consistently with the intensification of the rainy season and the convergence of inter-tropical zones. This suggests that higher areas will receive more than 280 cm of rainfall per year in the current climate, reaching 1,000 cm per year by 2070 until environmental stability is achieved. The temperature required for optimal leaf growth and development is 31.6ºC with a relatively humid climate, which can be achieved year round in tropical areas.

In this study, areas with a high level of probability indicate regions with the most potential and tend to be stable. This stability is influenced by the location's altitude above 1,000 m.a.s.l. (Argent, 1976). The large size of this species allows it to compete for sunlight from the surrounding trees. However, there are significant changes based on each scenario. Areas with moderate probability tend to be less stable, and their condition worsens when bioclimatic parameters change. This situation is exacerbated by complex topographic conditions, which result in higher hydraulic resistance (Domec et al., 2019) because water needs to be transported over long distances as the temperature increases. It is reasonable to assume that *M. ingens* is limited to the highlands because the relatively low temperatures, frequent fog, and low evaporation requirements create favorable conditions for transporting water 15 m upwards without damaging its xylem vessels. The central part of the island of Papua changed significantly, with an increase in precipitation during the warmest quarter. The continental index may rise due to climate change, and this impact seems to affect the highland areas as well. This suggests that the temperature differences in the region are very pronounced.

Changes in temperature and rainfall, relative humidity will significantly affect terrestrial biodiversity. The biodiversity we see today is the result of co-evolutionary processes and mechanisms that developed to coexist through spatial and temporal climate variability. Future tolerance to climate change will bring significant changes to many species, as it will take a long time for them to adapt. These pressures will also alter the composition of soil microbes, impacting the soil as a growth medium and affecting the soil ecosystem. This is crucial because soil microbes play an essential role in the decomposition of dead organic matter and the cycle of soil nutrients, both of which are vital for soil productivity and sustainable use.

The climate change scenario in this study illustrates that bananas require a warm subtropical climate and sufficient humidity. Adequate rainfall and soil moisture are necessary for plant growth (Pabst et al., 2016). Changes in soil moisture will reduce microbial activity, decreased leading to decomposition, and consequently, a reduction in total soil carbon (Meisner et al., 2021). According to Gunina et al. (2018), soil biota biomass is positively correlated with higher rainfall. However, the results of this research simulated a gradual increase in temperature and an indirect reduction inrainfall. This research indicates that climate changes affecting *M. ingens* plants influencethe distribution of soil nutrients fand changes in groundwater as a growing medium. This finding aligns with Becker (2017), who reported that in warm and dry climates (<1,900 m.a.s.l.), variations in total carbon and total nitrogen content in the soil are determined by climatic conditions, whereas in wet climates (>1,900 m.a.s.l.), these variations arestrongly controlled by tree biomass, which produces nutrients in the soil.

Changes in climate conditions have a significant negative impact on banana distribution. In cooler areas, banana distribution is limited, but higher temperatures caused by climate change can benefit productivity (Ramirez et al., 2011). This indicates that annual precipitation can be beneficial for plants, excessively high annual precipitation can be detrimental. High mean annual precipitation can increase the prevalence fungal diseases in bananas, reducing their ability to survive in the wild and lowering their productivity (Nyombi, 2010; Bebber, 2019). In contrast, some drier areas may experience positive effect. However, Bebber (2019) argues that temperature is a significant driving factor for this increased risk of fungal diseases. Climate change has created air temperatures more favorable for fungal spore growth.

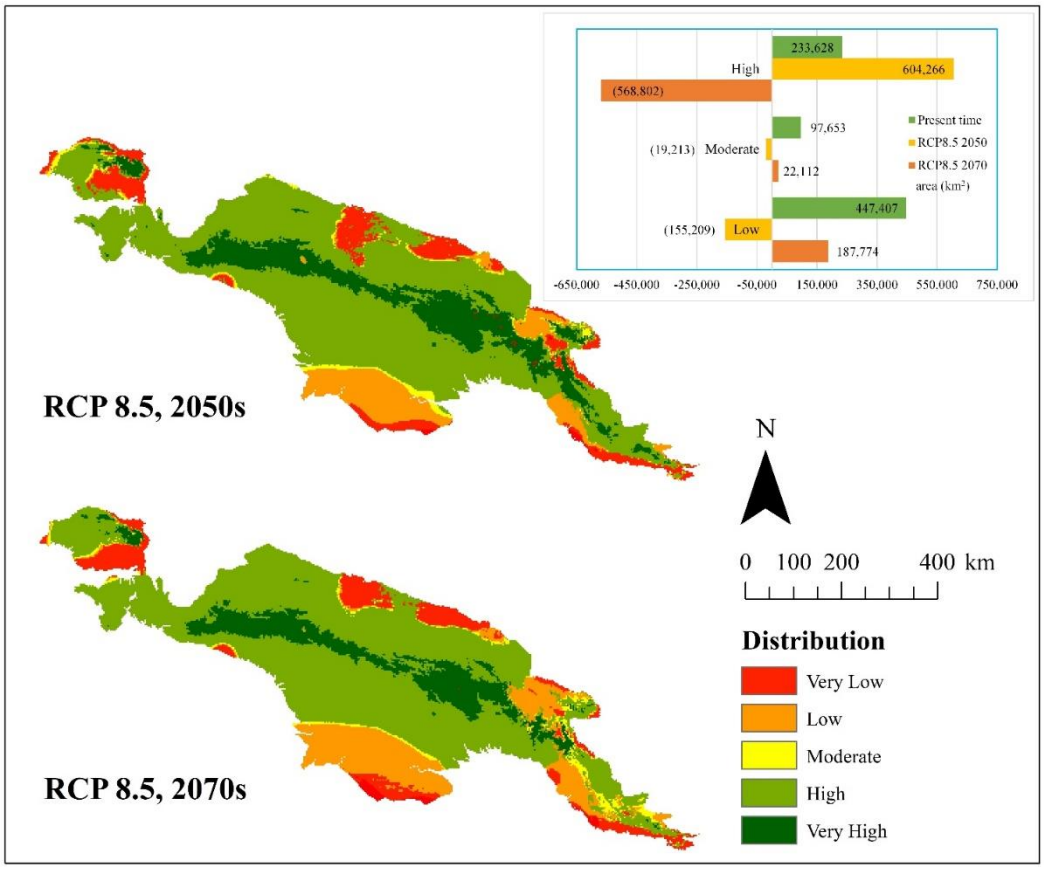

Figure 7. Bioclimatic range of *Musa ingens* to 2050 and 2070 according to RCP 8.5 scenario

Table 3. Bioclimatic area size (km^2) in *Musa ingens* according to RCP 2.6, RCP 4.5, RCP 6.0 and RCP 8.5 scenarios

Period	Bioclimatic range index				
	<0.30	0.30-0.49	0.50-0.59	0.60-0.79	0.80-1.00
Present time	134,980	312,427	97,653	109,037	124,590
RCP2.6 2050	160,626	168,349	107,874	222,497	119,342
RCP2.6 2070	473,667	120,929	23,001	98,796	62,295
RCP4.5 2050	621,765	67,225	34,216	24,609	30,872
RCP4.5 2070	219,937	112,317	307,264	71,478	67,691
RCP6.0 2050	293,193	332,889	28,312	77,340	46,954
RCP6.0 2070	25,561	61,935	26,323	508,813	156,055
RCP8.5 2050	75,732	79,477	19,213	476,925	127,341
RCP8.5 2070	77,890	109,884	22,112	472,926	95,876

Climate change is not the only factor that increases fungal infections in bananas. Diseases that reduce the fruit production tree may also be influenced by other factors. Besides fungal infections, water stress due to inadequate water intake will reduce banana yields. Under water stress, bananas close their stomata to conserve water, reducing carbon assimilation and crop yields (Turner et al., 2007). Most Banana varieties grow best with 12 hours of bright light and high humidity of 50% or higher. The ideal temperature range is around 26 to 30°C. Growth begins at 18ºC, reaches optimal growth at 27ºC, and stops completely when the temperature reaches 38ºC. This suggests that while tropical plants, including bananas, can tolerate temperatures near freezing, the cannot tolerate excessively high temperatures, which they rarely experience in the wild. Although Bananas grow best in bright sunlight, high temperatures will scorch the leaves and fruit, indirectly affecting their survival in the wild.

This research indicates that environmental parameter dynamics within the same distribution

across different years can influence the environmental suitability of *M. ingens*, although the long-term population abundance cycle remains unknown. Some scenarios suggest less concerning outcomes; areas to become drier in the future may experience reduce disease infections, but bananas need require amplewater to thrive. Therefore, addressing infection issues through drying out may necessitate effective water management for banana distribution in the future. These factors are crucial in shaping the bioclimatic range of this species. Lastly, this research can inform IUCN about the potential impact of climate change on *M. ingens* in the future. We believe this study is the first report to model the potential bioclimatic range of *M. ingens* across the mainland of Papua Island. Further research on the *Musa* species incorporating biophysical variables, distribution aspects, and habitat history could provide valuable insights for future management of this species.

4. CONCLUSION

The distribution of *M. ingens*, modeled through maximum entropy species distribution modeling, reveals that the key factors influencing its distribution including precipitation of warmest quarter, precipitation of driest month, precipitation of coldest quarter, and mean temperature of wettest quarter. Bioclimatic changes under the RCP 4.5 scenario are projected to result in a fourfold decrease in the current area of high abundance, with a shift towards isolated optimal climate areas in highlands spanning from the Osua Trikora Mountains to the Giluwe Mountains and Mount Victoria. Many areas areas became uninhabitable. Map forecasting species distributions under modeled scenarios ilustrate species-specific responses to potential climate change, indicating a significant reduction in current distribution range and a shift towards the central region, with fewer locations across the island of Papua.

ACKNOWLEDGEMENTS

Thank you to the University of Indonesia and IPB University for facilitating this research. Thanks also to Cendrawasih University for background information regarding in situ data.

REFERENCES

Abdoussalami A, Hu Z, Islam ARMT, Wu Z. Climate change and its impacts on banana production: A systematic analysis. Environment, Development and Sustainability 2023; 25(11):1-30.

Abdulai I, Vaast P, Hoffmann MP, Asare R, Jassogne L, Van Asten P, et al. Cocoa agroforestry is less resilient to sub-optimal and extreme climate than cocoa in full sun. Global Change Biology 2018;24(1):273-86.

Agresti A. An Introduction to Categorical Data Analysis. Canada: John Wiley and Sons; 2018.

Aldiansyah S, Madani I. Spatial model of wildfire susceptibility using machine learning approaches on Rawa Aopa Watumohai National Park, Indonesia. GeoScape 2024; 18(1):1-20.

Aldiansyah S, Risna R. Assessing potential habitat suitability of vulnerable endemic species: A case study of *Diospyros celebica* Bakh and *Rhyticeros cassidix*. Forum Geografic 2023;22(2):159-69.

Aldiansyah S, Risna, Saputra RA. Assessing potential distributions of bird endemic species: Case studies of *Macrocephalon maleo* and *Rhyticeros cassidix* and their threats. Geomatics and Environmental Engineering 2024; 18(3):45-61.

Aldiansyah S, Wahid KA. Species distribution modelling using bioclimatic variables on endangered endemic species (*Bubalus depressicornis* and *Bubalus quarlesi*). Geosfera Indonesia 2023;8(1):1-18.

Aldiansyah S, Wahid KA. Species distribution modelling using bioclimatic variables on critically endangered endemic species (*Macrocephalon maleo*) in Sulawesi. ASEAN Journal on Science and Technology for Development 2024;41(3):240-53.

Aldiansyah S, Wardani F. Assessment of resampling methods on performance of landslide susceptibility predictions using machine learning in Kendari City, Indonesia. Water Practice and Technology 2024;19(1):52-81.

Aldiansyah S, Wardani F. Evaluation of flood susceptibility prediction based on a resampling method using machine learning. Journal of Water and Climate Change 2023; 14(3):937-61.

Allouche O, Tsoar A, Kadmon R. Assessing the accuracy of species distribution models: Prevalence, kappa and the true skill statistic (TSS). Journal of Applied Ecology 2006; 3(6):1223-32.

Araújo MB, Cabeza M, Thuiller W, Hannah L, Williams PH. Would climate change drive species out of reserves? An assessment of existing reserve-selection methods. Global Change Biology 2004;10(9):1618-26.

Araújo MB, Whittaker RJ, Ladle RJ, Erhard M. Reducing uncertainty in projections of extinction risk from climate change. Global Ecology and Biogeography 2005;14(6):529-38.

Argent GCG. The wild bananas of Papua New Guinea. Notes from the Royal Botanic Garden Edinburgh 1976;35(1):77-114.

Bebber DP. Climate change effects on Black Sigatoka disease of banana. Philosophical Transactions of the Royal Society B 2019;374(1775):Article No. 20180269.

Becker JN. Carbon and Nutrient Cycles Depending on Climate and Land Use along the Elevation Gradient of Mount Kilimanjaro. German: Gorg-August University School of Science; 2017.

Blaser WJ, Oppong J, Hart SP, Landolt J, Yeboah E, Six J. Climate-smart sustainable agriculture in low-to-intermediate shade agroforests. Nature Sustainability 2018;1(5):234-9.

Butler RA. Papua New Guinea [Internet]. 2006 [cited 2023 Jun 3]. Available from: https://rainforests.mongabay.com/20png.html.

Canadell JG, Raupach MR. Managing forests for climate change mitigation. Science 2008;320(5882):1456-7.

Casajus N, Périé C, Logan T, Lambert MC, de Blois S, Berteaux D. An objective approach to select climate scenarios when

projecting species distribution under climate change. PLoS ONE 2016;11(3):e0152495.

Domec JC, Berghoff H, Way DA, Moshelion M, Palmroth S, Kets K, et al. Mechanisms for minimizing height-related stomatal conductance declines in tall vines. Plant, Cell and Environment 2019;42(11):3121-39.

Dukes JS, Mooney HA. Does global change increase the success of biological invaders? Trends in Ecology and Evolution 1999;14(4):135-9.

Feng H, Zhang M. Global land moisture trends: Drier in dry and wetter in wet over land. Scientific Reports 2015;5(1):Article No. 18018.

Fieberg JR, Forester JD, Street GM, Johnson DH, ArchMiller AA, Matthiopoulos J. Used-habitat calibration plots: A new procedure for validating species distribution, resource selection, and step-selection models. Ecography 2018; 41(5):737-52.

Food and Agriculture Organization (FAO). FAOSTAT. Food and Agriculture Organization of the United Nations [Internet]. 2018 [cited 2023 Apr 21]. Available from: https://www.fao.org/home/en.

Fourcade Y, Besnard AG, Secondi J. Paintings predict the distribution of species, or the challenge of selecting environmental predictors and evaluation statistics. Global Ecology and Biogeography 2018;27(2):245-56.

Gasparrini A, Guo Y, Sera F, Vicedo-Cabrera AM, Huber V, Tong S, et al. Projections of temperature-related excess mortality under climate change scenarios. Lancet Planet Health 2017;1(9):e360-7.

Gent PR, Danabasoglu G, Donner LJ, Holland MM, Hunke EC, Jayne SR, et al. The community climate system model version 4. Journal of Climate 2011;24(19):4973-91.

Global Biodiversity Information Facility (GBIF). GBIF Occurrence Download [Internet]. 2023 [cited 2023 Apr 9]. Available from: https://doi.org/10.15468/dl.rcqwuv.

Greve P, Seneviratne SI. Assessment of future changes in water availability and aridity. Geophysical Research Letters 2015; 42(13):5493-9.

Gunina A, Nico Becker J, Hemp A, Yu L, Jones DL, Kuzyakov Y. Determining the optimal temperature and precipitation for microbial community development in montane forest ecosystems: PLFA analysis along a 3,500 m altitudinal gradient on Mt Kilimanjaro. Proceedings of the EGU General Assembly Conference Abstracts; 2018 April 8-13; Vienna: Austria; 2018.

Hirzel AH, Hausser J, Chessel D, Perrin N. Ecological-niche factor analysis: How to compute habitat-suitability maps without absence data? Ecology 2002;83(7):2027-36.

Hirzel AH, Le Lay G, Helfer V, Randin C, Guisan A. Evaluating the ability of habitat suitability models to predict species presences. Ecological Modelling 2006;199(2):142-52.

Intergovernmental Panel on Climate Change (IPCC). Climate Change 2013: The Physical Science Basis. Contribution of Working Group I to the Fifth Assessment Report of the Intergovernmental Panel on Climate Change. Cambridge, UK and New York, USA: Cambridge University Press; 2013. p. 1217.

Intergovernmental Panel on Climate Change (IPCC). Climate Change 2014 Synthesis Report Fifth Assessment Report [Internet]. 2014 [cited 2024 Jun 1]. Available from: https://ar5-syr.ipcc.ch/topic_futurechanges.php.

Joshi RU, Singh AK, Singh VP, Rai R, Joshi P. A review on adaptation of banana (*Musa* spp.) to cold in subtropics. Plant Breeding 2023;142(3):269-83.

Kallow S, Longin K, Sleziak NF, Janssens SB, Vandelook F, Dickie J, et al. Challenges for ex situ conservation of wild bananas: Seeds collected in Papua New Guinea have variable levels of desiccation tolerance. Plants 2020;9(9):Article No. 1243.

Kennedy J. Bananas and people in the homeland of genus *Musa*: not just pretty fruit. Ethonobotany Research and Applications 2009;7:179-98.

Knutti R, Sedláček J. Robustness and uncertainties in the new CMIP5 climate model projections. Nature Climate Change 2013;3(4):369-73.

Kohonen T. Learning Vector Quantization: Self-Organizing Maps. Berlin: Springer; 1995.

Lawton JH. Range, population abundance and conservation. Trends in Ecology and Evolution 1993;8(11):409-13.

Lee JW, Hong SY, Chang EC, Suh MS, Kang HS. Assessment of future climate change over East Asia due to the RCP scenarios downscaled by GRIMs-RMP. Climate Dynamics 2014; 42:733-47.

Lee JY, Marotzke J, Bala G, Cao L, Corti S, Dunne JP, et al. Future Global Climate: Scenario-based Projections and Near-term Information. Climate Change 2021: The Physical Science Basis. Contribution of Working Group I to the Sixth Assessment Report of the Intergovernmental Panel on Climate Change. Cambridge and New York: Cambridge University Press; 2021. p. 553-672.

Lentfer C. Tracing domestication and cultivation of bananas from phytoliths: An update from Papua New Guinea. Ethnobotany Research and Applications 2009;7:247-70.

Lott JE, Ong CK, Black CR. Understorey microclimate and crop performance in a *Grevillea robusta*-based agroforestry system in semi-arid Kenya. Agricultural and Forest Meteorology 2009;149(6-7):1140-51.

McSweeney CF, Jones RG. No consensus on consensus: The challenge of finding a universal approach to measuring and mapping ensemble consistency in GCM projections. Climatic Change 2013;119:617-29.

Meisner A, Snoek BL, Nesme J, Dent E, Jacquiod S, Classen AT, et al. Soil microbial legacies differ following drying-rewetting and freezing-thawing cycles. The ISME Journal 2021; 15(4):1207-21.

Mongabay. Deforestation statistics for Papua New Guinea [Internet]. 2019 [cited 14 Jul 2023]. Available from: https://rainforests.mongabay.com/deforestation/archive/Papua_New_Guinea.htm.

Naimi B, Araújo MB. sdm: a reproducible and extensible R platform for species distribution modelling. Ecography 2016;39(4):368-75.

Nyombi K. Understanding Growth of East Africa Highland Banana: Experiments and Simulation [dissertation]. Wageningen University, Wageningen; 2010.

Olson DM, Dinerstein E, Wikramanayake ED, Burgess ND, Powell GVN, Underwood EC, et al. Terrestrial ecoregions of the world: A new map of life on earth. Bioscience 2001; 51:933-8.

Pabst H, Gerschlauer F, Kiese R, Kuzyakov Y. Land use and precipitation affect organic and microbial carbon stocks and the specific metabolic quotient in soils of eleven ecosystems

of Mt. Kilimanjaro, Tanzania. Land Degradation and Development 2016;27(3):592-602.

Pacific-Australia Climate Change Science Adaptation Planning (PACCSAP). Pacific-Australia Climate Change Science and Adaptation Planning Program: Current and future climate of Papua New Guinea. Papua New Guinea [Internet]. 2011 [cited 2024 Jun 2]. Available from: https://www.pacificclimatechangescience.org/wpcontent/uploads/2013/06/14_PACCSAPPNG-11pp_WEB.pdf.

Phillips ND, Reid N, Thys T, Harrod C, Payne NL, Morgan CA, et al. Applying species distribution modelling to a data poor, pelagic fish complex: The ocean sunfishes. Journal of Biogeography 2017;44(10):2176-87.

Platts PJ, Omeny P, Marchant R. AFRICLIM: High-resolution climate projections for ecological applications in Africa. African Journal of Ecology 2015;53(1):103-8.

Plummer J, Kallow S, Janssens S. The IUCN Red List of Threatened Species, *Musa ingens*, Giant Highland Banana [Internet]. 2020 [cited 2023 Dec 26]. Available from: https://dx.doi.org/10.2305/IUCN.UK.2020-3.RLTS. T158541237A201905546.en.

Pourghasemi HR, Kerle N. Random forests and evidential belief function-based landslide susceptibility assessment in Western Mazandaran Province, Iran. Environmental Earth Sciences 2016;75(185):1-17.

Quillfeldt P, Engler JO, Silk JR, Phillips RA. Influence of device accuracy and choice of algorithm for species distribution modelling of seabirds: A case study using black-browed albatrosses. Journal of Avian Biology 2017;48(12):1549-55.

Rahmstorf S, Cazenave A, Church JA, Hansen JE, Keeling RF, Parker DE, et al. Recent climate observations compared to projections. Science 2007;316(5825):Article No. 709.

Rahmati O, Haghizadeh A, Pourghasemi HR, Noormohamadi F. Gully erosion susceptibility mapping: The role of GIS-based bivariate statistical models and their comparison. Natural Hazards 2016;82:1231-58.

Rahn E, Vaast P, Läderach P, Van Asten P, Jassogne L, Ghazoul J. Exploring adaptation strategies of coffee production to climate change using a process-based model. Ecological Modelling 2018;371:76-89.

Ramirez J, Jarvis A, Van den Bergh I, Staver C, Turner D. Changing climates: Effects on growing conditions for banana and plantain (*Musa* spp.) and possible responses. In: Yadav SS, Redden RJ, Hatfield JL, Lotze-Campen H, Hall AE, editors. Crop Adaptation to Climate Change. John Wiley and Sons, Ltd.; 2011. p. 426-38.

Ravi I, Vaganan MM. Abiotic stress tolerance in banana. In: Abiotic Stress Physiology of Horticultural Crops. New Delhi: Springer India; 2016.

RStudio Team. RStudio: Integrated Development for R [Internet]. 2020 [cited 2023 Jun 9]. Available from: http://www.rstudio.com/.

Ruosteenoja K, Jylhä K, Kämäräinen M. Climate projections for Finland under the RCP forcing scenarios. Geophysica 2016;51(1):17-50.

Sadsoeitoeboen M, Sianipar FR, Lefaan PT, Kilmaskossu JP, Loupatty JI, Dimara KA, et al. Variation and distribution of bananas in the Arfak Mountains. Jurnal Natural 2021;17(2):175-83 (in Bahasa).

Serdeczny O, Adams S, Baarsch F, Coumou D, Robinson A, Hare W, et al. Climate change impacts in Sub-Saharan Africa: From physical changes to their social repercussions. Regional Environmental Change 2017;17:1585-600.

Shabani F, Kumar L, Ahmadi M. A comparison of absolute performance of different correlative and mechanistic species distribution models in an independent area. Ecology and Evolution 2016;6(16):5973-86.

Simmonds NW. Notes on banana taxonomy. Kew Bulletin 1960;14(2):198-212.

Simmonds NW. Where our bananas come from. New Scientist 1962;16(307):36-9.

Siyum ZG. Tropical dry forest dynamics in the context of climate change: Syntheses of drivers, gaps, and management perspectives. Ecological Processes 2020;9(1):Article No. 25.

Sterly J. Simbu Plant Lore: Plants used by the people in the central highlands of New Guinea. Berlin: Dietrich Reimer Verlag; 1997.

Termeh SVR, Kornejady A, Pourghasemi HR, Keesstra S. Flood susceptibility mapping using novel ensembles of adaptive neuro fuzzy inference system and metaheuristic algorithms. Science of the Total Environment 2018;615:438-51.

Thiele HU. Carabid Beetles in Their Environments. Berlin: Springer-Verlag; 1977.

Thuiller W, Brotons L, Araújo MB, Lavorel S. Effects of restricting environmental range of data to project current and future species distributions. Ecography 2004;27(2):165-72.

Turner DW, Fortescue JA, Thomas DS. Environmental physiology of the bananas (*Musa* spp.). Brazilian Journal of Plant Physiology 2007;19(4):463-84.

Watts M, Mpanda M, Hemp A, Peh KSH. The potential impact of future climate change on the production of a major food and cash crop in tropical (sub) montane homegardens. Science of the Total Environment 2023;865:Article No. 161263.

World Checklist of Selected Plant Families (WCSP). World Checklist of Selected Plant Families. Facilitated by the Royal Botanic Gardens [Internet]. 2018 [cited 2024 Jun 1]. Available from: http://wcsp.science.kew.org.

World Meteorological Organization (WMO). Guidelines on the Calculation of Climate Normals [Internet]. 2017 [cited 2024 Jun 1]. Available from: https://library.wmo.int/records/item/55797-wmo-guidelines-on-the-calculation-of-climate-.

World Wide Fund for Nature (WWF). Southeastern Asia: Extends across central New Guinea [Internet]. 2019 [cited 2023 Jun 22]. Available from: https://www.worldwildlife.org/ecoregions/aa0105.

Environment and Natural Resources Journal

Volume 22
Issue 5
2024

Remote Sensing Analysis of Smog-Inducing Aerosol Optical Depth: An Integrated Approach for Air Pollution Mitigation

Shazia Pervaiz[1,*], Kanwal Javid[2], Filza Zafar Khan[3], and Sikandar Hayat[4]

[1]*Environmental Protection Agency, Punjab, Lahore, Pakistan*
[2]*Department of Geography, Government College University, Lahore, Pakistan*
[3]*Pakistan Council of Scientific and Industrial Research, Lahore, Pakistan*
[4]*Institute of Molecular Biology and Biotechnology, the University of Lahore, Pakistan*

ARTICLE INFO

Received: 31 Jan 2024
Received in revised: 26 Jul 2024
Accepted: 31 Jul 2024
Published online: 26 Aug 2024
DOI: 10.32526/ennrj/22/20240025

Keywords:
AOD/ Lahore Division/ Clean Air Policy/ Smog Rules/ Vehicular Pollution

*** Corresponding author:**
E-mail:
shaziapervaiz@gmail.com

ABSTRACT

Aerosol aggravation poses a significant challenge in the administrative Lahore Division of Punjab, Pakistan and contributes greatly to the persistent issue of smog. Since 2017, the division has experienced recurrent episodes of smog pollution, most notably in the months of October and November. In the present study, aerosol optical depth (AOD) has been analyzed alongside three metrological parameters: temperature, humidity and rainfall. These were tracked in October and November of 2018, 2020, and 2022 using remote sensing data and satellite imaging. Additionally, anthropogenic emissions data from automobile exhaust, industries and stubble burning were derived from secondary sources. Ultimately, the study helped piece together the complex environmental picture in Lahore Division in October and November. The results showed that AOD levels not only increased during this time, they were significantly influenced by a full range of metrological variables such as low temperature, high relative humidity, lack of rainfall and emissions from a variety of human activities. It was found that trucks, tractors and buses were among the worst contributors, alongside industry and stubble burning. Therefore, the present study suggests multi sectoral plans to mitigate aerosol levels and combat the smog menace, promoting environmental sustainability in the Lahore Division. A full set of recommendation is included, divided into three categories: industry, transport and agriculture. These are focused on technology, control systems, disposal, incentives, green solutions and more. At all levels, commitment, collaboration, and coordination are absolutely vital.

1. INTRODUCTION

Atmospheric aerosols (Sun et al., 2022; Pervaiz and Shirazi, 2023) are dynamic mixtures of solid and liquid particles (Wang et al., 2023) suspended in the atmosphere (Ali et al., 2022a) having aerodynamic diameter of 0.001 to 100 μm (Bao et al., 2019). Generally, aerosol particles are injected into the ambient air from natural sources (Bahadur et al., 2023) such as desert, road and soil dust (Ali et al., 2020; Xun et al., 2021; Yousefi et al., 2023), wildfires (Yu et al., 2021) and sea salt (Wang et al., 2023). Whereas, anthropogenic aerosols originate from vehicular and industrial emissions, biomass and stubble burning (Jiang et al., 2019; Pervaiz et al., 2023). Aerosols originated from anthropogenic and natural sources vary in types, size, composition (Metangley et al., 2024) and have relationship with meteorological variables such as temperature, rainfall and humidity (Khan et al., 2024; Majeed et al., 2024). Notably, aerosols have a strong ability to absorb and scatter solar radiant energy and also have the ability to alter climate (Hassan et al., 2024), and deteriorate air quality (Wang et al., 2023; Endale et al., 2024). However, uncertainties exist regarding their properties

Citation: Pervaiz S, Javid K, Khan FZ, Hayat S. Remote sensing analysis of smog-inducing aerosol optical depth: An integrated approach for air pollution mitigation. Environ. Nat. Resour. J. 2024;22(5):408-419. (https://doi.org/10.32526/ennrj/22/20240025)

reported in the Intergovernmental Panel on Climate Change (IPCC) 5th and the 6th assessment reports (Chen et al., 2022; Metangley et al., 2024). On the other hand other common air pollutants such as $PM_{2.5}$ (Anggraini et al., 2024), carbon monoxide (CO), nitrogen dioxide (NO_2), sulfur dioxide (SO_2), and ground level ozone (O_3) are also associated with the formation of aerosols (Pervaiz et al., 2021; Wang et al., 2023) that increase the concentration level of troposphere aerosols. Therefore, aerosol optical depth (AOD) (Raptis et al., 2020) are used to determine the level of air pollution (Chen et al., 2021; Endale et al., 2024) and help in forecasting atmospheric pollutants (Pang et al., 2018; Waris and Tariq, 2024).

Like other developing countries, Pakistan is also facing severe challenge of air pollution. Especially, 'Lahore' Punjab, Pakistan has drawn significant attention globally because of being affected by smog (Pervaiz and Shirazi, 2023). Several studies have been conducted by the different researchers on Lahore so far. But, evaluation of AOD trend of Lahore Division is still lacking and remains unaddressed where regional smog particularly called as seasonal smog prominently engulfs the division during winter season. Keeping in view this grave concern, there is a dire need to analyze AOD of Lahore Division at local scale for environment development. Therefore, goal of the present study is identification of the key air pollution emitting sources and their contribution in smog formation with the objective to examine aerosol optical depth (AOD) and stubble burning with three meteorological elements i.e., temperature, rainfall and humidity in October and November of 2018 to 2022 using remote sensing data. The specific months i.e., October and November was chosen due to known stubble burning and smog formation months of the study area.

2. METHODOLOGY

2.1 Study site

Lahore Division (Saeed et al., 2019) is geographically located between 31°15′ N to 31°42′ N latitudes and 74°01′ E to 74°39′ E longitudes (Aslam et al., 2022), occupies an area of land about 11,413.5 km^2 (Hassan, 2018) (Figure 1). Administratively, Lahore Division comprises of four districts i.e., Lahore, Sheikhupura, Kasur and Nankana Sahib (Khan et al., 2022). Overall, a huge load of aerosols is contributed in Lahore Division from (i) vehicular and industrial emissions (ii) waste and stubble burning and (iii) fugitive dust.

Lahore Division is the commercial hub of industrial units (Abbas et al., 2022) and well known for its industrial produce and contributes significantly in the country's economy (Rana and Bhatti, 2018). The Division consists of semi-arid to arid climate and divisible into considerable distinct seasons namely spring, summer, autumn, and winter (Fowler and Archer, 2006) including dynamic monsoon season (Chand and Ahmad, 2020). Division is also the hot-spot of intense air pollution which is affected by regional and local transportation of aerosols.

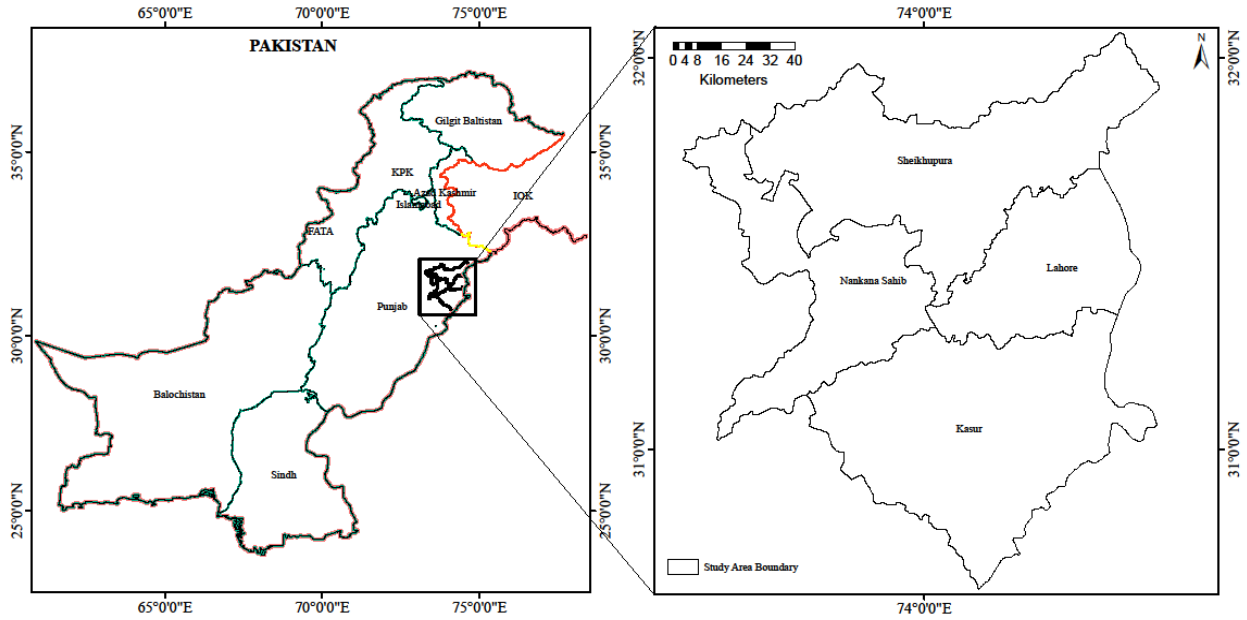

Figure 1. Map of the study area

2.2. Data acquisition

2.2.1 Ancillary data

Multiple studies have reported anthropogenic emissions of smog-causing aerosols (Pervaiz and Shirazi, 2023; Goheer et al., 2024). Therefore, this study focuses on the major contributing sectors that emit air pollutants into the ambient air. These sectors are categorized into three well-known major sources of air pollution i.e., automobiles, industries and agriculture. Data for these sectors were procured from published studies (FAO, 2018), reports (BOS, 2023), the Government of the Punjab, Excise and Taxation Department Pakistan and various published articles.

2.2.1 Remote sensing data

Remote sensing (Raptis et al., 2020) is an advanced approach widely employed for the surveillance and analysis of various environmental phenomena. Various satellite-based sensors are used for this purpose, such as Sentinel-5 Precursor (Sentinel 5P) for aerosol optical depth (AOD) (Zaman et al., 2024) and the Visible Infrared Imaging Radiometer Suite (VIIRS) to examine aerosol concentration and humidity in areas of stubble burning (Shen et al., 2021). Whereas, MERRA-2 (Borhani et al., 2024) is utilized for meteorological variables such as rainfall, humidity and temperature. The data sources, sensors specifications and spatial resolutions derived from these satellites are listed in Table 1.

However, Figure 2 presents an overview of the data acquisitions from different satellites and methods used in the present study categorized into four steps. In step 1, data on AOD; fire anomalies; temperature; rainfall; and relative humidity was derived from satellites. In step 2, the data for the study area was extracted. In steps 3 and 4, emissions data was scaled, as different satellite data with varying spatial resolutions was used. To ensure compatibility and accuracy for analysis, the data was transformed to a uniform resolution of 0.005 meters. This transformation involved converting pixels into points and then applying the Inverse Distance Weighting (IDW) interpolation method to standardize the spatial resolution to 0.005 meters. The map was produced using the following IDW formula:

$$Z_p = \frac{\Sigma\left(\frac{z_i}{d_i^p}\right)}{\Sigma\left(\frac{1}{d_i^p}\right)}$$

Table 1. Description of data

Data set name	Sensor	Spatial resolution	Data acquisition year	Months
Aerosol optical depth	Sentinel 5P	10 m	2018, 2020, 2022	October and November
Stubble burning	VIIRS S-NPP	250 m	2018, 2020, 2022	October and November
Temperature	MERRA 2	1 km	2018, 2020, 2022	October and November
Rainfall	MERRA 2	1 km	2018, 2020, 2022	October and November
Relative humidity	MERRA 2	1 km	2018, 2020, 2022	October and November

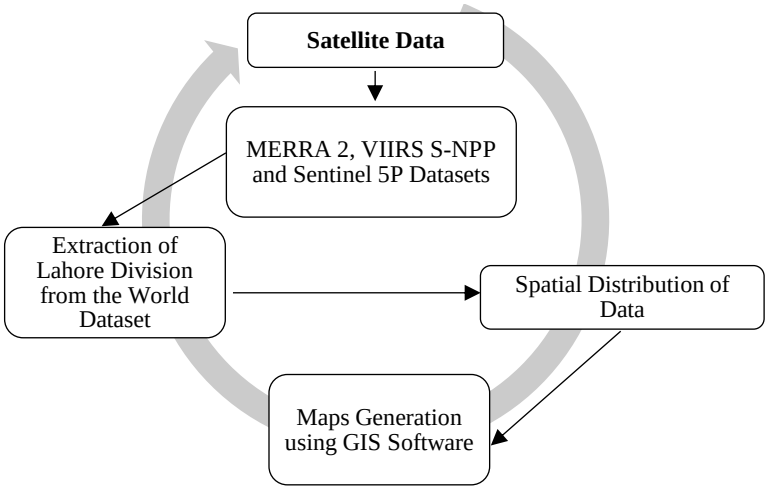

Figure 2. Schematic flowchart of data and methods used in the study

3. RESULTS AND DISCUSSION

3.1 Smog-causing aerosol emission from industry, transport and agriculture sectors

In the Lahore Division (Hassan, 2018), the cities of Lahore, Sheikhupura, and Kasur have a diverse array of industrial units (Paras et al., 2018) encompassing small, medium, and large-scale enterprises. Lahore Division is recognized for its significant industrial output including production of steel, leather, textile, auto parts, marble sheets, chemicals, pharmaceuticals, construction material, and engineering tools and sugar industry (Gilani et al., 2013; Amjad et al., 2019). Lahore Division is a one of the major contributor to deteriorate air by having high concentration of industries that rely on coal. Among all districts of division, Lahore has the largest number of industrial units of Sheikhupura and Kasur. Whereas, Nankana Sahib has more than 1,000 industries. In addition, Lahore Division is well known for its brick kilns (Hamid et al., 2023) furnaces. The large numbers of brick kilns are located in Kasur. However, Lahore and Sheikhupura have more than 200 brick kilns than Nanakana Sahib (Pervaiz et al., 2021). So, the use of fossil fuels and inferior quality of coal used in industrial units and brick kilns are one of the major sources of particulate matter and black carbon emissions (Pervaiz et al., 2022) causing smog.

Various factors of road transport (Muthu et al., 2021) are also linked to air emissions (Wang et al., 2023), encompassing factors like traffic density, traffic flow, congestion, vehicular speed, travel time, vehicle age and fuel characteristics (Pandian et al., 2009; Shrivastava et al., 2013; Khandar and Kosankar, 2014; Gately et al., 2017; Sharmilaa and Ilango, 2022). Moreover, Figure 3 illustrates the view of automobiles percentage in the study area and their contribution to discharge $PM_{2.5}$ emissions which is the most contributing factor in deteriorating ambient air. On comparing results of vehicular registration in the study area, it was noticed that highest population of registered vehicles is motorcycle and least is tractors. However, results of the figure have shown that highest concentration of $PM_{2.5}$ has been emitted by trucks. Similarly auto rickshaws, buses and tractors are also contributing factors to release particulate matter emissions into the ambient air and causing air pollution. Moreover, the previous study conducted by Ali et al. (2022b) supported the findings of the current research that automobiles emissions are one of the major sources of air pollutants.

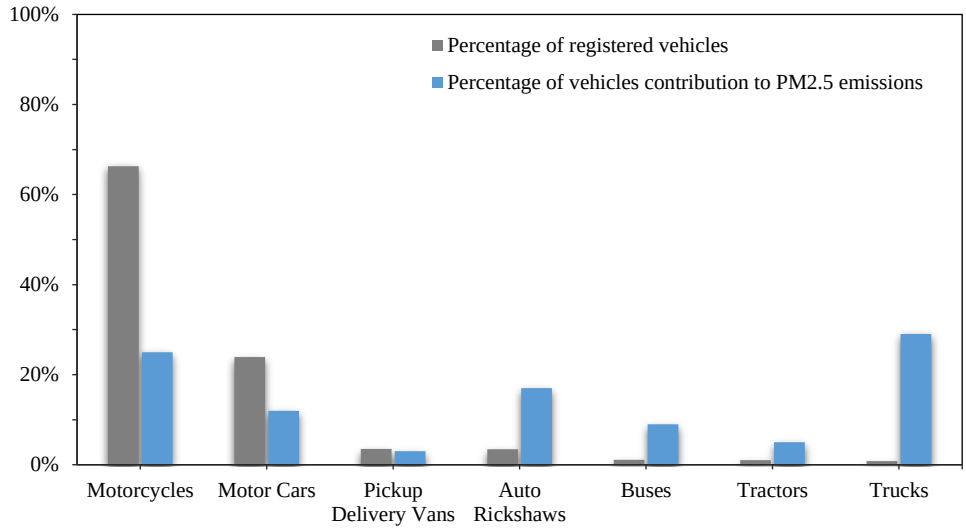

Figure 3. Percentage of registered vehicles and their contribution to $PM_{2.5}$ emissions (Source: Government of the Punjab, Excise and Taxation Department Pakistan 2018)

Furthermore, the Lahore Division claims to be a renowned agriculture sector particularly excelling in the cultivation of rice crops (FAO, 2018; Javed et al., 2023). In addition to this, agricultural processes such as 'slash and burn' (Tang and Yap, 2020) are contributing agents of smog creation (Pierobon et al., 2022), another is rice straw burning (Khalid et al., 2023). Lahore Division is one of the leading division where rice crop (Khan et al., 2021) is grown widely and known to generate high amount of dry residues (Jain et al., 2014). The crop burning emissions are one of the leading causes of smog (Figure 4) based on transportation of regional aerosols (Zeb et al., 2024).

Figure 4. Crop residue burning around Lahore (Shaikh, 2023)

According to the FAO (2018) study, the twelve districts of Punjab are categorized for Basmati Rice growing, namely: Mandi Bahuddin, Sialkot, Gujranwala, Lahore, Gujrat, Hafizabad, Jhang, Okara, Bahawalnagar, Nanka Sahib, Narowal, Sheikhupura and Faisalabad. Three out of the four districts in Lahore Division generate the highest produce of rice (Goheer et al., 2024). However, the breakdown of air pollutants generated from the above source is categorized below (Table 2).

Table 2. Sources of AOD emissions across various sectors

Industry sector	Air pollutants
Steel furnaces / re-rolling mills, paper, and board mills	PM_{10}, $PM_{2.5}$, CO
Brick kilns, fertilizers and pharmaceutical industries	PM_{10}, $PM_{2.5}$, CO, SO_2, NOx
Small resource recovery units, rice, and textile mills	PM_{10}, $PM_{2.5}$
Transport sector	
Motorcycle and motor car	$PM_{2.5}$, HC, CO
Pickup delivery van, auto rickshaw, bus, tractor, truck	$PM_{2.5}$, HC, CO, NOx
Agriculture sector	
Rice straw burning	PM_{10}, $PM_{2.5}$, CO

3.2 AOD trend over Lahore Division in October and November (2018 to 2022)

Lahore, Sheikhupura and Kasur are the industrial and urbanized cities of Lahore Division (Nadeem, 2017; Rana and Bhatti, 2018). Figure 5 has shown the significant variations of AOD in Lahore Division in October and November of 2018 to 2022. Upon comparison of AOD results, it has been noticed that Lahore is the most affected district of Lahore Division where vehicular emissions, industrial soot release into the ambient air and support the findings of the studies conducted by Pervaiz and Shirazi (2023) and Goheer et al. (2024). Furthermore, dust from the southern region of Punjab contributes to Lahore's AOD levels, a phenomenon previously documented in a study by Tariq et al. (2021). Additionally, during stubble burning months (Shabbir et al., 2024) air pollutants get transported in Lahore from India through its shared boundary (Majeed et al., 2024). Hence, AOD caused by stubble burning aerosols (Goheer et al., 2024) coupled with high relative humidity created favorable conditions for the elevation of smog level in Lahore.

3.3 Stubble burning trend over Lahore Division in October and November (2018 to 2022)

According to a 2018 study by FAO, three out of the twelve districts associated with the Lahore Division namely Lahore, Sheikhupura, and Nankana Sahib, are prominently involved in rice cultivation (Younas et al., 2015; Javed et al., 2023). The cultivated rice species in these cities generate a substantial amount of crop residues (Jain et al., 2014). Stubble burning, a common practice, not only releases greenhouse gases but also emits particulate matter into ambient air, typically peaking in the first week of November (Abdurrahman et al., 2020). In the Lahore Division, farmers often prefer stubble burning, believing it enhances soil fertility (Pervaiz et al., 2022). However, incidents of stubble burning have increased with the shift from manual to mechanical harvesting (Sanjay et al., 2021).

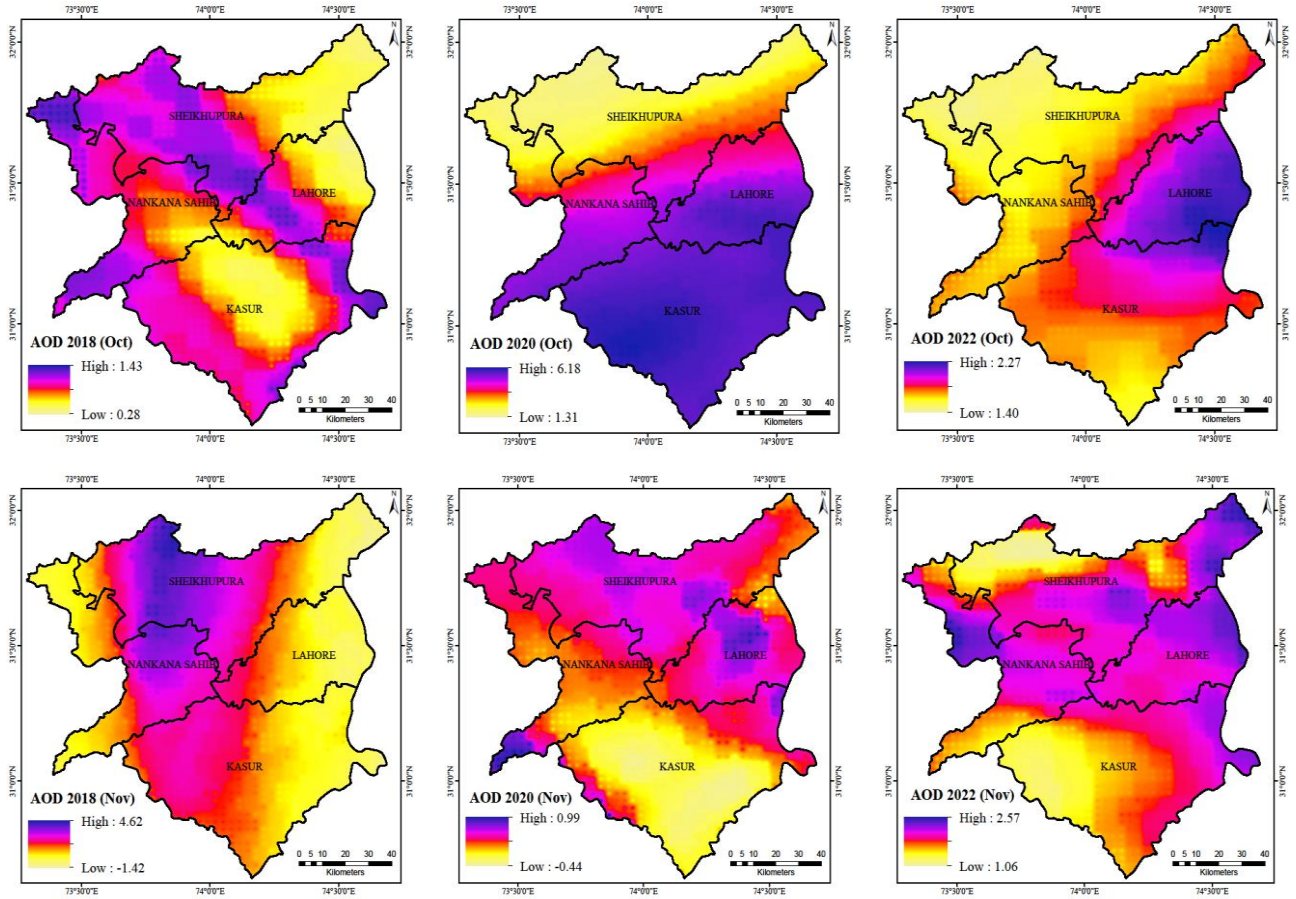

Figure 5. AOD trend over Lahore Division in October and November (2018 to 2022)

However, the results of spatial mapping (Figure 6) reveal the highest extent of stubble burning recorded in Nankana Sahib, a district well-known for its rice crop (Yameen et al., 2019; Shah et al., 2022). Furthermore, emissions from crop burning, when combined with pollutants from vehicular and industrial sources (Gaffney and Marley, 2009; Guo et al., 2024), along with high relative humidity, contribute to the formation of smog (Pervaiz and Shirazi, 2023). Moreover, the study conducted by Kundu et al. (2024) presented the similar findings of our study. In addition to this, our findings of the study also supported by Tariq et al. (2015), Singh (2024), Goheer et al. (2024), and Goenka et al. (2024) who examined that the AOD level increased after crop residue burning in October and November.

3.4 Temperature trend over Lahore Division in October and November (2018 to 2022)

Figure 7 of the study depicts temperature variations in Lahore Division. Notably, Kasur and Sheikhupura have consistently recorded higher temperatures compared to Lahore and Nankana Sahib. A comparative analysis reveals a persistent trend of lower temperature in Lahore from 2018 to 2022. The conjunction of low temperatures in Lahore coupled with high relative humidity significantly impacts air quality emerging as a prominent factor in the formation of smog. This observation aligns with earlier research on Lahore by various authors, reinforcing the current study's findings (Tariq et al., 2021; Pervaiz and Shirazi, 2023) as well as study conducted by Jiang et al. (2024) also reported the findings that low temperature helps to rise the AOD level and deteriorates the quality of air.

3.5 Rainfall trend over Lahore Division in October and November (2018 to 2022)

Meteorological variables, such as rainfall (Kayes et al., 2019; Pervaiz et al., 2022), play a crucial role in mitigating the concentration of air pollutants in the atmosphere. Figure 8 illustrates a consistent low trend of rainfall across most of Lahore Division during the study period. The scarcity of rainfall in October and November proved to be a contributing factor to the heightened levels of Aerosol Optical Depth (AOD) in Lahore, as corroborated by earlier study (Pervaiz et al., 2022). Furthermore, a focused examination of the

2020 spatial data for Kasur highlighted the influential role of low rainfall in elevating AOD levels aligns with the findings of previous studies conducted by Salma et al. (2012) and Kaur et al. (2013). Therefore, Kasur, being a well-known twin city of Lahore, demonstrates similar patterns and by showing the relationship with the meteorological factor i.e., rainfall having influence on air quality in the study area.

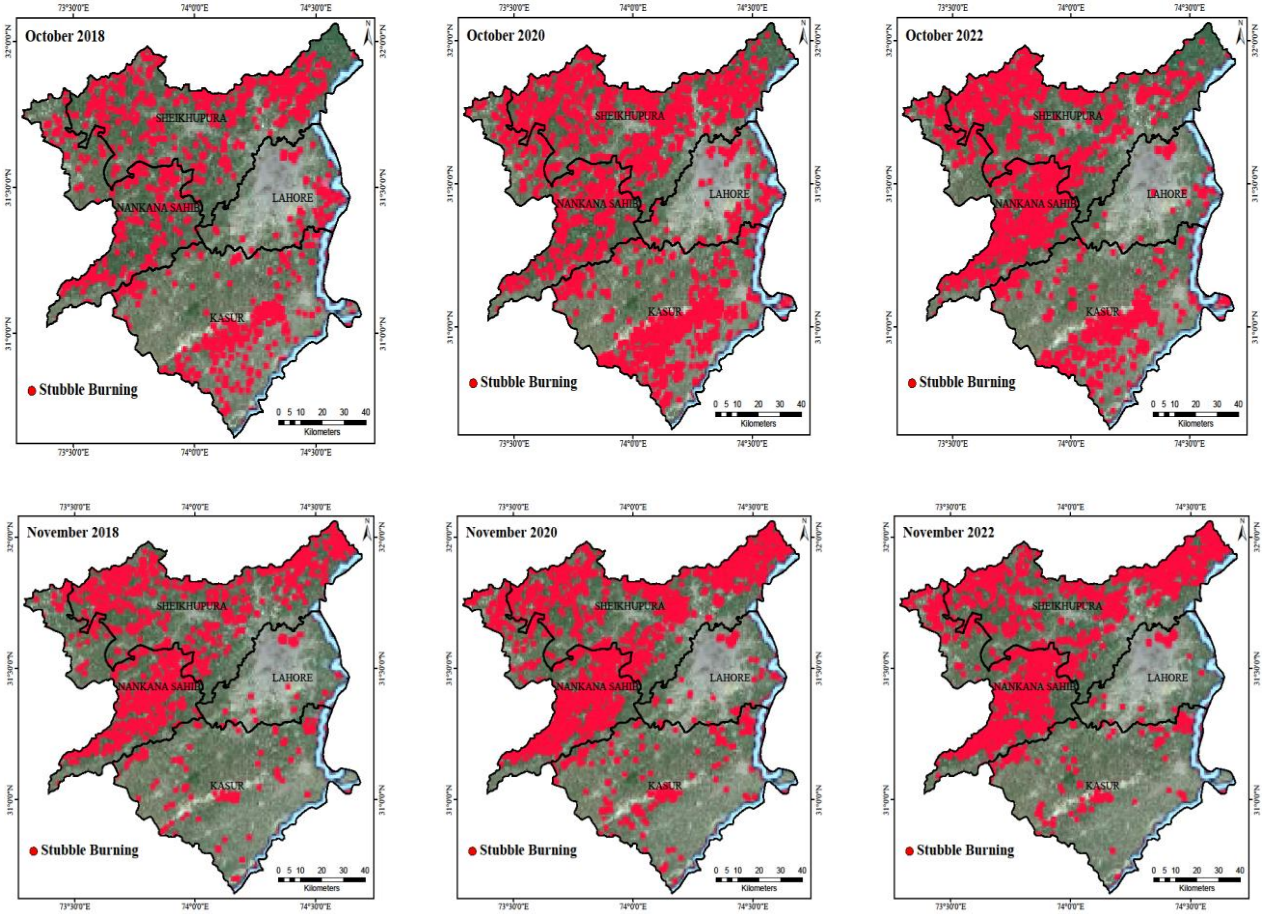

Figure 6. Stubble burning trend over Lahore Division in October and November (2018 to 2022)

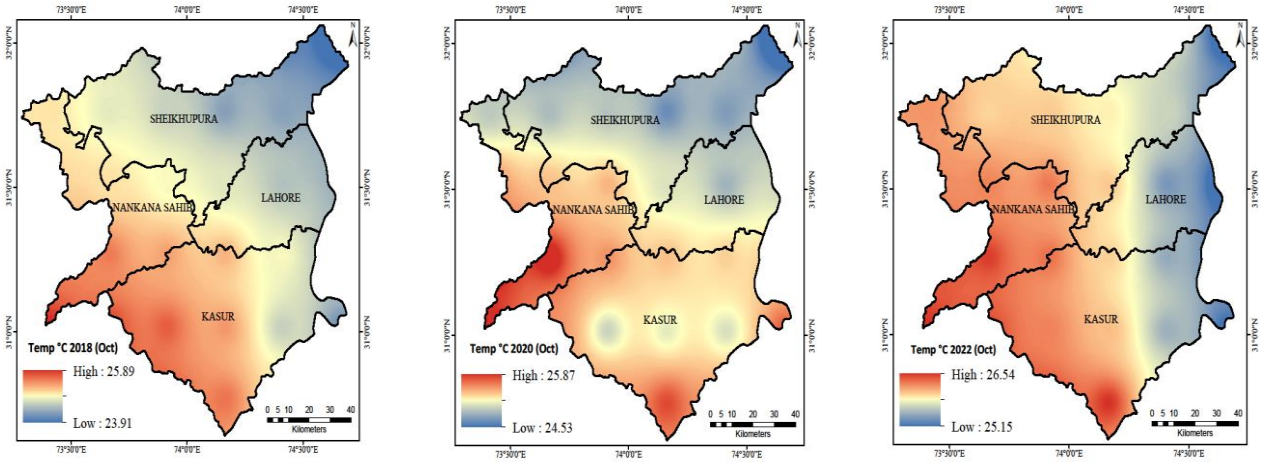

Figure 7. Temperature trend over Lahore Division in October and November (2018 to 2022)

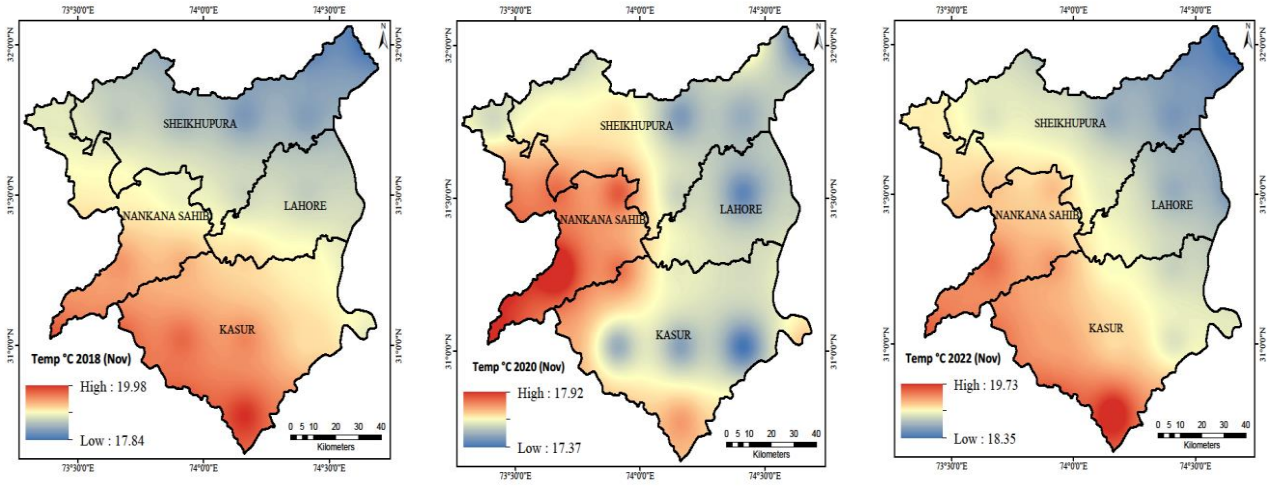

Figure 7. Temperature trend over Lahore Division in October and November (2018 to 2022) (cont.)

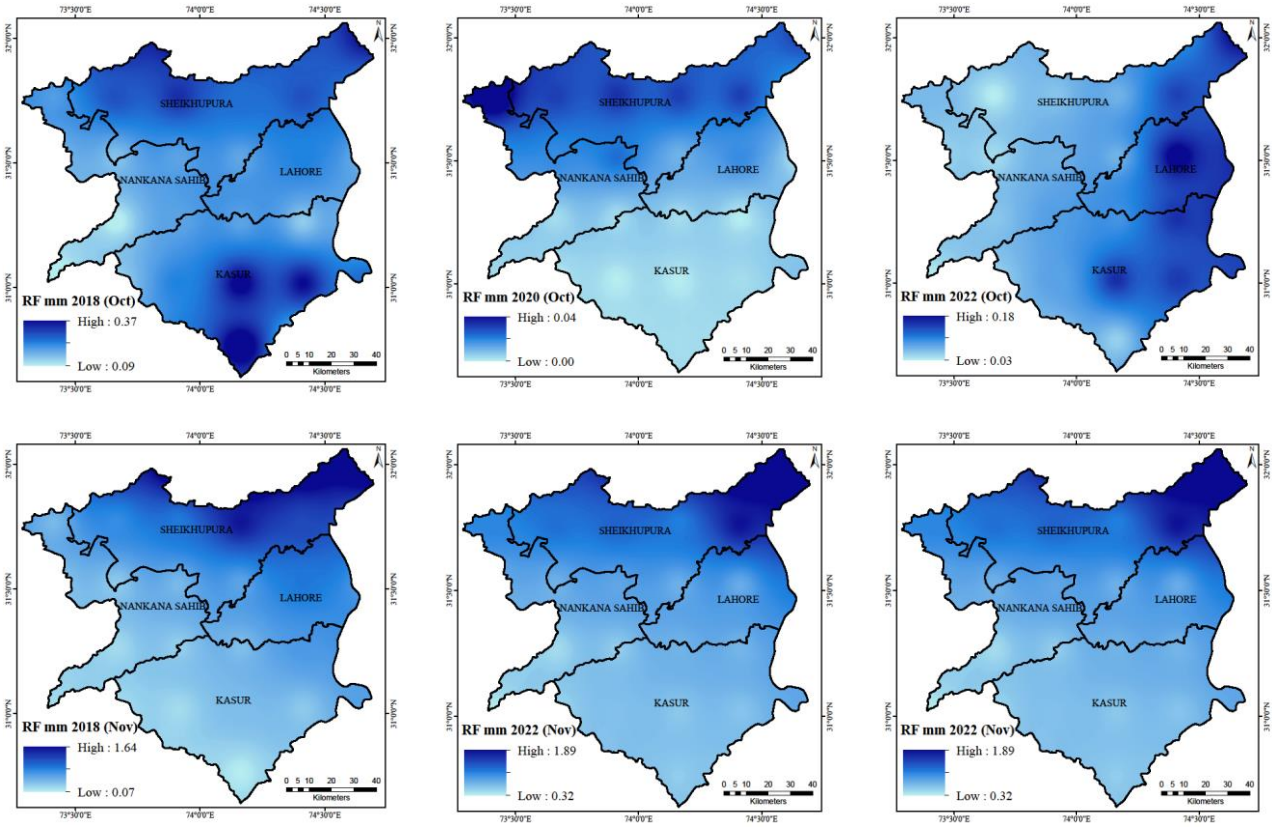

Figure 8. Rainfalltrend over Lahore Division in October and November (2018 to 2022)

3.6. Humidity trend over Lahore Division in October and November (2018 to 2022)

Figure 9 presents the variations in relative humidity in October and November of 2018 to 2022. In October 2018, a notably high trend of relative humidity was observed in Lahore and Sheikhupura and certain parts of Kasur. Similarly, in 2020, elevated relative humidity levels were noted in Lahore, Sheikhupura and central Kasur. However, in 2022, the highest levels of relative humidity were recorded in Lahore and Sheikhupura extending to the northern part of Kasur. In contrast, moderate to low levels of relative humidity were exhibited in Nankana Sahib. Hence, the results show that the high relative humidity levels are a significant contributor by increasing AOD levels into the atmosphere. This meteorological factor contributes to air pollution of Lahore being one of the most affected districts in the Lahore Division. Findings of the present study supported the results of prior study conducted on Lahore (Khan et al., 2021).

However, in support of our study results, studies conducted globally by Shahid et al. (2015), Basharat et al. (2023), Zhu et al. (2024), and Guo et al. (2024) reported the similar findings.

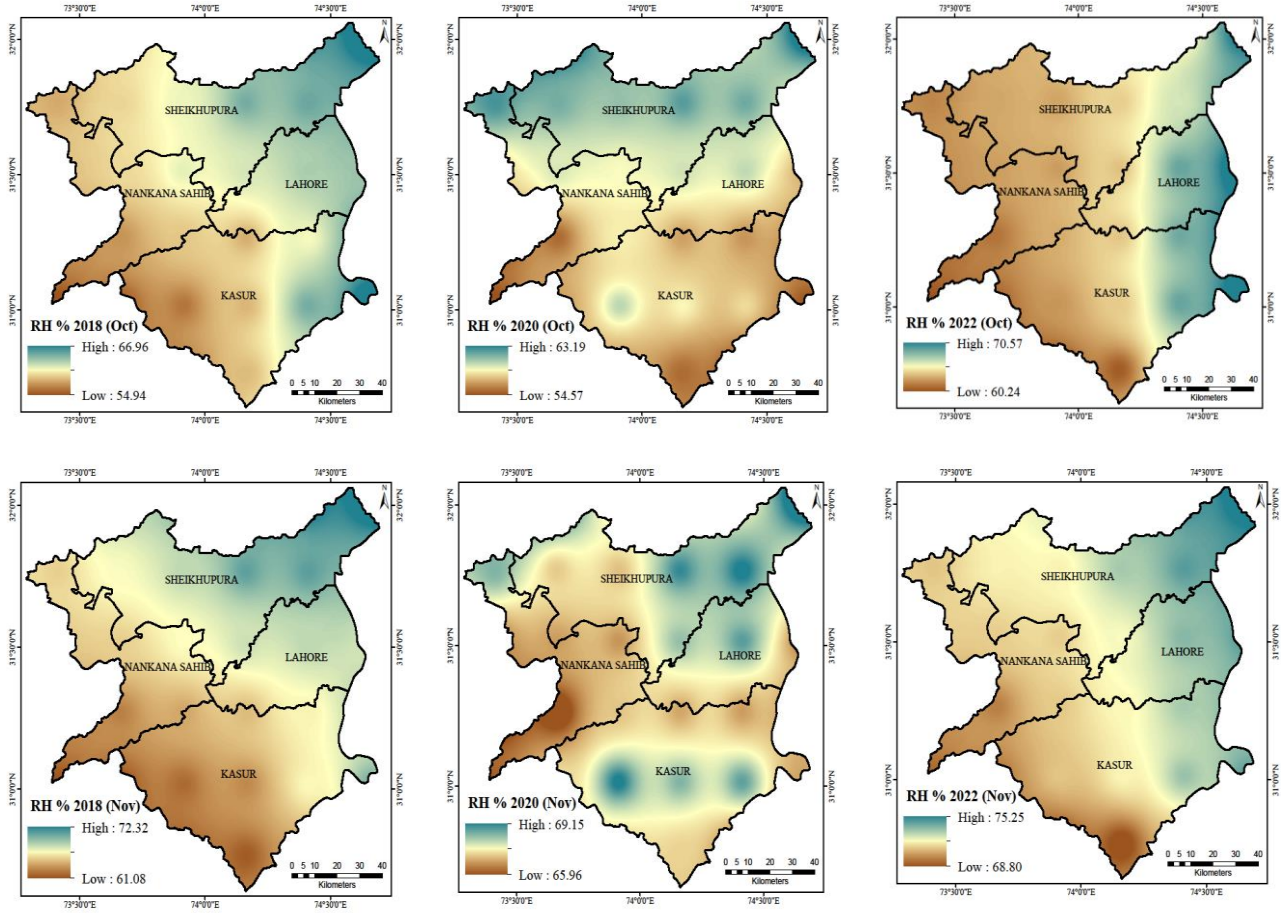

Figure 9. Relative humidity trend over Lahore Division in October and November (2018 to 2022)

4. CONCLUSION AND RECOMMENDATIONS

The government of Punjab has already taken measures to control emissions from road vehicles, crop waste burning, and stationary industrial sources using the Punjab Smog Prevention and Control Rules, 2023. Furthermore, to mitigate air pollution levels, the Punjab Clean Air Policy 2023 (with a phased action plan) has also been notified for clean air. The clean air policy consists of timelines: Short term (<1 year/2023-24), Mid term (1-3 years/2023-26), and Long term (>3 years/2023-30) for the transport, industrial, and agricultural sectors.

However, particular challenges in controlling the generation of anthropogenic aerosols need immediate measures. The current study recorded the highest AOD levels in Sheikhupura, Nankana Sahib, and Lahore in November 2022 compared to October which is known for stubble burning month. Moreover, it is pertinent to note that not only crop residue burning is in practice, but the vegetable and fruit markets in the Lahore Division also contribute significantly to air pollution. These markets burn leftover packing materials at night after delivering goods via high-transport vehicles. These overloaded goods vehicles are another major source of air pollutants by elevating the level of air pollutants.

Considering the study's findings, it becomes evident that a concerted effort is required to address environmental challenges in the context of ongoing economic development. Therefore, sectoral measures for mitigating environmental smog are proposed (Table 3). Implementing these steps requires robust commitment and coordination among government bodies, industries, and citizens to control air pollutants. This collaborative approach is mandatory to ensure the long-term sustainability of a healthier environment in the Lahore Division especially in light of the current study results for the upcoming October and November, 2024.

Table 3. Industrial, transport and agricultural sectoral guide to mitigate environmental smog

Industry sector	Transport sector	Agriculture sector
• Introduction of self-monitoring reporting tools for air emission causing industries • Installation of emission control systems by training cameras using machine learning approaches to monitoring and track industry emission compliance • Adoption of cleaner production technologies • Incentivization of the use of low-emission fossil fuels • Introduction of green industrial zones • Planting ever-green trees as compared to deciduous trees' species, around industrial areas and industrial estates to trap particulate pollutants	• Mandatory vehicular fitness certificates, complying with the Punjab Environmental Quality Standards designed for motor vehicles, required for all public institutes • Reduction of mobility fares to promote train and bus travel for the public • Strict compliance at all entry points of Lahore Division for heavy transport vehicles	• Strict surveillance of vegetable and fruit markets at night • Providing platforms to promote crop waste management practices • Exploring and implementing alternative crop residue disposal methods such as briquetting and waste to energy • Introduction a uniform threshold limit for fire counts using remote sensing data such as for SNPP-VIIRS 7 and MODIS 30%

GRANT SUPPORT DETAILS: The present research did not receive any financial support.

CONFLICTS OF INTEREST: The authors declare no conflict of interest.

REFERENCES

Abbas S, Ali G, Qamer FM, Irteza SM. Associations of air pollution concentrations and energy production dynamics in Pakistan during lockdown. Environmental Science and Pollution Research 2022;29(23):35036-47.

Abdurrahman MI, Chaki S, Saini G. Stubble burning: Effects on health and environment, regulations and management practices. Environmental Advances 2020;2:Article No. 100011.

Ali G, Bao Y, Ullah W, Ullah S, Guan Q, Liu X, et al. Spatiotemporal trends of aerosols over urban regions in Pakistan and their possible links to meteorological parameters. Atmosphere 2020;11(3):Article No. 306.

Ali MA, Bilal M, Wang Y, Qiu Z, Nichol JE, de Leeuw G, et al. Evaluation and comparison of CMIP6 models and MERRA-2 reanalysis AOD against Satellite observations from 2000 to 2014 over China. Geoscience Frontiers 2022a;13(2):Article No. 101325.

Ali M, Siddique I, Abbas S. Characterizing air pollution and its association with emission sources in Lahore: A guide to adaptation action plans to control pollution and smog. Applied Sciences 2022b;12(10):Article No. 5102.

Amjad H, Hamid S, Niaz Y, Ashraf M, Yasir U, Chaudhary A, et al. Efficiency assessment of wastewater treatment plant: A case study of Pattoki, District Kasur, Pakistan. Earth Science Pakistan 2019;3(2):1-4.

Anggraini Z, Santoso M, Sofyan A. Characteristics of fine particulate matter (PM2.5) chemical composition in the North Jakarta Industrial Area. Environment and Natural Resources 2024;22(3):222-31.

Aslam RA, Shrestha S, Usman MN, Khan SN, Ali S, Sharif MS, et al. Integrated SWAT-MODFLOW modeling-based groundwater adaptation policy guidelines for Lahore, Pakistan under projected climate change, and human development scenarios. Atmosphere 2022;13(12):Article No. 2001.

Bao Y, Zhu L, Guan Q, Guan Y, Lu Q, Petropoulos GP, et al. Assessing the impact of Chinese FY-3/MERSI AOD data assimilation on air quality forecasts: Sand dust events in northeast China. Atmospheric Environment 2019;205:78-89.

Bahadur FT, Shah SR, Nidamanuri RR. Applications of remote sensing vis-à-vis machine learning in air quality monitoring and modelling: A review. Environmental Monitoring and Assessment 2023;195(12):Article No. 1502.

Basharat U, Tariq S, Chaudhry MN, Khan M, Agyekum EB, Mbasso WF, et al. Seasonal correlation of aerosols with soil moisture, evapotranspiration, and vegetation over Pakistan using remote sensing. Heliyon 2023;9(10):e20635.

Borhani F, Ehsani AH, Shafiepour Motlagh M, Rashidi Y. Estimate ground-based $PM_{2.5}$ concentrations with Merra-2 aerosol components in Tehran, Iran: Merra-2 $PM_{2.5}$ concentrations verification and meteorological dependence. Environment, Development and Sustainability 2024; 26(3):5775-816.

Bureau of Statistics Punjab (BOS). Punjab Development Statistics 2023. Punjab, India: Planning and Development Board Government of the Punjab; 2023.

Chand S, Ahmad M. Appraisal of spatial and temporal behavior in monsoon precipitation series of Punjab-Pakistan using hierarchical Bayesian Models. Environmental Earth Sciences 2020;79(12):Article No. 304.

Chen G, LiY, Zhou Y, Shi C, Guo Y, Liu Y. The comparison of AOD-based and non-AOD prediction models for daily PM2.5 estimation in Guangdong province, China with poor AOD coverage. Environmental Research 2021;195:Article No. 110735.

Chen C, Dubovik O, Schuster GL, Chin M, Henze DK, Lapyonok T, et al. Multi-angular polarimetric remote sensing to pinpoint global aerosol absorption and direct radiative forcing. Nature Communications 2022;13(1):Article No. 7459.

Endale TA, Raba GA, Beketie KT, Feyisa GL. Exploring the trend of aerosol optical depth and its implication on urban air quality using multi-spectral satellite data during the period from 2009 to 2020 over Dire Dawa, Ethiopia. Nature Environment and Pollution Technology 2024;23(1):1-15.

Food and Agriculture Organization (FAO). Remote Sensing for Spatio-Temporal Mapping of Smog in Punjab and Identification of the Underlying Causes using GIS Techniques

(R-Smog). Punjab, India: Department of Agriculture Punjab; 2018.

Fowler HJ, Archer DR. Conflicting signals of climatic change in the upper Indus Basin. Journal of Climate 2006;19(17): 4276-93.

Gaffney JS, Marley NA. The impacts of combustion emissions on air quality and climate: From coal to biofuels and beyond. Atmospheric Environment 2009;43(1):23-36.

Gately CK, Hutyra LR, Peterson S, Wing IS. Urban emissions hotspots: Quantifying vehicle congestion and air pollution using mobile phone GPS data. Environmental Pollution 2017;229:496-504.

Gilani SR, Hussain M, Baig Y, Mahmood Z, Abbas Z, Batool S. A study of drinking water of industrial area of Sheikhupura with special concern to arsenic, manganese and chromium. Pakistan Journal of Engineering and Applied Sciences 2013;13:118-26.

Goenka R, Thakur J, Taori A, Bothale RV, Chauhan P. The prevailing smog conditions over the Delhi-NCR during the 2022 post monsoon. Advances in Space Research 2024; 73(5):2609-17.

Goheer MA, Hassan SS, Sheikh AS, Malik Y, Uzair M, Satti TN. Assessing smog trends and sources of air pollutants across northeastern districts of Punjab, Pakistan using geospatial techniques. International Journal of Environmental Science and Technology 2024. DOI: https://doi.org/10.1007/s13762-024-05754-x.

Guo L, Gu C, Dong K, Ou S, Zhao X, Wang X, et al. Composition characteristics and potential regions of PM2.5 during winter haze pollution in typical industrial areas, NW-China. Aerosol and Air Quality Research 2024;24(7):Article No. 230290.

Hamid A, Riaz A, Noor F, Mazhar I. Assessment and mapping of total suspended particulate and soil quality around brick kilns and occupational health issues among brick kilns workers in Pakistan. Environmental Science and Pollution Research 2023;30(2):3335-50.

Hassan I. Rapid commercial conversion of agriculture land in Lahore Division, Pakistan. Advancements in Life Sciences 2018;5(4):192-203.

Hassan T, Zhang K, Li J, Singh B, Zhang S, Wang H, et al. Impacts of spatial heterogeneity of anthropogenic aerosol emissions in a regionally refined global aerosol-climate model. Geoscientific Model Development 2024;17(8):3507-32.

Jain N, Bhatia A, Pathak H. Emission of air pollutants from crop residue burning in India. Aerosol Air Quality Research 2014;14:422-30.

Jiang T, Chen B, Chan KKY, Xu B. Himawari-8/AHI and MODIS aerosol optical depths in China: Evaluation and comparison. Remote Sensing 2019;11(9):Article No. 1011.

Jiang X, Wang Y, Wang L, Tao M, Wang J, Zhou M, et al. Characteristics of daytime-and-nighttime AOD differences over China: A perspective from CALIOP satellite observations and GEOS-Chem model simulations. Journal of Geophysical Research: Atmospheres 2024;129(8):e2023JD039158.

Javed K, Muhammad S, Khan Z, Fatima S, Nawaz H, Mahrukh TK, et al. Synecological analysis of weeds of wheat, rice and sugar cane crops of tehsil Muridke, District Sheikhupura (Punjab) Pakistan. Pakistan Journal of Weed Science Research 2023;29(2):107-14.

Kaur S, Lubana PPS, Aggarwal R. Groundwater management for adaptation under changing climate conditions in Indian Punjab. Journal of Water and Climate Change 2013;4(1):38-51.

Kayes I, Shahriar SA, Hasan K, Akhter M, Kabir MM, Salam MA. The relationships between meteorological parameters and air pollutants in an urban environment. Global Journal of Environmental Science and Management 2019;5(3):265-78.

Khalid A, Guerriero E, Cerasa M, Mahmood T, Khalid A, Paris E, et al. Estimation inventories of persistent organic pollutants from rice straw combustion as an agricultural waste. Fire 2023;6(12):Article No. 459.

Khandar C, Kosankar S. A review of vehicular pollution in urban India and its effects on human health. Journal of Advanced Laboratory Research in Biology 2014;5(3):54-61.

Khan R, Kumar KR, Zhao T, Ullah W, de Leeuw G. Interdecadal changes in aerosol optical depth over Pakistan based on the MERRA-2 reanalysis data during 1980-2018. Remote Sensing 2021;13(4):Article No. 822.

Khan HU, Rashid I, Israr J, Zhang G. Geotechnical characterization and statistical evaluation of alluvial soils of Lahore. Arabian Journal of Geosciences 2022;15(9):Article No. 845.

Khan, MN, Tariq S, Ehsan N, Haseeb T. Classification of aerosol types in mega-city of Lahore (Pakistan) using ground-based remote sensing. Air Quality, Atmosphere and Health 2024;7:1361-72.

Kundu N, Hooda RS, Sandeep. Does stubble burning really contribute in Delhi's air pollution? Evidences from ground, model, and satellite data. Water, Air, and Soil Pollution 2024;235(5):Article No. 320.

Majeed R, Anjum MS, Imad-ud-din M, Malik S, Anwar MN, Anwar B, et al. Solving the mysteries of Lahore smog: The fifth season in the country. Frontiers in Sustainable Cities 2024;5:Article No. 1314426.

Metangley S, Middey A, Kadaverugu R. Modern methods to explore the dynamics between aerosols and convective precipitation: A critical review. Dynamics of Atmospheres and Oceans 2024;106:Article No. 101465.

Muthu M, Gopal J, Kim DH, Sivanesan I. Reviewing the impact of vehicular pollution on road-side plants: Future perspectives. Sustainability 2021;13(9):Article No. 5114.

Nadeem F. Monitoring urbanization and comparison with city master plans using remote sensing and GIS: A case study of Lahore District, Pakistan. International Journal of Advance Remote Sensing GIS 2017;6:2234-45.

Pandian S, Gokhale S, Ghoshal AK. Evaluating effects of traffic and vehicle characteristics on vehicular emissions near traffic intersections. Transportation Research Part D: Transport and Environment 2009;14(3):180-96.

Pang J, Liu Z, Wang X, Bresch J, Ban J, Chen D, et al. Assimilating AOD retrievals from GOCI and VIIRS to forecast surface PM2.5 episodes over Eastern China. Atmospheric Environment 2018;179:288-304.

Paras I, Mohey-ud-din G, Fareed F. Infrastructure development in Punjab, Pakistan: From assessment to spatiotemporal analysis at district level. Journal of Quantitative Methods 2018;2(2): 75-103.

Pervaiz S, Akram MAN, Khan FZ, Javid K, Zahid Y. Brick sector and air quality: An integrated assessment towards 2020 challenge of environment development. Environment and Natural Resources Journal 2021;19(2):153-64.

Pervaiz S, Khan F, Javid K, Altaf A, Aslam F, Tahir M, et al. Development of air quality and brick Kilns during the onset of Covid-19: An analysis. Biological and Clinical Sciences Research Journal 2022;2022(1):1-11.

Pervaiz S, Shirazi SA. Intervention of urban criteria pollutants in air quality: A satellite based analysis of world's smog-induced City. International Journal of Chemical and Biochemical Sciences 2023;24:1-15.

Pervaiz S, Shirazi SA, Ahamad MI. Greenhouse gas emissions and aerosol distribution in brick kiln zones of Punjab, Pakistan: An appraisal using spatial information technology. Natural and Applied Sciences International Journal 2023;4(1):62-79.

Pierobon F, Sifford C, Velappan H, Ganguly I. Air quality impact of slash pile burns: Simulated geo-spatial impact assessment for Washington State. Science of the Total Environment 2022;818:Article No. 151699.

Raptis IP, Kazadzis S, Amiridis V, Gkikas A, Gerasopoulos E, Mihalopoulos N. A decade of aerosol optical properties measurements over Athens, Greece. Atmosphere 2020; 11(2):Article No. 154.

Rana IA, Bhatti SS. Lahore, Pakistan: Urbanization challenges and opportunities. Cities 2018;72:348-55.

Saeed A, Saeed H, Saleem Z, Fang Y, Babar ZUD. Evaluation of prices, availability and affordability of essential medicines in Lahore Division, Pakistan: A cross-sectional survey using WHO/HAI methodology. PLoS ONE 2019;14(4):e0216122.

Salma S, Rehman S, Shah MA. Rainfall trends in different climate zones of Pakistan. Pakistan Journal of Meteorology 2012; 9(17):37-47.

Sanjay, Swamy HM, Seidu M, Singh SB. Issues of paddy stubble burning in Haryana: Current perspective. Paddy and Water Environment 2021;19:55-69.

Shabbir Y, Guanhua Z, Shah SRA, Ishaq RA. Trans-boundary spatio-temporal analysis of Sentinel 5P tropospheric nitrogen dioxide and total carbon monoxide columns over Punjab and Haryana Regions with COVID-19 lockdown impact. Environmental Monitoring and Assessment 2024; 196(3):Article No. 291.

Shahid MZ, Liao H, Li J, Shahid I, Lodhi A, Mansha M. Seasonal variations of aerosols in Pakistan: Contributions of domestic anthropogenic emissions and transboundary transport. Aerosol Air Quality Research 2015;15(1):1580-600.

Shah SHIA, Jianguo Y, Jahangir Z, Tariq A, Aslam B. Integrated geophysical technique for groundwater salinity delineation, an approach to agriculture sustainability for Nankana Sahib Area, Pakistan. Geomatics, Natural Hazards and Risk 2022;13(1):1043-64.

Sharmilaa G, Ilango T. A review on influence of age of vehicle and vehicle traffic on air pollution dispersion. Materials Today: Proceedings 2022;60:1629-32.

Shen L, Wang H, Cheng M, Ji D, Liu Z, Wang L, et al. Chemical composition, water content and size distribution of aerosols during different development stages of regional haze episodes over the North China Plain. Atmospheric Environment 2021;245:Article No. 118020.

Shrivastava RK, Neeta S, Geeta G. Air pollution due to road transportation in India: A review on assessment and reduction strategies. Journal of Environmental Research and Development 2013;8(1):Article No. 69.

Singh J. Is Agri-residue burning a menace for air quality and public health in Delhi, India? Atmosfera 2024. DOI: https://doi.org/10.20937/ATM.53365.

Sun J, Wang Z, Zhou W, Xie C, Wu C, Chen C, et al. Measurement report: Long-term changes in black carbon and aerosol optical properties from 2012 to 2020 in Beijing, China. Atmospheric Chemistry and Physics 2022;22(1):561-75.

Tang KHD, Yap PS. A systematic review of slash-and-burn agriculture as an obstacle to future-proofing climate change. Proceedings of the 4th International Conference on Climate Change; 2020 Feb; 27-28; Kuala Lumpur, Malaysia; 2020.

Tariq S, Ali M. Analysis of optical and physical properties of aerosols during crop residue burning event of October 2010 over Lahore, Pakistan. Atmospheric Pollution Research 2015;6(6):969-78.

Tariq S, Mehmood S, Nisa A, Ul-Haq Z, Mehmood U. Remote sensing of aerosol properties during intense smog events over Lahore (Pakistan). Kuwait Journal of Science 2021;48(4):1-6.

Waris U, Tariq S. Temporal dynamics and forecasting of aerosol optical depth in megacities Lahore and Karachi: Insights from the Indo-Gangetic Basin and southern Pakistan, and implications for Sustainable development. Atmospheric Pollution Research 2024;15(7):Article No. 102146.

Wang P, Tang Q, Zhu Y, He Y, Yu Q, Liang T, et al. Coupling coordination degree of AOD and air pollutants in Shandong Province from 2015 to 2020. Atmosphere 2023;14(4):Article No. 654.

Yameen Q, Arshad MF, Saqlain M. Normalized difference vegetation index as a tool for wheat crop coefficient and evapotranspiration estimation: A case study of Nankana Sahib District Pakistan. Acta Science Agriculture 2019;3(10):32-9.

Younas M, Rehman MA, Hussain A, Ali L, Waqar MQ. Economic comparison of direct seeded and transplanted rice: Evidences from adaptive research area of Punjab Pakistan. Asian Journal of Agriculture and Biology 2015;4(1):1-7.

Yousefi R, Wang F, Ge Q, Shaheen A, Kaskaoutis DG. Analysis of the winter AOD trends over Iran from 2000 to 2020 and associated meteorological effects. Remote Sensing 2023; 15(4):Article No. 905.

Yu X, Lary DJ, Simmons CS. PM2.5 modeling and historical reconstruction over the continental USA utilizing GOES-16 AOD. Remote Sensing 2021;13(23):Article No. 4788.

Xun L, Lu H, Qian C, Zhang Y, Lyu S, Li X. Analysis of aerosol optical depth from sun photometer at Shouxian, China. Atmosphere 2021;12(9):Article No. 1226.

Zaman NAFK, Kanniah KD, Kaskaoutis DG, Latif MT. Improving the quantification of fine particulates (PM2.5) concentrations in Malaysia using simplified and computationally efficient models. Journal of Cleaner Production 2024;448:Article No. 141559.

Zeb B, Alam K, Khan R, Ditta A, Iqbal R, Elsadek MF, et al. Characteristics and optical properties of atmospheric aerosols based on long-term AERONET investigations in an urban environment of Pakistan. Scientific Reports 2024;14(1): Article No. 8548.

Zhu H, Martin R, van Donkelaar A, Hammer M, Li C, Meng J, et al. Global Spatial variation in the PM2.5 to AOD relationship strongly influenced by aerosol composition. EGUsphere 2024. DOI: https://doi.org/10.5194/egusphere-2024-950.

Environment and Natural Resources Journal

Volume 22
Issue 5
2024

Seasonal Diversity of Arbuscular Mycorrhizal Fungi (AMF) in the Mangrove Forests of Bakkhali, Sundarban, India

Supriti Paul[1*], Vipin Parkash[1], Ranjna Kaundal[1], Bikram Dhara[2,3], Meghna Thapa[1], and Arup Kumar Mitra[2]

[1]Forest Research Institute University (FRIDU), Forest pathology, Dehradun, Uttarakhand, India
[2]Department of Microbiology, St. Xavier's College (Autonomous), Kolkata, India
[3]Centre for Global Health Research, Saveetha Institute of Medical and Technical Sciences, Saveetha University, Chennai, India

ARTICLE INFO

Received: 219 Feb 2024
Received in revised: 26 Jul 2024
Accepted: 31 Jul 2024
Published online: 30 Aug 2024
DOI: 10.32526/ennrj/22/20240042

Keywords:
Arbuscular Mycorrhizal Fungi (AMF)/ Seasonal diversity/ Spores/ Colonization/ Mangroves

*** Corresponding author:**
E-mail:
manapaul2021@gmail.com

ABSTRACT

Mangroves, despite thriving at the fringes of habitat tolerance in coastal regions, stand out as one of the world's most highly productive ecosystems. This study delves into the remarkable symbiotic relationship between mangroves and arbuscular mycorrhizal fungi (AMF). Specifically, it assesses seasonal diversity in six true mangrove species and four associated species, situated in Henry's Island, Bakkhali, India. Spore density and root colonization were examined across different seasons. The highest spore density was observed in *Heritiera fomes* (a timber-producing mangrove) during the post-monsoon season, followed by pre-monsoon and monsoon periods. Root colonization was notably prominent in *Ceriops tagal* (Indian mangrove), *Bruguira gymnorrhiza* (Oriental mangrove), and *Sonneratia alba* (flowering evergreen mangrove) during both pre- and post-monsoon seasons. This study unveiled a rich fungal diversity, with a total of 60 AMF species belonging to 13 genera. Among these, the genus *Glomus* emerged as the dominant group, with species such as *G. deserticola* along with another genus *Rhizophagus intraradics* displaying widespread distribution. Notably, *Glomus* consistently ranked as the most prevalent genus throughout the year, indicating its remarkable adaptability and strong dispersal capacity in both true and associate mangrove plant species. This research sheds light on the seasonal dynamics of AMF associations in mangrove ecosystems, emphasizing the significance of *Glomus* as a key player in this symbiotic relationship. These findings contribute to our understanding of the ecological intricacies within mangrove habitats and highlight the adaptability of certain AMF genera to varying environmental conditions.

IMPLICATIONS FOR PRACTICE

- Our study found major AMF diversity with highest significance of *Glomus* sp. indicating remarkable dominance rate throughout the coastal area of Bakkhali, India.
- Keeping in view our results, it is important to increase mass multiplication of salt-tolerant AMF spores to improve threatened mangrove recovery throughout the coastal land.

1. INTRODUCTION

Mangroves are well recognised as ecologically as well as economically important, dynamic coastal ecosystems, playing crucial roles in protecting the habitat from natural disasters through maintaining the productivity, health, carbon sequestration, and tolerance to various abiotic stresses (Akram et al., 2023). Recent research (Constance et al., 2022) has revealed that mangrove growth is frequently impeded by the scarcity of some essential macronutrients like

Citation: Paul S, Parkash V, Kaundal R, Dhara B, Thapa M, Mitra AK. Seasonal diversity of Arbuscular Mycorrhizal Fungi (AMF) in the mangrove forests of Bakkhali, Sundarban, India. Environ. Nat. Resour. J. 2024;22(5):420-430. (https://doi.org/10.32526/ennrj/22/20240042)

phosphorus (P) and nitrogen (N). Through colonization, arbuscular mycorrhizal fungi (AMF) could fulfil such nutrient requirements in saline and poor-nutrient soils in mangrove ecosystem (Akaji et al., 2022). The external hyphae of AMF penetrate into the deeper soil around the plant roots and increase the root surface area (Finlay, 2008). Long-term salinization enhances AMF biomass, which is in turn involved in primary mineral P mobilization in coastal soils (Fan et al., 2023).

Therefore, having a wide range of ecological functions (Marro et al., 2022), AMF are commonly known as keystone organisms in mangrove habitats (Shankarammal, 2023). In coastal ecosystem, AMF play a major role in improving rhizospheric soil characteristics, developing nutrients uptake, and ameliorating plant resilience to a variety of abiotic stressors (Wang et al., 2022). Finding the multifunctional role of glomalin related soil protein (GRSP) in preservation and restoration of Soil Organic Carbon (SOC), recent research has revealed that plantations using AMF can be a useful tool for increasing carbon sequestration during coastal forest restoration (Li et al., 2023). Defining the seasonal diversity of AMF is important to comprehend the multiple ecological attributes through the symbiotic relationship, which in turn gives a clear idea on seasonal impacts in mangrove ecosystem as well as on its conservation strategies (D'Souza and Rodrigues, 2013; Su et al., 2011). Therefore, it is necessary to measure the seasonal AMF biodiversity of mangrove habitats (Gaonkar and Rodrigues, 2020). However, no studies have been reported on the seasonal variation of AMF in true and associate mangroves in Henry Island, India. In this paper, seasonal differences of various ecological parameters associated with mangroves were been explained.

2. METHODOLOGY

2.1 Study site and sample collection

Henry Island (21.5769°N 88.2923°E) is located on the southern triangle of West Bengal, on the North-East coast of India, and in-between the Saptamukhi River and the Bakkhali River. The total area of Henry Island is 470 ha, which has a mangrove cover of about 200 ha. This area is characterized by a tropical climate with annual precipitation of approximately 2,000 mm. The major mangrove flora of the island is dominated by 10 plant species, and of these, 6 are true mangroves while 4 are associates. Rhizospheric soil and root samples were randomly collected in pre-monsoon (March-May 2022), monsoon (July-September 2022), and post-monsoon (October 2022-February 2023) seasons from the study site. All total 90 soil samples were collected, placed in separate Ziploc bags, and then transported to the laboratory. Samples were air-dried through 2 mm sieve and mixed thoroughly to obtain a composite sample and further divided into two parts, one for AMF spore isolation, identification, enumeration, and trap culture preparation, and the other for soil physico-chemical analyses.

2.2 Soil physico-chemical analysis

A total of 30 soil samples (0-25cm) from each season were randomly collected and air-dried in the laboratory. Soil pH was measured in soil water (1:2) suspension and electrical conductivity (EC) was measured at room temperature in 1:5 soil suspension using a pH meter (LI 120 Elico, India) and EC meter (CM-180 Elico, India), respectively. Further, soil physico-chemical properties were detected by standard soil analysis techniques, namely, Walkley and Black (1934) rapid titration method for soil organic carbon (OC), Bray and Kurtz (1945) method for available phosphorus (P), Potassium permanganate oxidation method (Jackson, 1973) for available soil nitrogen (N), and ammonium acetate method (Hanway and Heidel, 1952) for available potassium estimation.

2.3 Isolation, identification of AMF spores, and trap culture preparation

Using the wet sieving and decanting method (Gerdemann and Nicolson, 1963), AMF spores were isolated from collected seasonal soil samples. Trap cultures were prepared for further AMF identification. *Zea mays* was used as trap plant and culture pots were thoroughly maintained at 27°C and well-watered condition in glass house for almost 6 months. Hoagland's solution without phosphorus (P) was added in every 15 days. Isolated AMF spores from both soil samples and trap cultures were then mounted on glass slides in polyvinyl alcohol lacto- glycerol (PVLG) and prepared to examine under bright field microscope. Identification was based on spore morphology along with wall characteristics, dimensions, and other relevant traits, following the international website of VAM fungi (invam.wvu.edu) for taxonomic identification.

2.4 AMF root colonization

Approximately 1 cm long secondary and tertiary root pieces were bleached in H_2O_2 and then

cleaned in 10% KOH for almost 1 h at 90°C. After that, they were acidified in 5 N HCL and stained the with 0.05% Tryphan blue (Phillips and Hayman, 1970). Following the overnight staining process, PVLG-mounted roots were examined under bright-field research microscope (20X, 40X, 100X). The presence of hyphae, arbuscles, or vesicles in root segments was considered as mycorrhizal colonization.

2.5 Statistical analysis

AMF diversity was seasonally analysed for each mangrove plant species by calculating Simpson's diversity index (D) - measurement of relative abundance (RA) of each species, Shannon diversity index (H) - measurement of species diversity in a community, species richness (SR) - number of species present, and species evenness (E) - distribution of abundance across the species. Isolation frequency (IF) reflects the distribution status of AMF species, whereas relative abundance (RA) reveals the similarity or dissimilarity of species.

Following formulae were used to calculate Shannon-Wiener diversity index (H) and Simpson's diversity index (D):

$$H = -\sum pi \ln pi$$

$$D = 1 - [\frac{\sum n(n-1)}{N(N-1)}]$$

Where; pi is the proportion of individual species that contributes to the total number of individuals, n is the number of individuals of a given species, and N is the total number of individuals in a community. Species evenness was estimated as (∑(H)=H/H max) where; H max=lnS, S=total number of species in the community (richness). Also, RA was evaluated using formula: RA=(number of spores of a species/total no of spores in all soil samples) × 100, while IF=(no of soil samples possessing spores of a particular species/total no of soil sample analysed) × 100.

Pearson's correlation coefficient was calculated to evaluate the relationship between relative abundance (RA) and isolation frequency (IF), Simpson index and Shannon index, Species evenness and richness, by using the PAST software 4.03 (details in data availability statement) ($p \leq 0.05$). All data on seasonal variation was statistically analysed using SPSS software (version 16.0). Later, a paired t-test was done to compare the soil parameters between 'true' and 'associate' mangrove plants. Further, a cluster analysis (Bray-Curtis similarities) was performed to understand the AMF species' distribution among the mangrove plants by using the PAST software 4.03.

3. RESULTS AND DISCUSSION

3.1 Soil analysis

The results of soil physico-chemical analysis gave a clear indication on basic (pH range 6.01-8.61) nature of soil throughout the year. Electrical conductivity (EC) ranged from 0.59 to 3.9 d/Sm. Organic carbon (OC) was higher at the true mangrove site in the post monsoon season. In both types of mangroves, phosphate (P) deficiency was found throughout the year. Also, low nutrient (especially nitrogen and organic carbon) availability was seen at both mangrove types. Therefore, paired t-test showed (Table 1) significant differences ($p<0.05$) between the soil parameters in both types of mangroves. The positive t-value indicated that the mean value of P was higher in associate mangrove plants, in the monsoon season.

Table 1. 1-Associate mangrove, 2- true mangrove; paired t-test

Soil parameters	Pre-monsoon			Monsoon			Post-monsoon		
	t	df	p	t	df	p	t	df	p
pH_1-pH_2	-4.29	2	0.5	-3.857	2	0.5	-6.9	2	0.5
EC_1-EC_2	-6.09	2	0.5	-67.66	2	0.5	-3.63	2	0.5
N_1-N_2	-3.23	2	0.5	-1.47	2	0.37	-0.14	2	0.9
OC_1-OC_2	-1.55	2	0.36	-1.73	2	0.33	-3.85	2	0.16
P_1-P_2	6.6	2	0.09	2.2	2	0.27	1.66	2	0.34

3.2 Mycorrhizal colonization, AMF spore density, and AMF species diversity

The seasonal alterations had a significant impact on variations in spore density among mangrove plants. Seasonal variations in spore density (SD) of AM fungi is presented in Table 2. The mean SD was significantly higher in *Heritiera fomes* throughout the year, whereas in *Acanthus ilicifolius*, SD was higher only in the monsoon season. Besides, minimum SD was recorded in *Ceriops tagal* and *Avicennia marina*

in monsoon, premonsoon, and post monsoon seasons, respectively.

A total of 60 AM fungal species (Figure 1) representing 13 genera were recorded (Table 3). *Glomus* was the dominant genus, followed by *Rhizophagus*, *Scutellospora*, *Gigaspora*, and *Diversispora*. Maximum relative abundance (RA) was recorded for *G. deserticola* and *R. intraradics* in monsoon, *F. geosporum* in premonsoon, and *F. verruculosum* in the post monsoon season. Whereas minimum RA was recorded for *G. multicaule*, *G. myriocarpa*, *Racocetra castanea*, *R. clarus*, and *Septoglomus constricum* in monsoon, *Claroideoglomus luteum* in premonsoon, and *A. kentinensis* in the post monsoon season. Along with, *A. polonica* showed minimal RA both in the pre and post monsoon season. Besides, here was no significant change in relative abundance (RA%=0) for several species of *Glomus*, *Rhizophagus*, *Claridioglomus*, *Septoglomus*, and *Scutellospora* in different season. Further, a significant correlation (Table 4) existed between RA and isolation frequency (IF) throughout the year (M. r=0.685, Pr. r=0.600, Po. r= 0.872).

Table 2. Seasonal variation in AMF spore density in selected mangrove species

Mangrove species	Monsoon	Pre-monsoon	Post monsoon
Avicennia marina	59.00±19.08	28.00±2.51	24.3±6.2
Suaeda salsa	30.0±5.5	68.0±8.5	58.7±8.8
Heritiera fomes	99.33±10.47	89.30±15.72	107.70±17.46
Acanthus ilicifolius	92.33±2.33	16.0±2.3	25.70±3.28
Excoecaria agallocha	25.00±5.13	29.7±9.6	34.00±10.97
Sonneratia alba	27.00±3.21	76.70±6.94	56.00±6.11
Aegiceras corrticulatum	21.30±2.02	67.70±9.74	30.80±3.28
Bruguira gymnorrhiza	14.66±3.71	60.30±9.49	42.00±6.24
Porteressia coarctata	62.33±6.38	19.70±3.93	51.30±4.41
Ceriops tagal	8.33±1.45	14.00±3.61	46.0±11.7

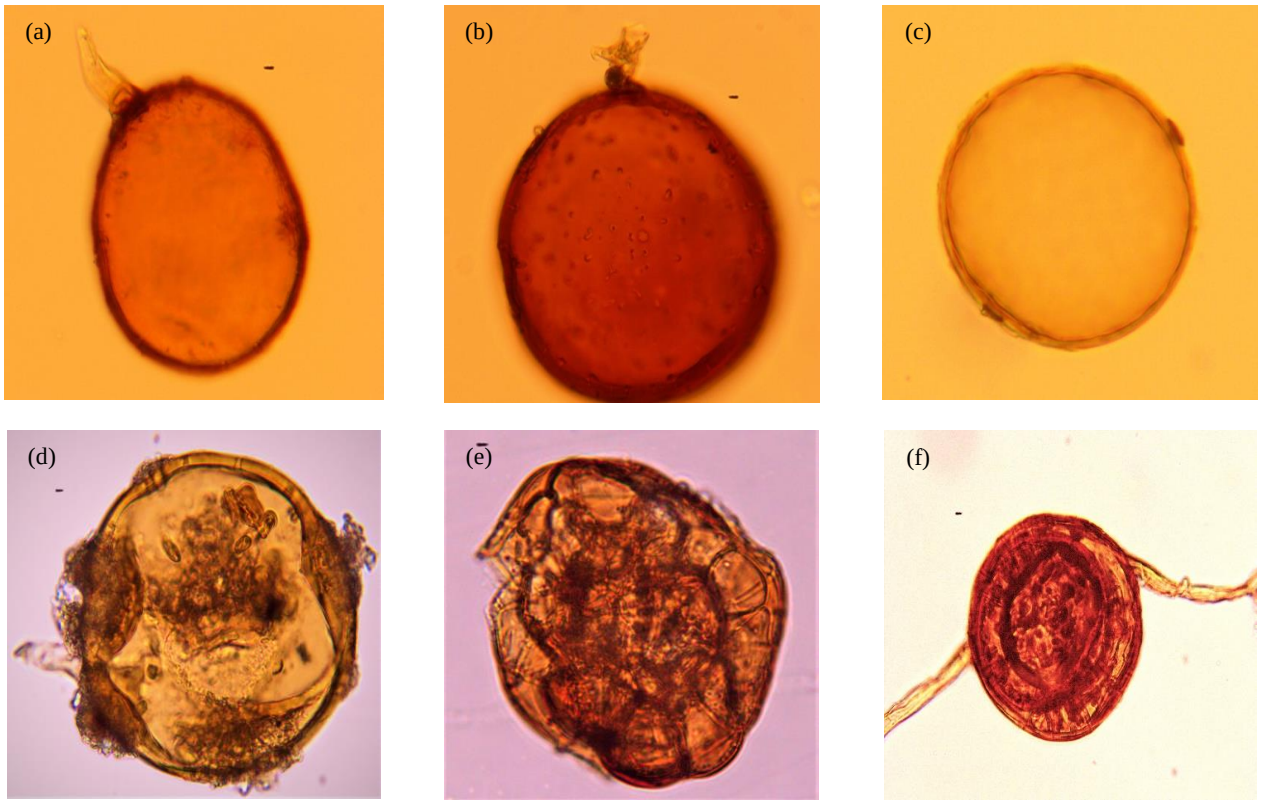

Figure 1. Tentative identification of spores; (a) *Glomus mossae*, (b) *G. macrocarpon*, (c) *Acaulospora* sp., (d) *Gigaspora* sp., (e) *Sclerocystis* sp., (f) *Glomus multicauli*

Table 3. Seasonal variance of relative abundance (RA) of AM fungi in selected study site

Species	Monsoon RA (%)	Pre-monsoon RA (%)	Post monsoon RA (%)
Acaulospora kentinensis	0.457	1.5	0.42
A. laevis	0.685	2.6	0.63
A. dilatata	0.685	1.9	2.1
A. excavata	0.913	2.1	1.26
A. foveata	1.826	1.3	2.31
A. morrowiae	0.457	1.3	1.47
A. polonica	0.457	0.2	0.42
A. scorbiculata	0.913	0.4	2.94
A. spinosa	1.37	1.3	2.94
Ambispora apendiculata	0.685	0.4	1.89
Cetraspora pellucida	0.457	0.6	1.89
Chlyamidospore	0.457	1.1	2.1
Claroideoglomus claroideum	1.826	0.9	0
C. luteum	0.685	0.2	0
Dentiscutata heterogama	1.826	1.3	2.31
Diversispora eburnea	3.881	1.5	3.14
D. epigaea	3.425	3.4	4.19
D. jakucsiae	0.457	2.8	0.84
D. spurca	0.685	3	3.98
Entrophospora	1.142	3	2.31
Funneliformis geosporum	1.142	3.8	3.35
F. mosseae	1.142	2.3	5.03
F. verruculosum	0.685	3.8	5.24
Glomus coronatum	1.826	2.6	1.68
G. diaphanum	1.142	2.3	0.63
G. macrocarpum	2.74	3.2	0
G. microcarpum	1.37	1.1	0
G. multicaule	0.228	2.3	0
G. myriocarpa	0.228	1.3	0
G. versiforme	0.457	0.9	0
Gigaspora gigantes	1.826	2.1	0
Gigaspora margarita	3.196	2.3	1.68
G. australe	1.826	0.9	3.56
G. badium	2.968	0.9	3.14
G. caledonius	2.968	0.4	2.52
G. clarum	2.74	0.6	2.31
G. deserticola	5.023	1.1	0.84
G. glomerulatum	4.795	0.9	1.05
G. halontatum	2.283	0.9	0
G. hoi	0.457	1.3	0
G. maculosum	2.74	1.9	0
G. pellucidum	2.055	3.2	0
G. warcupii	1.826	2.8	0
Rhizophagus aggregatum	4.795	3	0
R. fasciculatus	4.11	2.8	2.94
R. intraradics	5.023	2.6	3.14
R. manihotis	2.74	1.5	3.77
Racocetra castanea	0.228	1.1	5.03
R. clarus	0.228	0.6	1.05
R. fasciculatus	1.826	2.3	2.73
R. invermaius	0.457	1.1	3.14

Table 3. Seasonal variance of relative abundance (RA) of AM fungi in selected study site (cont.)

Species	Monsoon RA (%)	Pre-monsoon RA (%)	Post monsoon RA (%)
R. irregularis	0.685	1.3	2.52
Sclerocystis pubescens	0.685	0.9	0.84
Sclerocystis sinuosum	1.598	0.9	1.68
Scutellospora	3.881	0.9	0.84
Scutellospora dipurpurascens	0.913	1.3	0
Scutellospora fulgida	1.598	1.7	1.68
Scutellospora heterogama	0.913	1.1	1.05
Septoglomus	1.142	3	0.63
Septoglomus constricum	0.228	0.9	0.84

Table 4. Pearson correlation of coefficient between RA vs. IF, Simpson vs. Shannon index and Species evenness vs. richness

Ecological parameters	Monsoon	Pre-monsoon	Post-monsoon
RA vs. IF	0.6851	0.6004	0.872
Evenness vs. Richness	-0.374	-0.215	-0.589
Simpson vs. Shannon	-0.343	0.1539	0.9592

Species richness as well as evenness was maximum in the monsoon season, and minimum in pre and post monsoon seasons. Whereas, Simpson and Shannon index were higher in monsoon but lower in the post monsoon season. Species evenness showed a non-significant correlation (Figure 2) with species richness only in post monsoon, (r=-0.589) pre, and monsoon season (r=-0.215, r=-0.374). However, the Simpson index showed a significant correlation with the Shannon index (Table 4) only in the post monsoon season (r=0.9592), but a non-significant correlation in both monsoon and pre-monsoon season (M. r=-0.343, Pr. r=0.1539).

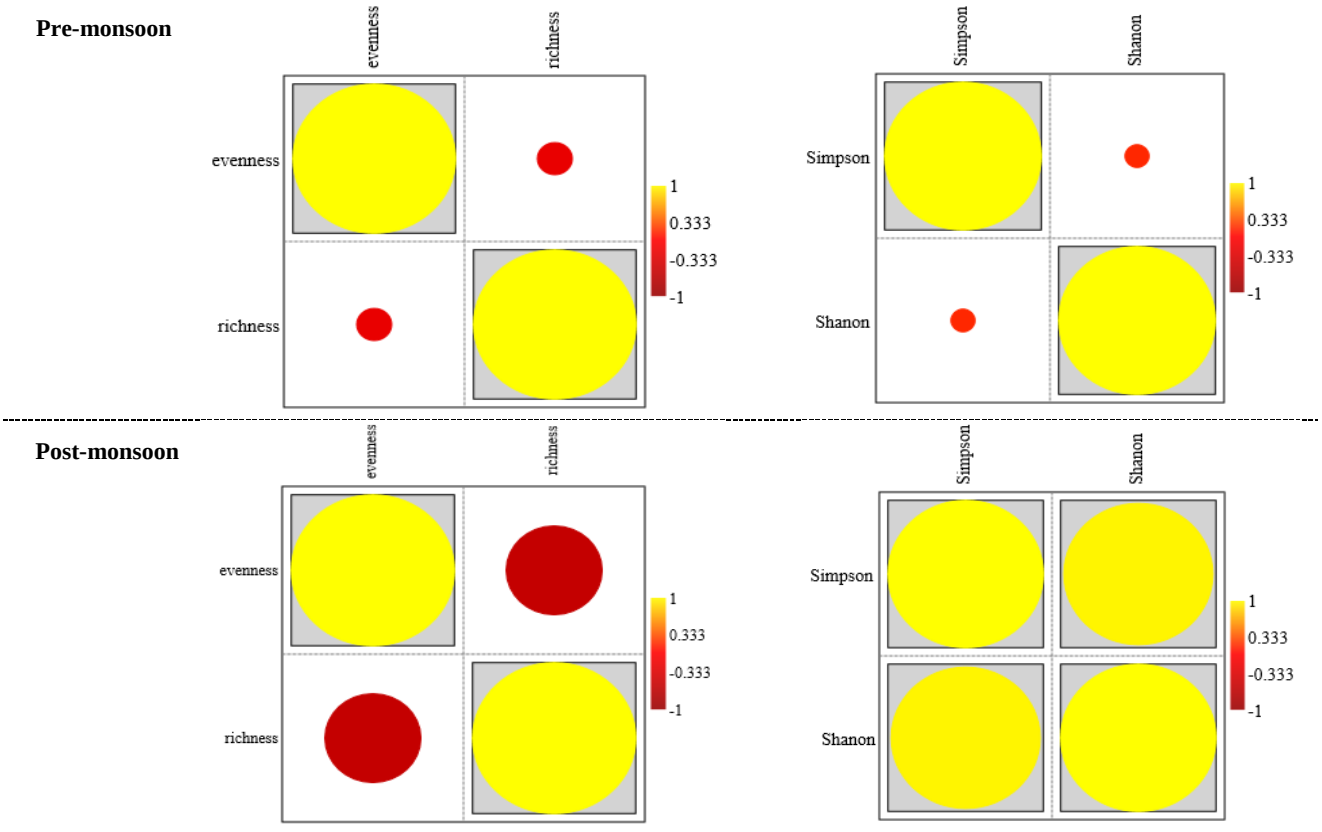

Figure 2. Plot diagram of seasonal variation in Pearson correlation coefficient of AMF species in listed a mangrove plants; Species evenness vs. richness-left one and Simpson vs. Shannon index -right one, boxed circle: p≤0.05

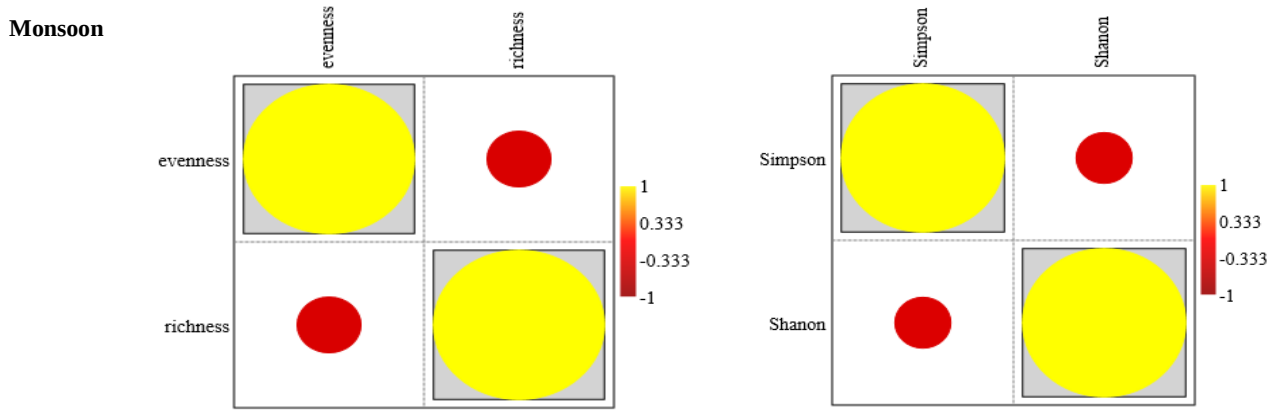

Figure 2. Plot diagram of seasonal variation in Pearson correlation coefficient of AMF species in listed a mangrove plants; Species evenness vs. richness-left one and Simpson vs. Shannon index -right one, boxed circle: p≤0.05 (cont.)

3.3 Cluster analysis

Cluster analysis (Figure 3) was done based on the RA of AMF species. All the AMF species were grouped into 7 clusters at a similarity level 33%. Further, cluster I subdivided into two sub-clusters at 77% similarity, cluster II at 69% similarity, cluster III at 75%, cluster IV at 69%, cluster V at 65%, cluster VI at 77%, and cluster VII at 65% similarity. *G. deserticola* and *G. glomerulatum* showed the highest similarity at 95% in cluster VI, whereas *A. polonica* and *Claridioglomus* showed the lowest similarity in cluster VII, with 65%.

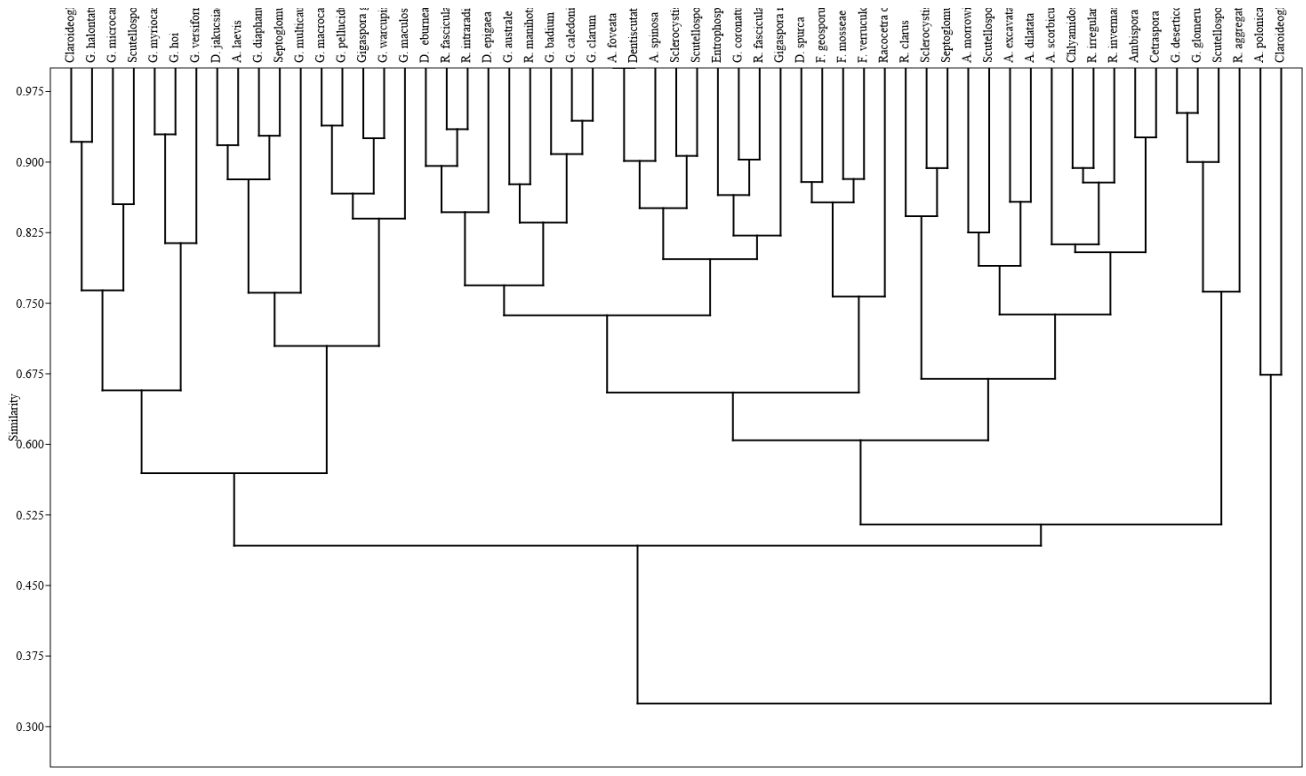

Figure 3. Bray-Curtis cluster analysis showing similarity in abundance of AMF species

4. DISCUSSION

The present study notes the variations in pH and EC values in mangrove soils which could be attributed by the continuous influx of tidal water, further leading to salt deposition (Rodrigues and Anuradha, 2009). In both type of mangroves, the level of most of the macronutrients were low, including available P. However, it is well known that AMF can grow more rapidly in low nutrient soils, especially regarding P (Hindumathi and Reddy, 2011). Along with this, AMF contributions in improving nutrition uptake and community development in nutrient-deficient soil of

mangroves are also widely known (Sridhar et al., 2011). Inadequate formation of root hairs of mangrove plants may restrict the nutrient absorption, perhaps making them mycotrophic (Baylis, 1975; Tomlinson, 2016).

In this study, higher root colonization was found in associate mangroves such as *Acanthus ilicifolius* and *Aegiceras corrticulatum* rather than true mangroves (Figure 4) in monsoon season, whereas in true mangroves such as *Ceriops tagal*, *Bruguira gymnorrhiza*, and *Sonneratia alba*, colonization was higher in both the pre and post monsoon seasons. A similar kind of observation has been reported earlier (Gaonkar and Rodrigues, 2020; Wang et al., 2015). Seasonal variation in AMF spore density has also been found in selected mangrove species. An earlier study revealed that spore density patters might indicate a wide range of environmental factors that are conductive to sporulation rather than AMF activity in roots (Miller and Bever, 1999). In our study, a high spore density was observed in the pre and post monsoon rather than in the monsoon season. Previous studies have revealed similar observations (Gaonkar and Rodrigues, 2020; Sivakumar, 2013). During the dry season, increased spore density is believed to be a sign of accessible nutrients and root senescence, which in turn stimulates fungal sporulation as plant nutrients requirements decrease (Gemma et al., 1989).

In the present study, a significant positive correlation existed between RA and IF throughout the year, indicating that species with higher spore production are widely distributed, while fewer spore production clearly indicates a confined geographic range (Dandan and Zhiwei, 2007).

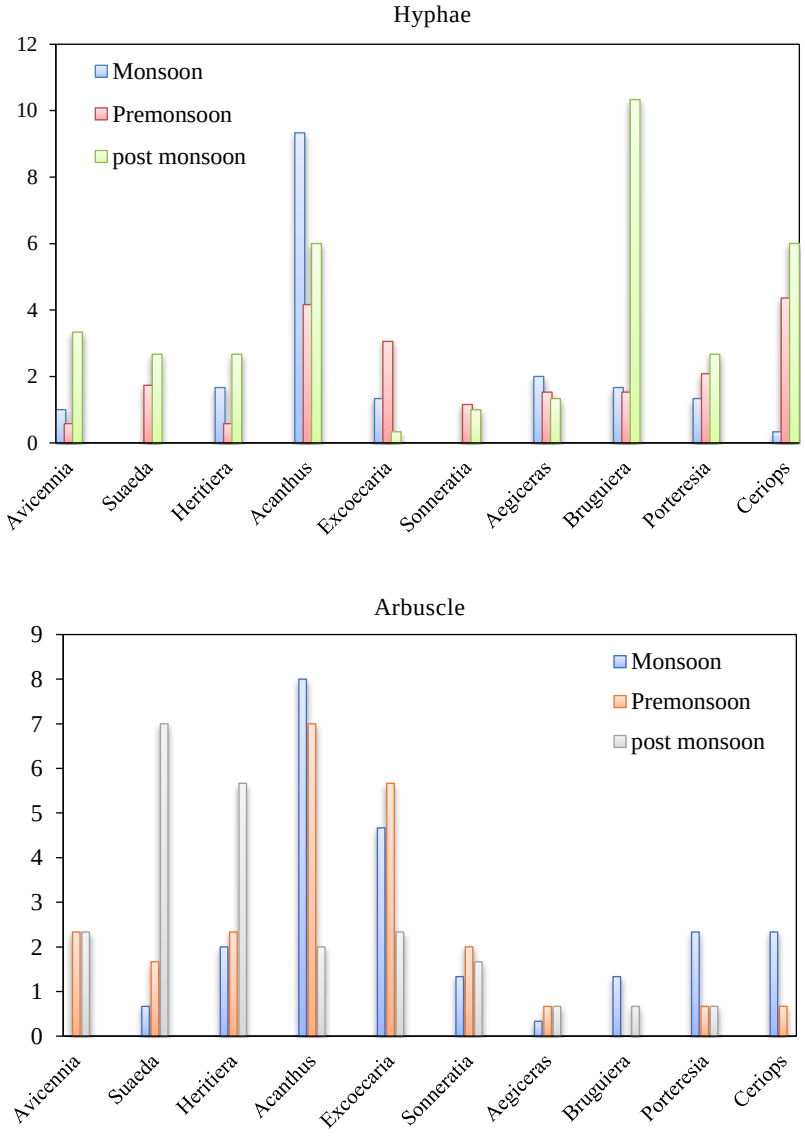

Figure 4. Graphical representation of seasonal data of root colonization

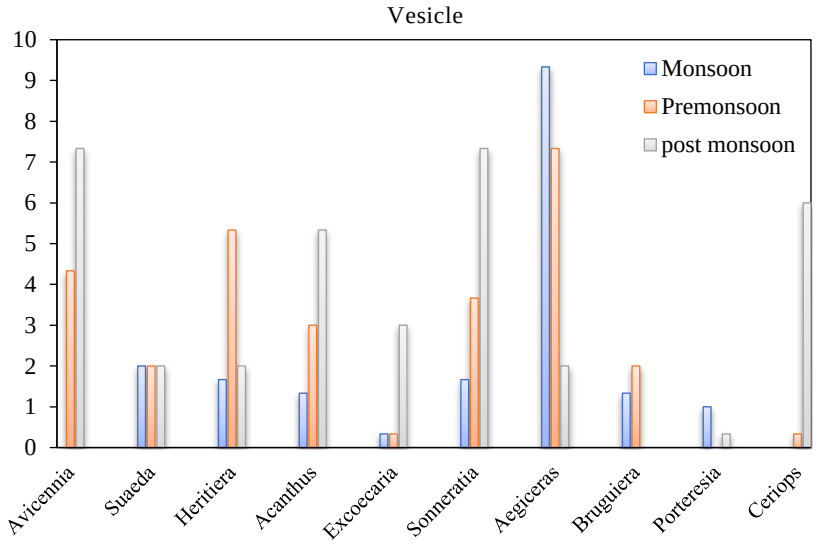

Figure 4. Graphical representation of seasonal data of root colonization (cont.)

G. deserticola and *R. intraradics* had the highest RA compared to other AMF species. It is well known that *Glomus* species are extensively dispersed and frequently found in various geographic regions (Stutz et al., 2000). Furthermore, this genus exhibits higher adaptability to changes in sporulation patterns under diverse environmental conditions, leading to their dominance (Stutz and Morton, 1996). A previous study revealed that the basic nature of mangrove soil might assured *Glomus* presence (Wang et al., 2011). The presence of a high AMF species diversity in Henry Island gives a clear indication of the site's diversity. Greater AMF diversity might be facilitated by the high environmental factors found in mangrove ecosystems (Fabián et al., 2018). A significant resemblance amongst AM species (almost 77%) suggested this widespread distribution. A similar kind of observation was recorded in a previous study (Sridhar et al., 2011).

The seasonal diversity found in the present study is higher than an early discovery in Indian mangroves, where 11 AM species representing 5 genera were recorded (D' Souza and Rodrigues, 2023), and then in South China, where only 6 species were reported (Wang et al., 2010). Our study supported previous findings that *Glomus* and *Rhizophagus* were the most widely distributed genus under alkaline condition (Parihar et al., 2019). AMF species were shown to be negatively impacted by soil alkalinity, whereas Glomeraceae family members registered more frequently, indicating a strong adaptation, which could be beneficial in restoring a damaged and disturbed alkaline ecoregion (Parihar et al., 2019).

5. CONCLUSION

These findings hold significant ecological implications, as they provide a deeper understanding of the role of AMF in enhancing the resilience and productivity of mangrove ecosystems in the Sundarban coastal region, India. Furthermore, the adaptability of certain AMF genera, such as *Glomus*, suggests their potential utility in ecosystem restoration and conservation efforts. Overall, this study contributes to the broader body of knowledge surrounding mangrove ecology in the Asian coastal ecosystem, highlighting the intricate dynamics of AMF associations and their ecological importance. Further research in this area could lead to more targeted conservation and restoration strategies for mangrove habitats, which are vital for both biodiversity and coastal protection.

ACKNOWLEDGEMENTS

The authors would like to thank the council of scientific and industrial research (CSIR), New Delhi, India, for awarding Junior Research Fellowship to Ms Supriti Paul and Ms. Ranjna Kaundal for their Ph.D. programme and Vipin Parkash also would like to thank the director, Forest Research Institute (ICFRE), Dehradun,Mr. Samim Pradhan-Deputy ranger of Bakkhali, Sundarban, India and Mr. Pranab Roy, asst. teacher, WB This research did not receive any specific grant from funding agencies in the public, commercial

or non-profit sectors. Although Ms. Supriti Paul and Ms. Ranjna Kaundal are receiving SRF for their Ph.D. programme. This research was supported by the faculties of Forest pathology department of FRIDU, Dehradun, Uttarakhand and department of Microbiology of St. Xaviers College, Kolkata, India.

SOFTWARE AVAILABILITY STATEMENT

The software used in this study are free and these are: PAST software version 4.03 is available upon registration at (https://past.en.lo4d.com/windows), while SPSS software is available upon downloaded version at (https://www.ibm.com/support/pages/downloading-ibm-spss-modeler-160).

AUTHOR'S CONTRIBUTION

Supriti Paul wrote the manuscript and designed the project. Ranjna Kaundal, Bikram Dhara, Meghna Thapa contributed to the editing. Vipin Parkash (Correspondence) contributed to supervision and Arup Kumar Mitra to co-supervision. All the authors approved the final version of the manuscript.

CONFLICT OF INTEREST

The authors have no conflicts of interest to declare.

REFERENCES

Akaji Y, Inoue T, Taniguchi T, Baba S. Arbuscular mycorrhizal fungal communities of a mangrove forest along a salinity gradient on Iriomote Island. Plant and Soil 2022;472:145-59.

Akram H, Hussain S, Mazumdar P, Chua KO, Butt TE, Harikrishna JA. Mangrove health: A review of functions, threats, and challenges associated with mangrove management practices. Forests 2023;14(9):Article No. 1698.

Baylis GTS. *Magnolioid mycorrhiza* and mycotrophy in root systems derived from it. In: Endomycorrhizas. Academic Press; 1975. p.373-89.

Bray RH, Kurtz LT. Determination of total, organic, and available forms of phosphorus in soils. Soil Science 1945;59(1):39-46.

Constance A, Oehri J, Bunbury N, Wiesenberg GL, Pennekamp F, A'Bear L, et al. Soil nutrient content and water level variation drive mangrove forest aboveground biomass in the lagoonal ecosystem of Aldabra Atoll. Ecological Indicators 2022; 143:Article No. 109292.

D'Souza J, Rodrigues BF. Seasonal diversity of arbuscular mycorrhizal fungi in mangroves of Goa, India. International Journal of Biodiversity 2013;2013(1):Article No. 196527.

Dandan Z, Zhiwei Z. Biodiversity of arbuscular mycorrhizal fungi in the hot-dry valley of the Jinsha River, Southwest China. Applied Soil Ecology 2007;37(1-2):118-28.

Fabián D, Guadarrama P, Hernadez-Cuevas L, Ramos-Zapata JA. Arbuscular mycorrhizal fungi in a coastal wetland in Yucatan, Mexico. Botanical Sciences 2018;96(1):24-34.

Fan T, Luo M, Tan J, Hu D, Chen X, Huang J, et al. Incorporating biotic phosphorus-acquisition strategies into soil phosphorus transformation under long-term salinization in a tidal wetland. Catena 2023;231:Article No. 107274.

Finlay RD. Ecological aspects of mycorrhizal symbiosis: With special emphasis on the functional diversity of interactions involving the extraradical mycelium. Journal of Experimental Botany 2008;59(5):1115-26.

Gaonkar S, Rodrigues BF. Diversity of arbuscular mycorrhizal (AM) fungi in mangroves of Chorao Island, Goa, India. Wetlands Ecology and Management 2020;28:765-78.

Gemma JN, Koske RE, Carreiro M. Seasonal dynamics of selected species of VA mycorrhizal fungi in a sand dune. Mycological Research 1989;92(3):317-21.

Gerdemann JW, Nicolson TH. Spores of mycorrhizal Endogone species extracted from soil by wet sieving and decanting. Transactions of the British Mycological Society 1963;46: 235-44.

Hanway JJ, Heidal H. Soil analysis methods as used in Iowa State College Soil Testing Laboratory. Iowa State College of Agriculture Bulletin 1952;57:1-31.

Hindumathi A, Reddy BN. Occurrence and distribution of arbuscular mycorrhizal fungi and microbial flora in the rhizosphere soils of mungbean [*Vigna radiata* (L.) wilczek] and soybean [*Glycine max* (L.) Merr.] from Adilabad, Nizamabad and Karimnagar Districts of Andhra Pradesh state, India. Advances in Bioscience and Biotechnology 2011; 2(4):275-86.

Jackson ML. Soil Chemical Analysis. New Delhi, India: Pentice Hall of India Pvt. Ltd.; 1973. p. 151-4.

Li T, Yuan Y, Mou Z, Li Y, Kuang L, Zhang J, et al. Faster accumulation and greater contribution of glomalin to the soil organic carbon pool than amino sugars do under tropical coastal forest restoration. Global Change Biology 2023; 29(2):533-46.

Marro N, Grilli G, Soteras F, Caccia M, Longo S, Cofré N, et al. The effects of arbuscular mycorrhizal fungal species and taxonomic groups on stressed and unstressed plants: A global meta-analysis. New Phytologist 2022;235(1):320-32.

Miller SP, Bever JD. Distribution of arbuscular mycorrhizal fungi in stands of the wetland grass *Panicum hemitomon* along a wide hydrologic gradient. Oecologia 1999;119(4):586-92.

Parihar M, Rakshit A, Singh HB, Rana K. Diversity of arbuscular mycorrhizal fungi in alkaline soils of hot sub humid eco-region of Middle Gangetic Plains of India. Acta Agriculturae Scandinavica, Section B - Soil and Plant Science 2019; 69(5):386-97.

Phillips JM, Hayman DS. Improved procedures for clearing roots and staining parasitic and vesicular-arbuscular mycorrhizal fungi for rapid assessment of infection. Transactions of the British mycological Society 1970;55(1):158-61.

Rodrigues BF, Anuradha N. Arbuscular mycorrhizal fungi in Khazan land agro-ecosystem. In: Frontiers in Fungal Ecology, Diversity and Metabolites. New Delhi: I.K International Pvt Ltd.; 2009. p. 141-50.

Shankarammal C, Kalaiselvam M. Diversity of arbuscular mycorrhizal fungi in association with mangrove plants in Tamil Nadu, India. Kavaka 2023;59(1):16-24.

Sivakumar N. Effect of edaphic factors and seasonal variation on spore density and root colonization of arbuscular mycorrhizal fungi in sugarcane fields. Annals of Microbiology 2013; 63:151-60.

Sridhar KR, Roy S, Sudheep NM. Assemblage and diversity of arbuscular mycorrhizal fungi in mangrove plant species of the

southwest coast of India. In: Metras JN, editor. Mangroves Ecology, Biology and Taxonomy. New York: Nova Science Publishers; 2011. p. 257-74.

Stutz JC, Morton JB. Successive pot cultures reveal high species richness of arbuscular endomycorrhizal fungi in arid ecosystems. Canadian Journal of Botany 1996;74(12):1883-9.

Stutz JC, Copeman R, Martin CA, Morton JB. Patterns of species composition and distribution of arbuscular mycorrhizal fungi in arid regions of southwestern North America and Namibia, Africa. Canadian Journal of Botany 2000;78(2):237-45.

Su YY, Sun X, Guo LD. Seasonality and host preference of arbuscular mycorrhizal fungi of five plant species in the inner Mongolia steppe, China. Brazilian Journal of Microbiology 2011;42:57-65.

Tomlinson PB. The Botany of Mangroves. Cambridge, UK: Cambridge University Press; 2016.

Walkley A, Black IA. An examination of the Degtjareff method for determining soil organic matter, and a proposed modification of the chromic acid titration method. Soil Science 1934;37(1):29-38.

Wang L, Mu M, Li X, Lin P, Wang W. Differentiation between true mangroves and mangrove associates based on leaf traits and salt contents. Journal of Plant Ecology 2011;4(4):292-301.

Wang XQ, Wang YH, Song YB, Dong M. Formation and functions of arbuscular mycorrhizae in coastal wetland ecosystems: A review. Ecosystem Health and Sustainability 2022;8(1):Article No. 2144465.

Wang Y, Li T, Li Y, Qiu Q, Li S, Xin G. Distribution of arbuscular mycorrhizal fungi in four semi-mangrove plant communities. Annals of Microbiology 2015;65(2):603-10.

Wang Y, Qiu Q, Yang Z, Hu Z, Tam NFY, Xin G. Arbuscular mycorrhizal fungi in two mangroves in South China. Plant and Soil 2010;331:181-91.

Environment and Natural Resources Journal

Volume 22
Issue 5
2024

Comparison of the Yield and Quality of Teak Wood from Different Plantations in Phrae Province, Thailand

Thiti Wanishdilokratn[1], Siriluk Sukjareon[1], Itsaree Howpinjai[1], Teeka Yotapakdee[2], Wanwasa Wirojanarome[2], Ratchaneewan Kamton[2], Siriporn Kiratikarnkul[3], and Lamthai Asanok[4*]

[1]Department of Forest Industry Technology, Maejo University Phrae Campus, Thailand
[2]Department of Applied Economics for Community Development, Maejo University Phrae Campus, Thailand
[3]Department of Economics, Maejo University, Thailand
[4]Department of Agroforestry, Maejo University Phrae Campus, Thailand

ARTICLE INFO

Received: 18 Mar 2024
Received in revised: 26 Jul 2024
Accepted: 2 Aug 2024
Published online: 29 Aug 2024
DOI: 10.32526/ennrj/22/20240069

Keywords:
Phrae/ Teak plantation/ Thailand/ Wood industry/ Wood quality

*** Corresponding author:**
E-mail: lamthainii@gmail.com

ABSTRACT

This study aims to compare the yield and quality of Teak wood from a Forest Industry Organization (FIO) plantation and a private teak plantation (PTP) in Thailand to provide guidelines for the sustainable utilization of teak wood. To quantify yields, we employed a randomized design at two locations (FIO and PTP), and determined volumetric proportions, the yields of milled teak and wood properties. We found that the whole lumber yield differed significantly ($p \leq 0.05$) between the two locations, although the yield of lumber sheets did not differ ($p > 0.05$). While more teak wood was produced at the FIO plantation than the PTP, the sawing techniques used at the two locations resulted in no significant difference in wood yield. Wood drying had significantly different effects ($p \leq 0.05$) between the two locations, but the drying method did not differ ($p > 0.05$). Overall, the lumber yields were greater for timber harvested from an FIO plantation than a PTP. Even though there are differences in sawing techniques adopted, the final lumber yield did not differ significantly between these two sources. The mechanical properties of teak wood improved with kiln drying, FIO plantation exhibits better properties than dried wood from the PTP.

1. INTRODUCTION

There is a huge demand for timber resources worldwide (Abdulah et al., 2020). However many countries, including Thailand, are experiencing decrease in forest area due to deforestation and illegal logging and the country imposed a total ban of export of round logs since 1989. Given their large economic impact, forest resources require careful management. Teak (*Tectona grandis*) is an important forest product (Dotaniya et al., 2013; Seviset et al., 2017; Udayana et al., 2019). Teak-wood is renowed for its wood qualities such as its appearance, strength, and durability and is being used in a variety of exterior and interior applications including furniture manufacture (Lima et al., 2021). In Thailand, teak wood production is being solely managed by the Forest Industry Organization (FIO); however, production did not meet the demand under this framework (Kalu and Adeyoju, 2011; Tewari and Mariswamy, 2013). Therefore, Thai government enacted a policy allowing smallholder farmers plant teak tress in their homesteads and promoting and commercial private teak plantations (PTPs).

Several studies have reported that the quantity and quality of teak sourced from the FIO and PTPs differs (Solorzano et al., 2012; Adi et al., 2016). Therefore, efforts are underway to adopt various technologies that improve these wood characteristics to avoid wastage. For instance, saw milling technologies and sawyer expertise impact lumber quantity and efficiency in sawn timber recovery processess. Kaakkurivaara (2022) suggested many

Citation: Wanishdilokratn T, Sukjareon S, Howpinjai I, Teeka Yotapakdee T, Wirojanarome W, Kamton R, Kiratikarnkul S, Asanok L. Comparison of the yield and quality of teak wood from different plantations in Phrae Province, Thailand. Environ. Nat. Resour. J. 2024;22(5):431-436. (https://doi.org/10.32526/ennrj/22/20240069)

ways of timber processing technologies to eliminate skidding and harvesting loss of teakwood from FIO plantations before being transported to sawmills. Circular saws are widely used in the lumber industry as they are efficient, stable and precise, thus limiting wastage (Krilek et al., 2014; Li and Zhang, 2017). Moreover, wood drying (seasoning) is the most important stages among wood processing because dried wood at moisture content around 12% offers major advantages over freshly sawn wood, including improved mechanical properties (Batista et al., 2017). For instance, timber intended for furniture and other interior woodwork should be dried to a target moisture content (MC) of 12-15% (Loucanova et al., 2017; Rabidin et al., 2017) under tropical conditions. Various wood seasoning kiln methods are adopted with different characteristics such as steam-heated kilns, dehumidification kilns, electric kilns, solar kilns, and other advanced wood-drying processes.

Phrae province in northern Thailand has a large teakwood industry that employs more than 12,000 people and is valued at >1,800 million baht per year (Yotapakdee et al., 2015). Improving this industry will add value to the local economy and develop infrastructure (Stone et al., 2011). However, there are no authentic data available comparing teak wood is sourced from the FIO and PTPs.

This study investigated the lumber yield and wood properties of teak from FIO plantations and PTPs in Phrae Province, Thailand, with the aim of providing information to help support the sustainable use of this valuable resource.

2. METHODOLOGY

2.1 Study site

The study was undertaken in FIO's teak plantation (47Q, x=656673, y=2040833) and a PTP (47Q, x=618202, y=1996767) located in Phrae Province, Thailand. In each site, timber yields of whole lumber, wood slabs, and sawdust produced by two types of sawmills was determined: a "standard" sawmill (The sawmill has been inspected and complies with the standards for sawing) and a "general" sawmill (The sawmill that uses traditional local wisdom for sawing). The yield of lumber sheets, wood residues and was also assessed and quantified. The properties of wood dried using different technologies of wood-drying kiln with direct heat ("standard" wood-drying kiln and "general" wood-drying kiln).

2.2 Wood sample preparation

Twenty numbers of defect-free (without bends or insect holes or knots) 25 year old teak trees were randomly selected from both the FIO plantation and PTP and harvested, cross cut with a length of about 2.5 m having a girth of 30-40 cm. The lumber was dried for 120 h in a standard kiln at the FIO plantation and in a general kiln at the PTP. To assess the teak wood properties, samples were cut from middle part of tree for each tests: 60 samples measuring 20×20×40 mm was used to determine the MC after drying in an oven for 24 h at 103±2°C; 60 samples measuring 20×20×300 mm were used to assess shrinkage in the cross-sectional or Longitudinal (X), radial (R), and tangential (T) directions after soaking in water for 24 h; and 60 samples measuring 20×20×300 mm were used to assess the modulus of rupture (MOR) and modulus of elasticity (MOE) using a Universal testing machine (BPS INSTRUMENT; BA-100) with BS373 standard (1985) and ASTM D143 (2014).

2.3 Experimental design

For the quantitative wood-sawing experiments, a randomized design was used involving two treatments (FIO and PTP), with 20 replicates per treatment. The first experiment assessed the yields of the whole lumber, wood slabs, and sawdust. Wood slabs and sawdust were measured and calculated based on sawblade thickness, number of cuts, and lumber width and length. Then, the yields after milling were quantified based on the volumes of whole lumber and each sheet produced; the difference between these values corresponded to the wood residue.

Next, wood properties were assessed following a randomized design with six treatments: two locations (FIO and PTP) and three drying methods ("standard" wood drying kiln, "general" wood drying kiln, and no drying- control). The treatment groups were as follows: FIO_1, FIO wood dried in a standard kiln; FIO_2, FIO wood dried in a general kiln; FIO_{ND}, undried FIO wood; PTP_1, PTP wood dried in a standard kiln; PTP_2, PTP wood dried in a general kiln; and PTP_{ND}, undried PTP wood. The average values were calculated for FIO_1 and FIO_2 (FIO_D); and PTP_1 and PTP_2 (PTP_D) for comparison with the undried control samples. For each treatment group, MC, MOR, MOE, and shrinkage were tested. Thus, a total of 120 samples (6 groups×4 tests×5 replicates) were used.

2.4 Data collection

The timber volume was calculated based on the volume of a cylinder:

$$\text{Timber volume } (m^3) = \pi \times r^2 \times h \quad (1)$$

Where; π is 3.14, r is the log radius (m), and h is the log length (m).

Lumber volume was calculated based on the following formula (Lima et al., 2018):

$$\text{Lumber volume } (m^3) = L \times T \times W \quad (2)$$

Where; L is the length (m), T is the thickness (m), and W is the width (m).

Sawdust volume was determined as follows:

$$\text{Sawdust volume } (m^3) = T_{sb} \times N \times W \times L \quad (3)$$

Where; T_{sb} is the thickness of the sawblade (m), N is the sawing time, W is width of the lumber (m), and L is the length of the lumber (m).

The MC was determined as the difference in wood weight before and after drying (Moghanaki et al., 2013):

$$Mc\ (\%) = \frac{(W_1 - W_2)}{W_2} \times 100 \quad (4)$$

Where W_1 and W_2 are the weights before and after drying (g).

Finally, volumetric shrinkage was calculated as a percentage:

$$\text{Wood shrinkage } (\%) = \frac{(\text{Wood swelling change})}{(\text{Wood swelling size})} \times 100 \quad (5)$$

2.5 Data analysis

Statistical differences in yields were analyzed using a t-test. Wood properties were analyzed using one-way analysis of variance (ANOVA). All analyses were performed using SPSS for Windows software (ver. 20.0; IBM Corp., Armonk, NY, USA).

3. RESULTS AND DISCUSSION

3.1 Teak timber yield

The whole lumber yield from the FIO plantation (57.21±1.27%) was significantly higher than that of PTP (49.56±1.44%, p≤0.05). However, the proportion of timber processed into wood slabs was significantly lower from the FIO plantation (36.69±1.28%) than the PTP (44.94±1.60%, p≤0.05). There was no significant difference in the sawdust proportion between the FIO plantation (6.10±0.24%) and the PTP (5.50±0.16%, p>0.05) (Table 1). These results were similar to those of a previous study that reported that a lumber yield of 28-64% maximizes the economic value of wood (Adu et al., 2014).

The volumetric yield from timber is related to the sawblades, equipment capacity, timber dimensions, and human factors (Baltrušaitis and Pranckevičienė, 2005). For instance, Ovrum et al. (2009) suggested that timber length and diameter strongly influence the lumber yield. One study estimated a total volumetric yield of 47.6% after milling (Munoz et al., 2013). In another study, it was found that when the timber (including bark) was processed into boards, 40% yield was obtained, and of the remaining 60% planer shavings (10%), cutter shavings (26%), sawdust (13%), and bark (11%) (Melo et al., 2016). A previous study found that teak trees in FIO plantations had fewer buttress roots than those in PTPs, resulting in higher yields (Warner et al., 2016). Overall, these findings highlight the importance of intensive silvicultural management for lumber yield (Bermejo et al., 2004).

Table 1. Average percentage yields of whole lumber, wood slabs, and sawdust produced from timber harvested from an FIO plantation and PTP.

Source	Whole lumber yield	Wood slab yield	Sawdust yield
FIO	57.21±1.27	36.69±1.28	6.10±0.24
PTP	49.56±1.44	44.94±1.60	5.50±0.16
p value	≤0.001	≤0.001	0.347

Note: ANOVA was performed followed by t-test; p≤0.05 indicates statistical significance.

3.2 Teak lumber yield

There were no group differences in the proportion of lumber processed into sheets (FIO: 93.90±1.82%; PTP: 92.54±1.48%, p>0.05) or wood residues (FIO: 6.10±1.82%; PTP: 7.46±1.48%, p>0.05) (Table 2). These results were similar to those of Bomba et al. (2016). The milling equipment capacity, technology, and techniques impact the final lumber volume and wood residues produced (Wang and Rolf, 2003).

Table 2. Average percentage yields of lumber processed into sheets and wood residues from an FIO plantation and PTP.

Source	Lumber sheets	Wood residues
FIO	93.90±1.82%	6.10±1.82%
PTP	92.54±1.48%	7.46±1.48%
p value	0.307	0.307

Note: ANOVA was performed followed by t-test; p≤0.05 indicates statistical significance.

3.3 Impact of drying on teak wood properties

The MCs of teak wood were significantly lower in the FIO_D (10.38%) and PTPD (11.16%) treatments compared to the FIOND (29.95%) and PTPND (44.03%) treatments (all p≤0.05). This was similar to the results of Wanneng et al. (2014), who measured an initial MC of 47% in 25-year-old teak.

The MOR was significantly higher in FIO_D (100.91 MPa) than in PTP_D (83.35 MPa), FIO_{ND} (83.06 MPa), and PTP_{ND} (77.10 MPa) (all p≤0.05). The MOE of FIO_D (9,144.90 MPa) was significantly different from that of PTP_{ND} (7,993.20 MPa, p≤0.05), but not from those of PTP_D (8,541.50 MPa) or FIO_{ND} (8,375.80 MPa) (both p>0.05). Djati et al. (2015) measured MOR values in teakwood of 91.57 to 141 MPa, and MOE values of 9,332 to 10,684 MPa. Thulasidas and Bhat (2012) reported that wet, dry, and plantation teakwood at air-dry condition (12% m.c) had MOR values of 109.89, 118.01, and 111.20 MPa, respectively, and MOE values of 9,102.28, 9,709.90, and 10,045.21 MPa, respectively. Teak wood in all sites, dry sites, and wet sites had MOR values of 87, 75, and 88 MPa, respectively, and MOE values of 12,240, 9,920, and 12,420 MPa, respectively (Amoah and Inyoung, 2019; Rizanti et al., 2018) Kiln drying reduces the moisture content within the wood, which affects its strength.

Our FIO_D and PTP_D samples exhibited significantly less shrinkage values than the FIO_{ND} and PTP_{ND} samples in the X direction (0.14% and 0.18% vs. 0.34% and 0.45%, respectively), R direction (0.31% and 0.41% vs. 1.12% and 2.20%, respectively), and T direction (0.39% and 0.46% vs. 1.70% and 3.87%, respectively) (all p≤0.05; Table 3). These values are comparable to those measured in a previous study of teakwood, i.e., 0.49% (X), 3.50% (R), and 5.17% (T) (Miranda et al., 2010).

Table 3. Average MC, MOR, MOE, and shrinkage of dried and undried teak wood harvested from an FIO plantation and PTP.

Treatment	MC (%)	MOR (MPa)	MOE (MPa)	Shrinkage (%)		
				X	R	T
FIO_D	10.38^a	100.91^a	$9,144.90^a$	0.14^a	0.31^a	0.39^a
FIO_{ND}	29.95^b	83.06^b	$8,375.80^{ab}$	0.34^b	1.12^b	1.70^b
PTP_D	11.16^a	83.35^b	$8,541.50^{ab}$	0.18^a	0.41^a	0.46^a
PTP_{ND}	44.03^c	77.10^b	$7,993.20^b$	0.45^c	2.20^c	3.87^c
p value	≤0.001	≤0.001	≤0.04	≤0.001	≤0.001	≤0.001

Note: Different superscript letters (a-c) indicate significant differences among the treatments for each property in a column; ns, non-significant. ANOVA was performed followed by Duncan's new multiple range test at p≤0.05

3.4 Impact of drying method on teak wood properties

The lowest teakwood MC was obtained in FIO_1 (9.62%), which differed significantly from the MCs of FIO_2 (11.13%), PTP_1 (11.16%), and PTP_2 (11.18%) (all p≤0.05). In the tropical conditions, the optimum moisture content is around 12-15% with slight variations depending on the season and surrounding atmospheric humidity.

In addition, the mechanical properties of standing bending tests like MOR values of FIO_1 (104.28 MPa) and FIO_2 (97.54 MPa) were significantly higher than those of PTP_1 (84.51 MPa) and PTP_2 (82.20 MPa) (all p<0.05). Although FIO_1 (9,331.20 MPa) had the highest MOE, it did not differ significantly from those of FIO_2 (8,958.90 MPa), PTP_1 (8,647.00 MPa), and PTP_2 (8,436.00 MPa) (all p>0.05). These results were similar to those of Bhat and Priya (2004), who recorded MOR, MOE of 91.8 MPa and 8,436 Ma, respectively.

In this study, the lowest X shrinkage was observed in FIO_1 (0.14%), but it did not differ significantly from those of FIO_2 (0.15%), PTP_2 (0.17%), and PTP_1 (0.18%) (all p>0.05). The lowest R shrinkage was observed in FIO_1 (0.28%), which was not significantly different from that of FIO_2 (0.35%, p>0.05) but differed significantly from those of PTP_1 (0.39%) and PTP_2 (0.43%) (all p<0.05). The lowest T shrinkage was again observed in FIO_1 (0.33%), which differed significantly from those of FIO_2 (0.45%),

PTP_1 (0.45%), and PTP_2 (0.47%) (all $p<0.05$; Table 4). For teak wood harvested from 15, 20, and 25-year-old teak trees, Izekor and Fuwape (2011) reported mean R shrinkages of 1.51%, 1.30%, and 0.73% and mean T shrinkages of 3.14%, 2.23%, and 1.27%, respectively. Overall, the quality of the drying oven impacts the mechanical properties of wood (Alteyrac et al., 2006).

Table 4. Impact of drying treatment and lumber source on the MC, MOR, MOE, and shrinkage of teak wood harvested from an FIO plantation and PTP.

Treatment	MC (%)	MOR (MPa)	MOE (MPa)	Shrinkage (%)		
				X	R	T
FIO_1	9.62^{a}	104.28^{a}	$9{,}331.20^{ns}$	0.14^{ns}	0.28^{a}	0.33^{a}
FIO_2	11.13^{b}	97.54^{a}	$8{,}958.60^{ns}$	0.15^{ns}	0.35^{ab}	0.45^{b}
PTP_1	11.16^{b}	84.51^{b}	$8{,}647.00^{ns}$	0.18^{ns}	0.39^{b}	0.45^{b}
PTP_2	11.18^{b}	82.20^{b}	$8{,}436.00^{ns}$	0.17^{ns}	0.43^{b}	0.47^{b}
p value	<0.001	<0.001	0.25	0.58	0.01	0.05

Note: Different superscript letters (a-c) indicate significant differences among the treatments for each property in a column; ns, non- significant. ANOVA was performed followed by Duncan's new multiple range test at $p \leq 0.05$

4. CONCLUSION

The lumber yields were greater for timber harvested from an FIO plantation than a PTP in Thailand; however, even though there are differences in sawing techniques adopted, the final lumber yield did not differ significantly between these two sources. The mechanical properties of teak-wood improved with kiln drying, FIO plantation exhibits better properties than dried wood from the PTP.

ACKNOWLEDGEMENTS

We are grateful to Thailand Science Research and Innovation for financial support and the Knowledge Network Institute of Thailand. We are also indebted to Maejo University Phrae Campus and the Office of Agricultural Research and Extension Maejo University.

REFERENCES

Abdulah L, Suhendang E, Purnomo H, Matangaran JR. Measuring the sustainability of wood consumption at the household level in Indonesia: Case study in Bogor, Indonesia. Biodiversitas 2020;21(2):457-64.

Adi DS, Sudarmanto, Ismadi, Gopar M, Darmawan T, Amin Y, et al. Evaluation of the wood quality of platinum Teak wood. Teknologi Indonesia 2016;39(1):36-44.

Adu S, Adu G, Mensah KF, Boasiako CA, Effah B, Adjei S. Maximizing wood residue utilization and reducing its production rate to combat climate change. International Journal of Plant and Forestry Sciences 2014;1(2):1-12.

Alteyrac J, Cloutier A, Ung CH, Zhang SY. Mechanical properties in relation to selected wood characteristics of black spruce. Wood and Fiber Science 2006;38(2):229-37.

American Society for Testing and Materials (ASTM). D 143. Standard Methods of Testing Small Clear Specimens of Timber. American Society for Testing and Materials International; 2014.

Amoah M, Inyoung S. Comparison of some physical, mechanical and anatomical properties of smallholder plantation Teak (*Tectona grandis* Linn.f.) from dry and wet localities of Ghana. Journal of the Indian Academy of Wood Science 2019;16(2):125-38.

Baltrušaitis A, Pranckevičienė V. The influence of log offset on sawn timber volume yield. Materials Science (Medžiagotyra) 2005;11(4):403-6.

Batista DC, Lube VM, Silva JGMD, Barbieri J, Vitoria RD. Analysis of the kiln drying process of a sawmill in Espírito Santo state, Brazil: A case study. Brazilian Journal of Wood Science 2017;8(3):177-86.

Bermejo I, Canellas I, Miguel AS. Growth and yield models for Teak plantations in Costa Rica. Forest Ecology and Management 2004;189(1-3):97-110.

Bhat KM, Priya PB. Influence of provenance variation on wood properties of teak from the Western Ghat Region in India. IAWA Journal 2004;25(3):273-82.

Bomba J, Bohm M, Sedivka P, Friess F, Oralkova R. Influence of selected factors on the sawing capacity of sawmills in the Czech Republic. Scientia Agriculturae Bohemica 2016; 47(4):174-80.

British Standard (BS). BS 373. Method of Testing Small Clear Specimens of Timber. British Standards Institution; 1985.

Djati ID, Tauchi T, Kubo M, Terauchi F. Mechanical properties and characteristics of young Teak for making products. Bulletin of Japanese Society for the Science of Design 2015:62(3):25-34.

Dotaniya ML, Meena VD, Lata M, Meena HP. Teak plantation: A potential source of income generation. Popular Kheti 2013;1(3):61-3.

Izekor DN, Fuwape JA. Performance of Teak (*Tectona grandis* L.F) wood on exposure to outdoor weather conditions. The Journal of Applied Science 2011;15(1):217-22.

Kalu C, Adeyoju SK. Socioeconomic causes of unregulated Teak plantation exploitation in Edo State, Nigeria. Journal of Sustainable Forestry 2011;30(5):406-18.

Krilek J, Kovac J, Kucera M. Wood crosscutting process analysis for circular saws. BioResources 2014;9(1):1417-29.

Kaakkurivaara N. Chapter 6: Teak Timber Harvesting. p. 202-2011. In: Trisurat Y, Hwan-ok Ma, Yanuariadi T, Kant P,

Thulasidas PK, editors. Teak in Mekong for a Sustainable Future. Kasetsart University, Bangkok, Thailand; International Tropical Timber Organization; 2022. p. 359.

Li B, Zhang Z. Research on the effect of yield strength of circular saw blade on roll tensioning process. Journal of Wood Science 2017;63(2):140-6.

Lima ILD, Ranzini M, Longui EL, Barbosa JDA. Wood characterization of *Tectona grandis* L.F. cultivated in Brazil: A review of the last 30 years. Society and Development 2021;10(14):e162101421549.

Lima RBD, Ferreira RLC, Silva JAAD, Guedes MC, Oliveira CPD, Silva DASD, et al. Lumber volume modeling of Amazon Brazilian species. Journal of Sustainable Forestry 2018;38(3):262-74.

Loucanova E, Palus H, Dzian M. A course of innovations in wood processing industry within the forestry-wood chain in Slovakia: A Q methodology study to identify future orientation in the sector. Forests 2017;8(6):Article No. 210.

Melo RRD, Rocha MJ, Junior FR, Stangerlin DM. Análise da influência do diâmetro no rendimento em madeira serrada de cambará. Pesquisa. Florestal Brasileira 2016;36(88):393-8.

Miranda I, Sousa V, Pereira H. Wood properties of Teak (*Tectona grandis*) from a mature unmanaged stand in East Timor. Journal of Wood Science 2010;57(1):171-8.

Moghanaki SK, Khoshandam1 B, Mirhaj MH. Calculation of moisture content and drying rate during microwave drying. Applied Mechanics and Materials 2013;423-426:746-9.

Munoz GR, Gete AR, Regueiro MG. Variation in log quality and prediction of sawing yield in oak wood (*Quercus robur*). Annals of Forest Science 2013;70(7):695-706.

Ovrum A, Hoibo OA, Vestoi GI. Grade yield of lumber in Norway spruce (*Picea abies* (L.) Karst.) as affected by forest quality, tree size, and log length. Forest Products Journal 2009;59(6):70-8.

Rabidin ZA, Seng GK, Wahab MJA. Characteristics of timbers dried using kiln drying and radio frequency-vacuum drying systems. MATEC Web of Conferences 2017;108(10001):1-5.

Rizanti DE, Darmawan W, George B, Merlin A, Dumarcay S, Chapuis H, et al. Comparison of Teak wood properties according to forest management: Short versus long rotation. Annals of Forest Science 2018;75(2):1-12.

Seviset S, Piromgram T, Saributr U, Porncharoen R, Raerai K, Charoensettasilp S. Mechanical property of 9 years old thinning of Teak plantation in Thailand. Proceedings of the 3rd International Conference on Mechatronics and Mechanical Engineering; 2016 Oct 21-23; Shanghai: China; 2017.

Solorzano S, Moya R, Murillo O. Early prediction of basic density, shrinking, presence of growth stress, and dynamic elastic modulus based on the morphological tree parameters of *Tectona grandis*. Journal of Wood Science 2012;58(4):290-9.

Stone IJ, Benjamin JG, Leahy J. Applying innovation theory to Maine's logging industry. Journal of Forestry 2011; 109(8):462-9.

Tewari VP, Mariswamy KM. Heartwood, sapwood and bark content of Teak trees grown in Karnataka, India. Journal of Forestry Research 2013;24(4):721-5.

Thulasidas PK, Bhat KM. Mechanical properties and wood structure characteristics of 35-year old home-garden Teak from wet and dry localities of Kerala, India in comparison with plantation Teak. Journal of the Indian Academy of Wood Science 2012;9(1):23-32.

Udayana C, Andreassen HP, Skarpe C. Understory diversity and composition after planting of teak and mahogany in Yogyakarta, Indonesia. Journal of Sustainable Forestry 2019;39(5):494-510.

Wang CY, Rolf C. Frame sawing of stone: Theory and technology. Key Engineering Materials 2003;250:171-80.

Wanneng PX, Ozarska B, Daian MS. Physical properties of *Tectona Grandis* grown in Laos. Journal of Tropical Forest Science 2014;26(3):389-96.

Warner AJ, Jamreonprucksa M, Puangchit L. Development and evaluation of Teak (*Tectona grandis* L.f.) taper equations in northern Thailand. Agriculture and Natural Resources 2016;50(5):362-7.

Yotapakdee T, Kongsuban N, Lattirasuvan T, Mangkita W. Determinants of food bank from *Melientha suavis* Pierre in a rural community in Phrae Province, Thailand. Environment and Natural Resources Journal 2018;13(2):44-54.

Environment and Natural Resources Journal

Volume 22
Issue 5
2024

Space-Time Variability of Drought in Tay Nguyen Provinces, Vietnam Using Satellite-Based Vegetation Time Series from 2000 to 2023

Nguyen Quang Thi[1*] and Hoang Van Hung[2]

[1]*Faculty of Resources Management, Thai Nguyen University of Agriculture and Forestry, Mo Bach Str, Thai Nguyen City, Thai Nguyen Province 250000, Vietnam*
[2]*Thai Nguyen University, Tan Thinh Ward, Thai Nguyen City, Thai Nguyen Province 250000, Vietnam*

ARTICLE INFO

Received: 8 Mar 2024
Received in revised: 2 Aug 2024
Accepted: 5 Aug 2024
Published online: 30 Aug 2024
DOI: 10.32526/ennrj/22/20240063

Keywords:
Drought/ Earth observation/ Satellite data/ Vegetation condition/ MODIS/ Drought trends/ Vietnam

*** Corresponding author:**
E-mail:
nguyenquangthi@tuaf.edu.vn

ABSTRACT

Droughts are among the most costly hazards in Tay Nguyen (known as Vietnamese Central Highlands), causing significant threats to agriculture and vegetation ecosystems. This study investigated the spatial and temporal dynamics of vegetation-based drought in the Tay Nguyen Provinces of Dak Lak and Dak Nong, using a long-term series of Moderate Resolution Imaging Spectro-radiometer (MODIS) Vegetation Condition Index (VCI) from 2000 to 2023. The results exhibited a high positive correlation (R=0.73) between VCI and soil moisture-based drought index in drought-detected areas. Monthly analysis revealed severe drought events during the dry months, notably in 2005, 2010, 2013, 2016, and 2019. In contrast, wetter conditions were primarily observed during 2017-2018 and 2022-2023. Despite temporal variability of drought, larger trends of decreasing and increasing vegetation-based drought were detected during the dry season. These trends remained a relatively stable during the rainy season. Among vegetation types, shrubland exhibited the lowest VCI trends. This research offers valuable insights for stakeholders and policymakers to develop targeted strategies for sustainable land management and regional drought resilience.

1. INTRODUCTION

Drought, a recurring and inherent climatic phenomenon, exerts profound and far-reaching impacts on the environment and the economy (Gampe et al., 2021; Ha et al., 2022). It is a widespread occurrence, affecting nearly all climate zones and ecosystems across the globe. Traditionally, drought monitoring relied on station-based climate indices, and the Standardized Precipitation Index (SPI) was probably the most used drought index over the past decades (Mishra and Singh, 2010; Vicente-Serrano et al., 2010). However, in-situ climate observations are challenging to collect over large areas, especially in remote areas. Historical climate data records are often incomplete and fragmented, complicating long-term drought trend analysis and the derivation of spatial and temporal drought characteristics (AghaKouchak et al., 2015). Also, developing countries with limited resources often face challenges in establishing and maintaining a comprehensive network of weather and soil monitoring stations (Vu et al., 2018).

Recent advances in remote sensing enable near-real-time, consistent, and frequent drought observations over large areas (Le et al., 2020a). Also, open-source data policies in recent years have unlocked the archive of long-term remote sensing time series. Consequently, several satellite-derived vegetation-based drought indices have been developed for deriving vegetation-based drought information. Among the different vegetation-based drought indices, the Normalized Difference Vegetation Index (NDVI) was the most widely used index for detecting vegetation health and drought-related details (Kogan, 1990). However, this indicator has been criticized due to its susceptibilities to soil background reflectance and atmospheric interferences (Ha et al., 2023; Kogan,

Citation: Thi NQ, Hung HV. Space-time variability of drought in Tay Nguyen Provinces, Vietnam using satellite-based vegetation time series from 2000 to 2023. Environ. Nat. Resour. J. 2024;22(5):437-448. (https://doi.org/10.32526/ennrj/22/20240063)

1990). The Vegetation Condition Index (VCI) has emerged as a compelling alternative, demonstrating superior effectiveness in tracking drought-related conditions associated with vegetation (Le et al., 2021). Several recent studies have employed the VCI for monitoring and characterizing drought patterns across scales and climate zones (Marumbwa et al., 2020; Shahfahad et al., 2022; Wei et al., 2021; Zou et al., 2020).

In the Tay Nguyen Provinces, known as the Central Highlands in English, the agricultural sector plays a significant role in the local and national economy. Coffee crops in this region, such as Dak Lak and Dak Nong Provinces, account for nearly 90% of Vietnamese coffee production (Maskell et al., 2021). However, this region is drought-prone and frequently suffers from intense drought conditions. Ha et al. (2023) have reported multiple drought events (e.g., drought events in 2004-2005, 2015-2016, and 2019-2020) across Mainland Southeast Asia, including Vietnam. Also, Tran et al. (2023) reported a high risk of drought in some provinces of the Central Highlands, such as Dak Lak. Statistically, the 2015-2016 drought event damaged nearly 11 thousand hectares of cropland, including seasonal and industrial crops in the Central Highlands (Byrareddy et al., 2021; Le et al., 2021). Alarming projections indicate that drought hazards in this region are poised to intensify and occur more frequently in the coming decades (Nguyen-Ngoc-Bich et al., 2021). Consequently, there could be a threat of disruptions to crop production, posing a substantial risk to food security in the region.

In this study, our primary objectives are to monitor and assess the spatiotemporal variability of vegetation-based drought conditions using long time-series MODIS-based VCI observations in large-area industrial croplands and forest ecosystems of the two Vietnamese Central Highlands provinces. Firstly, we cross-verified the quality and reliability of time-series vegetation-based drought products. Subsequently, we assessed the spatial and temporal patterns of vegetation-induced drought conditions using monthly MODIS-based VCI time series during the dry and rainy seasons from 2000 to 2023. Lastly, a detailed analysis of spatiotemporal trends of vegetation-induced drought was explored in consideration of various land cover types over the study period. The findings of this study could provide valuable information for local agricultural and natural ecosystem management in mitigating vegetation-related drought impacts and developing drought adaptation plans in the face of the ongoing climate crisis.

2. METHODOLOGY

2.1 Study area

The study area spans the two provinces of Dak Lak and Dak Nong, located in the Central Highlands of Vietnam (Figure 1). Plateau landscapes and various elevations mainly characterize this area. Climate conditions are primarily controlled by tropical characteristics with annual temperature and precipitation ~22^{o}C and ~1,800 mm, respectively. There are two main climate seasons in the Central Highlands, Vietnam (Vu-Thanh et al., 2014): dry (November-April) and rainy (May-October) seasons. This area often lacks precipitation during the dry season, resulting in water and vegetation stress. By contrast, heavy rainfall during the rainy season impacts topsoil, such as soil erosion.

In the Central Highlands, basalt soils are predominantly distributed, accounting for nearly 60% of Vietnamese basalt soil. Due to its unique climate, soil, and elevation characteristics, Dak Lak and Dak Nong are considered the provinces of industrial crops (e.g., coffee and pepper) and had diverse vegetation types. Here, we classified the area into four main land cover types from Copernicus's land cover service product (Buchhorn et al., 2020): cropland, forests, shrubland, and others (e.g., built-up, water bodies, and bare land). Croplands account for 40% of the area and is primarily distributed in Dak Lak province, whereas forests ranked second with nearly 45% and mainly distributed in Dak Nong Province.

2.2 Datasets

This study utilized a set of various publicly available datasets, including time-series MODIS NDVI, Copernicus Global Land Service product, Digital elevation model (DEM), and soil moisture observations. Each dataset has different spatial resolution and coordinate systems, so we standardized them to the spatial resolution of MODIS NDVI 250 m and used a geographic coordinate system. This approach enables the power of multi-source data seamless integration for consistent, accurate, and timely drought monitoring and assessment. Although each dataset may come from different providers, these datasets are available from the Google Earth Engine (GEE) computing platform (Gorelick et al., 2017).

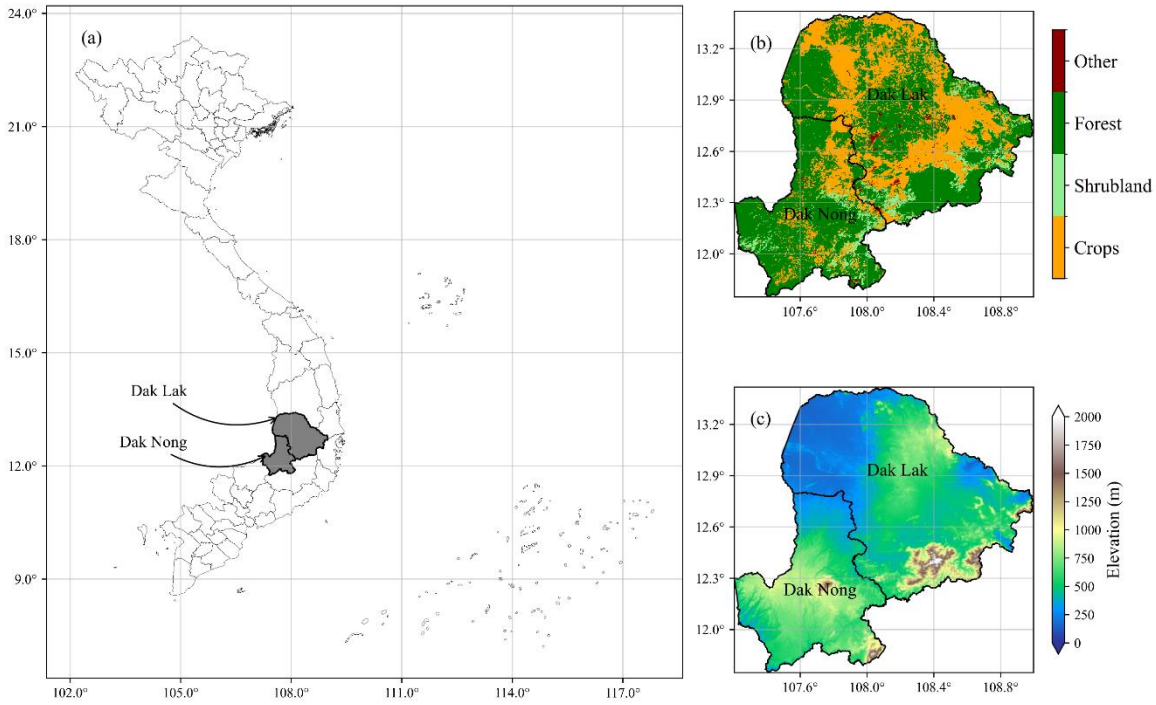

Figure 1. Map of the study area covers the two provinces of the Central Highlands Dak Lak and Dak Nong (a) and their land cover types (b) and elevation characteristics (c).

Monthly NDVI time series are aggregated from MODIS Terra (MOD13Q1 V6.1) and Aqua (MYD13Q1 V6.1) sensor collections at 250 m spatial resolution. These datasets are available through the NASA Land Processes Distributed Active Archive Center (LP DAAC) at the USGS Earth Resources Observation and Science (EROS) Center and can be accessed via the GEE catalog (https://developers.google.com/earth-engine/datasets/catalog/modis). Here, this study used both Terra and Aqua MODIS NDVI 16-day data products from 2000 to 2023 due to the challenges posed by cloud cover in tropical areas. The frequent and persistent cloud cover in these regions can significantly obstruct satellite observations (Li et al., 2018), leading to data gaps and reduced accuracy in monitoring drought dynamics. By leveraging the combined datasets from both MODIS sensors, we could mitigate the impact of cloud-related obstructions, ensuring a more comprehensive and continuous assessment of drought over the study period. Firstly, we removed cloud-related pixels from both MODIS NDVI 16-day products using its quality mask layers (DetailedQA band). Subsequently, we combined the two collections in time order and interpolated the missing observations using the linear interpolation method from the nearest temporal measurement. Next, we reconstructed the time series of MODIS NDVI observations using the Savitzky-Golay filter method with a 5-moving window and second-order polynomial (Ha et al., 2023; Savitzky and Golay, 1964). Finally, we aggregated the MODIS NDVI 16-day products into a monthly window using the median approach. A total of 287 monthly NDVI composites are used to investigate the spatiotemporal variability of vegetation-based drought conditions in the Central Highlands of Vietnam from 2000 to 2023.

The Copernicus Global Land Service provides a high-resolution, accurate, and consistent global land cover product from 2015 to 2019 at 100 m spatial resolution (Buchhorn et al., 2020) and can accessed via the GEE https://developers.google.com/earth-engine/datasets/catalog/COPERNICUS_Landcover_100m_Proba-V-C3_Global). This data product is produced from PROBA-V satellite observations using machine learning random forest algorithm with an overall accuracy of 80%, and its details can be found in a study by Buchhorn et al. (2020). This study employed the land cover product 2019, and we reclassified this data into four main land cover types, namely cropland, shrubland, forests, and others (e.g., built-up, water, and bare land). Non-vegetation types are masked from the formal analysis, and we finally resampled them to the spatial resolution of the MODIS NDVI at 250 m using the nearest neighbor method.

Monthly topsoil moisture (at 10 cm depth) observations were sourced from the Goddard Earth

Sciences Data and Information Services Center within the Famine Early Warning Systems Network Land Data Assimilation System (FLDAS). This dataset is produced monthly and spans from 1981 to the present at global scale, and it is commonly used to monitor agricultural drought (McNally et al., 2017). Here, soil moisture, together with soil properties (e.g., clay, sand, and organic carbon contents) was employed to derive a soil-based drought indicator from 2000 to 2023, and this index was used to cross-verify the MODIS-based drought. The soil moisture and soil properties data are in different spatial resolutions, but they are resampled to 250 m spatial resolution using the bilinear method to ensure the compatibility with the MODIS data.

The Shuttle Radar Topography Mission (SRTM) high-resolution DEM data was provided by NASA Jet Propulsion Laboratory (JPL) and downloaded from the GEE. This dataset has a spatial resolution of 30 m and covers a near-global scale. Here, we resampled the DEM into 250 m spatial resolution using the bilinear technique and converted it into a geographic coordinate system. In this study, the bilinear resampling method was chosen due to its computational efficiency and image quality. This approach produces smoother and better images than nearest-neighbor resampling, which selects the closest pixel and can result in blocky and jagged edges (Pu, 2021; Wu et al., 2022).

2.3 Vegetation-based drought index

Changes in vegetation health are reflective of altered ecosystem dynamics and can be indicative of water limitations and drought. Drought-induced shifts in vegetation cover, composition, and productivity provide more direct and early warning signs of impending water scarcity, making it a reliable and cost-effective tool for monitoring and characterizing drought. In this study, we used the Vegetation Condition Index (VCI) to monitor and assess drought dynamics in the two provinces of Central Highlands Dak Lak, and Dak Nong, from 2000 to 2023. The VCI has been developed by Kogan (1990) and is widely used for monitoring and characterizing drought conditions. The calculation of VCI relies on time series NDVI observations and is expressed in the following equation. At each pixel, monthly NDVI values are linearly scaled over the selected study period.

$$VCI_i = \frac{NDVI_i - NDVI_{min,j}}{NDVI_{max,j} - NDVI_{min,j}} \times 100$$

Where; VCI_i and $NDVI_i$ are the NDVI at month i, respectively. The $NDVI_{min}$ represents minimum NDVI values at month j (j=1, 2, 3, …, 12) across the years, while $NDVI_{max}$ indicates maximum NDVI values at respective j months. The VCI values are measured in percentage and range from zero to 100, indicating extreme drought conditions (stressed vegetation) to wet conditions (healthy vegetation), respectively. Generally, the VCI values are classified into five different levels of drought severity (Kogan, 1990): extreme drought (0-10%), severe drought (10-20%), moderate drought (20-30%), mild drought (30-50%), and normal condition (≥50).

2.4 Time series trends of vegetation-based drought

In this analysis, we used non-parametric Sen's slope and Mann-Kendall (MK) methods to identify the trends of time series vegetation-based drought between 2000 and 2023. These methods are proven to be robust to non-normality and widely employed to assess the presence and significance of trends in climate and vegetation time series. Sen's slope estimator, introduced by (Sen, 1968), is a non-parametric technique that calculates the median slope of all possible pairs of data points in the time series, providing an estimate of the magnitude of the monotonic trend. This approach is particularly advantageous because it is resistant to the effects of outliers and non-normality in the data. The Mann-Kendall test is a statistical test used to determine the significance and direction of the trend (Li et al., 2021; Mann, 1945). It is a rank-based method that evaluates the correlation between time and the variable of interest, thus identifying whether a significant upward or downward trend exists in the time series.

In this study, we computed per-pixel trends within a 95% confidence interval, examining both the dry and rainy seasons. The division of the data into these two distinct seasons serves a dual purpose, including mitigating potential issues arising from seasonality and addressing concerns related to the stationarity of the vegetation time series. This way we aim to enhance the precision of our trend calculations and provide a better understanding of the temporal dynamics, shedding light on variations specific to dry and rainy periods. The trend values range from negative to positive, where negative (positive) values represent the decreasing (increasing) direction of vegetation-based drought during the study period.

2.5 Cross-validation of vegetation-based drought condition

Spatially dense in-situ data observations play a key role in assessing and validating remote sensing-based drought products. However, it is very challenging to collect time-series station-based measurements such as soil moisture in Vietnamese Central Highlands. In this study, we derived the Soil Water Deficit Index (SWDI) (Mishra et al., 2017), a soil-based drought index, from monthly time-series FLDAS soil moisture and soil properties (e.g., clay and sand contents). The SWDI values generally range from -10 to +10, where negative (positive) values indicate drought (non-drought) conditions (Fang et al., 2021; Mishra et al., 2017). Due to its sensitivity and early detection of crop water stress, the SWDI has been widely used to monitor agricultural drought and offers crucial insights into the availability of moisture for plant growth and survival (Mishra et al., 2017). Specifically, we used the SWDI to cross-check the quality of MODIS-based drought using Pearson correlation analysis. Here, we checked the agreement in the percentage of detected drought areas between the VCI and SWDI, and we subsequently calculated Pearson correlation at each pixel using time-series VCI and SWDI observations over the selected study period. The Pearson correlation coefficients range from -1 to 1, where higher negative (positive) values represent a larger negative (positive) correlation between the two drought indices.

3. RESULTS AND DISCUSSION

3.1 Cross-validation of vegetation-based drought

We assessed the spatial correlation and drought-detected areas between the two datasets using Pearson correlation analysis during the dry season. Here, we cross-verified the VCI-SWDI relationship during the dry season because of the higher frequent and severe droughts in the study region. The annual average data over the dry season was prepared, and the Pearson coefficients were computed per-pixel over the study period.

Overall, a good agreement exists between VCI-based and SWDI-based drought indices. Spatially, higher correlations were more observed along the northern area of Dak Nong Province, while lower correlations were scattered across southern Dak Nong and central Dak Lak Provinces (Figure 2(a)). Notably, nearly 91% of the study area exhibited positive correlations between VCI and SWDI indices, indicating that soil moisture is positively associated with vegetation condition (Cao et al., 2022). It is also noted that statistically non-significant correlations are found in Dak Nong and Dak Lak Provinces, accounting for 20% of the study area.

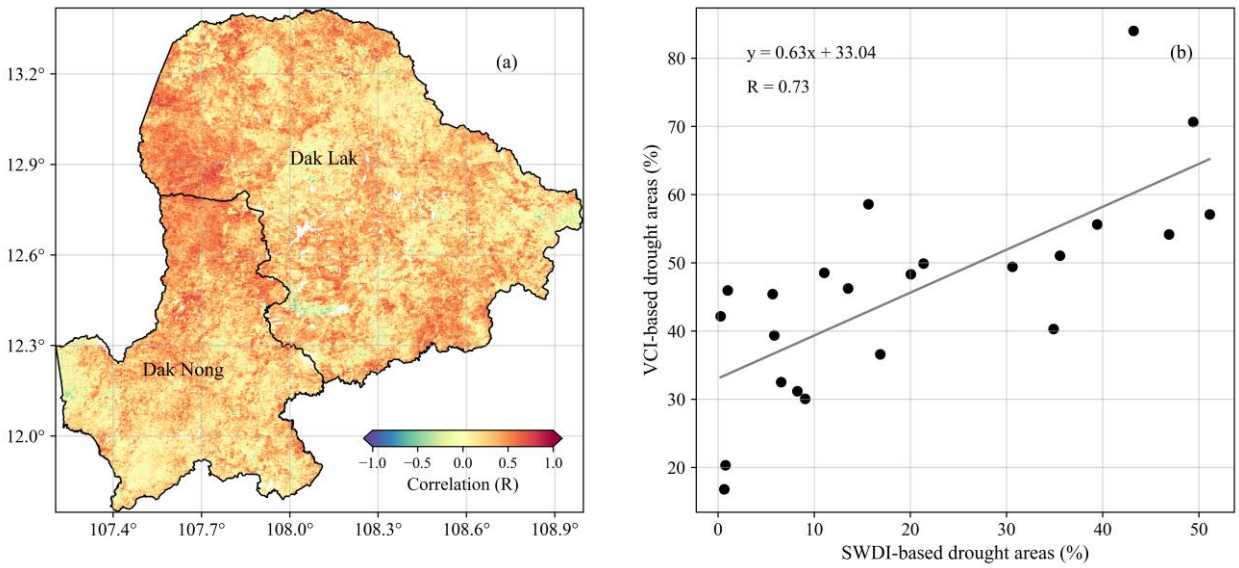

Figure 2. Spatial map and scatter plot show Pearson's correlation coefficients (a) and the agreement of drought-detected areas (b) between VCI and SWDI over the study period.

Apart from spatial assessment, Figure 2(b) displayed the agreement of drought-detected areas between VCI-based and SWDI-based drought indices. Overall, there is a high positive correlation between VCI and SWI indices in the percentage of the drought-affected areas from 2000 to 2023. The R-value is 0.73

and its relationship is linearly correlated, indicating that an increase in VCI-based drought areas is associated with an increase in SWDI-based drought areas. This agreement indicates that VCI-based drought can be effective and reliable in detecting drought-affected areas.

3.2 Spatiotemporal patterns of vegetation-based drought

3.2.1 Spatial patterns of seasonal droughts

In this section, we presented the spatiotemporal variability of vegetation-based drought (VCI) during both dry and rainy seasons from 2000 to 2023. Overall, there are significant spatial and temporal variations in VCI-based drought conditions across the study period. Notably, the dry seasons experienced higher exposure to drought vulnerability, particularly in the years 2004-2005, 2015-2016, and 2019-2020 (Figure 3). These timeframes marked critical phases of vegetation stress, possibly indicative of environmental factors such as reduced rainfall or elevated temperatures that exacerbated the impact of drought on the region's vegetation (Le et al., 2021). In addition, human activities might exaggerate the vegetation-based drought, such as agricultural shifting (Chen et al., 2023) and deforestation (Mermoz et al., 2021). Temporally, the dry season of 2005 suffered from the most severe drought (Figure 3), while the wettest conditions were observed during the periods 2017-2018 and 2022-2023. Notably, recent drought conditions were primarily found in the northern area of Dak Lak, for example, in 2019 (Figure 3).

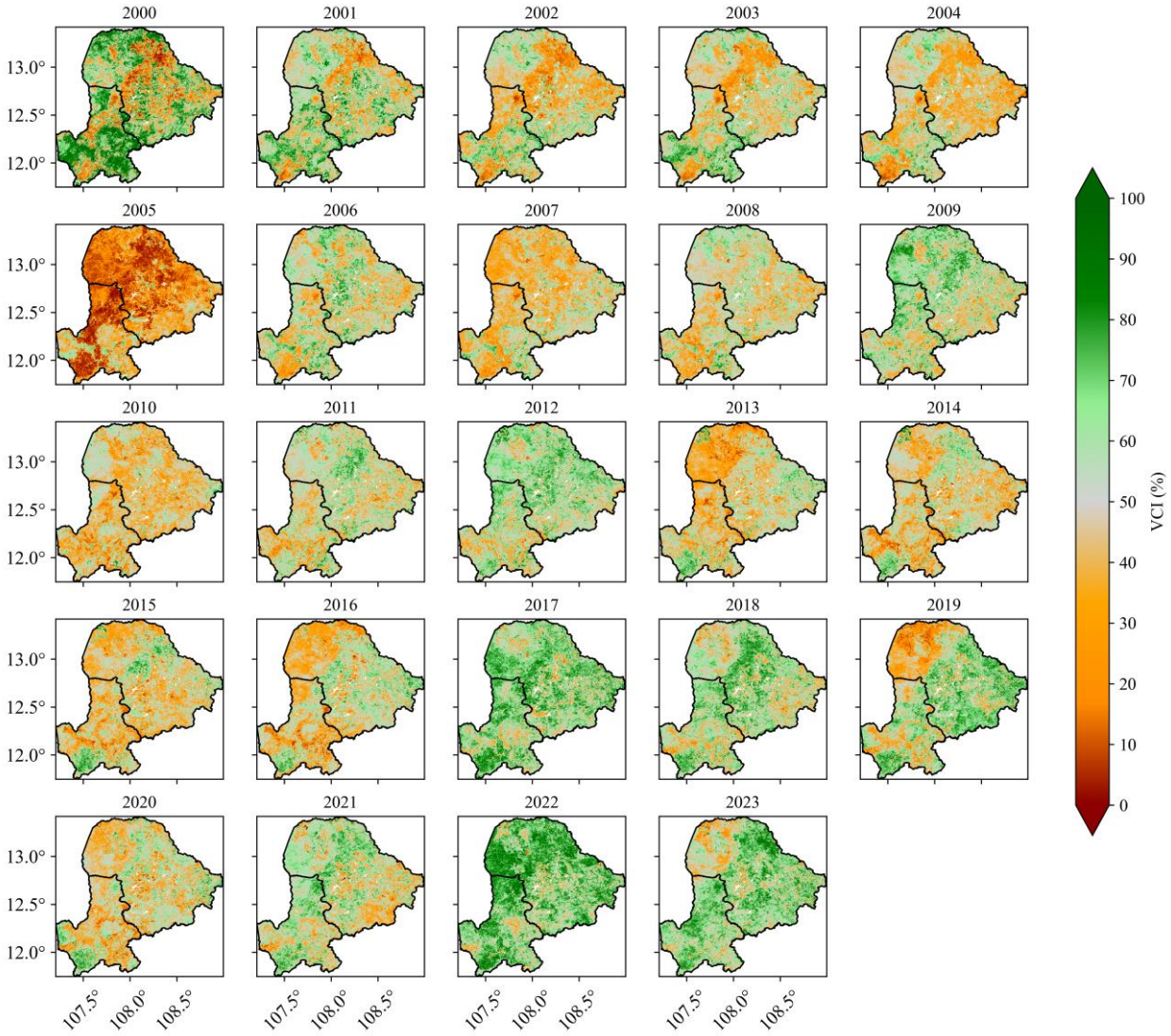

Figure 3. Annual variability of mean drought conditions during the dry seasons from 2000 to 2023. Red indicates severe drought, while green indicates wet conditions. Gray refers to normal conditions.

Likewise, the study area experienced VCI-based drought conditions during the rainy season, particularly in the early 2000s. However, the degree of drought severity was much lower compared to the dry season (Figure 4). For example, larger areas of drought were detected in Dak Lak Province from 2000 to 2005, but in recent years, the province experienced wetter conditions, especially in 2022 and 2023 (Figure 4). These findings shed light on the dynamic nature of VCI-based drought conditions, emphasizing the need for a better understanding of the interplay between climatic variables and vegetation health. The discerned patterns provide valuable insights for stakeholders and policymakers to develop targeted strategies for drought resilience and sustainable land management practices in the study area. For example, some areas in the northern Dak Lak Province and southern Dak Nong Province suffered more frequent drought, so it may require attention with respect to agriculture and vegetation ecosystems in these areas.

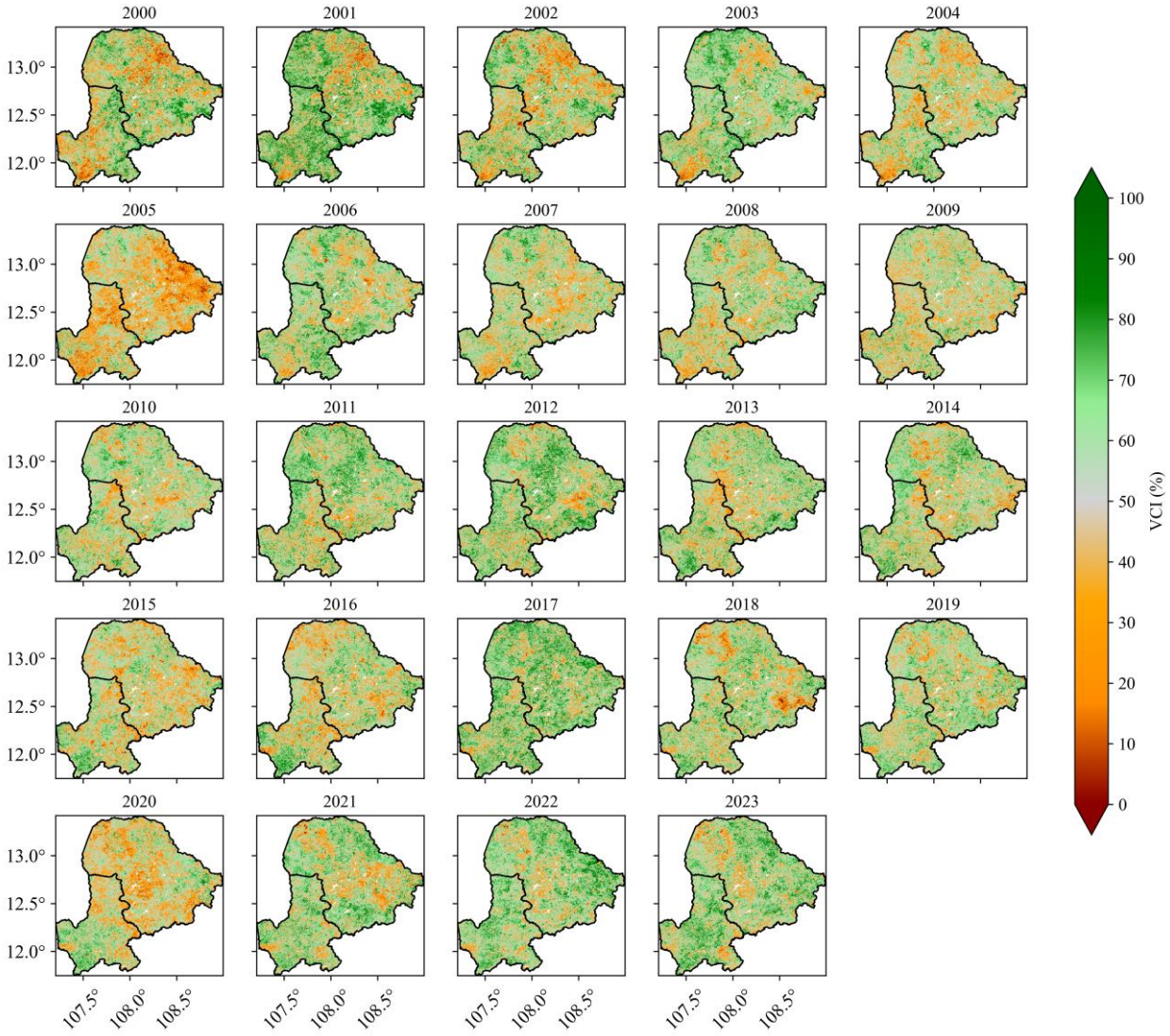

Figure 4. Annual variability of mean drought conditions during the rainy seasons from 2000 to 2023. Red indicates severe drought, while green indicates wet conditions. Gray refers to normal conditions.

3.2.2 Temporal analysis of drought

Figure 5 showed the monthly evolution of drought conditions over the two provinces of Dak Lak and Dak Nong from 2000 to 2023. It is clear that almost all drought events occurred in the region during the dry months. The lowest VCI values were observed in 2005, 2016, and 2020 (Figure 5), indicating the severe drought conditions during these periods. Also, the highest VCI values were found during the periods 2017-2018 and 2022-2023, suggesting a wetting condition during these years. The 2005 drought in the study region was the most severe, possibly due to the prolonged El Niño conditions (Phan-Van et al., 2022), which led to significantly reduced rainfall and higher-

than-average temperatures, exacerbating water shortages. In addition, changes in land cover and hydrological pattern could be also responsible for variations in the vegetation-based measurements (Le et al., 2020b; Mondal et al., 2022). These observations are aligned with recent studies in Vietnam (Le et al., 2020b; Le et al., 2021; Thien et al., 2024; Tran et al., 2023) and mainland Southeast Asia (Ha et al., 2023; Li et al., 2022).

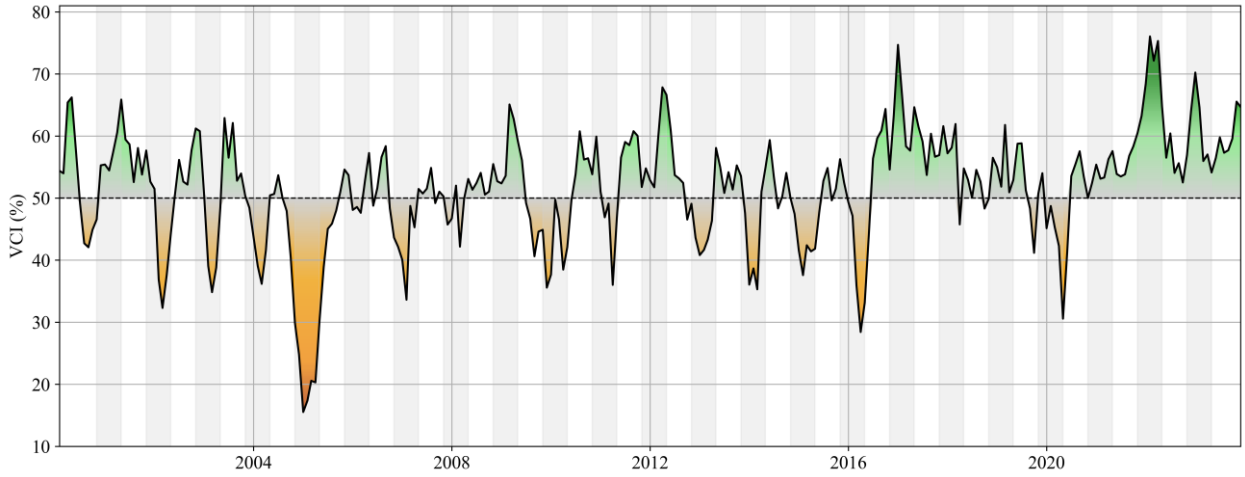

Figure 5. Temporal pattern of drought and wet conditions from 2000 to 2023. Vertical gray colors indicate the dry seasons from October to April.

Apart from the overall pattern, Figure 6 displayed the temporal pattern of the monthly VCI-based drought condition across three main land cover types from 2000 to 2023. Clearly, a similar pattern of the VCI was found in cropland, forests, and shrubland. However, forests and cropland had the lowest VCI values in 2005 (Figure 6), indicating that these types of vegetation are more sensitive to drought. Interestingly, cropland in 2010 suffered from lower VCI values than forests and shrublands. Cropland and forests had the highest VCI value in 2022, while shrublands witnessed the largest VCI value in 2000s (Figure 6). These observations might indicate that shrublands suffered from larger variations in recent years.

In recent years, however, higher VCI values were primarily observed in cropland and forests, which indicated an improvement in forest plantations or irrigated systems. In comparison, shrubland had relatively lower VCI values and had a longer duration of drought in recent years. For example, shrubland suffered from lower VCI values over nearly 12 months during the period 2020-2021. Also, the VCI values in shrubland during the last two years were lower than those of cropland and forests, suggesting not only the potential influence of drought but also the impact of human-induced activities such as land use disturbance. These patterns highlight the need for targeted conservation efforts in shrubland areas to mitigate further degradation and promote ecosystem resilience.

3.3 Time series trend of vegetation-based drought

In this study, we assessed the time-series trend of vegetation-based drought using the MK and Sen's slope tests over the two provinces of Vietnamese Central Highlands from 2000 to 2023. Overall, large areas of increasing VCI-based trends were detected in the study area over the study period (Figure 7), indicating a decline in vegetation-based drought trends. During the dry season, nearly 50% of the study area experienced significant positive VCI trends (Figure 7(a)), while the declining VCI values accounted for 20%. In comparison, the rainy season witnessed a smaller area of increasing VCI trends (~47%) from 2000 to 2023. Notably, it is estimated that the deviation of the VCI trends during the dry season was larger than that of the rainy season. For example, the estimated standard deviation of VCI trends for the dry season stood at 1.65%, in contrast to the lower figure of 1.32% observed for the rainy season. These observations suggested that the dry season witnessed more profound variations in drought than the rainy seasons and aligned with recent studies (Ha et al., 2023; Le et al., 2021; Tran et al., 2023; Vu and Ngo-Duc, 2024).

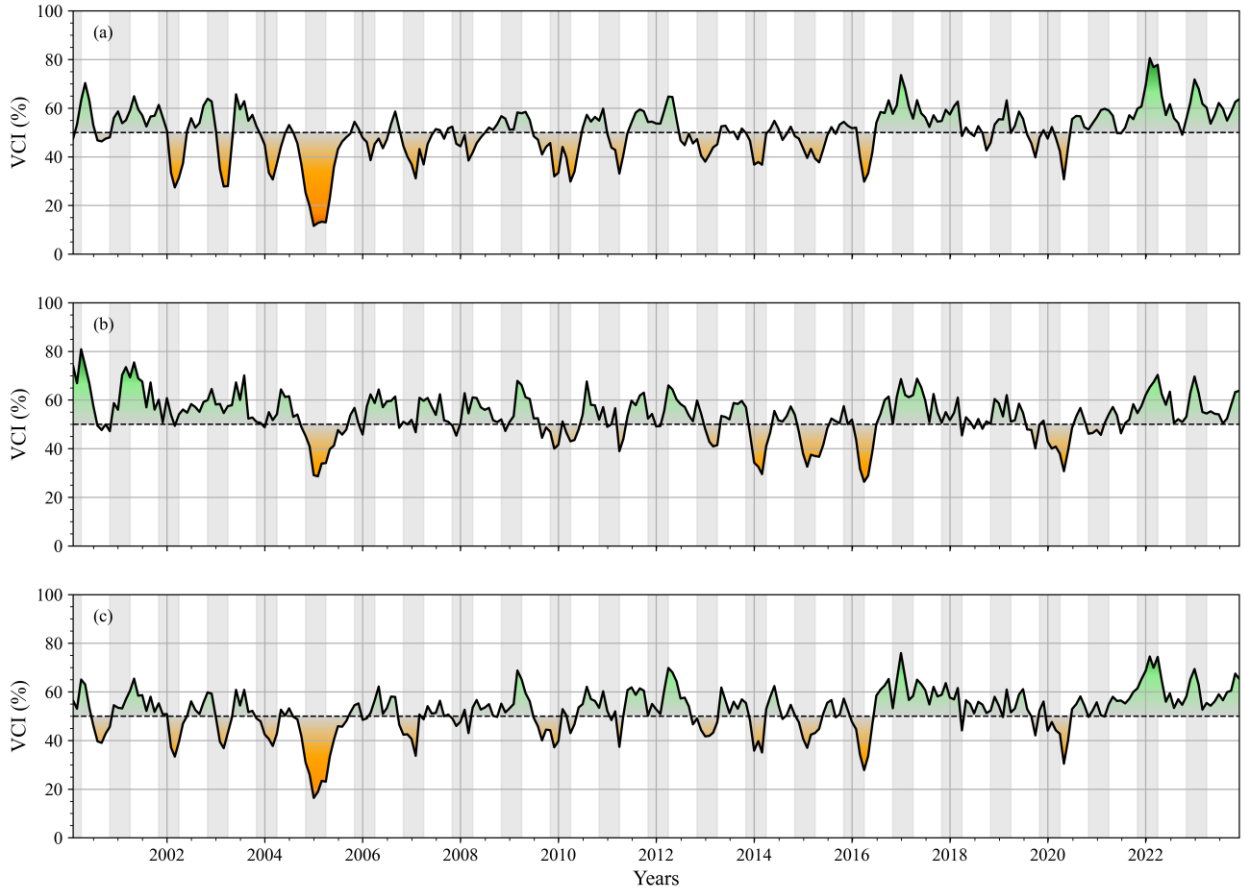

Figure 6. Monthly variability of drought conditions across land cover types (a) croplands, (b) shrubland, (c) forests across the study area. Color represents the VCI values from the lowest (red) to the highest (dark green). The gray color indicates dry season during the study period.

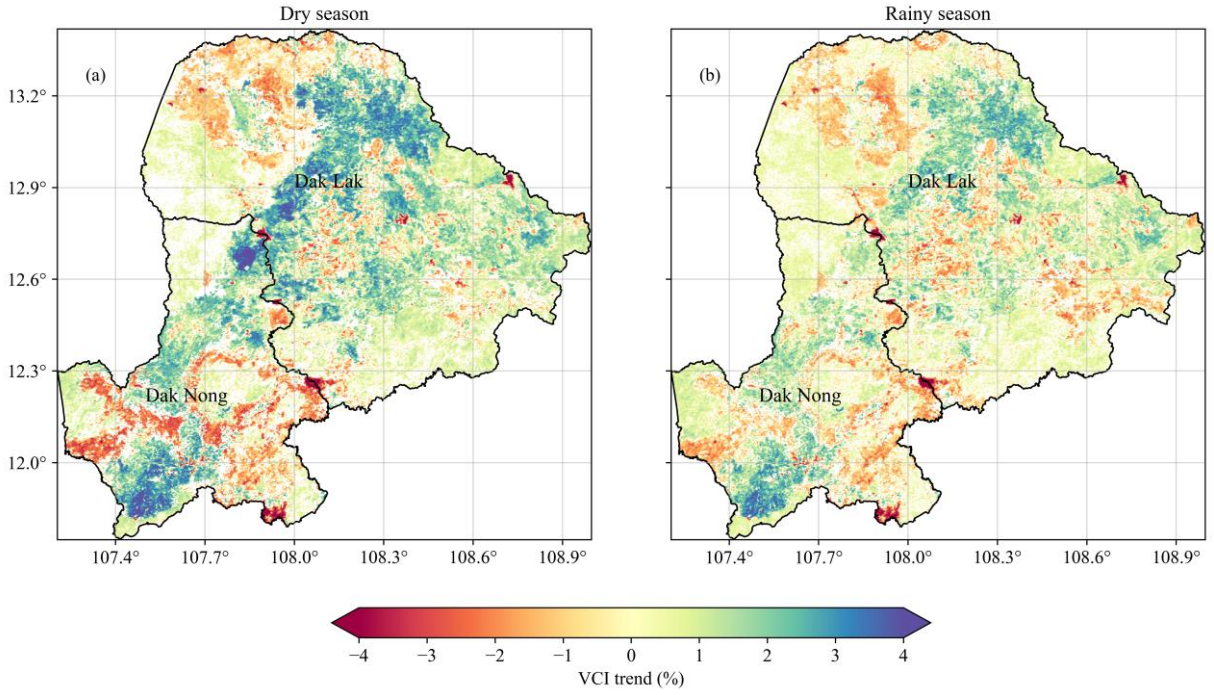

Figure 7. Spatial trends of per-pixel vegetation-based drought during the dry (a) and rainy (b) seasons from 2000 to 2023 at p-value≤0.05. Reddish color represents the declining VCI trends, while blue color indicates the increasing VCI trends.

Interestingly, significant increasing or declining VCI-based trends were primarily detected in the southern and central areas of Dak Nong and Dak Lak Provinces, respectively. For example, nearly 23% of Dak Nong Province witnessed declining VCI trends during the dry season, while Dak Lak has smaller areas of declining VCI trends (~17%) over the same period. Notably, Dak Lak Province had larger areas of increasing VCI trends compared to the rainy season, and these observations are mainly found in the forests and industrial crops. Coffee plantations are primarily detected around the central area of Dak Lak Province (Maskell et al., 2021).

The disparities observed in VCI trends between the two seasons in Dak Lak Province could be attributed to climate and human activities. For example, Dak Lak Province had large areas of industrial croplands, and farmers may store water during the dry season to cope with frequent droughts. Clearly, cropland had the highest VCI trend, an average of 1.1%, whereas the shrubland had the lowest VCI trend (-0.4%) during the dry season (Figure 8(a)). Likewise, cropland and forests experienced positive VCI trends during the rainy season. Negative shrubland VCI trends could be due to human activities such as agricultural shifting (Chen et al., 2023). Also, the rapid pace of rural urbanization across various regions has also contributed to these variable vegetation trends, reflecting the impact of expanding infrastructure and land use changes on natural ecosystems (Ha et al., 2020; Jeganathan et al., 2014).

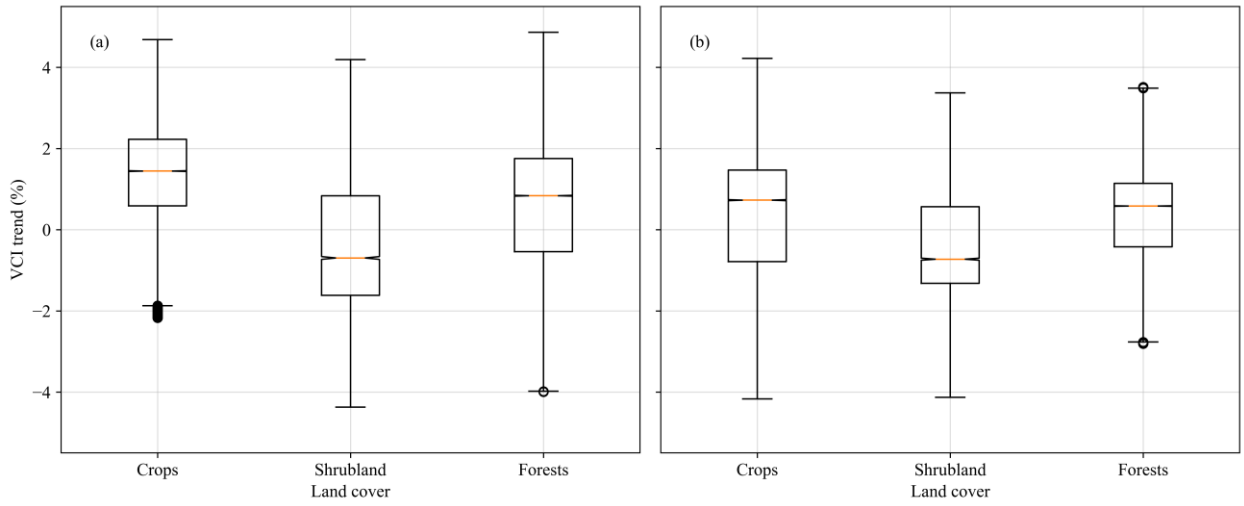

Figure 8. Trends of VCI-based conditions during the dry (a) and wet (b) seasons from 2000 to 2023 across land cover types of croplands, shrubland, forestland.

4. CONCLUSION

In this study, we employed a vegetation-based index to assess the spatiotemporal variability of drought conditions in the Vietnamese Central Highlands, Dak Lak, and Dak Nong Provinces, from 2000 to 2023. Spatial correlation analysis between the Vegetation Condition Index (VCI) and the Soil Water Deficit Index (SWDI) demonstrated a robust agreement, with nearly 91% of the study area exhibiting positive correlations. The comparison of drought-affected areas between VCI and SWDI revealed a high positive correlation (R-value=0.73), confirming the effectiveness and reliability of VCI-based drought detection.

The monthly evolution of drought conditions indicated a clear prevalence during the dry months, with severe episodes in 2005, 2010, 2013, 2015-2016, and 2019. The VCI patterns across land cover types revealed sensitivity variations, with forests and cropland being particularly vulnerable in certain years. The time-series analysis highlighted large areas of increasing VCI-based trends during both dry and rainy seasons over the study period. Nearly 50% of the study area experienced an increasing VCI trend during the dry season, whereas this figure for the rainy season was about 47%. Higher declining VCI trends were primarily detected in Dak Nong and northern Dak Lak Province.

These findings are crucial for informing stakeholders and policymakers, enabling the development of targeted strategies for drought resilience and sustainable land management practices in the region. In future studies, we would conduct a more detailed investigation into the localized impacts

of extreme drought events, as well as the incorporation of additional drought indices and environmental variables. Such approaches could provide a more comprehensive understanding of drought dynamics and improve the effectiveness of adaptation and mitigation strategies in the region.

ACKNOWLEDGEMENTS

This study received no external support. We thank two anonymous reviewers for their feedback and comments to enhance this manuscript.

REFERENCES

AghaKouchak A, Farahmand A, Melton FS, Teixeira J, Anderson MC, Wardlow BD, et al. Remote sensing of drought: Progress, challenges and opportunities. Reviews of Geophysics 2015;53(2):452-80.

Buchhorn M, Lesiv M, Tsendbazar NE, Herold M, Bertels L, Smets B. Copernicus global land cover layers: Collection 2. Remote Sensing 2020;12(6):Article No. 1044.

Byrareddy V, Kouadio L, Mushtaq S, Kath J, Stone R. Coping with drought: Lessons learned from robusta coffee growers in Vietnam. Climate Services 2021;22:Article No. 100229.

Cao M, Chen M, Liu J, Liu Y. Assessing the performance of satellite soil moisture on agricultural drought monitoring in the North China Plain. Agricultural Water Management 2022;263:Article No.107450.

Chen S, Olofsson P, Saphangthong T, Woodcock CE. Monitoring shifting cultivation in Laos with Landsat time series. Remote Sensing of Environment 2023;288:Article No. 113507.

Fang B, Kansara P, Dandridge C, Lakshmi V. Drought monitoring using high spatial resolution soil moisture data over Australia in 2015-2019. Journal of Hydrology 2021;594:Article No. 125960.

Gampe D, Zscheischler J, Reichstein M, O'Sullivan M, Smith WK, Sitch S, et al. Increasing impact of warm droughts on northern ecosystem productivity over recent decades. Nature Climate Change 2021;11(9):772-9.

Gorelick N, Hancher M, Dixon M, Ilyushchenko S, Thau D, Moore R. Google earth engine: Planetary-scale geospatial analysis for everyone. Remote Sensing of Environment 2017;202:18-27.

Ha TV, Huth J, Bachofer F, Kuenzer C. A review of earth observation-based drought studies in Southeast Asia. Remote Sensing 2022;14(15):Article No. 3763.

Ha TV, Tuohy M, Irwin M, Tuan PV. Monitoring and mapping rural urbanization and land use changes using Landsat data in the northeast subtropical region of Vietnam. The Egyptian Journal of Remote Sensing and Space Science 2020;23(1):11-9.

Ha TV, Uereyen S, Kuenzer C. Agricultural drought conditions over mainland Southeast Asia: Spatiotemporal characteristics revealed from MODIS-based vegetation time-series. International Journal of Applied Earth Observation and Geoinformation 2023;121:Article No. 103378.

Jeganathan C, Dash J, Atkinson P. Remotely sensed trends in the phenology of northern high latitude terrestrial vegetation, controlling for land cover change and vegetation type. Remote Sensing of Environment 2014;143:154-70.

Kogan FN. Remote sensing of weather impacts on vegetation in non-homogeneous areas. International Journal of Remote Sensing 1990;11(8):1405-19.

Le M-H, Kim H, Moon H, Zhang R, Lakshmi V, Nguyen L-B. Assessment of drought conditions over Vietnam using standardized precipitation evapotranspiration index, MERRA-2 re-analysis, and dynamic land cover. Journal of Hydrology: Regional Studies 2020b;32:Article No. 100767.

Le M-H, Lakshmi V, Bolten J, Du Bui D. Adequacy of satellite-derived precipitation estimate for hydrological modeling in Vietnam basins. Journal of Hydrology 2020a;586:Article No. 124820.

Le T, Sun C, Choy S, Kuleshov Y. Regional drought risk assessment in the Central Highlands and the South of Vietnam. Geomatics, Natural Hazards and Risk 2021;12(1):3140-59.

Li J, Wang J, Zhang J, Zhang J, Kong H. Dynamic changes of vegetation coverage in China-Myanmar economic corridor over the past 20 years. International Journal of Applied Earth Observation and Geoinformation 2021;102:Article No. 102378.

Li P, Feng Z, Xiao C. Acquisition probability differences in cloud coverage of the available Landsat observations over mainland Southeast Asia from 1986 to 2015. International Journal of Digital Earth 2018;11(5):437-50.

Li Y, Lu H, Entekhabi D, Gianotti DJS, Yang K, Luo C, et al. Satellite-based assessment of meteorological and agricultural drought in Mainland Southeast Asia. IEEE Journal of Selected Topics in Applied Earth Observations and Remote Sensing 2022;15:6180-9.

Mann HB. Nonparametric tests against trend. Econometrica: Journal of the Econometric Society 1945:13(3):245-59.

Marumbwa FM, Cho MA, Chirwa PW. An assessment of remote sensing-based drought index over different land cover types in southern Africa. International Journal of Remote Sensing 2020;41(19):7368-82.

Maskell G, Chemura A, Nguyen H, Gornott C, Mondal P. Integration of Sentinel optical and radar data for mapping smallholder coffee production systems in Vietnam. Remote Sensing of Environment 2021;266:Article No. 112709.

McNally A, Arsenault K, Kumar S, Shukla S, Peterson P, Wang S, et al. A land data assimilation system for sub-Saharan Africa food and water security applications. Scientific Data 2017; 4(1):1-19.

Mermoz S, Bouvet A, Koleck T, Ballère M, Le Toan T. Continuous detection of forest loss in Vietnam, Laos, and Cambodia using Sentinel-1 data. Remote Sensing 2021; 13(23):Article No. 4877.

Mishra A, Vu T, Veettil AV, Entekhabi D. Drought monitoring with soil moisture active passive (SMAP) measurements. Journal of Hydrology 2017;552:620-32.

Mishra AK, Singh VP. A review of drought concepts. Journal of Hydrology 2010;391(1-2):202-16.

Mondal A, Le M-H, Lakshmi V. Land use, climate, and water change in the Vietnamese Mekong Delta (VMD) using earth observation and hydrological modeling. Journal of Hydrology: Regional Studies 2022;42:Article No. 101132.

Nguyen-Ngoc-Bich P, Phan-Van T, Ngo-Duc T, Vu-Minh T, Trinh-Tuan L, Tangang FT, et al. Projected evolution of drought characteristics in Vietnam based on CORDEX-SEA downscaled CMIP5 data. International Journal of Climatology 2021;41(12):5733-51.

Phan-Van T, Nguyen-Ngoc-Bich P, Ngo-Duc T, Vu-Minh T, Le PV, Trinh-Tuan L, et al. Drought over Southeast Asia and its association with large-scale drivers. Journal of Climate 2022;35(15):4959-78.

Pu R. Assessing scaling effect in downscaling land surface temperature in a heterogenous urban environment. International Journal of Applied Earth Observation and Geoinformation 2021;96:Article No. 102256.

Savitzky A, Golay MJ. Smoothing and differentiation of data by simplified least squares procedures. Analytical Chemistry 1964;36(8):1627-39.

Sen PK. Estimates of the regression coefficient based on Kendall's tau. Journal of the American Statistical Association 1968; 63(324):1379-89.

Shahfahad, Talukdar S, Ali R, Nguyen K-A, Naikoo MW, Liou Y-A, et al. Monitoring drought pattern for pre-and post-monsoon seasons in a semi-arid region of western part of India. Environmental Monitoring and Assessment 2022;194(6): Article No. 396.

Thien BB, Ovsepyan AE, Phuong VT. Monitoring land surface temperature relationship to land use and land cover in Hai Duong Province, Vietnam. Environment and Natural Resources Journal 2024. DOI: 10.32526/ennrj/22/20230194.

Tran TV, Bruce D, Huang C-Y, Tran DX, Myint SW, Nguyen DB. Decadal assessment of agricultural drought in the context of land use land cover change using MODIS multivariate spectral index time-series data. GIScience and Remote Sensing 2023;60(1):Article No. 2163070.

Vicente-Serrano SM, Beguería S, López-Moreno JI. A multiscalar drought index sensitive to global warming: The standardized precipitation evapotranspiration index. Journal of Climate 2010;23(7):1696-718.

Vu-Thanh H, Ngo-Duc T, Phan-Van T. Evolution of meteorological drought characteristics in Vietnam during the 1961-2007 period. Theoretical and Applied Climatology 2014;118:367-75.

Vu N, Ngo-Duc T. Spatial distribution and trends of heat stress in Vietnam. Environment and Natural Resources Journal 2024. DOI: 10.32526/ennrj/22/20230227.

Vu TM, Raghavan SV, Liong SY, Mishra AK. Uncertainties of gridded precipitation observations in characterizing spatio-temporal drought and wetness over Vietnam. International Journal of Climatology 2018;38(4):2067-81.

Wei W, Zhang H, Zhou J, Zhou L, Xie B, Li C. Drought monitoring in arid and semi-arid region based on multi-satellite datasets in northwest, China. Environmental Science and Pollution Research 2021;28:51556-74.

Wu J, Lin L, Li T, Cheng Q, Zhang C, Shen H. Fusing Landsat 8 and Sentinel-2 data for 10-m dense time-series imagery using a degradation-term constrained deep network. International Journal of Applied Earth Observation and Geoinformation 2022;108:Article No. 102738.

Zou L, Cao S, Sanchez-Azofeifa A. Evaluating the utility of various drought indices to monitor meteorological drought in Tropical Dry Forests. International Journal of Biometeorology 2020;64:701-11.

Environment and Natural Resources Journal

Volume 22
Issue 5
2024

Warming Effect from Soil Greenhouse Gas Emission of Each Mangrove Zone during the Dry Season in Ngurah Rai Forest Park, Bali, Indonesia

I Putu Sugiana[1*], Tri Prartono[2], Rastina[2], and Alan Frendy Koropitan[2]

[1]*Graduate Program of Marine Science, School of Graduates, IPB University, IPB Dramaga Campus, Bogor 16680, West Java, Indonesia*
[2]*Department of Marine Science and Technology, Faculty of Fisheries and Marine Science, IPB University, IPB Dramaga Campus, Bogor 16680, West Java, Indonesia*

ARTICLE INFO

Received: 5 Feb 2024
Received in revised: 31 Jul 2024
Accepted: 8 Aug 2024
Published online: 22 Aug 2024
DOI: 10.32526/ennrj/22/20240029

Keywords:
Closed-chamber technique/ CO_2/ CH_4/ N_2O/ Mangrove zones/ GHG flux variations

*** Corresponding author:**
E-mail: iptsugiana@apps.ipb.ac.id

ABSTRACT

In addition to functioning as a carbon sink, mangrove soil also releases greenhouse gases (GHGs) through microbial metabolism. GHG flux fluctuates according to the ecological parameters of mangroves and climate variability. We quantified GHG fluxes from the soil using a closed-chamber technique and assessed soil and porewater conditions in three primary mangrove zones (each zone was dominated by one of the mangrove types) at Ngurah Rai Forest Park, Bali, Indonesia, categorized by genera: *Bruguiera*, *Rhizophora*, and *Sonneratia*. We found that the CO_2 flux ranged from 322.5 to 3,494.5 µg/m^2/h, CH_4 flux ranged from -24.7 to 60.9 µg/m^2/h, and N_2O flux ranged from -1.2 to 2.3 µg/m^2/h. None of the GHG fluxes varied significantly between mangrove zones. Overall, the highest CO_2 fluxes were observed in the *Bruguiera* zones, while the highest CH_4 and N_2O fluxes were found in the *Sonneratia* and *Rhizophora* zones, respectively. A significant relationship between GHG fluxes and soil properties, including soil organic carbon (SOC), total Kjeldahl nitrogen (TKN), water content, bulk density, and soil type. The average warming effect on GHG fluxes ranged from 0.9 and 1.8 $MgCO_2$/ha/year, accounting for only 1.1% to 2.2% of the annual plant carbon sequestration rate of 75.9 to 81.6 $MgCO_2$/ha/year. These findings suggest that the variability of GHG fluxes is not significantly influenced by mangrove type; instead, soil conditions play a crucial role. Calculations of the net carbon stock may overlook the relatively low warming effect of GHG fluxes in this area.

1. INTRODUCTION

Global warming is the phenomenon of the Earth's average atmospheric temperature increasing due to the presence of greenhouse gases (GHGs) such as carbon dioxide (CO_2), methane (CH_4), and nitrous oxide (N_2O) (Montzka et al., 2011; Kweku et al., 2018). The IPCC report (2021) states that atmospheric CO_2 concentrations have reached 409.9 parts per million (ppm) since the pre-industrial era in 1750. Additionally, the report indicates that CH_4 and N_2O have increased by 5-10 parts per billion (ppb) and one ppb each year, respectively (Reay et al., 2018). Despite their lower concentrations compared to CO_2, CH_4, and N_2O have a global warming potential of 29.8 and 273 times greater than CO_2 over a 100 year period (IPCC, 2021). Hence, their influence must not be overlooked when calculating the atmosphere's Global Warming Potential (GWP).

In addition to serving as a carbon sink in the form of CO_2 absorption, mangrove forests also release GHG fluxes (Alongi, 2014; Chen et al., 2016). Indonesia has the highest proportion of mangrove forests worldwide, accounting for about 19.5% (Bunting et al., 2018). These forests have a carbon uptake rate of 1,190,814 tonsC/ha/year. Nevertheless, GHG emissions are notably substantial, particularly in

Citation: Sugiana IP, Prartono T, Rastina, Koropitan AF. Warming effect from soil greenhouse gas emission of each mangrove zone during the dry season in Ngurah Rai Forest Park, Bali, Indonesia. Environ. Nat. Resour. J. 2024;22(5):449-463. (https://doi.org/10.32526/ennrj/22/20240029)

mangrove forests impacted by pollution, including organic matter (Das et al., 2022). The decomposition of organic matter results in the production of carbon dioxide (CO_2) in the oxic/aerobic soil layer and methane (CH_4) in the anoxic/anaerobic soil layer (Wang et al., 2009; Treat et al., 2015). In addition, N_2O is produced through denitrification processes that utilize NO_3^- (nitrate) or NO_2^- (nitrite) nutrients derived from the nitrification process of NH_4^+ (ammonia). These processes are typically found in mangrove forests with high soil carbon and nitrogen content and low oxygen conditions (Zhu et al., 2013; Queiroz et al., 2019). Hence, accurate data regarding GHG fluxes is necessary to accurately determine the net carbon stock of the mangrove ecosystem.

Variations in environmental condition, such as water salinity, soil type, and soil carbon accumulation capability, are responsible for the differences observed in mangrove vegetation types (Ewel et al., 1998; Srikanth et al., 2016; Raganas and Magcale-Macandog, 2020). The arrangement of mangrove trees differs depending on the dominant species, affecting the amount of organic matter that is contributed to the surrounding environment (Prasad et al., 2010; Mulya and Arlen, 2018). This, in turn, impacts greenhouse gas fluxes and the extent of the warming effect in terms of CO_2-equivalent (Chen et al., 2016; Xu et al., 2021). Various studies have shown that comparing the warming effect caused by GHG emissions with the annual carbon sequestration rate varies across different zones. For instance, the warming effect value of GHG flux in *Kandelia candel* dominated mangrove area is 20.5% (Chen et al., 2016), while it is 24% for CH_4 in *Kandelia obovata* zone (Liu et al., 2020). In the mixed zone consisting of *K. obovata*, *Avicennia marina*, and *Aegiceras corniculatum*, the warming effect of CH_4 is only 4.6% (Zhu et al., 2013). These findings highlight the significant impact of mangrove zoning factors on the warming effect of soil GHG fluxes.

The mangrove ecosystem at Ngurah Rai Forest Park (TAHURA) is the largest mangrove area in Bali, Indonesia. The zonation patterns of mangrove species are evident, with the dominant zones occupied by the genera *Rhizophora*, *Sonneratia*, and *Bruguiera* (Sugiana et al., 2022). The environmental conditions also vary, regarding to salinity, pH, oxidation-reduction potential (ORP), and substrate type (Prinasti et al., 2020; Dewi et al., 2021; Sugiana et al., 2021). These parameters are key factors that control the greenhouse gas flux from mangrove soil (Chen et al., 2016; Kitpakornsanti et al., 2022). Previous research measured GHG flux during the rainy season (Sugiana et al., 2023). However, due to the potential variations that may occur due to seasonal factors (Padhy et al., 2020; Cameron et al., 2021), measurements during the dry season are also necessary.

In this study, we quantified the warming effect from GHG fluxes through the dry season from different mangrove zones. The selection of three prominent mangrove zones (*Rhizophora*, *Sonneratia*, *Bruguiera*) in the Ngurah Rai Grand Forest Park, Bali, was made to assess the overall state of the mangrove ecosystem accurately. This research aims to add data related to the seasonal fluctuations in GHG levels and their warming effect that have not been previously recorded in the same area. The research findings indicate that mangrove ecosystems also emit greenhouse gases (GHGs) from soil which increase the warming effect in the atmosphere, albeit in negligible amounts in this area. Because this is not the case in all mangrove areas GHG emissions need tobe known in order to calculate the blue carbon stock accurately. The research result also contributes to the FoLU (Forestry and Other Land Use) Net Sink 2030 program by collecting GHG data in the forestry sector in Indonesia.

2. METHODOLOGY

2.1 Study site and condition

This research is located in Ngurah Rai Forest Park, Bali (8°42'50.46"S, 8°47'49.92"S, 115°10'9.42"E, and 115°15'13.19"E). The majority of the mangrove forests have undergone conversion from shrimp ponds within the past three decades (JICA, 1999). Mangrove forests are primarily characterized by three primary genera: *Bruguiera*, *Rhizophora*, and *Sonneratia*. The general health of mangroves based on the mangrove health index (MHI) has been categorized as moderate (Sugiana et al., 2022). Fine sand dominates the mangrove soil in this area (Prinasti et al., 2020; Imamsyah et al., 2020). pH and salinity of the porewater vary across different zones depending on their proximity to the sea (Sugiana et al., 2021). A total of 12 study plots were allocated among the three mangrove zones, including 3 plots in the *Bruguiera* zone, 4 plots in the *Sonneratia* zone, and 5 plots in the *Rhizophora* zone (Figure 1). During the data collection, the weather conditions had clear skies, and the tide conditions reached their lowest point. The sampling time was carried out between August 23-28, 2023, in the daytime (1 pm to 3 pm; UTC+8 time

zone). Data collection was only conducted once per plot. We also recorded the field air temperatures, which varied between 25.0 and 28.3°C (mean: 26.7°C), and humidity levels which ranged from 73 to 88% (mean: 80%).

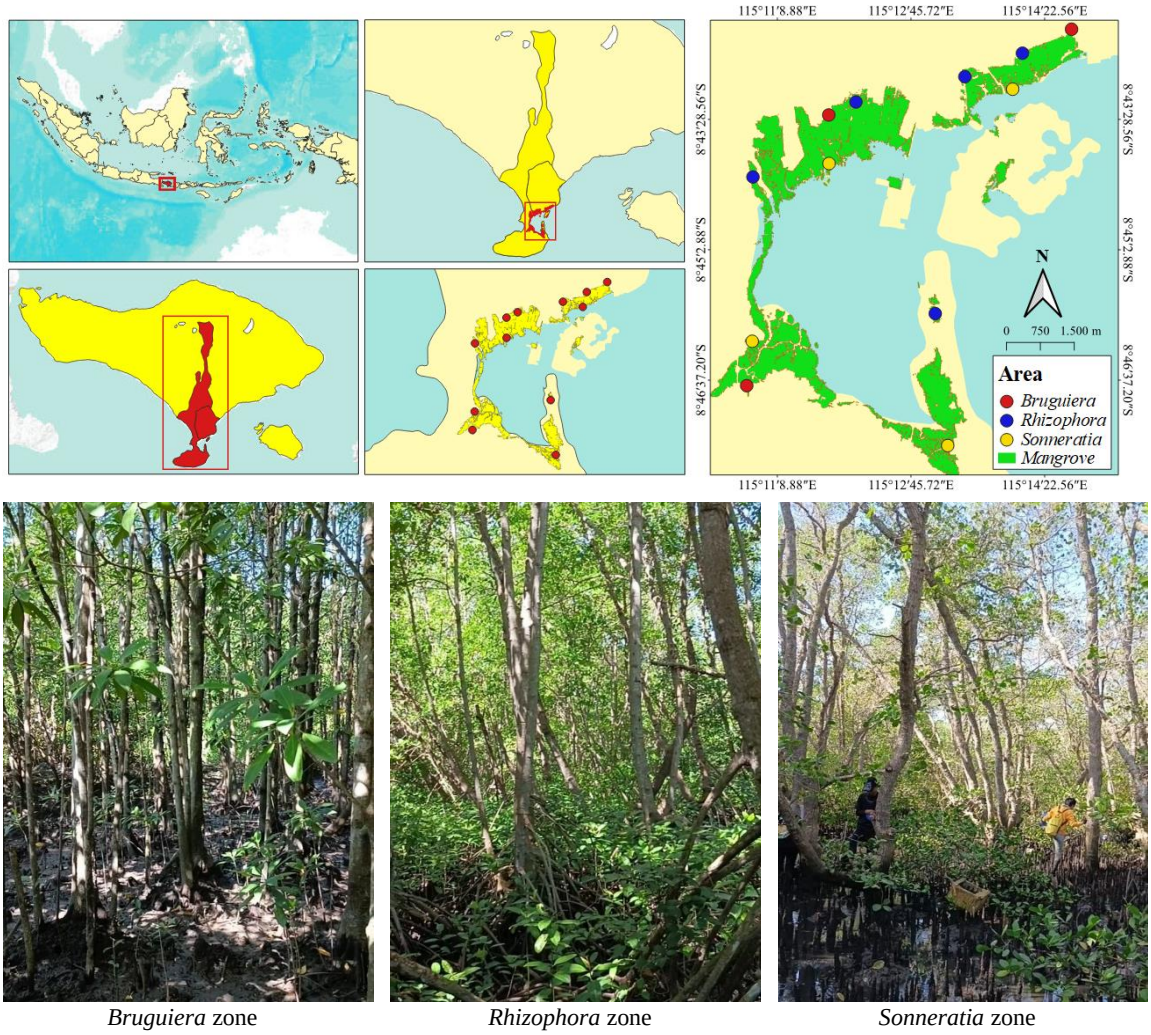

Figure 1. Distributions and conditions of research data collection plots in Bali, Indonesia

The mangrove forest structure conditions and carbon sequestration rates vary across each mangrove zone, as shown in Table 1. The data for measuring the structure of the stand was collected following the guidelines for monitoring mangrove communities (Dharmawan and Ulumuddin, 2021). The carbon sequestration rates of each mangrove zone were derived by combining the parameters of stem diameter growth, burial rate, and litterfall production, yielding the annual rate of carbon sequestration. The data previously been published by Sugiana et al. (2024).

2.2 Greenhouse gases data collection

Each sampling plot has three subplots that serve as measuring points for GHG fluxes, positioned as shown in Figure 2. Each subplot is constrained by a 10×10 m transect that was previously employed to delimit measurements of the structure of mangrove stands. GHG samples were collected using a 10 mL syringe. The samples were taken after being incubated in a clear container constructed of acrylic, which had dimensions of 20×20×25 cm. The samples were collected at 10-minute intervals, four times in total (at t=0, 10, 20, and 30 minutes), following the methodology described by Chen et al. (2016). The incubation method involves submerging the chamber in mangrove soil, which is free from crab holes and debris, at a depth of around 2 cm. Gas samples were only collected in August 2023, marking the transitional period from the dry season to the rainy season. A total of 144 gas samples were collected from 12 plots, with each plot yielding twelve samples. The collected gas is transferred into a vacutainer tube with a capacity of 10 mL.

Table 1. Average forest structure of each mangrove zones and annual carbon sequestration rate

Parameter	Zone		
	Bruguiera	*Rhizophora*	*Sonneratia*
Dominance of mangrove	*B. gymnorrhiza*	*R. mucronata*	*S. alba*
Number of spp.	1	3	1
Tree density (stands/ha)	3,030	3,576	2,121
Sapling density (stands/ha)	1,414	1,333	985
Diameter at breast height (cm)	8.3	8.8	11.5
Canopy coverage (%)	75.18	74.59	49.17
Mangrove health index (%)	56.03	55.99	42.13
Carbon sequestration rate ($MgCO_2$/ha/year)	75.6	79.3	81.8

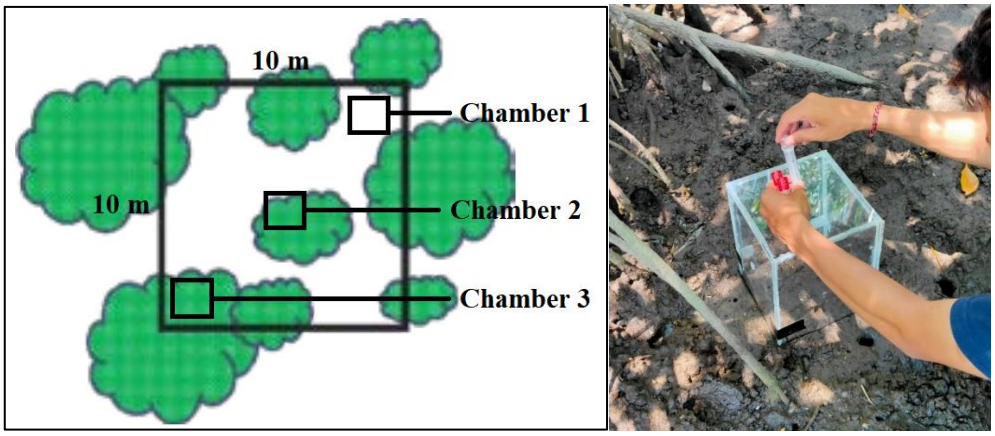

Figure 2. Position of incubation chamber between sampling plots (left; image is a modification from Dharmawan et al., 2020) and GHGs sampling (right)

The GHG samples were subsequently sent to the laboratory of the Agricultural Environmental Research Institute in Pati, Central Java, Indonesia to measure the concentration of each GHG. Determination of CH_4, CO_2, and N_2O in the samples was carried out using a gas chromatograph (450-GC Varian) was used. This machine had a flame ionization detector (FID), a thermal conductivity detector (TCD), and a ^{63}Ni electron capture detector (μECD). The 450-GC Variant is further furnished with a PAL autosampler injector that operates as an auto-injector with a capacity of 2 mL. It utilizes Ar, H_2, He, and N_2 as carrier gases. The measuring procedure was conducted at a temperature of 25°C, and the obtained measurements are compared to a standard curve that serves as a reference. The determination of concentration values is derived by comparing the peak area with the value obtained from the standard curve. Subsequently, the concentrations of CO_2, CH_4, and N_2O are transformed into flux values by applying the equation derived by Chen et al. (2016):

$$Fm = \frac{V \times \Delta M \times 10^6}{A \times P} \quad (1)$$

Where; Fm=GHG fluxes (μg/m^2/h), ΔM=the slope of the linear regression line between GHG concentrations (ppm) and sampling frequency (10 min transformed to an hour), V=chamber volume (L), A= chamber area (m^2), P=constant gas volume (22.414 L/mol).

The CH_4 and N_2O fluxes are transformed into CO_2-equivalent form in order to standardize their warming impact with that of CO_2 by using the following formula:

$$Fe = Fm \times M \times GMP \quad (2)$$

Where; Fe=warming effect in CO_2-equivalent fluxes ($gCO_2/m^2/h$ converted to $MgCO_2$/ha/year), Fm=GHG fluxes (mol/m^2/h), M=molecular weight of the GHGs (CH_4: 16.04 g/mol and N_2O: 44.013 g/mol), GMP=warming effect or the conversion factor of CH_4 and N_2O emissions to CO_2 equivalents as 29.8 and 273, respectively, over a 100-year timeframe (IPCC, 2021).

2.3 Soil and porewater physicochemical characteristics measurement

Environmental condition measurement is divided into two components: soil and porewater. We collected the soil sample using a soil auger with a diameter of 5 cm at a depth ranging from 0 to 100 cm. Subsequently, the soil pH was measured using a Lutron 212 pH meter. We first homogenized the soil, and then 300 grams were collected and stored in plastic containers. One hundred grams of soil samples were dried at 70°C until a consistent weight was achieved (approximately 48 h) to obtain the percentage of the water content. We also dried another 100 g of the soil at 105°C to measure the bulk density value. A dried soil used for water content measurement is then used again for grain size analysis (10 g), soil organic carbon (SOC) measurement (3 g), and the rest (around 100 g) for total Kjeldahl nitrogen (TKN) and phosphorus (TP) analysis. We used the dry sieve method (gravel: 2 mm, sand: 1.1 mm-75 µm) and the settling time method for silt and clay categorization for soil grain size analysis. For SOC, we used the loss on ignition (LOI) method, where the samples were burned at a temperature of 550°C (Chen et al., 2014). TKN analysis was performed using a flow injection analyzer (FIA) method, and TP was measured using the colorimetric persulfate digestion method. Since the data collection was conducted during low tide, porewater samples were mostly found at 50-100 cm from the soil surface. We measured several parameters, including temperature, pH, salinity, and ORP, using the Multimeter COM-600 Water Quality Tester, and the dissolved oxygen (DO) was measured using a Lutron DO-5519 meter. The soil sampling for these measurements was performed after the GHG samples were collected to avoid soil disturbance affecting the GHG data.

2.4 Statistical analysis

We used ANOVA analysis to see if there are notable disparities in GHG emission rates and environmental variables, specifically soil and porewater. All the data, including GHG production rates, mangrove stand structure, carbon sequestration, and ecological condition, had a normal distribution ($\rho>0.05$) based on the Shapiro-Wilk test. We then used the Tukey Honestly Significant Difference (HSD) follow-up test to determine the zones that exhibited statistically significant differences. A Pearson correlation test was also performed using R Studio version 4.0.2 software to establish the relationship between GHG flux and mangrove ecological parameters (stand structure and environment condition). Principal component analysis (PCA) with MVSPW software was used to determine the correlation among all parameters and GHG emission in the study areas.

3. RESULTS AND DISCUSSION

3.1 Soil and porewater physicochemical characteristics

Generally, each mangrove zone is categorized by the predominant sandy soil type. According to Shepard's categorization, the soil composition varies, ranging from primarily sandy (with a sand content of at least 75%) to a mixture of sand and silt/clay known as sandy loam (with a sand content between 50-75% and a combined silt and clay content of at least 25%) (Table 2). In detailed information, the main soil types are categorized into four: rough sand, medium sand, fine sand, and very fine sand. Fine sand dominated the *Bruguiera* and *Sonneratia* zones by 38.7% and 19.3%, respectively, while medium sand dominated the *Rhizophora* zone by 22.5% (Figure 3).

No soil properties, including pH, moisture content, bulk density, SOC, TKN, TP, C:N, and N:P Ratio, show significant differences based on the ANOVA test ($\rho>0.05$). However, when looking at the average values, the highest values for soil pH, water content, SOC, and C:N Ratio were found in the *Sonneratia* zone, while the lowest was in the *Rhizophora* zone (Table 2). Furthermore, the bulk density and total phosphorus are higher in the *Bruguiera* zone, while the TN and N:P ratios are highest in the *Rhizophora* zone (Table 2).

The discrepancies in values among soil properties can be attributed to their interdependent relationship. The *Sonneratia* zone, characterized by greater clay content, exhibits the highest organic carbon levels. This is because clay soil can bind carbon tightly more than coarser soil types (Matus, 2021; Amorim et al., 2023). Similarly, the lower bulk density value relates to a higher presence of organic carbon, indicating an inverse relationship with soil organic carbon concentration (Perie and Ouimet, 2008; Matus, 2021). Soil that contains a high amount of organic material has a greater capacity to absorb water, resulting in higher water content values (Gao et al., 2019). Given its proximity to these water sources, the *Sonneratia* zone exhibits a slightly higher soil pH, perhaps due to the influx of surface water from the nearby sea and neighboring rivers (Figure 4). Microbial metabolic activities, specifically

nitrification and denitrification processes, and the dark cycle process of photosynthesis in plants, can cause minor fluctuations in TKN and TP content. These processes indirectly involve the utilization of nitrogen and phosphorus available in the soil (Lovelock et al., 2006; Inoue et al., 2011; Zhu et al., 2013; Queiroz et al., 2019).

Table 2. Comparison of GHG fluxes in mangroves soil of Ngurah Rai Forest Park, Bali with other regions (NA: not available)

Location	Dominated mangrove species	Region	GHG Fluxes (µg/m^2/h)			References
			CO_2	CH_4	N_2O	
Ngurah Rai Forest Park, Bali (Dry season)	*Bruguiera*, *Rhizophora*, *Sonneratia*	Tropical	322.5-3,494.5	-24.7-60.9	-1.2-2.32	This study
Ngurah Rai Forest Park, Bali named as Benoa Bay, Bali (Wet season)	*Bruguiera*, *Rhizophora*, *Sonneratia*	Tropical	98-8,953	0.9-88.0	0.24-3.6	Sugiana et al. (2023)
Tampamachoco coastal lagoon, Mexico	*Avicennia germinans*	Tropical	-242.9-358	-3.0-5.6	-1.1-2.9	Romero-Uribe et al. (2022)
Budai, Taiwan	*Kandelia*, *Avicennia*	Sub-Tropical	NA	14.1-316.9	NA	Lin et al. (2020)
Honda bay, Philipines	*Rhizophora*	Tropical	252-33,300	-5.95-17.53	-0.67-5.54	Castillo et al. (2017)
Bhitarkanika, India	*Rhizophora*	Sub-Tropical	NA	5	0.20	Chauhan et al. (2015)
Sulawesi, Indonesia	*Rhizophora*, *Bruguiera*	Tropical	-1,340-3,880	-6.1-13.1	-0.35-0.61	Chen et al. (2014)
Maipo, Hongkong	*Kandelia*, *Acanthus*	Sub-Tropical	31	NA	11.6	Chen et al. (2012)
Futian, China	*Kandelia*, *Acanthus*, *Bruguiera*	Sub-Tropical	-560-20.6	10.1-5,168.6	0.14-23.8	Chen et al. (2010)
Brisbane, Australia	*Avicennia*, *Aegiceras*	Sub-Tropical	NA	272.5	40.4	Allen et al. (2007)

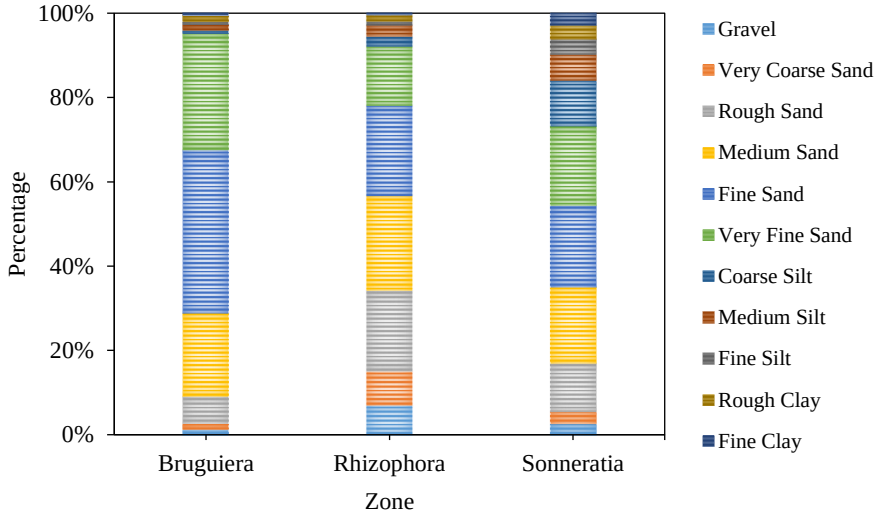

Figure 3. Soil type classification from each mangrove zone in TAHURA Ngurah Rai, Bali

Several porewater parameters, including salinity, oxidation-reduction potential (ORP), and dissolved oxygen (DO), demonstrate substantial differences ($\rho<0.05$) across mangrove zones. However, the rest of the parameters were not significantly different ($\rho>0.05$). The *Bruguiera* zone had the highest average temperature, salinity, ORP, and DO values in porewater, whereas the *Sonneratia* zone displayed the lowest values. Unlike other conditions, pH levels are high in the Sonneratia zone and low in the *Rhizophora* zone. This pattern is also observed in soil pH, as shown in Table 3.

Figure 4. Fresh water irrigation flows were found at the two southernmost *Sonneratia* plots

Table 3. Soil and porewater properties of each mangrove zone

Media	Parameter	Zone		
		Bruguiera	*Rhizophora*	*Sonneratia*
Soil	Dominant soil type	Sand (Gravel: 1%, Sand: 94%, Silt: 3%, Clay: 2%)	Sand (Gravel: 7%, Sand: 85%, Silt: 6%, Clay: 2%)	Sandy Loam (Gravel: 3%, Sand: 71%, Silt: 21%, Clay: 6%)
	Soil pH	6.32±0.25[a]	6.23±0.22[a]	6.66±0.26[a]
	Water content (%)	42.8±2.9[a]	37.4±4.8[a]	50.9±12.5[a]
	Bulk density (g/cm^3)	0.81±0.16[a]	0.80±0.06[a]	0.66±0.07[a]
	Soil organic carbon (SOC) (%)	1.24±0.47[a]	1.16±0.40[a]	1.96±0.36[a]
	Total Kjeldahl Nitrogen (TKN) (%)	0.05±0.04[a]	0.06±0.02[a]	0.05±0.03[a]
	Total phosphor (TP) (%)	0.013±0.001[a]	0.009±0.003[a]	0.012±0.002[a]
	C:N ratio	47.9±35.5[a]	21.3±6.4[a]	50.0±24.0[a]
	N:P ratio	3.8±3.8[a]	7.0±3.2[a]	4.2±2.8[a]
Porewater	Temperature (°C)	28.3±1.0[a]	27.8±0.9[a]	27.5±0.6[a]
	pH	6.43±0.17[a]	6.37±0.19[a]	6.81±0.34[a]
	Salinity (ppt)	22.94±1.94[a]	22.19±1.00[ab]	19.50±2.07[b]
	ORP (mV)	6±53[a]	-58±29[ab]	-95±59[b]
	Dissolved oxygen (DO) (mg/L)	2.44±0.71[a]	1.30±0.38[b]	1.25±0.36[b]

Similar to soil conditions, porewater properties are also related each other. High porewater pH in the *Sonneratia* zone may be caused by the flushing of tides or the proximity of river flow near the monitoring area (Figure 4). This also caused low salinity values found in the same zone. Generally, *Bruguiera* mangroves grow near land with low salinity conditions (Dangremond et al., 2015). However, this condition was found due to multiple measurement locations inside the area predominantly occupied by the *Sonneratia* species with low porewater salinity. This caused the *Bruguiera* zone to have the highest salinity value compared to the *Sonneratia* zone. The *Sonneratia* zone also has lower levels of ORP and DO, which can be attributed to the breakdown of organic matter by high aerobic microbial metabolism. Consequently, the soil in mangrove areas tends to have a reducing tendency, as seen by negative ORP values (Hall et al., 2013).

3.2 Soil greenhouse gas fluxes

No significant variations were found between mangrove zones in the CO_2, CH_4, and N_2O fluxes ($\rho>0.05$). The average CO_2 flux in the *Bruguiera* and *Sonneratia* zones is twice as high as in the *Rhizophora* zone, measuring 2,660.0±611.9 µg/m^2/h and 2,456.1±1,261.1 µg/m^2/h, respectively. The *Sonneratia* zone produced 35.4±17.4 µg/m^2/h CH_4 gas, while the *Bruguiera* and *Rhizophora* zones only comprised 7% and 21% of the average CH_4 gas production compared to the *Sonneratia* zone. However, while considering the N_2O flux, it was seen

that the *Rhizophora* zone had the highest flux value, specifically 0.6±0.9 µg/m^2/h. This value was 1.2 times higher than in the *Bruguiera* zone and six times higher than in the *Sonneratia* zone (Figure 5).

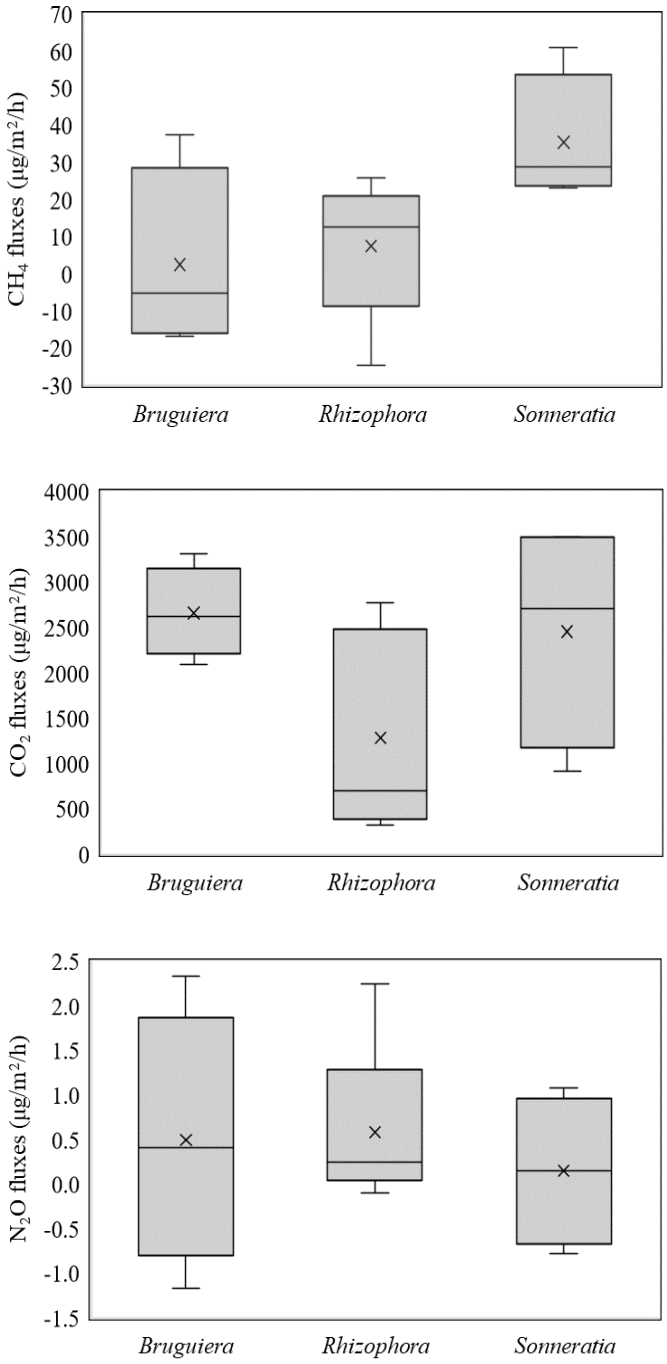

Figure 5. Greenhouse gas fluxes of each mangrove zone in TAHURA Ngurah Rai, Bali

Other study have shown that mangrove soil can act as both sources (positive value) and sinks (negative value) of GHGs (Konnerup et al., 2014; Atwood et al., 2017; Cabezas et al., 2018; Romero-Uribe et al., 2022). There is no discernible pattern in the GHG fluxes trend between mangrove zones. Nevertheless, a positive trend of CO_2 fluxes demonstrates that mangrove soil always emits CO_2 into the atmosphere. Meanwhile, the CH_4 and N_2O fluxes exhibit inconsistent trends, varying between positive and negative values. Most GHG fluxes with negative values were seen in the *Bruguiera* zone for CH_4 and the *Sonneratia* zone for N_2O. The maximum and minimum CH_4 flux values throughout all mangrove zones are 60.85 µg/m^2/h and -24.67 µg/m^2/h, while N_2O fluxes are 2.25 µg/m^2/h and -1.17 µg/m^2/h,

respectively. CH_4 and N_2O fluxes can exhibit negative values in certain instances, as observed in studies conducted in North Sulawesi, Indonesia (Chen et al., 2014) and Tampamachoco coastal lagoon, Mexico (Romero-Uribe et al., 2022). This phenomenon is mostly attributed to microbial activity and environmental conditions.

Wetland soil, including mangrove ecosystems, mostly has high organic matter with limited oxygen. Methanogenic bacteria produce more CH_4 gas in anaerobic conditions. Conversely, when there is an ample oxygen supply, CO_2 is predominantly produced (Adame and Lovelock, 2011; Chen et al., 2016; Sugiana et al., 2023). The CH_4 flux may vary due to environmental conditions or the presence of specific microbes in the soil, particularly methanogenic (methane producer) and methanotrophic (methane consumer) bacteria. Methanotrophic bacteria utilize CH_4 as an energy source and metabolize it into methanol and then formaldehyde which is subsequently metabolized further to produce carbon-containing biomass and CO_2 (Kalyuzhnaya et al., 2019; Nazir and Zaffar, 2021). When the activity of methanotrophic bacteria exceeds that of methanogenic bacteria, the CH_4 production will drop. For example, in the *Bruguiera* zone, where oxygen levels are high, methane production is generally lower than in other zones.

In addition, N_2O is a greenhouse gas produced by bacteria during the denitrification process in anaerobic environments (Marton et al., 2012; Queiroz et al., 2019). The energy requirements for microbial adaptation and the stability of nitrogen molecules influence the production of N_2O. The primary conversion of N_2O to N_2 instead of the formation of N_2O from nitrogen monoxide (NO) leads to a decline in N_2O production in the soil. As a result, measurements of N_2O flux sometimes provide negative values or demonstrate a downward trend. Denitrifying bacteria rely on nitrous oxide (N_2O) molecules as electron acceptors during anaerobic respiration to generate energy. The breakdown of N_2O into N_2 liberates a greater amount of energy, hence facilitating the proliferation and viability of bacteria (Conrad, 1996; Zumft and Kroneck, 2006; Ussiri and Lal, 2013). In addition, N_2 is more stable than other nitrogen forms, leading to higher production quantities in this form (Robertson and Groffman, 2024).

Multiple research studies have demonstrated varying levels of GHG fluxes. Despite their shared tropical locations, GHG emissions exhibit significant variability. This is also true in other sub-tropical regions, as indicated in Table 2. We found that GHG fluxes in Ngurah Rai Forest Park, Bali, are lower during the dry season compared to the wet season. These findings demonstrate that fluctuations in GHG emissions are also influenced by seasonal factors, similar to other studies conducted in the Ayeyarwady Delta, Myanmar (Cameron et al., 2021) and Sudarban, India (Padhy et al., 2020). In addition, the features of the mangrove type also appear to impact the rate of greenhouse gas flux indirectly. Table 2 demonstrates that various research locations are primarily characterized by a specific type of mangrove, resulting in distinct GHG emissions compared to other areas dominated by different mangrove species. However, despite being predominantly influenced by the Rhizophoraceae group in Sulawesi, Indonesia, and Honda Bay, Philippines, the greenhouse gas (GHG) emissions show notable disparities compared to the current findings. This suggests that more factors, such as hydro-oceanic conditions, affect GHG fluxes.

3.3 Soil GHG relationship with environmental parameters

We found no relationship between atmospheric conditions and GHG fluxes. However, stand structure, sapling density seems to correlate with N_2O flux. Most soil properties, including water content, bulk density, TOC, TKN, C:N ratio, N:P ratio, and soil types, have positive or negative correlations with GHG fluxes. The pore water characteristics did not significantly correlate with GHG fluxes, as indicated in Table 4.

The correlation between the sapling density and the N_2O flux can be attributed to the state of the roots of mangrove plants. Increased sapling density leads to a greater accumulation of organic matter, including nitrogen, in the soil, which bacteria can exploit to create N_2O gas (Xiong et al., 2017; Alongi, 2020). In addition, high sapling density leads to greater soil stability and enhanced microbial diversity, all of which contribute to the production of N_2O (Braker and Conrad, 2011; Craig et al., 2021).

Low bulk density with high sand composition (mostly mineral content) can indicate high CO_2 production (Chen et al., 2016; Yost and Hartemink, 2019; Sugiana et al., 2023). Sandy soil has a looser porosity, making it easier for dissolved oxygen to enter the porewater. Meanwhile, a low bulk density with silty and clayed soil, mostly with high water content, indicated a high TOC concentration used to produce CO_2 gas through microbial activity (Matus, 2021; Amorim et al., 2023). However, it also triggers

high CH_4 production because silt and clay soil reduce dissolved oxygen levels in porewater, causing anoxic environmental conditions (Wang et al., 2009; Gao et al., 2019; Liu et al., 2020; Matus, 2021).

Table 4. Pearson correlation coefficient values (r) among atmospheric condition, mangrove structure, soil, and porewater properties with greenhouse gases (*=correlation coefficient at ρ<0.05, while ** at ρ<0.01)

Parameter	Correlation coefficient		
	CO_2	CH_4	N_2O
Atmospheric condition			
Temperature (°C)	0.13	0.28	-0.04
Humidity (%)	-0.41	-0.37	-0.05
Mangrove structure			
Tree density (ind/ha)	-0.27	-0.31	-0.08
Sapling density (ind/ha)	-0.36	-0.18	**0.59***
Diameter (cm)	0.57	0.33	-0.16
Canopy cover (%)	-0.44	0.05	0.21
Health index (%)	-0.46	-0.03	0.19
Soil properties			
Soil pH	0.09	0.02	0.32
Water content (%)	0.57	**0.59***	-0.02
Bulk density (g/cm^3)	**-0.74****	**-0.58***	0.46
TOC (%)	**0.72****	**0.74****	-0.31
TKN (%)	-0.06	0.09	**0.87****
TP (%)	0.18	0.12	-0.24
C:N Ratio	0.27	0.30	**-0.73****
N:P Ratio	-0.09	0.05	**0.69***
Gravel (%)	-0.36	**-0.93****	0.11
Sand (%)	**-0.65***	**-0.59***	0.04
Silt (%)	**0.64***	0.51	-0.06
Clay (%)	**0.75****	**0.69***	-0.17
Porewater properties			
Temperature (°C)	-0.43	0.03	0.42
pH	0.36	0.03	0.10
Salinity (ppt)	-0.35	-0.02	0.02
ORP (mV)	-0.17	0.11	0.23
DO (mg/L)	-0.25	0.27	0.44

Only three soil properties, including TKN, C:N ratio and N:P ratio, strongly correlate with N_2O flux. Nitrogen availability in mangrove soil is an energy source for denitrifying bacteria to produce N_2O gas (Queiroz et al., 2019). Measured TKN includes organic nitrogen and also ammonium (NH_4^+) and ammonia (NH_3). Since N_2O flux highly correlates with TKN, it shows that nitrification and denitrification processes in the nitrogen cycle are occurring in the mangrove ecosystem. The nitrification process converts NH_4^+ and NH_3 into nitrate (NO_3), while denitrification converts NO_3 into nitrite (NO_2^-)- > NO- > N_2O- > N_2 (stable) (Robertson and Groffman, 2024).

In addition, another parameter could have a significant relationship with GHG fluxes in different conditions and locations. Vegetation stand structure and composition may impact GHG fluxes indirectly since they could affect soil organic matter production. A high density of mangrove stands and canopy cover leads to higher organic matter, including TOC and TN, which are the sources of GHG production (Weiss et al., 2016; Alongi, 2020; Dermawan et al., 2023). Soil and porewater pH are also one of the important indicators, especially for CH_4 production. A low pH value could show high CH_4 production due to anoxic conditions (Koebsch et al., 2013; Ulumuddin, 2018). Porewater ORP and DO are also other crucial parameters. CO_2 is mostly produced when their values increase, while low ORP and DO will cause increased fluxes of CH_4 and N_2O. Temperature also plays a

crucial role in influencing the rate of micrometabolic processes, thereby impacting variations in GHG production. Another last parameter that could affect GHG production is salinity. Salinity often affects CH_4 synthesis by enhancing the activity of sulfate-reducing bacteria, which compete with methanogens for resources (Chen et al., 2014; Welti et al., 2017; Sugiana et al., 2023).

The first principal component (PC1) explains 55.161% of the total variance, while the second principal component (PC2) accounts for 22.579% of the variance. Together, these components explain 77.74% of the total variability, which indicates that the two principal components effectively capture the primary patterns in the data. Sapling Density shows a strong positive contribution to both PC1 and PC2, suggesting that areas with higher sapling density are significantly distinct in terms of the environmental variables considered. N_2O contributes positively to PC2, implying that higher N_2O levels are associated with variations captured by the second principal component. CO_2, Clay, TOC, and CH_4 exhibit strong positive contributions to PC1, indicating that these variables are closely related and influence the first principal component. C:N has a strong negative contribution to PC1, suggesting that lower C:N are characteristic of the environmental gradient represented by PC1.

Bruguiera plots (represented by red triangles) predominantly cluster in the negative quadrant of PC1, except for B1 (Figure 6). This clustering suggests that *Bruguiera* dominated area are associated with environments characterized by lower levels of CO_2, Clay, TOC, and CH_4, but higher C:N. *Rhizophora* plots (depicted by blue triangles) are distributed across the negative sides of both PC1 and PC2, with the exception of R5, indicating that these species are adapted to environments with lower levels of most considered environmental variables. *Sonneratia* plots (represented by yellow squares) exhibit a broader distribution across the biplot. S4 and S2 plots are positioned in the positive quadrant of PC1, suggesting that *Sonneratia* dominated area are more tolerant of or associated with higher levels of CO_2, Clay, TOC, and CH_4. These results indicate that mangrove soil dominated by *Sonneratia* may exhibit both oxic and anoxic conditions, as indicated by high production of CO_2 and CH_4.

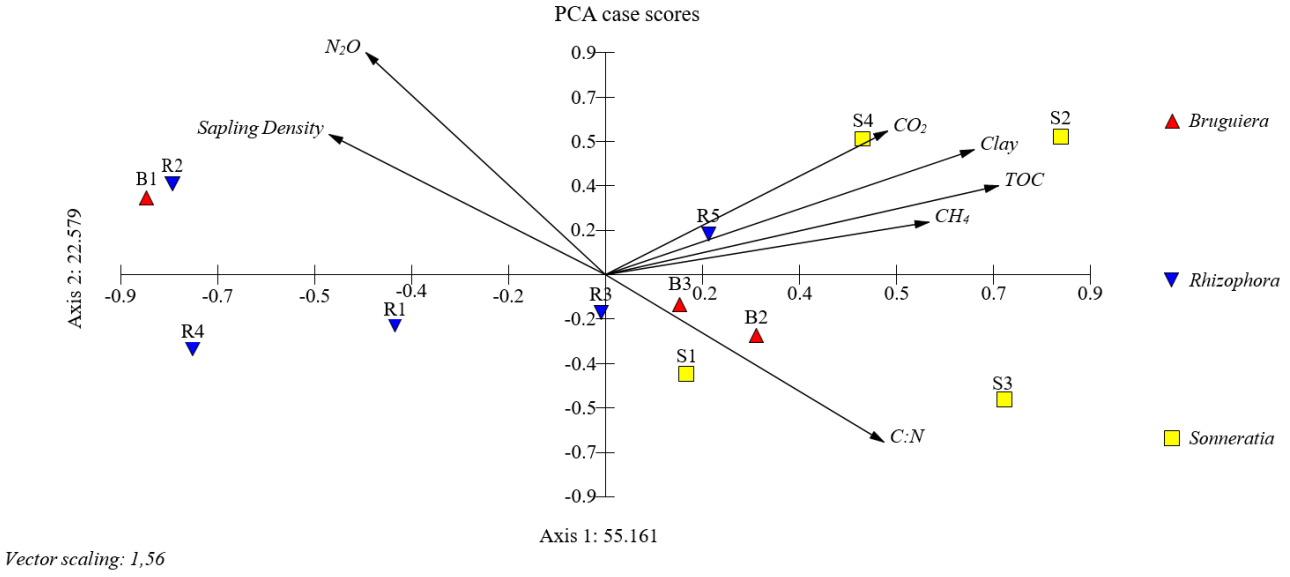

Figure 6. PCA analysis result of GHG fluxes and mangrove ecological parameters (B: *Bruguiera*, R: *Rhizophora* and S: *Sonneratia* zones)

3.4 Contribution to warming effect

The average GHG flux value of CO_2-equivalent (warming effect) showed positive results across mangrove zones but with a high variability. N_2O is the primary factor contributing to high warming in the *Bruguiera* and *Rhizophora* zones, while CH_4 is the major contributer in the *Sonneratia* zone. The *Sonneratia* zone has emerged as the primary driver of the warming effect, contributing the highest amount of 1.8±1.4 $MgCO_2$/ha/year (Table 5).

Compared to other studies, the global warming effect of GHG fluxes from mangrove sediments in Bali's Ngurah Rai Forest Park is relatively low. In Sulawesi, Indonesia, with an almost similar mangrove

zonation, the warming effect from mangrove soil GHGs is nearly 16 times greater than this result (Table 6). This demonstrates that factors other than the mangrove genera zonation pattern affect GHG emissions. We have summarised several comparisons of the warming effect of each GHG in several regions of the world, as shown in Table 6.

Table 5. Soil greenhouse gases warming effect from each mangrove zones in Ngurah Rai Forest Park, Bali, Indonesia

Zone	CO_2-equivalent flux ($MgCO_2$/ha/year)			
	CO_2	CH_4	N_2O	Total
Bruguiera	0.2±1.3	0.1±0.1	0.5±1.9	0.9±1.1
Rhizophora	0.1±0.8	0.3±0.1	0.6±1.0	1.0±1.3
Sonneratia	0.2±0.7	1.5±0.1	0.2±0.9	1.8±1.4
Average	0.2±1.0	0.6±0.1	0.4±1.1	1.2±1.2

Table 6. Warming effect of soil greehouse gases from several regions (NA: data not available)

Region	Condition	Warming effect ($MgCO_2$/ha/year)			Total	References
		CO_2	CH_4	N_2O		
Ngurah Rai Forest Park, Bali, Indonesia	Peak of dry season (August), three dominated genera	0.6±0.1	0.2±1.0	0.4±1.1	1.2±1.2	This study
	Wet season (December) three dominated genera	0.2±0.1	0.6±0.4	1.1±0.4	1.9±0.7	Sugiana et al. (2023)
Ayeyarwady Delta, Myanmar	Dry season (February)	8±0.5	0.2±0.1	1.6±0.3	9.8±0.9	Cameron et al. (2021)
	Wet season (October)	78.5±16.2	0.3±0.1	NA	78.8±16.3	
North Sulawesi, Indonesia	High *Ceriops tagal*/*R. apiculata*/*S. alba* covers, 10 years old mangroves	25.7±2	3.1±0.5	0.7±0.3	29.5±2.8	Cameron et al. (2019)
South Sulawesi, Indonesia	*R. apiculata*/*S. alba*/*B. gymnorrhiza* dominated zone	16.7±0.8	1.4±0.2	1.3±0.1	19.4±1.1	Cameron et al. (2019)
	Inudated, operating ponds	0.5±0.0	0.6±0.3	NA	1.1±0.2	
Perancak Estuary, Bali, Indonesia	*Avicennia*, *Rhizophora*, *Sonneratia*, and *Bruguiera* dominated zones	44.8±6.6	NA	NA	44.8±6.6	Sidik et al. (2019)
Northern Vietnam	*Kandelia candel* dominated site	15.3±14.3	NA	NA	15.3±14.3	Hien et al. (2018)
Honday Bay, Philippines	Abandoned pond with little regrowth mangroves	15.9±3.7	NA	NA	15.9±3.7	Castillo et al. (2017)
Global average of mangrove forest	Sum of autotrophic and heterotrophic respiration	17.6	19.5	NA	19.5	Alongi (2014)

Compared to the rate of CO_2 sequestration (as shown in Table 1), which effectively decreases the warming impact on the atmosphere, the proportion of greenhouse gas emissions to CO_2 storage rate is only approximately 1.1-2.2% for all the mangrove zones in Ngurah Rai Forest Park. Therefore, the emission of GHG does not substantially impact the mangrove ecosystem's ability to mitigate global warming. Consequently, it can be disregarded when calculating the carbon stock in the case of the mangrove ecosystem in Ngurah Rai Forest Park, Bali. However, to determine the significance of the warming impact value, conducting a thorough and evaluation is imperative. Multiple studies have shown that the warming effect value can account for up to 20.5% of the overall carbon sequestration rate in the mangrove ecosystem in China, specifically in areas dominated by the genus Kandelia (Chen et al., 2016). Furthermore, considering only CH_4 emissions, the warming effect value can reach as high as 24% (Liu et al., 2020). Zoning characteristics and the environmental conditions that facilitate greenhouse gasses (GHGs) production can contribute to this variation (Zhu et al., 2013).

4. CONCLUSION

In summary, there are no substantial variations in soil GHG fluxes across mangrove zones. Mangrove

soil can function as both sources and sinks of GHGs. The flux of GHGs is closely associated with several parameters, such as SOC, TKN, water content, bulk density, and soil type. CH_4 significantly contributed to the *Sonneratia* zone's warming effect, while N_2O was the major contributor in the other two zones. Soil GHGs warming effect only reduces small amounts of mangrove ecosystem effectivness in mitigating global warming. Hence, the impact of greenhouse gas emissions in each mangrove zone can be disregarded when estimating the carbon stock at TAHURA Ngurah Rai, Bali.

ACKNOWLEDGEMENTS

We express our gratitude to the Indonesian Ministry of Education, Culture, Research, and Technology (Kemendikbudristek) for providing financial support for this research project under the master's thesis research plan (18930/IT3.D10/ PT.01.02/M/T/2023). We also thank Putri, Nova, Echa, Ilham, and Wahyu for their valuable contributions in collecting field data and Dr. Bruce Campbell for his help in improving the English grammar in this paper. The authors declare no conflict of interest in preparing this paper.

REFERENCES

Adame MF, Lovelock CE. Carbon and nutrient exchange of mangrove forests with the coastal ocean. Hydrobiologia 2011;663:23-50.

Allen DE, Dalal RC, Rennenberg H, Meyer RL, Reeves S, Schmidt S. Spatial and temporal variation of nitrous oxide and methane flux between subtropical mangrove sediments and the atmosphere. Soil Biology and Biochemistry 2007;39(2):622-31.

Alongi DM. Carbon cycling and storage in mangrove forests. Annual Review of Marine Science 2014;6:195-219.

Alongi DM. Nitrogen cycling and mass balance in the world's mangrove forests. Nitrogen 2020;1(2):167-89.

Amorim HC, Araujo MA, Lal R, Zinn YL. What C:N ratios in soil particle-size fractions really say: N is preferentially sorbed by clays over organic C. Catena 2023;230:Article No. 107230.

Atwood TB, Connolly RM, Almahasheer H, Carnell PE, Duarte CM, Ewers Lewis CJ, et al. Global patterns in mangrove soil carbon stocks and losses. Nature Climate Change 2017; 7(7):523-8.

Braker G, Conrad R. Diversity, structure, and size of N_2O-producing microbial communities in soils: What matters for their functioning? Advances in Applied Microbiology 2011; 75:33-70.

Bunting P, Rosenqvist A, Lucas RM, Rebelo LM, Hilarides L, Thomas N, et al. The global mangrove watch: A new 2010 global baseline of mangrove extent. Remote Sensing 2018; 10(10):Article No. 1669.

Cabezas A, Mitsch WJ, MacDonnell C, Zhang L, Bydałek F, Lasso A. Methane emissions from mangrove soils in hydrologically disturbed and reference mangrove tidal creeks in southwest Florida. Ecological Engineering 2018;114:57-65.

Cameron C, Hutley LB, Friess DA. Estimating the full greenhouse gas emissions offset potential and profile between rehabilitating and established mangroves. Science of the Total Environment 2019;665:419-31.

Cameron C, Hutley LB, Munksgaard NC, Phan S, Aung T, Thinn T, et al. Impact of an extreme monsoon on CO_2 and CH_4 fluxes from mangrove soils of the Ayeyarwady Delta, Myanmar. Science of the Total Environment 2021;760:Article No. 143422.

Castillo JAA, Apan AA, Maraseni TN, Salmo SG. Soil greenhouse gas fluxes in tropical mangrove forests and in land uses on deforested mangrove lands. Catena 2017;159:60-9.

Chauhan R, Datta A, Ramanathan AL, Adhya TK. Factors influencing spatio-temporal variation of methane and nitrous oxide emission from a tropical mangrove of eastern coast of India. Atmospheric Environment 2015;107:95-106.

Chen G, Chen B, Yu D, Tam NF, Ye Y, Chen S. Soil greenhouse gas emissions reduce the contribution of mangrove plants to the atmospheric cooling effect. Environmental Research Letters 2016;11(12):Article No. 124019.

Chen GC, Tam NF, Ye Y. Spatial and seasonal variations of atmospheric N_2O and CO_2 fluxes from a subtropical mangrove swamp and their relationships with soil characteristics. Soil Biology and Biochemistry 2012;48:175-81.

Chen GC, Tam NF, Ye Y. Summer fluxes of atmospheric greenhouse gases N_2O, CH_4 and CO_2 from mangrove soil in South China. Science of the Total Environment 2010; 408(13):2761-7.

Chen GC, Ulumuddin YI, Pramudji S, Chen SY, Chen B, Ye Y, et al. Rich soil carbon and nitrogen but low atmospheric greenhouse gas fluxes from North Sulawesi mangrove swamps in Indonesia. Science of the Total Environment 2014;487:91-6.

Conrad R. Soil microorganisms as controllers of atmospheric trace gases (H_2, CO, CH_4, OCS, N_2O, and NO). Microbiological Reviews 1996;60(4):609-40.

Craig H, Antwis RE, Cordero I, Ashworth D, Robinson CH, Osborne TZ, et al. Nitrogen addition alters composition, diversity, and functioning of microbial communities in mangrove soils: An incubation experiment. Soil Biology and Biochemistry 2021;153:Article No. 108076.

Dangremond EM, Feller IC, Sousa WP. Environmental tolerances of rare and common mangroves along light and salinity gradients. Oecologia 2015;179:1187-98.

Das N, Mondal A, Mandal S. Polluted waters of the reclaimed islands of Indian Sundarban promote more greenhouse gas emissions from mangrove ecosystem. Stochastic Environmental Research and Risk Assessment 2022;36: 1277-88.

Dermawan EP, Siregar YI, Efriyeldi E. Estimation of carbon reserves in sediments in the mangrove ecosystem of Bukit Batu Village, Bengkalis Regency, Riau. Asian Journal of Aquatic Sciences 2023;6(1):93-101.

Dewi IG, Faiqoh E, As-syakur AR, Dharmawan IW. Natural regeneration of mangrove seedlings in Benoa Bay, Bali. Journal of Tropical Marine Science and Technology 2021;13(3):395-410.

Dharmawan IWE, Ulumuddin YI, Prayudha B. Guide to Monitoring Mangrove Community Structure in Indonesia. Bogor, Indonesia: PT Media Sains Nasional; 2020.

Dharmawan IWE, Ulumuddin YI. Mangrove Community Structure Data Analysis, A Guidebook for Mangrove Health Index (MHI) Training. Makassar, Indonesia: NAS Media Pustaka; 2021.

Ewel K, Bourgeois J, Cole T, Zheng S. Variation in environmental characteristics and vegetation in high-rainfall mangrove forests, Kosrae, Micronesia. Global Ecology and Biogeography Letters 1998;7(1):49-56.

Gao Y, Zhou J, Wang L, Guo J, Feng J, Wu H, et al. Distribution patterns and controlling factors for the soil organic carbon in four mangrove forests of China. Global Ecology and Conservation 2019;17:e00575.

Hall SJ, McDowell WH, Silver WL. When wet gets wetter: Decoupling of moisture, redox biogeochemistry, and greenhouse gas fluxes in a humid tropical forest soil. Ecosystems 2013;16:576-89.

Hien HT, Marchand C, Aime J, Cuc NT. Seasonal variability of CO_2 emissions from sediments in planted mangroves (Northern Viet Nam). Estuarine, Coastal and Shelf Science 2018;213:28-39.

Imamsyah A, Bengen DG, Ismet MS. Structure and distribution of mangrove vegetation based on biophysical environmental quality in the Ngurah Rai Grand Forest Park, Bali. Ecotrophic 2020;14(1):88-99.

Inoue T, Nohara S, Matsumoto K, Anzai Y. What happens to soil chemical properties after mangrove plants colonize? Plant and Soil 2011;346:259-73.

Intergovernmental Panel on Climate Change (IPCC). Climate Change 2021: The Physical Science Basis. Contribution of Working Group I to the Sixth Assessment Report of the Intergovernmental Panel on Climate Change. Cambridge, USA: Cambridge University Press; 2021.

Japan International Cooperation Agency (JICA). The Final Report of Project Administration: The Development of Sustainable Mangrove Management Project Bali and Lombok, Republic of Indonesia. Jakarta, Indonesia: Ministry of Forestry and Estate Crops in Indonesia - Japan International Cooperation Agency; 1999.

Kalyuzhnaya MG, Gomez OA, Murrell JC. The methane-oxidizing bacteria (methanotrophs). In: McGenity T, editor. Taxonomy, Genomics and Ecophysiology of Hydrocarbon-Degrading Microbes: Handbook of Hydrocarbon and Lipid Microbiology. Switzerland: Springer Nature; 2019. p. 245-78.

Kitpakornsanti K, Pengthamkeerati P, Limsakul A, Worachananant P, Diloksumpun S. Greenhouse gas emissions from soil and water surface in different mangrove establishments and management in Ranong Biosphere Reserve, Thailand. Regional Studies in Marine Science 2022;56:Article No. 102690.

Koebsch F, Glatzel S, Jurasinski G. Vegetation controls methane emissions in a coastal brackish fen. Wetlands Ecology and Management 2013;21:323-37.

Konnerup D, Betancourt-Portela JM, Villamil C, Parra JP. Nitrous oxide and methane emissions from the restored mangrove ecosystem of the Ciénaga Grande de Santa Marta, Colombia. Estuarine, Coastal and Shelf Science 2014;140:43-51.

Kweku DW, Bismark O, Maxwell A, Desmond KA, Danso KB, Oti-Mensah EA, et al. Greenhouse effect: Greenhouse gases and their impact on global warming. Journal of Scientific Research and Reports 2018;17(6):1-9.

Lin CW, Kao YC, Chou MC, Wu HH, Ho CW, Lin HJ. Methane emissions from subtropical and tropical mangrove ecosystems in Taiwan. Forests 2020;11(4):Article No. 470.

Liu J, Zhou Y, Valach A, Shortt R, Kasak K, Rey-Sanchez C, et al. Methane emissions reduce the radiative cooling effect of a subtropical estuarine mangrove wetland by half. Global Change Biology 2020;26(9):4998-5016.

Lovelock CE, Feller IC, Ball MC, Engelbrecht BM, Ewe ML. Differences in plant function in phosphorus-and nitrogen-limited mangrove ecosystems. New Phytologist 2006; 172(3):514-22.

Marton JM, Herbert ER, Craft CB. Effects of salinity on denitrification and greenhouse gas production from laboratory-incubated tidal forest soils. Wetlands 2012;32: 347-57.

Matus FJ. Fine silt and clay content is the main factor defining maximal C and N accumulations in soils: A meta-analysis. Scientific Reports 2021;11(1):Article No. 6438.

Montzka SA, Dlugokencky EJ, Butler JH. Non-CO_2 greenhouse gases and climate change. Nature. 2011;476(7358):43-50.

Mulya MB, Arlen HJ. Production of litter and detritus related to the density of mangrove. Proceeding of the International Conference on Biological Sciences and Biotechnology (ICBSB); 2018 March 1; Grandhika Setiabudi Medan Hotel, North Sumatra: Indonesia; 2018.

Nazir R, Zaffar R. Climate change extenuation by greenhouse gas quenching microflora. In: Lone SA, Malik A, editors. Microbiomes and the Global Climate Change. Singapore: Springer Nature; 2021. p. 23-41.

Padhy SR, Bhattacharyya P, Dash PK, Reddy CS, Chakraborty A, Pathak H. Seasonal fluctuation in three mode of greenhouse gases emission in relation to soil labile carbon pools in degraded mangrove, Sundarban, India. Science of the Total Environment 2020;705:Article No. 135909.

Perie C, Ouimet R. Organic carbon, organic matter and bulk density relationships in boreal forest soils. Canadian Journal of Soil Science 2008;88(3):315-25.

Prasad MBK, Dittmar T, Ramanathan AL. Organic matter and mangrove productivity. In: Ramanathan AL, Bhattacharya P, Dittmar T, Prasad MBK, Neupane BR, editors. Management and Sustainable Development of Coastal Zone Environments. Netherlands: Springer Nature; 2010. p. 175-93.

Prinasti NK, Dharma IG, Suteja Y. Community structure of mangrove vegetation based on substrate characteristic in Ngurah Rai Forest Park, Bali. Journal of Marine and Aquatic Sciences 2020;6(1):90-9.

Queiroz HM, Artur AG, Taniguchi CA, da Silveira MR, do Nascimento JC, Nobrega GN, et al. Hidden contribution of shrimp farming effluents to greenhouse gas emissions from mangrove soils. Estuarine, Coastal and Shelf Science 2019;221:8-14.

Raganas AF, Magcale-Macandog DB. Physicochemical factors influencing zonation patterns, niche width and tolerances of dominant mangroves in Southern Oriental Mindoro, Philippines. Indo Pacific Journal of Ocean Life 2020;4(2):51-62.

Reay DS, Smith P, Christensen TR, James RH, Clark H. Methane and global environmental change. Annual Review of Environment and Resources 2018;43:165-92.

Robertson GP, Groffman PM. Nitrogen transformations. In: Paul EA, Frey SD, editors. Soil Microbiology, Ecology and Biochemistry. USA: Elsevier; 2024. p. 407-38.

Romero-Uribe HM, López-Portillo J, Reverchon F, Hernández ME. Effect of degradation of a black mangrove forest on seasonal greenhouse gas emissions. Environmental Science and Pollution Research 2022;29:11951-65.

Sidik F, Adame FM, Lovelock CE. Carbon sequestration and fluxes of restored mangroves in abandoned aquaculture ponds. Journal of the Indian Ocean Region 2019;15(2):177-92.

Srikanth S, Lum SK, Chen Z. Mangrove root: Adaptations and ecological importance. Trees 2016;30:451-65.

Sugiana IP, Andiani AAE, Dewi IGAIP, Karang IWGA, As-Syakur AR, Dharmawan IWE. Spatial distribution of mangrove health index on three genera dominated zones in Benoa Bay, Bali, Indonesia. Biodiversitas Journal of Biological Diversity 2022;23(7):3407-18.

Sugiana IP, Faiqoh E, Adame MF, Indrawan GS, Andiani AA, Dewi IG, et al. Soil greenhouse gas fluxes to the atmosphere during the wet season across mangrove zones in Benoa Bay, Indonesia. Asian Journal of Atmospheric Environment 2023;17(13):1-12.

Sugiana IP, Faiqoh E, Indrawan GS, Dharmawan IW. Methane concentration on three mangrove zones in Ngurah Rai Forest Park, Bali. Jurnal Ilmu Lingkungan 2021;19(2):422-31.

Sugiana IP, Prartono T, Rastina, Koropitan AF. Ecosystem carbon stock and annual sequestration rate from three genera-dominated mangrove zones in Benoa Bay, Bali, Indonesia. Biodiversitas 2024;25(1):287-99.

Treat CC, Natali SM, Ernakovich J, Iversen CM, Lupascu M, McGuire AD, et al. A pan-Arctic synthesis of CH_4 and CO_2 production from anoxic soil incubations. Global Change Biology 2015;21(7):2787-803.

Ulumuddin YI. Methane: Greenhouse gas emissions from blue carbon ecosystems, mangroves. Jurnal Ilmu Lingkungan 2018;17(2):359-72.

Ussiri D, Lal R. Formation and release of nitrous oxide from terrestrial and aquatic ecosystems. In: Ussiri D, Lal R, editors. Soil Emission of Nitrous Oxide and Its Mitigation. Netherlands: Springer Nature; 2013. p. 63-96.

Wang D, Chen Z, Sun W, Hu B, Xu S. Methane and nitrous oxide concentration and emission flux of Yangtze Delta plain river net. Science in China Series B: Chemistry 2009;52(5): 652-61.

Weiss C, Weiss J, Boy J, Iskandar I, Mikutta R, Guggenberger G. Soil organic carbon stocks in estuarine and marine mangrove ecosystems are driven by nutrient colimitation of P and N. Ecology and Evolution 2016;6(14):5043-56.

Welti N, Hayes M, Lockington D. Seasonal nitrous oxide and methane emissions across a subtropical estuarine salinity gradient. Biogeochemistry 2017;132:55-69.

Xiong Y, Liu X, Guan W, Liao B, Chen Y, Li M, et al. Fine root functional group-based estimates of fine root production and turnover rate in natural mangrove forests. Plant and Soil 2017;413:83-95.

Xu Y, Liao B, Jiang Z, Xin K, Xiong Y, Guan W. Emission of greenhouse gases (CH_4 and CO_2) into the atmosphere from restored mangrove soil in South China. Journal of Coastal Research 2021;37(1):52-8.

Yost JL, Hartemink AE. Soil organic carbon in sandy soils: A review. Advances in Agronomy 2019;158:217-310.

Zhu X, Burger M, Doane TA, Horwath WR. Ammonia oxidation pathways and nitrifier denitrification are significant sources of N_2O and NO under low oxygen availability. Proceedings of the National Academy of Sciences 2013;110(16):6328-33.

Zumft WG, Kroneck PM. Respiratory transformation of nitrous oxide (N_2O) to dinitrogen by bacteria and archaea. Advances in Microbial Physiology 2006;52:107-227.

Environment and Natural Resources Journal

Volume 22
Issue 5
2024

Distribution of Salinity in Surface Water Surrounding Salt Mines in Non Thai and Phra Thong Kham Districts, Nakhon Ratchasima Province, Thailand

Bantita Terakulsatit*, Sakchai Glumglomjit, Thanyalak Anuphan, and Namthip Nongse

School of Geotechnology, Institute of Engineering, Suranaree University of Technology, Nakhon Ratchasima 30000, Thailand

ARTICLE INFO

Received: 30 Jan 2024
Received in revised: 14 Aug 2024
Accepted: 19 Aug 2024
Published online: 4 Sep 2024
DOI: 10.32526/ennrj/22/20240022

Keywords:
Saline water/ Saline soil/ Sodium adsorption ratio/ Water quality/ Chlorite content

*** Corresponding author:**
E-mail: tbantita@sut.ac.th

ABSTRACT

Nakhon Ratchasima Province faces significant challenges due to saline soil and water, resulting from natural salt rock deposits and salt mining activities. This study investigates the physicochemical properties, salinity distribution, and surface water quality in Non Thai and Phra Thong Kham District. A total of 75 samples were collected, with 48 from Non Thai and 27 from Phra Thong Kham. The analysis focused on properties such as temperature, electrical conductivity (EC), pH, total dissolved solids (TDS), salinity, chloride, sodium, calcium, and magnesium. Water quality was assessed using standards from the Thai Department of Health and the World Health Organization. Additionally, the Sodium Adsorption Ratio (SAR) was employed to evaluate irrigation suitability, and ArcGIS 10.5 was utilized to map salinity and water quality distribution. Results indicated that surface water pH remained relatively neutral and within acceptable limits. However, salinity levels varied from 0.5 to 30 ppt, indicating brackish to saline conditions. In several areas, concentrations of salinity, sodium, and chloride exceeded standard limits. Factors such as proximity to salt mines, water flow direction, lower terrain, and smaller reservoirs were linked to increased salinity, with Phang Thiam Subdistrict in Phra Thong Kham District showing the highest levels. The SAR index further indicated that water quality in Phra Thong Kham was unsuitable for domestic use and irrigation, unlike Non Thai. Further research in other salt mine areas are essential for a deeper understanding of salinity distribution, which is crucial for assessing risks and making informed decisions to protect public health and the environment.

1. INTRODUCTION

The rock salt formation in Thailand is located in two basins (Sakon Nakhon and Khorat Basins) of the Khorat Plateau in Northeastern Thailand (Figure 1). The total rock salt reserve is estimated to be at least 18 trillion tons (Akhrajanthachot, 2010). Both basins contain three layers of evaporated deposits within the Maha Sarakham salt-bearing strata (Suwanich et al., 1986) as shown in Figure 2.

Salt mines in Thailand are mainly distributed in the northeastern region, including Chaiyaphum, Khon Kaen, Maha Sarakham, Udon Thani, Sakon Nakhon, Nakhon Phanom, and Nakhon Ratchasima Provinces. The Nakhon Ratchasima Province, in particular, hosts a significant number of salt mines, scattered across various areas such as Phimai, Non Sung, Dan Khun Thot, and Phra Thong Kham Districts (DPIM, 2009). Salt mines are usually in the form of halite and are extracted from evaporite formations, originating from dissolved rock salt in the Maha Sarakham Formation (El Tabakh et al., 1999). The salt mining activities in these areas have various impacts on the region in multiple dimensions, such as social, economic, and environmental aspects (DPIM, 2010).

Citation: Terakulsatit B, Glumglomjit S, Anuphan T, Nongse N. Distribution of salinity in surface water surrounding salt mines in Non Thai and Phra Thong Kham Districts, Nakhon Ratchasima Province, Thailand. Environ. Nat. Resour. J. 2024;22(5):464-475. (https://doi.org/10.32526/ennrj/22/20240022)

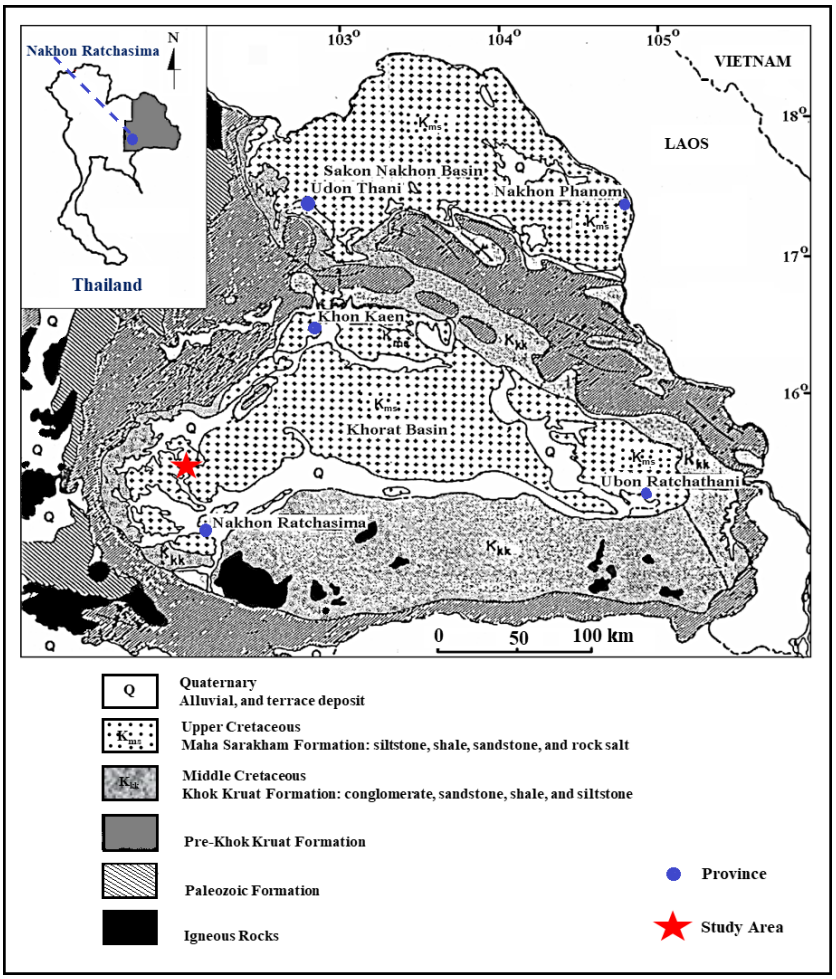

Figure 1. Sakon Nakhon and Khorat Basins in Northeastern Thailand containing rock salt (modified from Utha-aroon, 1993).

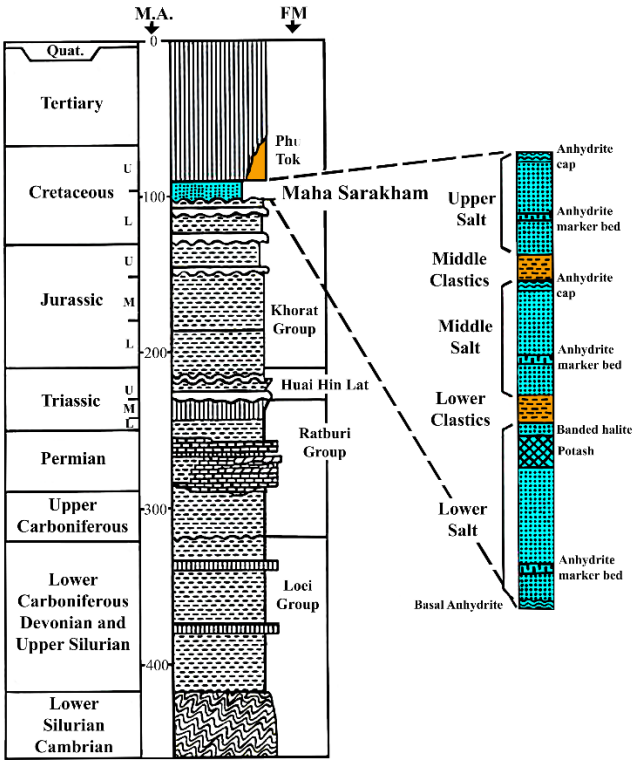

Figure 2. Lithostratigraphy and subdivisions of the Khorat Group and the Maha Sarakham Formation (modified from Suwanich, 1986).

The environmental impacts of salt mining in the Non Thai and Phra Thong Kham Districts of Nakhon Ratchasima Province have given rise to salinity issues in surface water, groundwater, and soil. This situation is exacerbated by the presence of saline soil and water originating from salt rock formation in the area (Wannakomol, 2005; Thongwat, 2018; Thongwat and Terakulsatit, 2019). The major causes of salinity are salts dissolving in groundwater and accumulating on the ground surface, sodium chloride, and shallow groundwater table depth depending on geomorphology, geology, and structural geology (Phoemphon and Terakulsatit, 2022; Wannakomol and Terakulsatit, 2018). Typically, this region encounters challenges associated with moderately to extremely saline soil (Figure 3), resulting in less prevalent cultivation of crops during the dry season compared to other regions. Additionally, issues related to the depletion of surface water and the presence of saline groundwater can be observed. The quality of the water is deemed inappropriate for consumption due to its excessive salinity (Royal Irrigation Department, 2020; Environment and Pollution Control, 2022). Furthermore, aside from the environmental impact of salt mining, certain regions are currently experiencing land subsidence (Wannakomol and Terakulsatit, 2018).

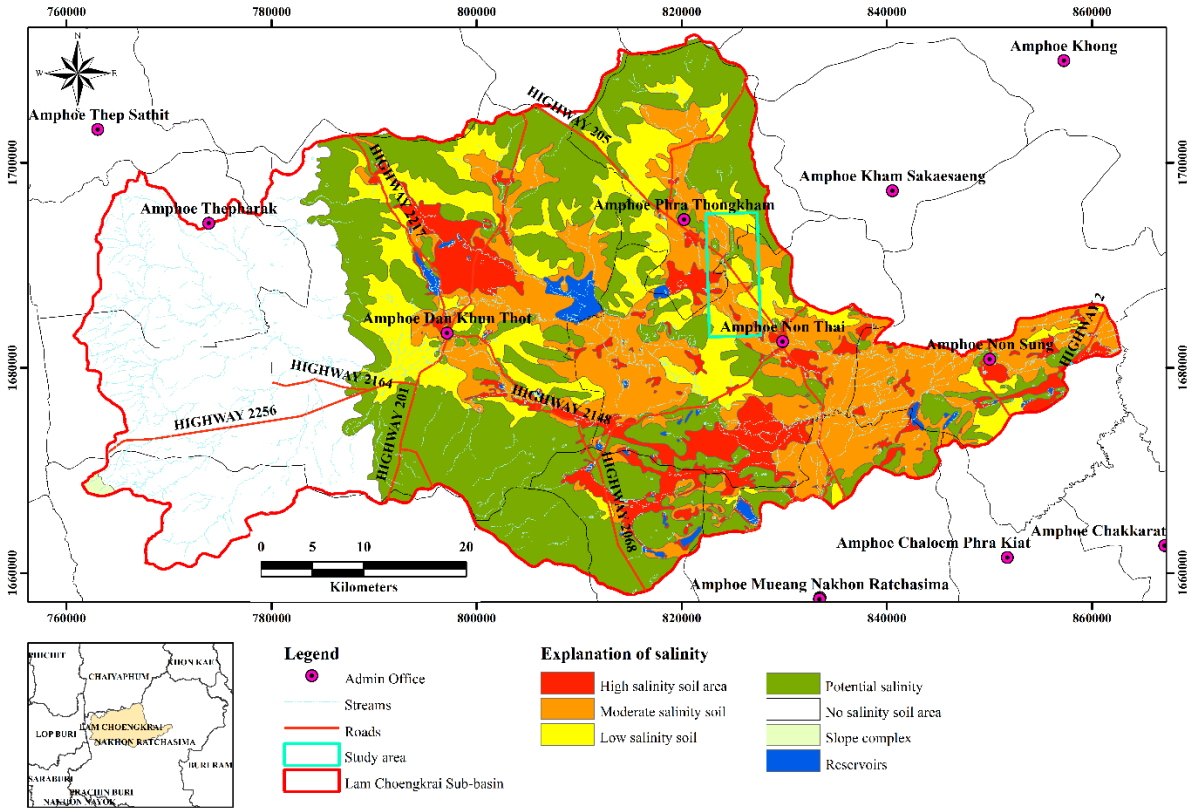

Figure 3. Saline soil area in Lam Chiang Krai River Basin in Non Thai and Phra Thong Kham Districts, Nakhon Ratchasima Provinces (modified from Royal Irrigation Department, 2020)

The unresolved conflict between the community and salt mine operators regarding the environmental impacts has resulted in a lack of understanding and awareness among community members (Green News, 2024; Prachathai News, 2023). The root cause lies in the dissemination of inaccurate information within the academic environment and the absence of proactive strategies to address associated issues. This has led to persistent conflicts without resolution. The community faces ongoing challenges due to water shortages, significantly impacting livelihoods, society, and the local economy near the salt mine. Thus, good management practices in salt mining are crucial for minimizing the negative impacts on both society and the environment in the long run. Monitoring and assessing the environmental impacts in the areas surrounding these salt mines helps to track the various impacts while assisting in managing and preventing the adverse effects that may occur. To address these issues and empower the community, this research aims to comprehensively investigate and assess the physical and chemical properties, as well as the distribution of salinity and surface water quality in the Non Thai and Phra Thong Kham Districts of Nakhon Ratchasima

Province. The anticipated outcomes of this study will serve to furnish the community with valuable insights into surface water quality and salinity within the study area. This information can be utilized in diverse applications, ensuring suitability and safety for purposes such as consumption, agriculture, and livestock. Furthermore, the findings will play a key role in developing water management strategies specifically suited to the needs of the study area.

2. METHODOLOGY

2.1 Study area

The study area encompasses coordinates 0178000E to 0183000E and 1689000N to 1695000N, covering 30 km^2. It is situated in two Districts, namely Non Thai (Sai-O and Non Thai Subdistricts) and Phra Thong Kham (Phang Thiam and Nong Hoi Subdistricts) within Nakhon Ratchasima Province (Figure 4). The salt mine is centrally located in the Phang Thiam Subdistrict of Phra Thong Kham District and the Banlang Subdistrict of Non Thai District (Figure 4), located at 15.25697 N and 101.98809 E (DPIM, 2009).

The general topography of this study area consists of plateaus interspersed with lowlands, with altitudes ranging from between 200 and 250 meters above sea level (LICD, 2022). The region features gently rolling low hills, except in mountainous areas where undulations are more pronounced. Flat valleys are found along various rivers, such as Lam Chiang Krai, Khlong Non Phao Phi, Khlong Sawai, Khlong Dan, Khlong Yang, and Khong Hut Phi Man (Royal Irrigation Department, 2020). The southern part of the study area is lower than the northern, influencing the flow direction of streams and canals, generally moving from northwest to southeast.

The prevalent soil type is sandy loam to coarse loamy, known for having low moisture retention, diminished fertility, and surface salt distribution (Land Development Department, 2021). The climate has three distinct seasons, with a general tendency toward dry conditions (Thongwat, 2018). Annual averages for rainfall, temperature, and relative humidity were approximately 924.4 mm, 27.4°C, and 71%, respectively.

2.2 Water samples and analysis

A total of 75 surface water samples in this study were collected between December 2022 and January 2023. This research involved the observation, measurement, and collection of 75 surface water samples in the area from both natural (canals) and man-made (reservoirs, ponds, and pools) water resources. Specifically, 48 samples (NT samples) were collected from Non Thai District, and 27 samples (PK samples) from Phra Thong Kham District in Nakhon Ratchasima Province (Figure 4). Water temperature, electrical conductivity (EC), pH, total dissolved solids (TDS), and salinity were measured using the Hanna Model EM-410-SS. The chloride content was analyzed by titration method according to the Mohr (Skoog et al., 1996). Chemical compounds, including ions of sodium (Na), calcium (Ca), and magnesium (Mg), were analyzed using Inductively Plasma Optical Emission Spectroscopy (ICP_OES) at the Suranaree University of Technology Laboratory, Thailand.

2.3 Sodium adsorption ratio (SAR) evaluation

The assessment of water samples for irrigation purposes involves the computation of the adjusted SAR index, following the methodology proposed by Lesch and Suarez (2009). The irrigation water classification is based on the correlation between the SAR and EC of the water samples. SAR is a pivotal parameter in determining the appropriateness of water for irrigation, serving as an indicator of the alkali/sodium hazard to crops. The SAR is determined using Equation (1) as follows:

$$\text{Sodium Adsorption Ratio (SAR)} = \frac{\text{Na}}{\sqrt{\text{Ca+Mg}}} \quad (1)$$

Based on the SAR values, the water type, quality, and suitability for irrigation as shown in Table 1.

Table 1. Classification of irrigation water based on SAR (Guettaf et al., 2017)

SAR values	Quality	Type of water and suitability for irrigation
<10	Excellent	Low-sodium water is suitable for all types of crops and soils, except for crops sensitive to sodium.
10-18	Good	Medium sodium water is suitable for coarse-textured or organic soil with good permeability. But relatively unsuitable in fine-textured soils.
18-26	Fair	High sodium water is harmful to almost all types of soil; requires good drainage, and the addition of high-leaching gypsum.
>26	Poor	Very high sodium water is unsuitable for irrigation.

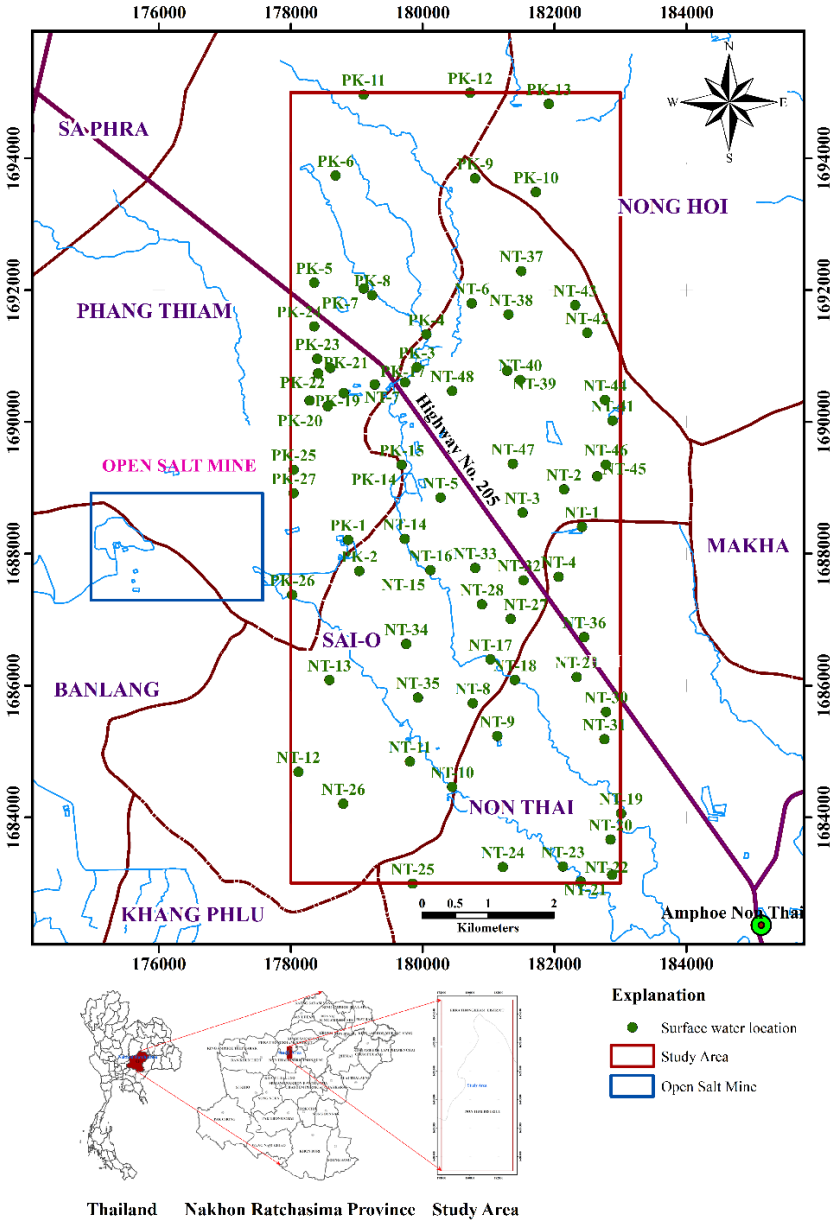

Figure 4. Study area and location of surface water samples around the salt mines in Non Thai and Phra Thong Kham Districts, Nakhon Ratchasima Province.

2.4 Water quality distribution mapping

The physicochemical parameters were applied to the ArcGIS 10.5 programmed and represented by the distribution of TDS, EC, salinity, chloride, sodium, and SAR content map of the surface water in the study area. Then, some physicochemical parameters were compared with the recommended limits set by the Department of Health (DoH, 2020) in Thailand and the World Health Organization (WHO, 2020) standards, as shown in Table 2.

Table 2. Criteria for assessing the quality of drinking water concerning saltwater adherence to the standards established by the DoH (2020) in Thailand and WHO (2022).

Parameters	Unit	DoH (2020)	WHO (2022)
pH (at 25°C)	-	6.5-8.5	6.5-8.5
Total dissolved solids (TDS)	mg/L	500	1,000
Electrical conductivity (EC)	µS/cm	2,000	2,500
Salinity	ppt	0.5	0.5
Chloride (Cl)	mg/L	250	250
Sodium (Na)	mg/L	200	200

3. RESULTS AND DISCUSSION

The results of surface water are predominantly clear, both from natural sources and human-made sources, with some areas having slight turbidity, especially for water sources used in agriculture and community areas affected by various human activities. Water temperatures vary with air temperatures, generally falling within the standard range of natural water sources in Thailand of 20 to 35°C.

3.1 General physical properties of surface water

As presented in Table 3, the pH value of most water is within the standard range of 6.5 to 8.5. This pH range does not have direct health implications, but it may harm agricultural water quality. The pH values in Non Thai District and Phra Thong Kham District range from 7.5 to 8.5, indicating a relatively neutral pH. The NT-5 sample exhibited acidic water with a pH of 6.53, while the PK-16 sample, taken from a large pool near the salt mine, showed alkaline water with a pH of 8.48. The distribution of these pH values correlates with the concentrations of Na, Ca, Mg, K, and salinity.

Figure 5(a) illustrates the distribution of TDS in surface water. Most samples exhibit TDS levels above 1,000 mg/L, surpassing the drinking water standard (DoH, 2020; WHO, 2022). In some instances, the TDS ranges from 600-1,000 mg/L, representing a rare distribution that exceeds the drinking water standard of the DoH (2020). However, it aligns with the WHO standard for good water quality, as the TDS level remains below 1,000 mg/L. It is essential to note that elevated TDS levels may pose concerns for consumers, leading to issues such as excessive scaling in water pipes, heaters, boilers, and household appliances (WHO, 2022). The presence of unusual tastes, such as saltiness and bitterness, may indicate water contamination. However, a few small areas in this study recorded TDS levels lower than 600 mg/L.

The EC of water in the study area ranges mainly between 2,500 and 10,000 µS/cm (Figure 5(b)). The water is brackish to salinity water and unsuitable for human consumption but acceptable for animal husbandry. The results were compared with the recommended limits of the drinking water standards, with values above 2,500 µS/cm (WHO, 2022) constituting highly saline water, requiring soil leaching. Additionally, areas near the salt mine have EC values exceeding 10,000 µS/cm, indicating extreme salinity. However, in the northern, eastern, and southern parts of the study area, values are below 1,500 µS/cm, which is within the drinkable water standard (DoH, 2020; WHO, 2022).

Table 3. Results of physical and chemical properties of surface water in the study area.

No	ID	MSL (m)	Water resources	pH	TDS (ppm)	EC (µS/cm)	Temp (°C)	Salinity (ppt)	Na (mg/L)	Ca (mg/L)	Mg (mg/L)	Cl (mg/L)	SAR
1	NT-1	186	Reservoir	7.41	598	1,197	27.30	0.60	713	46.94	11.84	386	93.00
2	NT-2	186	Pond	7.23	1,054	2,107	27.30	1.10	728	53.46	19.71	676	85.11
3	NT-3	187	Pond	7.36	463	925	27.30	0.40	1,149	27.45	6.38	1,224	197.55
4	NT-4	181	Pond	7.12	1,973	3,946	27.10	2.20	801	96.04	27.54	290	72.05
5	NT-5	185	Pond	6.53	2,639	5,272	27.30	3.00	990	141.30	39.76	1,674	73.57
6	NT-6	190	Pool	7.49	1,547	3,092	24.70	1.50	307	67.41	21.97	837	32.42
7	NT-7	190	Khlong Yang	7.60	673	1,354	24.90	0.60	115	41.05	11.71	354	15.87
8	NT-8	182	Pond	7.49	1,567	3,134	27.20	1.70	2,694	67.36	23.82	1,030	282.13
9	NT-9	181	Pond	7.63	484	967	27.00	0.40	117	37.43	7.48	322	17.46
10	NT-10	180	Khlong Non Phao Phi	7.27	4,484	8,968	27.20	5.20	53	126.10	68.49	3,027	3.81
11	NT-11	182	Pond	7.63	5,668	11,320	27.30	6.70	55	84.04	150.00	3,928	3.62
12	NT-12	182	Pond	7.26	900	1,801	27.40	1.00	47	77.62	32.69	612	4.49
13	NT-13	191	Reservoir	7.42	134	269	27.30	0.10	5	31.45	4.34	161	0.76
14	NT-14	185	Khlong Yang	7.53	301	602	27.40	0.20	42	37.32	7.19	258	6.34
15	NT-15	185	Khlong Sawai	7.21	2,571	5,143	27.90	2.90	47	166.60	46.44	1,674	3.24
16	NT-16	183	Pond	7.37	1,178	2,355	27.90	1.30	47	52.55	15.22	773	5.75
17	NT-17	182	Pond	7.11	3,906	7,808	27.80	4.60	50	264.10	88.12	2,640	2.65
18	NT-18	181	Khlong Sawai	7.30	1,035	2,070	27.80	1.10	46	60.31	17.59	676	5.23
19	NT-19	180	Khlong Sawai	7.51	1,366	2,733	27.80	1.50	46	57.43	18.89	902	5.28
20	NT-20	178	Reservoir	7.57	914	1,828	27.60	1.00	46	25.30	11.03	612	7.57

Remarks: Higher Cl content Higher SAR content

Table 3. Results of physical and chemical properties of surface water in the study area (cont.).

No	ID	MSL (m)	Water resources	pH	TDS (ppm)	EC (µS/cm)	Temp (°C)	Salinity (ppt)	Na (mg/L)	Ca (mg/L)	Mg (mg/L)	Cl (mg/L)	SAR
21	NT-21	180	Pond	7.02	297	595	27.70	0.20	57	19.13	5.87	225	11.43
22	NT-22	179	Khlong Dan	7.16	2,719	5,441	27.90	3.20	51	88.71	39.95	1,868	4.52
23	NT-23	177	Khlong Dan	7.32	2,860	5,719	27.70	3.40	49	110.50	41.24	1,996	4.01
24	NT-24	177	Pond	7.31	867	1,735	27.70	0.90	-	43.76	18.43	580	-
25	NT-25	181	Pond	7.51	495	990	27.70	0.50	94	32.24	17.67	354	13.31
26	NT-26	188	Pond	7.22	1,599	3,198	27.60	1.70	44	201.10	80.11	1,127	2.65
27	NT-27	182	Pond	7.52	906	1,812	27.40	0.90	-	54.09	15.18	547	-
28	NT-28	181	Pond	7.05	1,795	3,592	27.20	2.00	46	119.30	36.13	1,191	3.67
29	NT-29	183	Pond	7.22	6,142	12,290	27.40	7.40	56	167.90	106.40	4,315	3.40
30	NT-30	179	Pond	7.55	1,505	3,010	27.20	1.60	46	60.65	23.56	966	5.03
31	NT-31	180	Pond	7.48	514	1,027	27.30	0.50	-	14.82	4.97	322	-
32	NT-32	186	Pond	7.47	191	383	27.50	0.10	24	22.41	3.31	193	4.73
33	NT-33	182	Pond	7.04	5,930	11,850	27.20	6.90	55	386.60	107.20	4,025	2.49
34	NT-34	182	Pond	7.33	1,664	3,328	27.40	1.80	49	59.20	10.87	1,063	5.80
35	NT-35	182	Pond	7.67	533	1,066	27.40	0.50	119	30.62	8.17	354	19.04
36	NT-36	181	Pond	7.28	772	1,544	27.80	0.80	-	36.16	13.24	483	-
37	NT-37	193	Pool	7.40	1,799	3,606	27.40	2.00	345	79.24	65.56	1,143	28.66
38	NT-38	191	Pool	7.44	361	722	27.30	0.30	71	31.03	8.11	242	11.33
39	NT-39	191	Pool	7.10	2,391	4,743	27.30	2.70	-	88.41	31.96	1,530	-
40	NT-40	188	Pool	7.26	2,191	4,389	27.20	2.40	446	106.80	34.70	1,401	37.48
41	NT-41	187	Reservoir	7.33	861	1,722	27.30	0.90	197	46.69	14.13	564	25.27
42	NT-42	189	Pool	7.39	1,548	3,092	26.70	1.70	256	149.10	28.81	998	19.17
43	NT-43	190	Canal	7.53	972	1,944	26.80	3.50	596	167.20	93.92	2,061	36.90
44	NT-44	185	Reservoir	7.60	1,014	2,028	26.70	1.10	222	56.28	17.12	660	25.85
45	NT-45	187	Pond	6.82	3,431	6,861	26.80	3.90	717	164.80	66.10	2,302	47.15
46	NT-46	183	Pond	7.37	736	1,472	26.70	0.80	182	73.94	13.18	483	19.45
47	NT-47	186	Pool	7.36	1,462	2,924	27.00	1.60	289	77.92	44.76	934	26.07
48	NT-48	187	Pool	7.35	2,792	5,585	26.70	3.20	706	76.65	31.40	1,707	67.90
49	PK-1	187	Reservoir	7.34	944	1,888	27.30	1.00	2,893	41.47	13.27	580	391.02
50	PK-2	184	Pool	7.40	2,479	4,958	27.20	2.80	2,134	49.39	21.97	515	252.62
51	PK-3	190	Khlong Yang	7.25	751	1,498	24.90	0.70	161	40.95	11.02	483	22.31
52	PK-4	188	Khlong Yang	7.47	625	1,241	25.10	0.50	81	39.29	10.67	338	11.47
53	PK-5	190	Pool	7.34	905	1,801	26.90	1.00	111	52.21	18.17	81	13.17
54	PK-6	194	Pool	7.14	4,094	8,193	26.90	4.80	867	219.60	89.90	2,608	49.29
55	PK-7	193	Pool	7.23	413	827	27.00	0.40	67	33.54	9.04	258	10.29
56	PK-8	191	Khlong Kud Phi Man	7.29	818	1,636	27.00	0.80	180	55.36	16.70	161	21.17
57	PK-9	191	Pool	7.40	249	497	27.30	0.20	69	13.54	5.29	193	15.82
58	PK-10	195	Pool	7.23	2,441	4,953	27.20	2.80	254	203.80	150.40	1,658	13.48
59	PK-11	195	Pool	7.06	3,267	6,534	26.70	3.80	678	152.90	73.13	2,061	45.08
60	PK-12	195	Pool	7.32	2,971	5,938	26.70	3.40	682	128.00	43.32	1,964	52.11
61	PK-13	198	Pool	7.68	154	308	26.80	0.10	6	71.96	4.05	129	0.72
62	PK-14	187	Pool	7.22	2,282	4,567	27.40	2.60	387	197.70	53.61	1,546	24.39
63	PK-15	187	Pond	7.42	1,174	2,348	27.40	1.30	244	89.35	21.50	773	23.17
64	PK-16	189	Pool	8.48	9,689	19,380	27.80	12.80	6	74.81	118.50	6,698	0.42
65	PK-17	189	Pool	8.10	4,423	8,790	27.50	5.10	1,183	67.67	60.87	2,866	104.34
66	PK-18	189	Pond	8.02	2,220	4,436	27.70	2.50	471	96.37	56.98	1,481	38.06
67	PK-19	187	Pool	7.50	21,340	42,680	27.80	28.10	96	398.80	282.40	15,939	3.66
68	PK-20	188	Pond	7.61	8,013	16,010	27.70	9.90	-	255.00	139.10	5,764	-
69	PK-21	189	Pond	7.67	2,045	4,091	27.60	2.30	-	130.60	60.43	1,352	-
70	PK-22	192	Pond	7.64	1,177	2,353	27.70	1.20	185	115.30	38.38	773	14.89

Remarks: Higher Cl content Higher SAR content

Table 3. Results of physical and chemical properties of surface water in the study area (cont.).

No	ID	MSL (m)	Water resources	pH	TDS (ppm)	EC (µS/cm)	Temp (°C)	Salinity (ppt)	Na (mg/L)	Ca (mg/L)	Mg (mg/L)	Cl (mg/L)	SAR
71	PK-23	190	Pond	7.55	1,174	2,349	27.70	4.20	5,161	87.20	63.54	2,447	420.36
72	PK-24	190	Pond	7.64	2,687	5,370	27.80	3.10	4,796	112.90	48.10	1,803	377.98
73	PK-25	186	Pool	7.29	272	5,344	27.60	3.00	-	42.59	27.26	1,707	-
74	PK-26	183	Khlong Non Phao Phi	7.24	8,313	16,620	27.60	10.10	67	189.70	127.10	5,732	3.76
75	PK-27	185	Pond	7.38	677	1,353	27.20	0.70	1,875	42.33	11.78	419	254.90
	Max.	**198**		**8.48**	**21,340**	**42,680**	**27.9**	**28.10**	**5,161**	**398.80**	**282.4**	**15,939**	**420.36**
	Min.	**177**		**6.53**	**134.3**	**268.70**	**24.7**	**0.10**	**4.56**	**13.54**	**3.31**	**80.50**	**0.42**
	Avg.	**186.1**		**7.39**	**2,231.9**	**4,526.94**	**27.21**	**2.70**	**529.35**	**95.05**	**42.52**	**1,546.9**	**52.35**
	S.D.	**4.8**		**0.26**	**2,960.4**	**5,902.54**	**0.65**	**3.84**	**987.77**	**76.60**	**46.40**	**2,161.8**	**95.46**

Remarks: Higher Cl content Higher SAR content

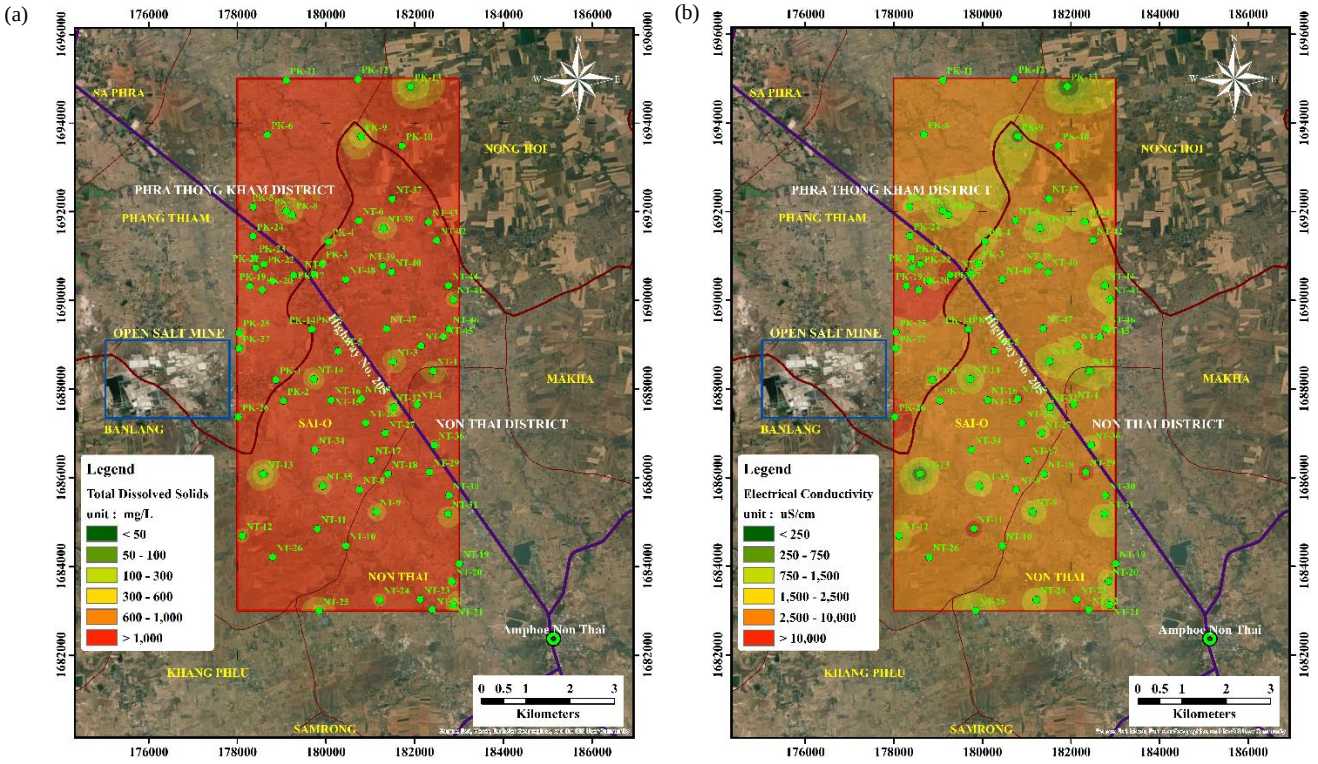

Figure 5. Distribution map of (a) total dissolved solids (TDS), and (b) electrical conductivity (EC) in the study area.

3.2 Salinity and chemical property distribution

The distribution of surface water salinity is illustrated in Figure 6(a). Salinity values range from 0.5 to 30 ppt, categorized as brackish water (1-10 ppt) to saltwater (over 10 ppt) according to the LEO EnviroSci Inquiry (2011). Regions with higher salinity, such as the 28.1 ppt reading in Phang Thiam Subdistrict (PK-19 sample) and Phra Thong Kham District, are associated with pools in proximity to salt mines. This phenomenon is attributed to surface runoff and sodium infiltration. Conversely, lower salinity (below 0.5 ppt) indicates freshwater suitable for human consumption, agriculture, and livestock.

The distribution of chloride (Cl) content, as depicted in Figure 7(b), has surpassed the standard limit of 250 mg/L. Concentrations of Cl ranging from 1,000 to 5,000 mg/L are observed across various communities and farmlands. Notably, the PK-19 sample from Phang Thiam Subdistrict in Phra Thong Kham District records the highest Cl content at 15,939 mg/L and is situated approximately 1 km from the salt mine.

High levels of chloride can give water and beverages a salty taste, usually noticeable at 200-300 mg/L for sodium, magnesium, and calcium chlorides. In the study area, chloride concentrations over 250 mg/L are likely to be tasted, though some people might

get used to it (WHO, 2022). However, in the northern and southern regions, chloride levels are generally below 250 mg/L, making the water suitable for consumption and use, according to DoH and WHO standards.

Figure 7(a) shows the sodium (Na) distribution, particularly in the western and eastern regions where most values exceed 500 mg/L. Water from the eastern region of this study area contains 200-300 mg/L of sodium, exceeding the drinking water standard of 200 mg/L (WHO, 2022). Areas with lower sodium concentrations, particularly those in the north and south can be found, aligning with the drinking water standards.

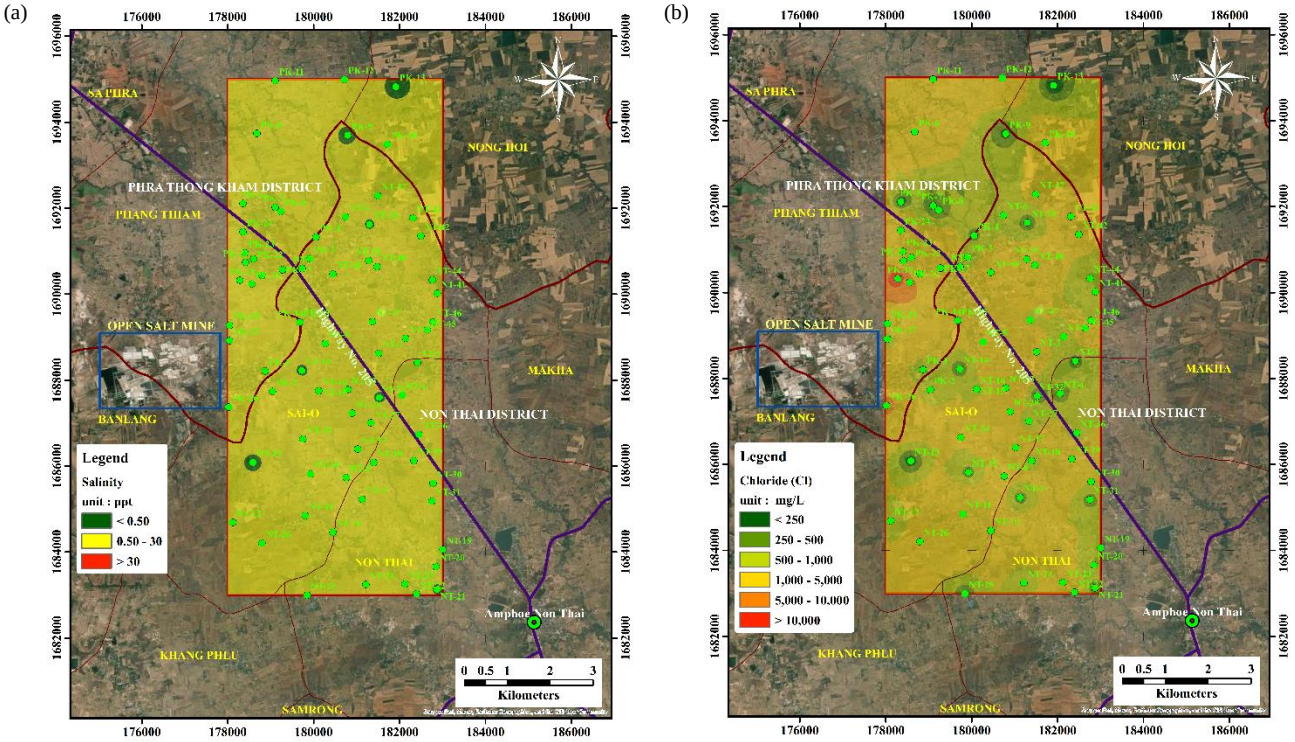

Figure 6. Distribution map of (a) salinity, and (b) chloride (Cl) in the study area

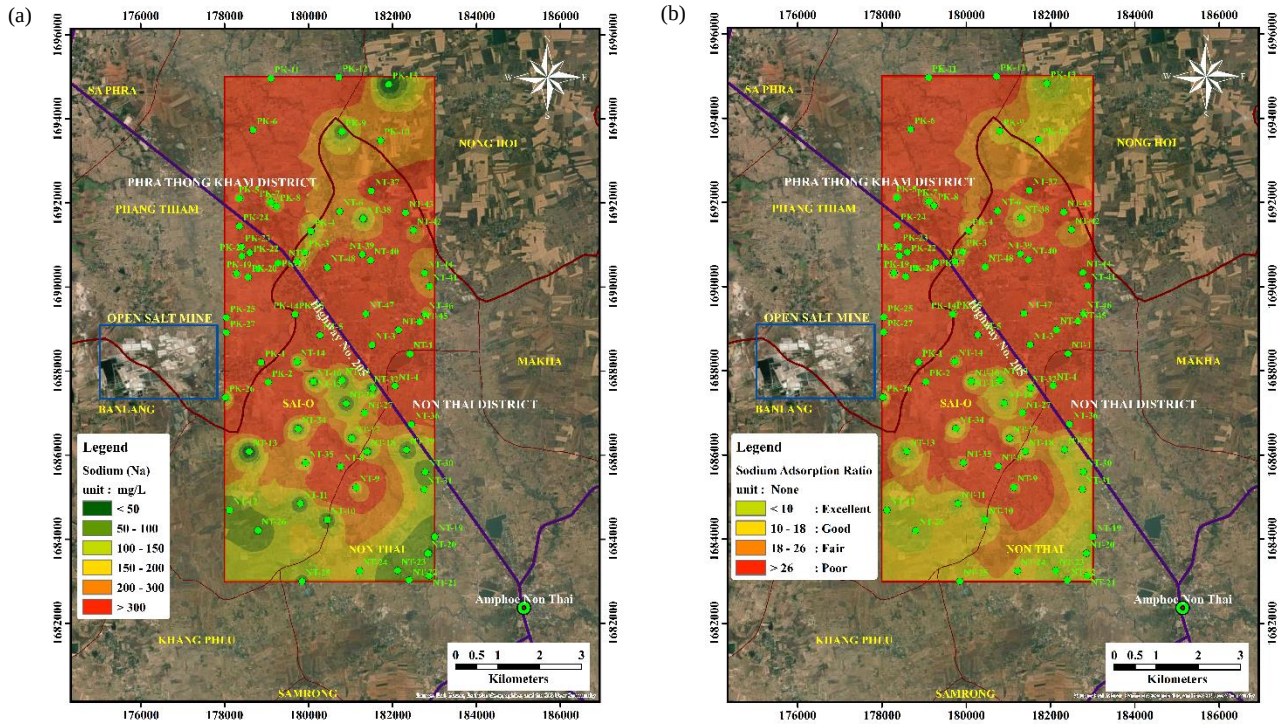

Figure 7. Distribution map of (a) sodium, and (b) Sodium Adsorption Ratio (SAR) in the study area

Based on the findings from the comparison of salinity and water quality across diverse water sources, the primary determinants influencing salinity include the proximity of the location to the salt mine and the lower altitude of the area. Additionally, the nature and scale of water resources play a crucial role. Specifically, water sources such as pools or small ponds exhibit higher salinity levels than larger reservoirs, rivers, and canals, which constitute flowing waterways and generally have lower salinity compared to other types of water sources.

3.3 Sodium adsorption ratio (SAR) evaluation

Based on the SAR values derived from this study, the range extends from 0.42 to 420.4, with an average SAR of 52.35 (Table 3). The SAR distribution in the Non Thai District generally remains below 10 (Figure 7(b)), indicating excellent water quality and a low susceptibility to sodium-related issues in crops (Guettaf et al., 2017). However, specific localized areas within the Non Thai District exhibit notably high SAR values exceeding 26. These elevated values suggest severely compromised water quality, posing a significant risk of sodium-related problems (Guettaf et al., 2017). Consequently, irrigation in these areas is considered unwise and requires extensive leaching to mitigate the potential detrimental effects. Conversely, the Phra Thong Kham District consistently shows SAR values exceeding 26 (Figure 7(b)), indicative of extremely poor water quality, rendering the water reservoirs unsuitable for irrigation. Despite this, isolated areas within the district exhibit low SAR values, suggesting fair to good water quality, and emphasizing the need for nuanced water management strategies in specific regions.

3.4 Dispersion of water salinity levels within each examined region

According to the salinity water distribution, several influencing factors contribute to saline water presence, encompassing the proximity of salt mines, low-lying topography, water flow direction (Thongwat, 2018), geological characteristics such as soil and rock types, the presence of rock salt, and the occurrence of joints and fractures in the formation (Royal Irrigation Department, 2020; Phoemphon and Terakulsatit, 2022; Wannakomol, 2005). Additionally, the size and nature of the water resource play a significant role in shaping salinity patterns. It is noteworthy that smaller, static sources, exemplified by pools, often exhibit higher salinity levels in comparison to larger, flowing waterways. The severity of salinity levels in the study area is further categorized based on specific villages and subdistricts.

3.4.1 Non Thai District

Areas with severe salinity distribution in Non Thai District can be determined as follows:

(i) Non Thai Subdistrict

The analysis of the salinity distribution in Non Thai Subdistrict encompasses seven villages ranked in descending order of severity: Ban Non Wai, Ban Non Thai, Ban Dan Tai, Ban Khok Phrom, Ban Dan Krong Krang, Ban Rai, and Ban Mai.

Ban Non Thai (NT-29 sample) encompasses a small agricultural pond situated at an altitude of 183 m. It registers the highest Cl concentration at 4,315 mg/L and a high salinity level of 7.4 ppt (Table 3). Additionally, the area exhibits the highest SAR value of 282.13 and a Na concentration of 2,694 mg/L. Another region, including Ban Non Wai and Ban Dan Tai, also showcases Cl levels surpassing 2,000 mg/L and salinity exceeding 5 ppt, indicating the presence of very saline water (Thongwat, 2018), which is unsuitable for use and consumption (DoH, 2020; WHO, 2022).

(ii) Sai O Subdistrict

The salinity distribution in the Sai O Subdistrict involves five villages, arranged in descending order of severity based on water salinity: Ban Sai O, Ban Khok, Ban Kut Chik, Ban Sawai, and Ban Khok Nong Phai.

The Ban Sai O area (NT-33 sample) encompasses a small agricultural pond situated at the highest altitude of 182 m, featuring a Cl concentration of 4025 mg/L and a salinity level of 6.9 ppt (Table 3). Additionally, Ban Sai O, Ban Kut Chik, and Khok Noi exhibit chlorite concentrations exceeding 2,000 mg/L and salinity levels surpassing 3.5 ppt, indicating the presence of extremely salty water, which is unsuitable for use and consumption (DoH, 2020; WHO, 2022).

3.4.2 Phra Thong Kham District

The areas in Phra Thong Kham District with severe salinity distribution can be determined as follows:

(i) Phang Thiam Subdistrict

The salinity distribution results for Phang Thiam Subdistrict, cover seven villages. Arranged in

descending order of water salinity severity, they are Ban Phang Thiam, Ban Yang Sam Ton, Ban Bueng Noi, Ban Chai Pha Nao, Ban Thonglang, Ban Non Sai Yong, and Ban Nong Pho.

Ban Phang Thiam Subdistrict (PK-19 sample) accommodates a large agricultural pond situated at an altitude of 187 m and is approximately 1 km away from the salt mine. This area demonstrates the highest Cl concentration at 15,939 mg/L and a high salinity of 28.1 ppt (Table 3). Furthermore, Ban Bueng Noi (PK-23 sample) displays the highest SAR value recorded at 420.36, along with a Na concentration of 5,161 mg/L (Table 3). Consequently, Ban Bueng Noi, Ban Thonglang, and Ban Non Sai Yong experienced elevated salinity levels, exceeding a SAR of 100. This indicates a severe level of saline quality, rendering it unsuitable for both use and consumption (DoH, 2020; WHO, 2022).

(ii) Nong Hoi Subdistrict

The results of the salinity distribution in the Nong Hoi Subdistrict, encompass two villages. These villages in descending order of severity based on water salinity are Ban Nong Hoi and Ban Tanon Hak, respectively.

The Nong Hoi Subdistrict encompasses small agricultural ponds situated approximately 7 km away from the salt mine. Ban Nong Hoi (PK-10 sample), positioned at an elevation of 195 m, exhibits a low Cl concentration of 129 mg/L and a low salinity of 0.1 ppt (Table 3). These values indicate good saltwater quality, although it is unsuitable for human consumption (DoH, 2020; WHO, 2022). In contrast, Ban Thanon Hak (PK-13 sample), situated at an elevation of 198 m, showcases a low Cl concentration of 1,658 mg/L and a high salinity of 2.8 ppt. These characteristics demonstrate good water quality, deeming it suitable for both use and consumption.

4. CONCLUSION

Most of the surface water in Non Thai and Phra Thong Kham Districts showed relatively neutral pH values. However, the TDS and EC values in many samples, surpassed the drinking water standards set by Thailand's DoH and the WHO. Elevated salinity, chloride, sodium, and SAR levels were concentrated near salt mines, influenced by surface runoff and sodium infiltration.

Non Thai District: (i) Non Thai Subdistrict, Ban Non Wai, Ban Non Thai, Ban Dan Tai, Ban Khok Phrom, Ban Dan Krong Krang, Ban Rai, and Ban Mai exhibited elevated chloride concentrations and salinity levels, rendering the water unsuitable for both consumption and use. (ii) Sai O Subdistrict, Ban Sai O displayed extremely salty water, making it unsuitable for consumption.

Phra Thong Kham District: (i) Phra Thong Kham Subdistrict Ban Phang Thiam demonstrated the highest chloride concentration and salinity, rendering the water unsuitable for both use and consumption. (ii) Nong Hoi Subdistrict revealed brackish to saline water in Ban Nong Hoi, while Ban Tanon Hak exhibited good water quality deeming it suitable for both use and consumption.

In summary, the study found that brackish to saline water is prevalent in the central and northern areas around the salt mine, with Phra Thong Kham District showing higher salinity levels, making the water unsuitable for domestic use and irrigation compared to Non Thai District. Key factors influencing salinity include proximity to the salt mine, lower terrain, seasonal changes, water flow direction, geological formations, and the size of water sources. The highest salinity risk is in areas near salt mines and their direct water flow paths, particularly in low-lying regions. Smaller water sources tend to have higher salinity. Water quality in this area is inconsistent, while some areas still have usable water. Additional research is necessary in other salt mine regions of Nakhon Ratchasima Province and beyond to gain a clearer understanding of salinity distribution. This work is crucial for assessing risks and making informed decisions to effectively manage and protect public health and the environment in areas surrounding salt mines.

ACKNOWLEDGEMENTS

This work was financially supported by (i) Suranaree University of Technology (SUT), (ii) Thailand Science Research and Innovation (TSRI), and (iii) National Science, Research and Innovation Fund (NSRF) under the grant numbers: NRIIS 179329. Special thanks go to Ms Mallika Nguanthaisong and the Geotechnology laboratory staff for their assistance with the laboratory work.

REFERENCES

Akhrajanthachot B. Potash and salt mine in the North-Eastern of Thailand. Proceedings of the Thai-Lao Technical Conference on Geology and Mineral Resources; 2010 Sep 7-8; Bangkok, Thailand: Rama Gardens Hotel; 2010.

Department of Health (DoH). Notification of the Department of Health on Criteria for Recommendation of Drinking Water

Quality Surveillance, B.E. 2563 (A.D. 2020). Thailand: Ministry of Public Health; 2020 (in Thai).

Department of Primary Industries and Mines (DPIM). General mining concession information [Internet]. 2009 [cited 2024 Jan 10]. Available from: https://www1.dpim.go.th/mne/mn.php?nox=&pltname=&status=*&ore1=&ore2=&prov=30&b1dx=00&b1mx=00&b1yx=0000&b2dx=00&b2mx=00&b2yx=0000&a1dx=00&a1mx=00&a1yx=0000&a2dx=00&a2mx=00&a2yx=0000. (in Thai).

Department of Primary Industries and Mines (DPIM). Study of saline soil in the Nakhon Ratchasima salt production area [Internet]. 2010 [cited 2024 Jan 10]. Available from: https://envi-mining.dpim.go.th/modules.php?m=article&op=detailnewsupdate&NUID=19. (in Thai).

El Tabakh M, Utha-Aroon C, Schreiber BC. Sedimentology of the cretaceous Maha Sarakham evaporites in the Khorat Plateau of northeastern Thailand. Sedimentary Geology 1999;123:31-62.

Environment and Pollution Control. Report Summarizing Water Quality Results Surface Water Resources, 4th Quarter, Fiscal Year 2022. Nakhon Ratchasima. Thailand: Pollution Control Department, Ministry of Natural Resources and Environment; 2022 (in Thai).

Green News. Revealing the cause of heavy saltwater spread "Khorat mine dug into the water source - will continue. Must make a new EIA" [Internet]. 2022 [cited 2024 Jan 24]. Available from: https://greennews.agency/?p=32079. (in Thai).

Guettaf M, Maoui A, Ihdene Z. Assessment of water quality: A case study of the Seybouse River (North East of Algeria). Applied Water Science 2017;7:295-307.

Land Development Department. Appropriate Agricultural Promotion Guidelines Nakhon Ratchasima Province. Thailand: Land Development Department, Ministry of Agriculture and Cooperatives; 2021.

LEO EnviroSci Inquiry. Lehigh University. Chloride and Salinity [Internet]. 2011 [cited 2024 Jan 29]. Available from: https://ei.lehigh.edu/envirosci/watershed/wq/wqbackground/chloridebg.html.

Lesch SM, Suarez DL. A short note on calculating the adjusted SAR index. Transaction of American Society of Agricultural and Biological Engineers 2009;52(2):493-6.

Local Information Center for Development (LICD). Basic Information of Nakhon Ratchasima Province. "General geography of Non Thai and Phra Thong Kham Districts". Nakhon Ratchasima, Thailand: Local Information Center for Development of Nakhon Ratchasima; 2022 (in Thai).

Phoemphon W, Terakulsatit B. Assessment of groundwater potential zones and mapping using GIS/RS techniques and analytic hierarchy process: A case study on saline soil area, Nakhon Ratchasima, Thailand. AIMS Geosciences 2022; 9(1):49-67.

Prachathai News. "Villagers demand a solution to the problems affecting the Dan Khun Thot" [Internet]. 2023 [cited 2024 Jan 24]. Available from: https://prachatai.com/journal/2023/12/107123. (in Thai).

Royal Irrigation Department. Developing Water Resources to Solve Drought and Flood Problems in the Lam Chiang Krai Basin 2019. Nakhon Ratchasima, Thailand: Thailand Ministry of Agriculture and Cooperatives; 2020 (in Thai).

Skoog DA, West DM, Holler FJ. Fundamentals of Analytical Chemistry. 7th ed. USA: Thomson Learning, Inc; 1996.

Suwanich P. Potash and rock salt in Thailand. In: Nonmetallic Minerals Bulletin No. 2. Bangkok, Thailand: Economic Geology Division, Department of Mineral Resources; 1986.

Thongwat W. Relationship between Soil Salinity and Chloride Content in Groundwater in Saline Soil Areas of Nakhon Ratchasima Province [dissertation]. Nakhon Ratchasima: Suranaree University of Technology; 2018.

Thongwat W, Terakulsatit B. Using GIS and map data for the analysis of the relationship between soil and groundwater quality at saline soil area of Kham Sakaesaeng District, Nakhon Ratchasima, Thailand. International Journal of Materials and Metallurgical Engineering 2019;13(1):32-9.

Utha-aroon C. Continental origin of the Maha Sarakham evaporates Northeastern Thailand. Journal of Southeast Asian Earth Sciences 1993;8(1-4):193-203.

Wannakomol A. Soil and Groundwater Salinization Problem in the Khorat Plateau, Northeast Thailand [dissertation]. Berlin, Germany: Freie University; 2005.

Wannakomol A, Terakulsatit B. Study and the land subsidence risk level mapping in the rock salt production area of Nakhon Ratchasima Province by using Synthetic Aperture Radar and Geophysical Data. Nakhon Ratchasima, Thailand: Suranaree University of Technology; 2018.

World Health Organization (WHO). World Health Organization's (WHO) Guidelines for Drinking-Water Quality. 4th ed. Geneva, Switzerland: World Health Organization; 2022.

Environment and Natural Resources Journal

Volume 22
Issue 5
2024

Enhancement of Shear Strength Properties of Soft Clay Using Coir Fiber-Coconut Husk Ash-Wood Ash Mixture

Anita Widianti[1*], Hafizh Pratama Wiandri[1], Anita Rahmawati[1], and Dian Eksana Wibowo[2]

[1]*Faculty of Engineering, Universitas Muhammadiyah Yogyakarta, Indonesia*
[2]*Faculty of Engineering, Universitas Negeri Yogyakarta, Indonesia*

ARTICLE INFO

Received: 11 Mar 2024
Received in revised: 9 Aug 2024
Accepted: 19 Aug 2024
Published online: 16 Sep 2024
DOI: 10.32526/ennrj/22/20240065

Keywords:
Soft clay/ Coir fiber/ Coconut husk ash/ Wood ash/ Shear strength

*** Corresponding author:**
E-mail: anitawidianti@umy.ac.id

ABSTRACT

Soft clay is a problematic type of soil because it has high water content, low shear strength, low bearing capacity, and high compressibility. This study explores the effectiveness of stabilizing soft clay using a combination of coir fiber, coconut husk ash, and wood ash. This research investigated the impact of incorporating 0.75% coir fiber and varying levels of a coconut husk ash-wood ash mixture (ranging from 0% to 10%) on the shear strength properties of soft clay. The study applied two different curing times: seven and 21 days. An unconsolidated-undrained triaxial test was conducted following ASTM D2850-03. The results demonstrated that combining coir fiber reinforcement with chemical stabilization through the ash mixture significantly enhanced the deviatoric stress, cohesion, internal friction angle, shear strength, and elastic modulus of soft soil. Specifically, an 8% ash content with a 21-day curing time achieved the highest deviatoric stress and shear strength. This highest shear strength value was 210% greater than soil solely reinforced with coir fiber.

1. INTRODUCTION

Soft clay is a problematic type of soil because its water content is high, so its shear strength is low. As a result, the compressibility level is high, and the bearing capacity is low (Hejazi et al., 2012). Hence, stabilization is necessary before employing soft soil as a structural base or fill (Karkush and Yassin, 2020). Adding a material with a high tensile strength is one of several stabilization methods. The materials that can be used are very diverse, including waste organic materials in the form of natural fibers from plants (Suffri et al., 2019).

Soil reinforced using randomly distributed fibers will behave as a composite material similar to plant roots, which is then known as an eco-composite. Fibers that can be used include coir, palm, sugar cane bagasse, rice husk, sisal, jute, barley straw, bamboo, and sawdust. These fibers have been proven to improve soil's geotechnical properties, such as bearing capacity, shear strength, and tensile strength (Hejazi et al., 2012; Medina-Martinez et al., 2022). Coir fiber is a widely used alternative due to its abundance in tropical countries, low cost, low environmental impact, and relatively lightweight (Das et al., 2016; Lone and Bawa, 2018). Cellulose accounts for 54% of coir fiber, lignin makes up 40%, and other water-soluble compounds constitute 6% (Khatri et al., 2017). The high cellulose concentration of coir fiber gives it superior flexural and tensile strength compared to other plant fibers (Gowthaman et al., 2018). Compared to synthetic fibers, natural fibers have a higher coefficient of friction and are more elastic (Maurya et al., 2015; Upadhyay and Singh, 2017). Fiber disintegration is slower than with other natural fibers and can take up to ten years because of the high lignin content, rendering coir fiber resistant to microbes (Hejazi et al., 2012).

Several studies have revealed that coir fiber mixed into the soil randomly will behave like plant roots. These fibers will increase friction between soil particles and the fiber surface, boosting its shear strength and bearing capacity. The mixture of fiber and

Citation: Widianti A, Wiandri HP, Rahmawati A, Wibowo DE. Enhancement of shear strength properties of soft clay using coir fiber-coconut husk ash-wood ash mixture. Environ. Nat. Resour. J. 2024;22(5):476-482. (https://doi.org/10.32526/ennrj/22/20240065)

soil will increase the bond or interlocking between the two. Fibers with relatively high tensile strength will help soil grains withstand horizontal forces (Peter et al., 2016; Upadhyay and Singh, 2017; Bhatt et al., 2017; Gupta et al., 2017).

Widianti et al. (2020) demonstrated that adding 0.75% coir fiber increased the soil's shear strength to its maximum value. However, it turns out that coir fiber cannot prevent air-induced swelling. Thus, it needs to be complemented with chemical stabilization, as demonstrated in subsequent research by Widianti et al. (2022). For this reason, Widianti et al. (2023) have mixed coconut husk ash and wood ash waste with coir fiber. This experiment combined the soil with 0.75% coir fiber and coconut husk ash-wood ash at varying levels (0%, 2%, 4%, 6%, 8%, and 10%). The test findings revealed that the highest values of California Bearing Ratio (CBR), Unconfined Compressive Strength (UCS), and tensile strength were achieved with a combination of coir fiber and coconut husk ash-wood ash with a content ranging from 6% to 8%. Additionally, the swelling was reduced to 0% with an ash content of 6-10%.

Trikarlina et al. (2018) explained that burning waste coir fiber produces coconut husk ash containing pozzolanic silica, calcium, and alumina. Multiple studies have proven that soil stabilized by coconut husk ash has superior physical and mechanical properties (Onyelowe, 2016; Chakraborty and Roy, 2016; Yusuf and Zava, 2019). This stabilization process is influenced by the ash concentration and curing time (Barman and Dash, 2022).

This study examined soft clay's shear strength and elastic modulus when mixed with 0.75% coir fiber and coconut husk ash-wood ash with varying contents. Higher shear strength values are expected due to combining chemical stability and strengthening with environmentally friendly additives. Soil shear strength is a significant parameter to consider when determining the bearing capacity of the soil and the stability of embankment slopes.

2. METHODOLOGY

2.1 Materials

This study utilized soft clay soil from Yogyakarta, Indonesia. Data on the physical and mechanical properties of the soil were obtained from previous research by Widianti et al. (2021a) and Widianti et al. (2021b). The data are shown in Table 1.

According to the particle size distribution and consistency limits test findings, the soil is categorized as clay with high plasticity, abbreviated as CH. Das and Sobhan (2016) defined soil as soft if its unconfined compressive strength (UCS) value fell within the 25 to 50 kPa range.

The coir fiber was sourced from waste at the market. The tensile strength test results exhibited tensile strength values from 107.4 MPa to 240.8 MPa, with strain values ranging from 20.53% to 34.10%. Before mixing with the soil, the fiber was cut into pieces about 5 cm long.

Table 1. The physical and mechanical properties of the soil (Widianti et al., 2021a; Widianti et al., 2021b).

Parameters	Values
Particle size distribution:	
Sand (%)	13.36%
Silt (%)	70.58%
Clay (%)	16.06%
Consistency limits:	
Liquid Limit	89.91%
Plastic Limit	38.86%
Shrinkage Limit	16.33%
Plasticity Index	51.05%
Specific Gravity	2.63
Proctor standard compaction:	
Maximum Dry Density	12.64 kN/m^3
Optimum Moisture Content	29.90%
Unconfined compressive strength	41.70 kPa
Cohesion	43.26 kPa
Internal friction angle	2.35^o

The research utilized a combination of coconut husk ash and wood ash derived from the waste of burning coconut husk and wood in the tofu home industry. The ash had been passed through a 200-mesh sieve and was dried in an oven for 24 h. Table 2 illustrates the chemical element content of the coconut husk ash-wood ash mixture examined at the GetIn-CICERO Laboratory, Department of Geological Engineering, Faculty of Engineering, Universitas Gadjah Mada, Indonesia. Several researchers stated that elements of the oxides SiO_2, Al_2O_3, Fe_2O_3, and CaO are essential to evaluate pozzolan characteristics (Muntohar et al., 2016).

2.2 Specimen preparation

This study utilized coir fiber at 0.75% of the mixture's overall weight and the coconut husk ash-wood ash mixture at different levels (0-10%) to determine the optimal mix yielding the maximum shear strength. Each specimen had a diameter of 3.5 cm and a height of 7 cm. Each variant was tested with

three specimens. Curing occurred for seven and 21 days before testing.

Table 2. Chemical element test results for a mixture of coconut husk ash-wood ash

Chemical element		Result
SiO_2	Silicon oxide	33.52%
CaO	Calcium oxide	27.58%
MgO	Magnesium oxide	4.96%
P_2O_5	Phosphorus oxide	3.95%
Fe_2O_3	Iron oxide	1.97%
Al_2O_3	Aluminium oxide	1.93%

2.3 Testing procedure

Unconsolidated-undrained triaxial testing was performed on the hardened specimens following STM D2850-03 (ASTM International, 2003). Each specimen was subjected to a specific cell pressure: 98.1 kPa, 196.2 kPa, and 294.3 kPa. Subsequently, the specimens were subjected to deviatoric stress with a 1 mm/minute loading speed until the soil collapsed or until the strain reached 15%. Testing was conducted at the Geotechnical Laboratory, Faculty of Engineering, Universitas Muhammadiyah Yogyakarta, Indonesia.

3. RESULTS AND DISCUSSION

3.1 Effect of ash content and curing time on deviatoric stress

Unconsolidated-undrained triaxial testing produces axial stress values in the form of deviator stress, which causes the specimen to collapse or the strain that occurs to reach 15%. Figure 1 summarizes the deviatoric stress values for each soil sample stabilized with coir fiber and varying ash content during the 7-day and 21-day curing.

Figure 1 demonstrates that the deviatoric stress value increased when the ash content and curing time rose. For a specimen containing 0.75% fiber and 10% ash, the maximum value obtained at a cell pressure of 294.3 kPa was 622.5 kPa.

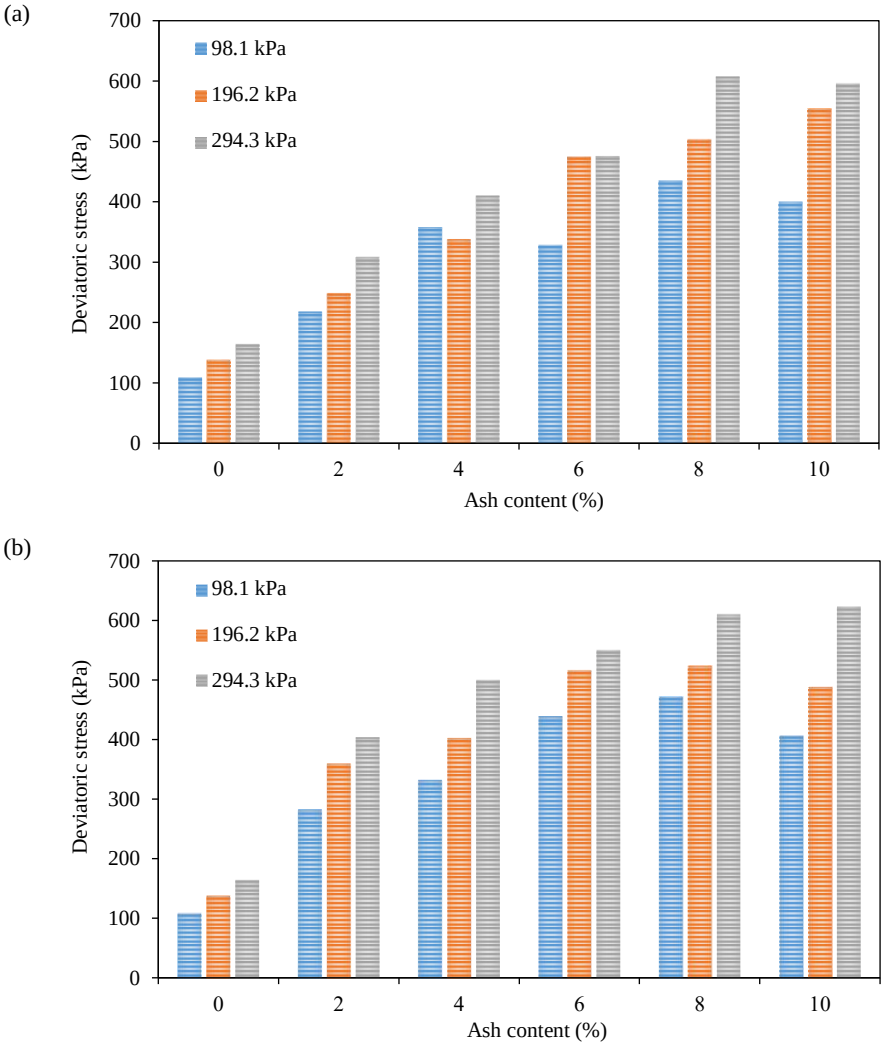

Figure 1. Effect of ash content on deviatoric stress values (a) seven-day curing, (b) 21-day curing

3.2 Effect of ash content and curing time on cohesion and internal friction angle

As demonstrated in Figure 2, the cohesion and internal friction angle values were examined by drawing a Mohr's circle graph based on the minor principal stresses (cell pressure) and the major principal stresses (cell pressure plus deviatoric stress).

Figures 3 and 4 summarize the internal friction angle and cohesion values obtained from Mohr's circle.

Figure 3 illustrates the difference in cohesion values between the soil reinforced with coir fiber before and after adding ash. The cohesion value of soil reinforced with coir fiber alone (with no ash) was 36.31 kPa, and it rose as the ash content was added and the curing time increased. The addition of 8% ash content and a curing time of 21 days resulted in the highest cohesion value, 154.92 kPa, indicating an increase of 327%.

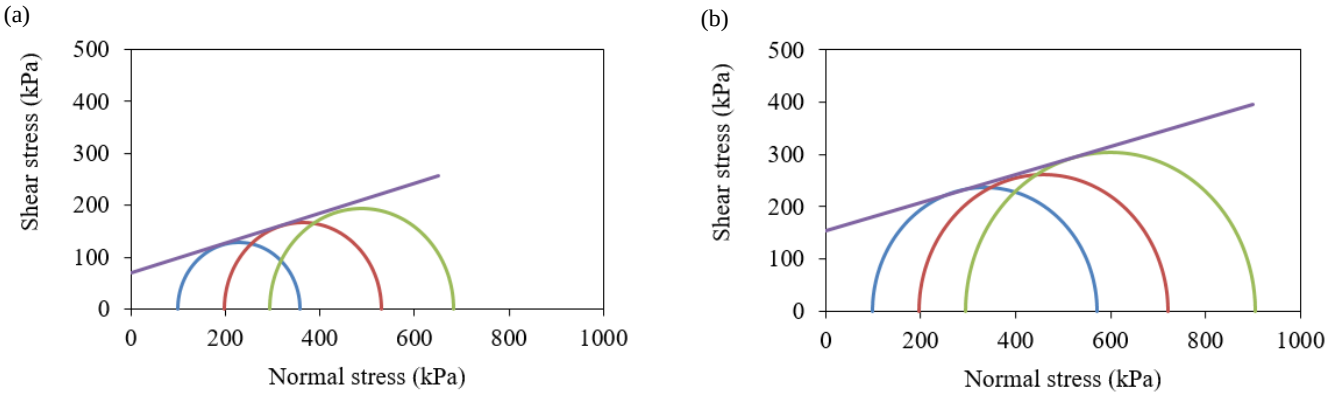

Figure 2. Mohr's circle of specimens (a) with 0.75% coir fiber and 0% ash, (b) with 0.75% coir fiber and 8% ash at 21 days of curing

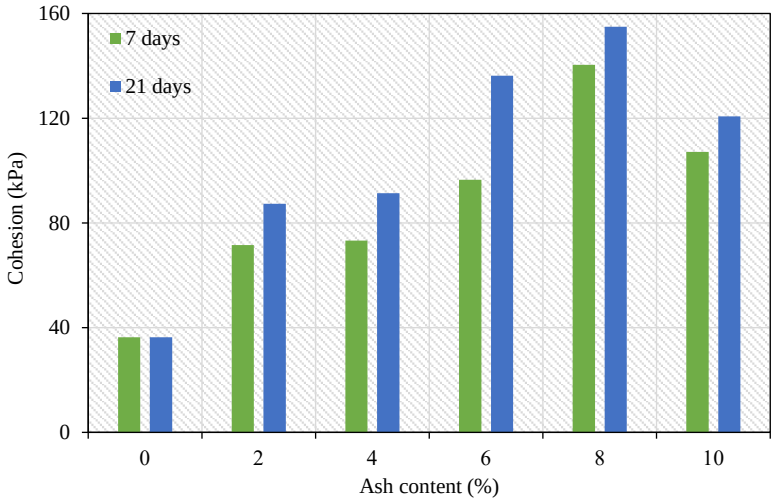

Figure 3. Effect of ash content on mixed soil cohesion values with curing times of seven and 21 days

The chemical reaction between the two raised the cohesion. When the calcium oxide (CaO) in coir fiber ash reacted with the silica (Si) in clay, the following pozzolanic reaction occurred.

$$Ca(OH)_2 + H_2O + SiO_2 \,\&\, Al_2O_3 \rightarrow CSH \,\&\, CAH$$

CSH and CAH are cement materials forming cementation in soil grains, raising the binding force between soil granules (Darwis, 2017; Tan et al., 2020).

The ash content and the curing time affected the internal friction angle, which tended to rise, as illustrated in Figure 4. Soil grains underwent flocculation and cementation due to a chemical reaction with ash, leading to this rise. As a result, the soil grains grew larger, and their surfaces became less smooth and flexible, leading to more friction between them (Fondjo et al., 2021).

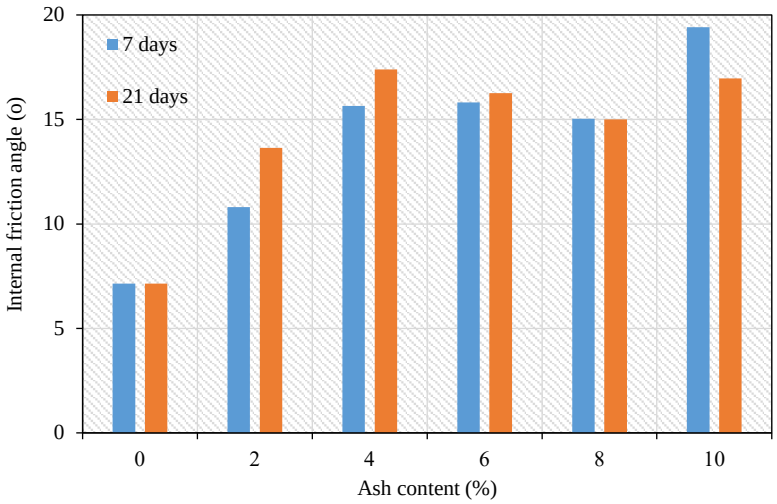

Figure 4. Effect of ash content on the internal friction angle of mixed soil with curing for seven and 21 days

3.3 Effect of ash content and curing time on shear strength

The tangent line depicted on the Mohr circle (Figure 2) is the failure envelope. If the soil has a normal stress value and the shear stress value is still below the failure envelope, then shear failure will not occur, and vice versa. In this study, the failure envelope for each specimen is shown in Figure 5. It can be seen that the failure envelope increases with each rise in ash content. An additional 8% ash content maximized the failure envelope.

Soil shear strength indicates how well soils resist moving or collapsing in the shear plane that cuts through them. According to Mohr (1980) in Das and Sobhan (2016), a material will only fail when shear stress and normal stress reach a critical combination. The shear strength values at specific normal stresses can be calculated using the cohesion and internal friction angle values pulled from Mohr's circle graph. Figure 6 exhibits the shear strength values of mixed soil at a curing time of seven and 21 days when a normal stress of 350 kPa was applied. The shear strength value in soil reinforced solely with coir fiber (and not with ash) was 80.21 kPa. The shear strength value rose over many days of curing in an ash mixture with varied concentrations. Adding 0.75% fiber and 8% ash to the soil elevated its shear strength to 248.73 kPa after 21 days of curing, signifying a 210% increase above the shear strength of fiber-reinforced soil.

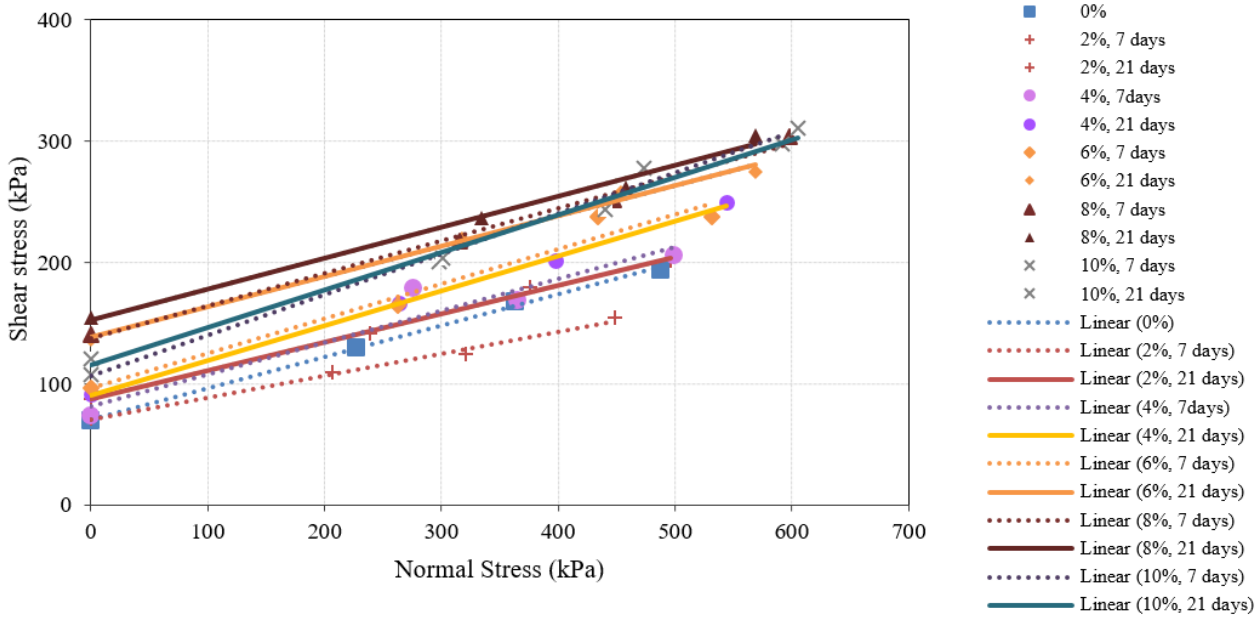

Figure 5. The failure envelope of the specimens during the curing time of seven days and 21 days

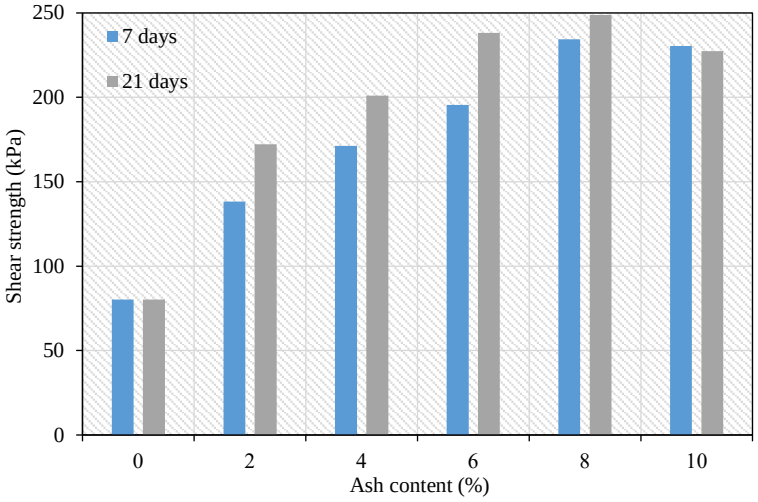

Figure 6. Effect of ash content on the shear strength of mixed soil with curing for seven and 21 days

3.4 Effect of ash content and curing time on the elastic modulus

Another parameter obtained from the triaxial test is the elastic modulus. This can be determined using the secant modulus method, obtained by comparing the deviatoric stress of 50% and the strain when it is 50%. Figure 7 displays a graph of the specimens' elastic modulus value at a cell pressure of 294.3 kPa.

As seen in Figure 7, the elastic modulus values continued to rise as the ash content increased. Curing the specimens for 21 days typically yielded a higher elastic modulus than curing it for seven days. The soil became stiffer as its elastic modulus rose (Widianti et al., 2021a).

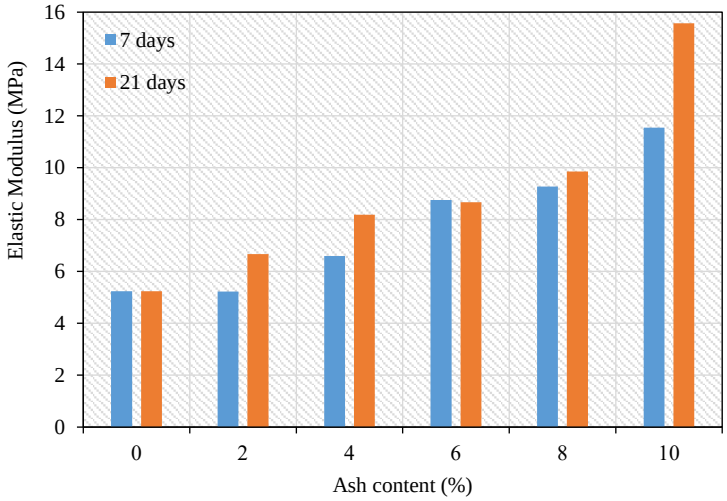

Figure 7. Effect of variations in ash content on the elastic modulus of mixed soil at a cell pressure of 294.3 kPa

4. CONCLUSION

The research yielded the following conclusions.

a) The combination of reinforcement using coir fiber and chemical stabilization using a mixture of coconut fiber ash and wood ash has significantly increased the deviatoric stress, cohesion, internal friction angle, shear strength, and elastic modulus of soft soil.

b) Cohesion, shear strength, elastic modulus, and internal friction angle all rose as cure time increased.

c) A mixture with an ash percentage of 8% and a curing time of 21 days achieved the highest deviatoric stress and shear strength. The highest shear strength value was 210% greater than soil solely reinforced with coir fiber.

ACKNOWLEDGEMENTS

The project presented in this article was supported by the Institute of Research and Innovation, Universitas Muhammadiyah Yogyakarta, Indonesia.

REFERENCES

American Society for Testing and Materials (ASTM). ASTM D2850-03: Standard Test Methods for Unconsolidated-Undrained Triaxial Compression Test on Cohesive Soils. Pennsylvania, USA; 2003.

Barman D, Dash SK. Stabilization of expansive soils using chemical additives: A review. Journal of Rock Mechanics and Geotechnical Engineering 2022;14(4):1319-42.

Bhatt H, Nitish J, Harshit V. Performance and analysis of coir fibre as soil reinforcement. International Journal for Research in Applied Science and Engineering Technology 2017;5(11): 67-72.

Chakraborty A, Roy S. Study on the properties of expansive clayey soil using Coconut Husk Ash (CHA) as stabilizer. ADBU Journal of Engineering Technology 2016;4(1):94-7.

Darwis H. Basics of Soil Improvement. Yogyakarta: Pustaka AQ; 2017 (in Indonesian).

Das BM, Sobhan K. Principles of Geotechnical Engineering. Boston, USA: Cengage Learning; 2016.

Das D, Kaundinya D, Sarkar R, Deb B. Shear strength improvement of sandy soil using coconut fibre. International Journal of Civil Engineering and Technology 2016;7:297-305.

Fondjo AA, Theron E, Ray RP. Stabilization of expansive soils using mechanical and chemical methods: A comprehensive review. Civil Engineering and Architecture 2021;9(5): 1295-308.

Gowthaman S, Nakashima K, Kawasaki S. A state-of-the-art review on soil reinforcement technology using natural plant fiber materials: Past findings, present trends and future directions. Materials 2018;11(4):Article No. 553.

Gupta HK, Maurya MC, Gupta AK. Shear strength enhancement of soil by using coconut fiber. Imperial Journal of Interdisciplinary Research 2017;3(6):366-72.

Hejazi SM, Sheikhzadeh M, Abtahi SM, Zadhoush A. A simple review of soil reinforcement by using natural and synthetic fibers. Construction and Building Materials 2012;30:100-16.

Karkush MO, Yassin SA. Using sustainable material in improvement the geotechnical properties of soft clayey soil. Journal of Engineering Science and Technology 2020; 15(4):2208-22.

Khatri VN, Dutta RK, Katre S. Shear strength, bearing ratio and settlement behavior of clay reinforced with chemically treated coir fibres. Jordan Journal of Civil Engineering 2017; 11(4):659-79.

Lone IA, Bawa EA. Utilization of fly-ash and coir fiber in soil reinforcement. International Journal of Civil Engineering and Technology 2018;9(8):341-6.

Maurya S, Sharma AK, Jain PK, Kumar R. Review on stabilization of soil using coir fiber. International Journal of Engineering Research 2015;4(6):296-9.

Medina-Martinez CJ, Sandoval-Herazo LC, Zamora-Castro SA, Vivar-Ocampo R, Reyes-Gonzalez D. Natural fibers: An alternative for the reinforcement of expansive soils. Sustainability 2022;14(15):Article No. 9275.

Muntohar AS, Hartono E, Diana W, Rahmawati A. Effect of cement replacement with carbide waste on the strength of stabilized clay subgrade. Civil Engineering Dimension 2016;18(1):8-15.

Onyelowe K. Effect of coconut shell husk ash and palm kernel shell husk ash on the grading and consistency behaviour of pozzolan stabilized oboro lateritic soil. Journal of Civil and Environmental Research 2016;8(3):55-63.

Peter L, Jayasree PK, Balan K, Raj SA. Laboratory investigation in the improvement of subgrade characteristics of expansive soil stabilised with coir waste. Transportation Research Procedia 2016;17:558-66.

Suffri N, Jeludin M, Rahim S. Behaviour of the undrained shear strength of soft clay reinforced with natural fibre. IOP Conference Series: Materials Science and Engineering 2019; 690:Article No. 12005.

Tan EH, Zahran EMM, Tan SJ. A review of chemical stabilisation in road construction. IOP Conference Series: Materials Science and Engineering 2020;943:Article No. 12005.

Trikarlina E, Sigalingging R, Munir AP. The utilization of coconut husk ash and effect of sikacim additive to manufacturing bricks. Jurnal Rekayasa Pangan dan Pertanian 2018;6(1):38-43 (in Indonesian).

Upadhyay P, Singh Y. Soil stabilization using natural fiber coir. International Research Journal of Engineering and Technology 2017;04(12):1808-12.

Widianti A, Diana W, Alghifari MR. Shear strength and elastic modulus behavior of coconut fiber-reinforced expansive soil. IOP Conference Series: Materials Science and Engineering 2021a;1144:Article No. 12043.

Widianti A, Diana W, Fikriyah ZS. Unconfined compressive strength of clay strengthened by coconut fiber waste. Advances in Engineering Research 2021b;199:47-50.

Widianti A, Diana W, Hasana M. Direct shear strength of clay reinforced with coir fiber. UKaRsT 2020;4(2):151-62.

Widianti A, Diana W, Rahmawati A, Wibowo DE. Combination of coir fiber waste and coir-wood ash for expansive clay stabilization. International Journal of GEOMATE 2023; 25(111):230-7.

Widianti A, Negara AAB, Elmino TS, Ramadhani L. Utilization of coir fibers to improve the bearing capacity and tensile strength of expansive clay. International Journal of GEOMATE 2022;23(95):20-6.

Yusuf IT, Zava AE. Investigating the suitability of coconut husk ash as a road soil stabilizer. International Journal of Technology 2019;10(1):27-35.

INSTRUCTION FOR AUTHORS

Publication and Peer-reviewing processes of Environment and Natural Resources Journal

Environment and Natural Resources Journal is a peer reviewed and open access journal that is published in six issues per year. Manuscripts should be submitted online at https://ph02.tci-thaijo.org/index.php/ennrj/about/submissions by registering and logging into this website. Submitted manuscripts should not have been published previously, nor be under consideration for publication elsewhere (except conference proceedings papers). A guide for authors and relevant information for the submission of manuscripts are provided in this section and also online at: https://ph02.tci-thaijo.org/index.php/ennrj/author. All manuscripts are refereed through a **single-blind peer-review** process.

Submitted manuscripts are reviewed by outside experts or editorial board members of **Environment and Natural Resources Journal**. This journal uses double-blind review, which means that both the reviewer and author identities are concealed from the reviewers, and vice versa, throughout the review process. Steps in the process are as follows:

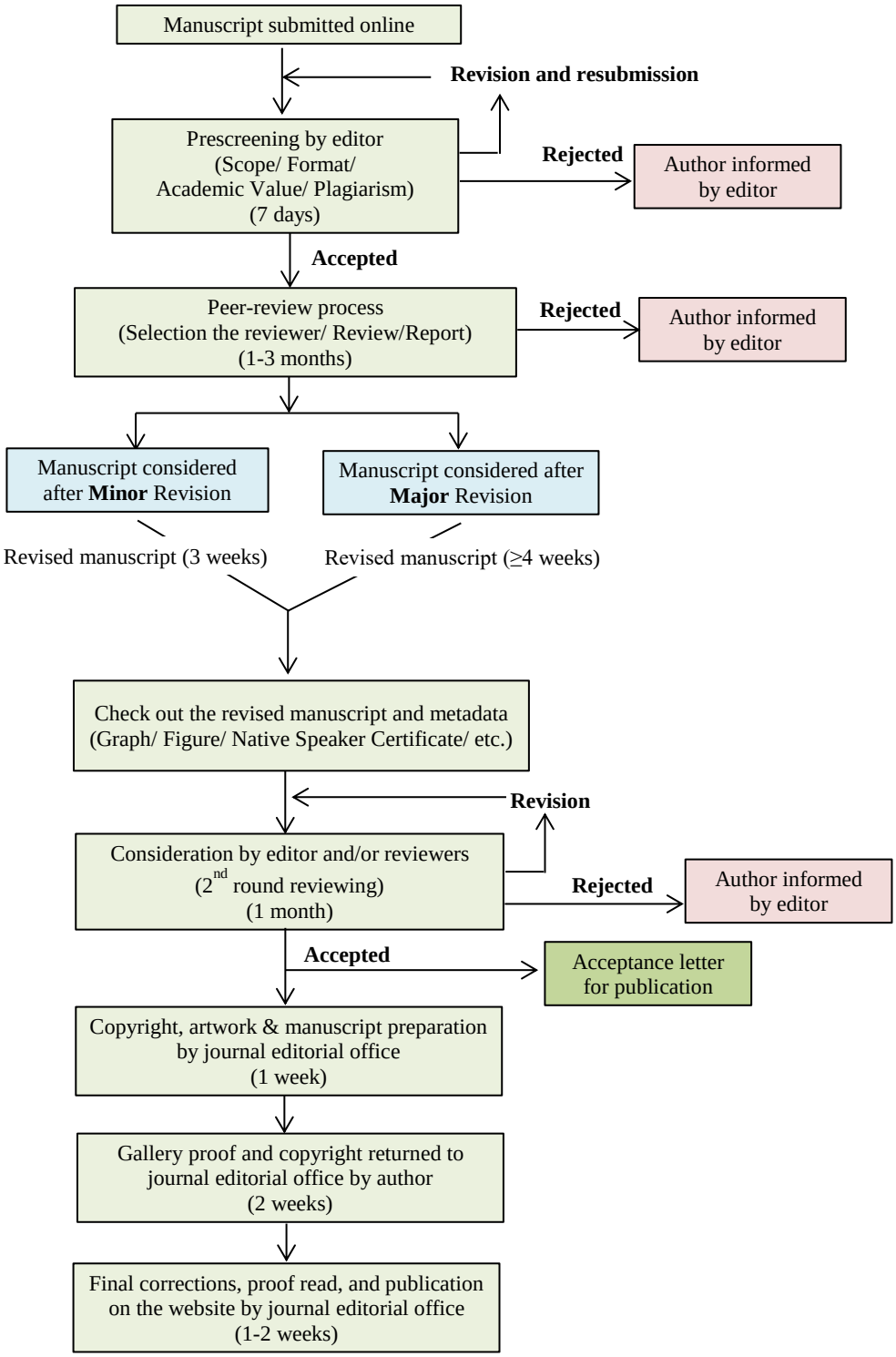

The Environment and Natural Resources Journal (EnNRJ) considers and accepts two types of articles for publication as follows:

- *Original Research Article*: This is the most common type of article. It showcases new, innovative or unique findings surrounding a focused research question. Manuscripts should not exceed 4,000 words (excluding references) - see more details in the Preparation of Manuscript section below.
- *Review Article (by invitation)*: This type of article focuses on the in-depth critical review of a special aspect of an environmental-related research question, issue, or topic. It provides a synthesis and critical evaluation of the state of the knowledge of the subject. Manuscripts should not exceed 6,000 words (excluding references).

Submission of Manuscript

The items that the author needs to upload for the submission are as follows:

Manuscript: The manuscript must be submitted as a Microsoft Word file (.doc or .docx). Refer to the **Preparation of Manuscript** section below for detailed formatting instructions.

Cover Letter: The letter should address the Editor and include the following: a statement declaring that the author's paper has not been previously published and is not currently under consideration by another journal.

- a brief description of the research the author reports in the paper, including why the findings are important and why the journal readers should be interested
- contact information of the author and any co-authors
- a confirmation that the author has no competing interests to disclose

Graphical Abstract (Optional): The author is encouraged to submit a graphical abstract with the manuscript. The graphical abstract depicts the research and findings with visuals. It attracts more potential readers as it lets them understand the overall picture of the article within a few glances. Note that the graphical abstract must be original and unpublished artwork. It should be a high-quality illustration or diagram in any of the following formats: TIFF, PDF, JPEG, or PNG. The minimum required size is 750 × 750 pixels (height × width). The size should be of high quality (600 dpi or larger) in order to reproduce well.

Reviewers Suggestion (mandatory): Please provide the names of three potential reviewers, with information about their affiliations as well as their email addresses. The recommended reviewers should not have any conflict of interest with the authors. Each reviewer must represent a different affiliation and not have the same nationality as the author. Please note that the editorial board retains the sole right to decide whether or not the recommended reviewers will be selected.

Declaration of Competing Interest: The author must include a declaration of competing interest form during submission. If there is no conflict of interest, please state, "The authors declare no conflict of interest." Otherwise, authors should declare all interests to avoid inappropriate influence or bias in their published work. Examples of potential conflicts of interest in research projects include but are not limited to financial interests (such as employment, consultancies, grants, and other funding) and non-financial interests (such as personal or professional relationships, affiliations, and personal beliefs).

CrediT (Contributor Roles Taxonomy) Author Statement or Author Contributions: For research articles with several authors, we require corresponding authors to provide co-author contributions to the manuscript using the relevant CRediT roles. CRediT is a taxonomy that shows the contributions of the author and co-author(s), reduces possible authorship disputes, and facilitates collaboration among research team members. The CRediT taxonomy includes 14 different roles describing each contributor's specific contribution to the scholarly output.

The roles are: Conceptualization; Data curation; Formal analysis; Funding acquisition; Investigation; Methodology; Project administration; Resources; Software; Supervision; Validation; Visualization; Roles/Writing – original draft; and Writing – review & editing.

Note that authors may have contributed through multiple roles, and those who contributed to the research work but do not qualify for authorship should be listed in the acknowledgments.

An example of a CRediT author statement is given below:
"Conceptualization, X.X. and Y.Y.; Methodology, X.X.; Software, X.X.; Validation, X.X., Y.Y. and Z.Z.; Formal Analysis, X.X.; Investigation, X.X.; Resources, X.X.; Data Curation, X.X.; Writing – Original Draft Preparation, X.X.; Writing – Review & Editing, X.X.; Visualization, X.X.; Supervision, X.X.; Project Administration, X.X.; Funding Acquisition, Y.Y."

Artwork for the Journal Cover: The author may provide and propose a piece of artwork (with a description) for the journal issue cover. This is an excellent opportunity for the author to promote their article, if accepted, on the cover of a published issue. Alternatively, the editorial team may invite the author to submit a piece of artwork for the cover after their manuscript has been accepted for publication. The final cover artwork selection will be made by the editorial team.

Final Author Checks: In addition to the basic requirements, the author should review this checklist before submitting their manuscript. Following it ensures the manuscript is complete and in accordance with all standards.

Preparation of Manuscript

Format and Style

The manuscript should be prepared strictly as per the guidelines given below. Any manuscript with an incorrect format will be returned, and the corresponding author may have to resubmit a new manuscript with the correct format.

Overall Format

The manuscript must be submitted as a Microsoft Word file (.doc or .docx). The formatting should be as follows:

- File format - .doc or .docx
- Page size - A4
- Page orientation - portrait (some landscape pages are accepted if necessary)
- Page margin - 2.54 cm (left and the right margin) and 1.9 cm (bottom and the top margin)
- Page number (bottom of the page)
- Line number
- Line spacing - 1.5
- Font - 12 point, Times New Roman (unless stated otherwise)

Unit - The use of abbreviation must follow the International System of Units (SI Unit) format.

- The unit separator is a virgule (/) and not a negative coefficient: 10 mg/L not 10 mgL^{-1}
- Liter always has a capital letter: mg/L

Equations

- Insert equations using the dedicated tool in Microsoft Word. Do not use pictures or text boxes.
- Equations that are referenced in the text should be identified by parenthetical numbers, such as (1), and should be referred to in the manuscript as “Equation 1”.

Inclusive Language: The language used in the manuscript acknowledges diversity, promotes equal opportunity, respects all people, and is sensitive to all aspects of differences. The manuscript content should not make assumptions about the beliefs or commitments of any individual. It should not imply superiority regarding age, race, ethnicity, culture, gender, sexual orientation, disability, or health conditions. Moreover, the manuscript must be free from bias, stereotypes, slang, and derogatory terms.

Reference Style: Vancouver style should be used for the reference list and in-text citations throughout the manuscript. Please follow the format of the sample references and citations, as shown in the Body Text Sections portion below.

Front Page

Title: The title of the manuscript should be concise and not longer than necessary. The title should be bold, 12-point size, and Times New Roman. The first letter of major words should be capitalized (as in standard title case).

Author(s) Name: The first and last names of all authors must be given, in bold, Times New Roman, and 12-point font.

Affiliation of All Author(s): Affiliation(s) must be in italics, Times New Roman, and 11-point font. Specify the Department/School/Faculty, University, City/Province/or State, and Country of each affiliation. Do not include positions or fellowships, or postal zip codes.
Each affiliation should be indicated with superscript Arabic numerals. The Arabic numeral(s) should appear immediately after the author’s name, and represent the respective affiliation(s).

Corresponding Author: One author should be responsible for correspondence, and their name must be identified in the author list using an asterisk (*).

- All correspondence with the journal, including article submission and status updates, must be handled by the corresponding author.

- The online submission and all associated processes should be operated by the corresponding author.

*Corresponding author: followed by the corresponding author's email address.

Example:

Papitchaya Chookaew[1], Apiradee Sukmilin[2], and Chalor Jarusutthirak[1*]
[1]Department of Environmental Technology and Management, Faculty of Environment, Kasetsart University, Bangkok, Thailand
[2]Environmental Science and Technology Program, Faculty of Science and Technology, Phranakhon Rajabhat University, Bangkok, Thailand
**Corresponding author: abcxx@xx.ac.th*

Abstract Page

Abstract: The abstract should include the significant findings paired with relevant data. A good abstract is presented in one paragraph and is limited to 250 words. Do not include a table, figure, or references.
Keywords - Up to six keywords are allowed, and they should adequately index the subject matter.

Highlights: Please include 3-5 concise sentences describing innovative methods and the findings of the study. Each sentence should contain at most 85 characters (not words).

Body Text Sections
The main body text of the manuscript normally includes the following sections: 1. Introduction 2. Methodology 3. Results and Discussion 4. Conclusions 5. Acknowledgments 6. Author Contributions 7. Declaration of Competing Interests 8. References

Introduction should include the aims of the study. It should be as concise as possible, with no subheadings. The significance of the problem and the essential background should also be given.

Methodology is sufficiently detailed so that the experiments can be reproduced. The techniques and methods adopted should be supported with standard references.
There should be no more than three levels of headings in the **Methodology and Results and Discussion** sections. Main headings are in bold letters, second-level headings are in bold and italic letters, and third-level headings are in normal letters.

Here is an example:

2. Methodology
2.1 Sub-heading
2.1.1 Sub-sub-heading

Results presents the key findings in figures and tables with descriptive explanations in the text.

Tables
- Tables - look best if all the cells are not bordered; place horizontal borders only under the legend, the column headings, and the bottom.

Figures
- Figures - should be submitted in color. The author must ensure that the figures are clear and understandable. Regardless of the application used to create them, when electronic artworks are finalized, please 'save as' or convert the images to TIFF or JPG and send them separately to EnNRJ. Images require a resolution of at least 600 dpi (dots per inch) for publication. The labels of the figures and tables must be Times New Roman, and their size should be adjusted to fit the figures without borderlines.
- Graph - The font style in all graphs must be Times New Roman, 9-10 size, and black color. Please avoid bold formatting, and set the border width of the graphs to 0.75 pt.

- Graph from MS Excel: Please attach an editable graph from MS Excel within your manuscript. Then please also submit the full MS Excel file used to prepare the graph as a separate document. This helps us customize our layout for aesthetic beauty.
- Graph from another program: Feel free to use whichever program best suits your needs. But as noted above, when your artwork is finalized, please convert the image to TIFF or JPG and send them separately Again, images should be at least 600 dpi. Do not directly cut and paste.

***All figures and tables should be embedded in the text, and also mentioned in the text.**

Discussion shows the interpretation of findings with supporting theory and comparisons to other studies. The Results and Discussion sections can be either separated, or combined. If combined, the section should be named Results and Discussion. **Conclusions** should include a summary of the key findings and take-home messages. This should not be too long, or repetitive but this section is absolutely necessary so that the argument of the manuscript is not uncertain or left unfinished.

Acknowledgments should include the names of those who contributed substantially to the work, but do not fulfill the requirements for authorship. It should also include any sponsor or funding agency that supported the work.

Author Contributions: For research articles with several authors, we require corresponding author contributions listed using the relevant CRediT roles. This should be done by the author responsible for correspondence.

Declaration of Competing Interest: The author must include a declaration of competing interest form during submission. If there is no conflict of interest, please state, "The authors declare no conflict of interest." Otherwise, authors should declare all interests to avoid inappropriate influence or bias in their published work.

References should be cited in the text by the surname of the author(s) and the year. This journal uses the author-date method of citation. The author's last name and date of publication are inserted in the text in the appropriate place. If there are more than two authors, “et al.” must be added after the first author’s name. Examples: (Frits, 1976; Pandey and Shukla, 2003; Kungsuwas et al., 1996). If the author’s name is part of the sentence, only the date is placed in parentheses: “Frits (1976) argued that . . .”

Please ensure that every reference cited in the text is also in the reference list (and vice versa).

In the list at the end of the manuscript, complete references must be arranged alphabetically by the surnames of the first author in each citation. Examples are given below.

Book

Tyree MT, Zimmermann MH. Xylem Structure and the Ascent of Sap. Heidelberg, Germany: Springer; 2002.

Chapter in a book

Kungsuwan A, Ittipong B, Chandrkrachang S. Preservative effect of chitosan on fish products. In: Steven WF, Rao MS, Chandrkachang S, editors. Chitin and Chitosan: Environmental and Friendly and Versatile Biomaterials. Bangkok: Asian Institute of Technology; 1996. p. 193-9.

Journal article

Muenmee S, Chiemchaisri W, Chiemchaisri C. Microbial consortium involving biological methane oxidation in relation to the biodegradation of waste plastics in a solid waste disposal open dump site. International Biodeterioration and Biodegradation 2015;102(3):172-81.

Journal article with Article Number

Sah D. Concentration, source apportionment and human health risk assessment of elements in $PM_{2.5}$ at Agra, India. Urban Climate 2023;49:Article No. 101477.

Non-English articles

Suebsuk P, Pongnumkul A, Leartsudkanung D, Sareewiwatthana P. Predicting factors of lung function among motorcycle taxi drivers in the Bangkok metropolitan area. Journal of Public Health 2014;44(1):79-92 (in Thai).

Article in press

Dhiman V, Kumar A. Biomass and carbon stock estimation through remote sensing and field methods of subtropical Himalayan Forest under threat due to developmental activities. Environment and Natural Resources Journal 2024. DOI: 10.32526/ennrj/22/20240018.

Published in conference proceedings

Wiwattanakantang P, To-im J. Tourist satisfaction on sustainable tourism development, Amphawa floating market Samut Songkhram, Thailand. Proceedings of the 1st Environment and Natural Resources International Conference; 2014 Nov 6-7; The Sukosol hotel, Bangkok: Thailand; 2014.

Ph.D./Master thesis

Shrestha MK. Relative Ungulate Abundance in a Fragmented Landscape: Implications for Tiger Conservation [dissertation]. Saint Paul, University of Minnesota; 2004.

Website

Orzel C. Wind and temperature: why doesn't windy equal hot? [Internet]. 2010 [cited 2016 Jun 20]. Available from: http://scienceblogs.com/principles/2010/08/17/wind-and-temperature-why-doesn/.

Report organization

Intergovernmental Panel on Climate Change (IPCC). IPCC Guidelines for National Greenhouse Gas Inventories: Volume 1-5. Hayama, Japan: Institute for Global Environmental Strategies; 2006.

Royal Gazette

Royal Gazette. Promotion of Marine and Coastal Resources Management Act 2059. Volume 132, Part 21, Dated 26 Mar B.E. 2558. Bangkok, Thailand: Office of the Council of State; 2015a. (in Thai).

Remark

** Please be note that manuscripts should usually contain at least 15 references and some of them must be up-to-date research articles.*

** Please strictly check all references cited in text, they should be added in the list of references. Our Journal does not publish papers with incomplete citations.*

Changes to Authorship

This policy of journal concerns the addition, removal, or rearrangement of author names in the authorship of accepted manuscripts:

Before the accepted manuscript

For all submissions, that request of authorship change during review process should be made to the form below and sent to the Editorial Office of EnNRJ. Approval of the change during revision is at the discretion of the Editor-in-Chief. The form that the corresponding author must fill out includes: (a) the reason for the change in author list and (b) written confirmation from all authors who have been added, removed, or reordered need to confirm that they agree to the change by signing the form. Requests form submitted must be consented by corresponding author only.

After the accepted manuscript

The journal does not accept the change request in all of the addition, removal, or rearrangement of author names in the authorship. Only in exceptional circumstances will the Editor consider the addition, deletion or rearrangement of authors after the manuscript has been accepted.

Copyright transfer

The copyright to the published article is transferred to Environment and Natural Resources Journal (EnNRJ) which is organized by Faculty of Environment and Resource Studies, Mahidol University. The accepted article cannot be published until the Journal Editorial Officer has received the appropriate signed copyright transfer.

Online First Articles

The article will be published online after receipt of the corrected proofs. This is the official first publication citable with the Digital Object Identifier (DOI). After release of the printed version, the paper can also be cited by issue and page numbers. DOI may be used to cite and link to electronic documents. The DOI consists of a unique alpha-numeric character string which is assigned to a document by the publisher upon the initial electronic publication. The assigned DOI never changes.

Mahidol University

Wisdom of the Land

Faculty of Environment and Resource Studies, Mahidol University, Thailand
999 Phutthamonthon Sai 4 Rd, Salaya, Phutthamonthon District, Nakhon Pathom 73170
E-mail: ennrjournal@gmail.com